AN ABSTRACT OF THE THESIS OF

Pierre J. Berbinau for the degree of Doctor of Philosophy in Mechanical Engineering presented on 3 April 1997

Title: A Study of Compression Loading of Composite Laminates

Abstract approved: Redacted for Privacy

Ernest G. Wolff

The compressive behavior of continuous fiber composites is not as well understood as their tensile behavior because research and industrial applications have until recently focused on the latter. Furthermore, most theoretical and experimental studies on the compression of composites have examined the case of unidirectional specimens with fibers along the loading direction (0° fibers). While this is a logical approach since it isolates the failure mode specific to this geometry (kinking), the study of multidirectional laminates is essential because these are used in all practical applications. Few theories model the compressive behavior of multidirectional laminates. None of the theories account for the stress field or the sequence and interaction of the various observed failure modes (kinking, delamination, matrix failure) specific to the multidirectional configuration.

The principal objective of this investigation is to construct a realistic theory to model the compressive behavior of multidirectional composites. Compression experiments have repeatedly shown that the initial failure mode was in-plane kinking of 0° fibers initiated at the edges of the specimens. We decided to base our compressive failure theory upon interlaminar stresses because in multidirectional laminates these are known to exist in a boundary layer along the edges. This required development of an analytical

theory giving the amplitude of these stresses at the free edges. We then incorporated these stresses into a new general microbuckling equation for 0° fibers. The global laminate failure strain was determined through several fiber and matrix failure criteria. Theoretical predictions were compared with experimental results obtained from compression testing of graphite/thermoplastic laminates with the same ply sequence but different off-axis ply angles. The theory correlated well with experiments and confirmed that in-plane kinking was the critical failure mode at low and medium angles, while revealing that out-of-plane buckling was responsible for failure at high angles. Furthermore, the theory correctly predicted the sequence of various fiber and matrix failure modes.

A Study of Compression Loading of Composite Laminates

by

Pierre J. Berbinau

A THESIS

submitted to

Oregon State University

in partial fulfillment of
the requirements for the
degree of

Doctor of Philosophy

Completed April 3, 1997

Commencement June 1997

Doctor of Philosophy thesis of Pierre J. Berbinau presented on April 3, 1997

APPROVED:

Redacted for Privacy

Major Professor, representing Mechanical Engineering

Redacted for Privacy

Head of Department of Mechanical Engineering

Redacted for Privacy

Dean of Graduate School

I understand that my thesis will become part of the permanent collection of Oregon State University libraries. My signature below authorizes release of my thesis to any reader upon request.

Redacted for Privacy

Pierre J. Berbinau, Author

ACKNOWLEDGEMENTS

First of all I would like to thank my Major Professor, Dr. Ernest G. Wolff, for accepting me as his Ph.D. graduate student; especially in light of a 4 years interruption between my Master's and my Ph.D. The memory of the two years spent doing a Master's under his supervision was a key factor in my decision to eventually come back to work on a Ph.D. with him. Beyond his guidance and advice throughout my Ph.D., Dr. Wolff also provided me with the opportunity to work on industrial research projects, and thus deserves much of the credit for the development of my own practical and analytical research skills. I would also like to thank Drs. Timothy C. Kennedy, William H. Warnes, Dawn Peters, and Charles K. Sollitt for serving as members of my graduate committee. In particular I would like to thank Dr. Sollitt for his careful review of my dissertation's work. Dr. Swavik A. Spiewak spent much time introducing me to mathematical software packages. His invaluable help and kind patience are much appreciated. Orrie Page carefully manufactured the fixtures needed for the experiments, and the completion of my thesis would not have been possible without him.

Aside for my thesis work, I very much enjoyed the mind-opening discussions I had on the topic of nonlocal elasticity with Dr. Kennedy, and especially with Dr. A.C. Eringen, Professor Emeritus Princeton University. My thanks also go to Dr. Enrique A. Thomann of the OSU Mathematics Dept. for his advice and the time he dedicated to me during my research on that topic.

Finally I thank all my friends here at OSU for their cheerful and moral support during these years working toward my Ph.D.

TABLE OF CONTENTS

TABLE OF CONTENTS (continued)

Page

LIST OF FIGURES

LIST OF FIGURES (continued)

LIST OF APPENDIX FIGURES

LIST OF APPENDIX FIGURES (continued)

LIST OF APPENDIX FIGURES (continued)

LIST OF APPENDIX FIGURES (continued)

LIST OF APPENDIX FIGURES (continued)

LIST OF APPENDIX FIGURES (continued)

NOMENCLATURE

The following is a list of the symbols used in the theory (Chapter 3) and subsequent Chapters. It does not apply to the literature review (Chapter 2), in which the original nomenclature from the various articles was kept.

$A^{(k)}$	Algebraic coefficients corresponding to ply (k)
$A_i^{(k)}$, $\overline{A}_i^{(k)}$	Algebraic coefficients corresponding to ply (k) and root (i)
A_f	Fiber cross-section area
$B^{(k)}$	Algebraic coefficients corresponding to ply (k)
$B_i^{(k)}$, $\overline{B}_i^{(k)}$	Algebraic coefficients corresponding to ply (k) and root (i)
c	Boundary condition coefficient for a beam varying from 1 (simply supported) to 4 (clamped)
C_{corr}	Correction coefficient (between 0 and 1)
C_{red}	Reduction coefficient (between 0 and 1)
e	Half thickness of the matrix layers between plies
E	Stiffness
E_f	Fiber stiffness
E_m	Matrix stiffness
E_b	Longitudinal stiffness of the (θ/-θ) beam
E_1	Ply longitudinal stiffness
E_2	Ply tranverse stiffness
$FacA_i^{(k)}$	Algebraic factor corresponding to ply (k) and root (i)
$FacB_i^{(k)}$	Algebraic factor corresponding to ply (k) and root (i)
g	Gage-length

NOMENCLATURE (continued)

G	Ply shear stiffness
G_m	Matrix shear stiffness
h	Thickness of a single ply
h_k	Thickness of ply (k)
i	Index for the number of roots ρ
I	Fiber moment of inertia
I_b	Moment of inertia of the (θ/-θ) beam
k	Index for the number of plies in the laminate
L	Specimen length
m	Distributed moment
M	Moment
$MM_i^{(k)}$	Algebraic coefficients corresponding to ply (k) and root (i)
$\vec{n}$	Unit vector normal to a surface
N	Half of the total number of plies in the laminate
$NN_i^{(k)}$	Algebraic coefficients corresponding to ply (k) and root (i)
p	Distributed axial force
p_k	Boundary stress (normal) on ply (k)
P	Buckling load
$q,\ q'$	Distributed normal force
Q	Shear force
$Q^{(k)}$	On-axis stiffness matrix for ply (k)
$\overline{Q}^{(k)}$	Off-axis stiffness matrix for ply (k)
r	Root of the determinant matrix
r_f	Fiber radius

NOMENCLATURE (continued)

$RR^{(k)}$	Algebraic coefficients corresponding to ply (k)
$SS^{(k)}$	Algebraic coefficients corresponding to ply (k)
t	Specimen thickness
t_k	Boundary stress (tangential) on ply (k)
$\overline{\overline{T}}$	Stress tensor
u_a	Applied displacement
u_k	Displacement in the x direction in ply number (k)
v	Amplitude of the buckling fiber in the y direction
v_k	Displacement in the y direction in ply number (k)
v_0	Initial amplitude of the buckling fiber in the y direction
V	Maximum amplitude of the buckling fiber in the y direction
V_0	Maximum initial amplitude of the buckling fiber in the y direction
V_f	Fiber volume fraction
w	Amplitude of the buckling fiber in the y direction
w_0	Initial amplitude of the buckling fiber in the y direction
W	Maximum amplitude of the buckling fiber in the y direction
W_0	Maximum initial amplitude of the buckling fiber in the y direction
Wi	Specimen width
x, y, z	Cartesian coordinates
β	Kink band boundary angle
δ	Bending amplitude of the $(\theta/-\theta)$ beam
ε_x	Strain in the x direction
ε_y	Strain in the y direction
ε_f	Fiber tensile strain

NOMENCLATURE (continued)

ε_{tf}	Fiber failure strain in tension
ϕ	Initial fiber misalignment angle
φ	Angle between the z direction and the direction of the unit normal $\vec{n}$
γ_{xy}	Shear strain in the (x,y) plane
λ	Half wavelength of fiber microbuckling
λ_0	Half wavelength of fiber microbuckling (measured)
ν_{12}, ν_{21}	Poisson's ratios
θ	Angle between the fibers and the loading direction
θ_k	Angle between the fibers and the loading direction in ply (k)
ρ	Root of the determinant matrix
ρ_i	Root number (i) of the determinant matrix
σ_c	Compressive strength
σ_e	Euler buckling strength
σ_f	Tensile failure stress of the matrix
σ_x	Normal stress in the x direction
σ_y	Normal stress in the y direction
σ_z	Interlaminar normal stress
$\sigma_{0°ply}$	Compressive stress in a 0° ply
τ_f	Shear failure stress of the matrix
τ_{xy}	Shear stress in the (x,y) plane
τ_{zx}	Interlaminar shear stress in the (x,z) plane
τ_{zy}	Interlaminar shear stress in the (y,z) plane
ω	Slope of the deflected fiber axis

Ce travail est dédié à mes parents,
Jean et Catherine Berbinau

... en mémoire des longues heures
passées à la table du salon...

A Study of Compression Loading of Composite Laminates

(1) INTRODUCTION

1.1 Review

Historically, as composite materials were being developed, and new fiber and matrices with improved mechanical properties were being used, the guiding principle was achieving better tensile properties for the overall laminate. Only fairly recently has attention broadened to include compression performance. It was found that compression strength of continuous fiber composites was clearly the limiting factor for failure [1], partly due to the fact that improvement in the tensile strength and modulus of the matrix were detrimental to the overall compressive strength of the composite [2]. Hence a thorough understanding of the compressive fracture process in multidirectional composites is essential for the prediction of the failure of these materials. Several investigators have studied experimentally the behavior of unidirectional, cross-ply and multidirectional composites in compression. For the high fiber volume fractions used in composites, kinking was found to be the universal failure mode [2-11]. But theoretical modeling of the compressive failure of composites has almost exclusively examined the case of unidirectional composites and, to our knowledge, only five attempts have been made to model the compression behavior of non-unidirectional composites: cross-ply composite [12], angle-ply composite [13], multidirectional composites [14-16].

However, none of these theories takes into account the so-called free-edge stresses which exist at the edges of composite specimens. We contend that these stresses play a role in the in-plane kinking of 0° fibers since experiments show that in-plane kinking starts at the edges [9,17-19]. Free-edge delamination has until now mostly examined the case of tensile loading but experiments on multidirectional composites indicate that interlaminar edge stresses play a role in compression failure by promoting delamination, as will be seen in the literature review section.

1.2 Scope of this investigation

It is our belief that a comprehensive understanding of the compression failure process hinges on a thorough modeling of the initiation of the failure modes arising during static compressive loading, namely kinking and free-edge delamination. To this end, we first developed a theory that predicts analytically interlaminar shear stresses τ_{zx} and τ_{zy}. Constructing an analytical theory for interlaminar stresses for any layup was a necessary step in order to create such a comprehensive model. We then incorporated these interlaminar shear stresses into an analytical model of the influence of the angle θ of adjacent plies onto the kinking of fibers in the 0° plies. Our final prediction for the compressive failure of a multidirectional composite comes as a general microbuckling equation for the 0° fibers that includes interlaminar stresses. Indeed, in line with main stream thinking among researchers, kinking is considered as an immediate outcome of microbuckling. While our theory is only valid in the case of symmetric composites, since it does not take into account warping effects, this is hardly a restriction because unsymmetric laminates are rarely used, and only for very specific applications. Derivation of the above theory is undertaken in Chapter 3, after a comprehensive literature review covering the various aspects of compression failure of composites in Chapter 2. To check

our predictions, and especially the influence of the supporting plies angle θ on the microbuckling strain, we performed experiments on a carbon/thermoplastic composite with the generic layup $[\theta/-\theta/0_2/\theta/-\theta/0]_s$ with θ varying between 10° and 90°. The fibers were AS4 carbon fibers, and the matrix a polyphenylene sulfide (PPS). To study the propensity for out-of-plane microbuckling, we performed additional experiments on specimens made up of a single 0° ply embedded in a thermoplastic. The test methodology and experimental setup are described in Chapter 4. Experimental results are then presented in Chapter 5. In Chapter 6 we compare our theoretical predictions for the above layup to the results from the experiments conducted in Chapter 4. Results from tests on the single embedded 0° ply are also discussed in the light of the study of the $[\theta/-\theta/0_2/\theta/-\theta/0]_s$ laminate. In Chapter 7 we summarize and conclude this work, and we give recommendations for further studies based on the present work.

(2) LITERATURE REVIEW

2.1 Overview

Experiments on compression of unidirectional composites show that failure takes place by the creation of a kink band [2-11], while for multidirectional composites, it is the initial failure mode [17-19]. This kink band is oriented at an angle β which for carbon fibers reinforced plastics takes the following values: $\beta = 15°$ [2,3,11], $\beta = 10°\text{-}30°$ [4], [5-8,17], $\beta = 20°\text{-}30°$ [10]. Figure 1 shows the geometry and kinematics of an in-plane kink band. The fibers in the kink band make an angle α with their initial direction. Experiments consistently showed $\alpha \approx 2\beta$. The kink band width is W. In the case of an out-of-plane kink, the global movement of the fibers is perpendicular to the ply plane. The difference between in-plane and out-of-plane kinking of a 0° ply is illustrated in Figure 2. While there is no full consensus among researchers about the exact mechanism leading to the formation of a kink band [20,21], it is acknowledged that kinking is eventually the end-result of microbuckling of 0° fibers and their subsequent failure in bending accompanied by large plastic rotation of the matrix. In view of experimental observations, theories for fiber microbuckling on foundation favor a gradual amplitude increase of initially wavy fibers versus an instability bifurcation of straight fibers. Indeed, an initial angle of axial fibers around 2°-3° is typical of hand-laid composite specimens [22], and gives a good agreement between the theoretical and experimental failure stresses for unidirectional composites [6,19]. This justifies the modeling of fiber alignment imperfections by the use of a microbuckling theory with fibers that are initially wavy in

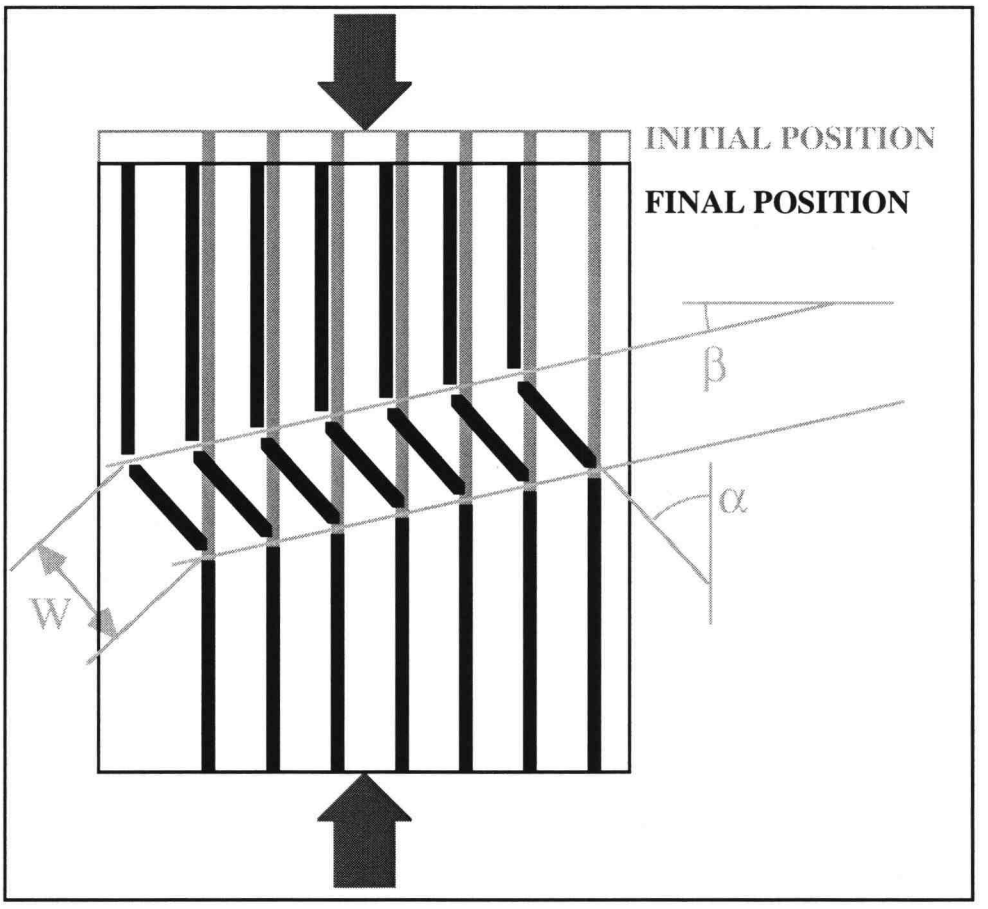

Figure 1. In-plane kink band formation

the ply plane. This will also be the approach used in this work. It is useful at this stage to review the existing theories for compression failure of composites. The three main categories of composite layups (unidirectional, cross-ply, and multidirectional) will be covered, and a separate section will be dedicated to the phenomenon of free-edge delamination.

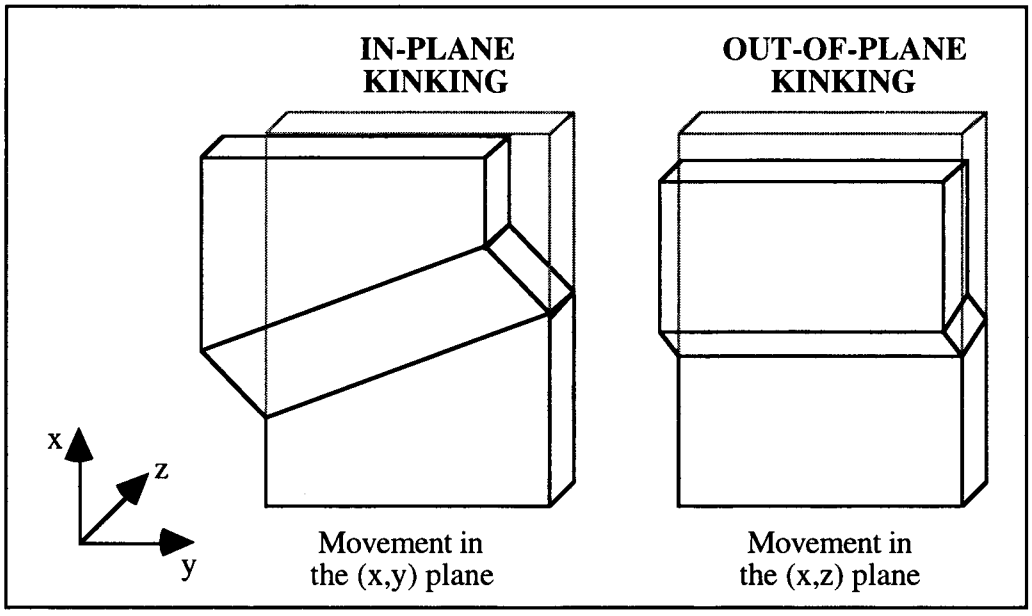

Figure 2. Comparison between in-plane kink and out-of-plane kink

2.2 0° specimens

Theoretical models for predicting failure loads are almost all for 0° specimens. They may be classified into two groups: microbuckling theories, which consider the microbuckling of a fiber on foundation with a fiber bending failure criterion, and kinking theories, which assume a-priori the existence of a kink band, and then study its stability. These various theories predict some or all of the following quantities: the applied stress σ_c or displacement u_c that triggers microbuckling/kinking, the kink band angle β, and the kink band width W.

2.2.1 Existing microbuckling theories:

The referenced theories are based on the microbuckling of a fiber on foundation (i.e. surrounded by a continuum), with various assumptions regarding the loading. For

reference purposes we show in Figure 3 the most general case of such microbuckling. When necessary we have changed the notation of the original article so that it corresponds to the one on Figure 3. P is the buckling load, p is the distributed axial load, q is the distributed transverse load, and m is the distributed couple. Q and M are respectively the shear force and moment induced in the fiber. The quantities u and v refer to displacements in the x and y directions respectively.

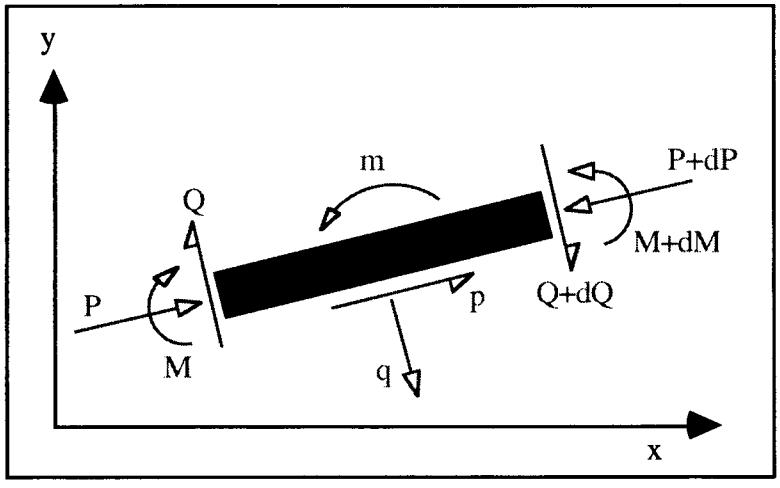

Figure 3. Fiber equilibrium

Rosen [23] was the first to investigate the microbuckling of fibers in composites. Using an energy method, he found the compressive stress σ_c for the shear mode (see Figure 10, Chapter 3) as:

$$\sigma_c = \frac{G_m}{1 - V_f}$$

where V_f is the fiber volume fraction and G_m is the matrix shear modulus. Microbuckling was elastic and the fibers were initially straight. The problem with this model is that it over predicts the compressive stress, and it contradicts experiments that show that the compressive stress is proportional to the fiber volume fraction [24, 25]. In addition, it

predicts a compressive stress independent of the fiber stiffness, contrary to experiments [26].

Hermann *et al* [27] considered the case p=0 (see Figure 3) and derived expressions for q and m from the elasticity solution of a foundation subjected to loads applied at the surface of a cylindrical cavity. Expressions for q and m depended on the buckling wavelength. The simplified case of m=0 was also considered.

Darby and Kanellopoulos [28] considered the buckling of a circular fiber with m=p=0 and q = q'v. It gave the same result as [29] for the buckling load:

$$P_c = 2\sqrt{E_f I q'}$$

or equivalently for the critical stress:

$$\sigma_c = \sqrt{E_f q'/\pi}$$

where q' is related to the matrix stiffness. Alternatively, by assuming that the deformation of the foundation is of exponential decay type, and by minimizing the total elastic strain energy, they obtained another expression for the critical stress (E_m is the matrix modulus):

$$\sigma_c = \sqrt{E_f/\pi} \cdot 4\left[E_m G_m/2\right]^{\frac{1}{4}}$$

thus finding q'. The predicted critical stress was however higher than the Rosen compressive stress in shear mode [23].

Lagoudas, Saleh and Tadsbakhsh [30-32] chose to model the composite as an inhomogeneous material by expressing mechanical properties as spatial Fourier series, and considering nonlinear strain measures. Solving equations up to the second order and assuming initial fiber waviness of varying wavelength lead them to a range of predictions for the compressive strength. The upper bound (straight initial fibers) is Rosen's model, and the lower bound (fibers with zero initial wavelength) is:

$$\sigma_c = \frac{G_m}{1-V_f} \cdot \left\{ \frac{1+\frac{sin(\pi V_f)}{2\pi V_f}\left[cos(\pi V_f) - \sqrt{cos^2(\pi V_f)+8}\right]}{1+\frac{sin(\pi V_f)}{2\pi V_f}\left[2cos(\pi V_f) - 4\frac{sin(\pi V_f)}{\pi V_f}\right]} \right\} \qquad \text{when} \quad E_m << E_f$$

The lower bound was close to experimental values for a boron/epoxy composite.

Taggart [29] considered the buckling of a single fiber on foundation with p=m=0. He obtained the buckling load:

$$P_c = 2\sqrt{E_f I E_s}$$

where L is the fiber length, E_f is the fiber stiffness, E_s is the stiffness of the surrounding material, and I is the moment of inertia. His FEA (Finite Elements Analysis) results showed that considering the foundation as orthotropic homogeneous with the effective properties of the composite gave a compressive strain an order of magnitude higher than experiments (made on glass/epoxy composite). Stress strain curves for various composite systems are all nonlinear. FEA also showed that matrix foundation support was less at free edges, not surprisingly.

Hahn and Williams [6] modeled microbuckling as a fiber on foundation submitted to a couple stress m, a distributed shear force p, and a distributed normal force q. For a single fiber in an infinite matrix (low fiber volume content), m=p=0 and q=Kv with K proportional to E_m. This gave a buckling load:

$$P_c = 2\sqrt{KE_fI}$$

and a half buckling wavelength λ:

$$\lambda = \pi\left(\frac{E_fI}{K}\right)^{\frac{1}{4}}.$$

For higher volume fractions where fibers buckle in-phase, they chose p=q=0 with m due to the shearing of the matrix. Considering the equilibrium of a rectangular fiber with the surrounding matrix gave $m = -\frac{h_f}{V_f}\tau_{LT}$ and the same buckling stress as Rosen [23]. Considering the equilibrium of a single circular fiber with an initial amplitude f_0 gave $m = -A_f\tau_{LT}$ and q=Kv. They obtained then the buckling stress:

$$\sigma_c = V_f\left[G_{LT} + \frac{EI}{A}\left(\frac{\pi}{\lambda}\right)^2 + \frac{K}{A}\left(\frac{\lambda}{\pi}\right)^2\right]\left(1 - \frac{f_0}{f}\right)$$

Minimizing with respect to λ gave:

$$\sigma_c = V_f\left[G_{LT} + \frac{2}{A}\sqrt{EIK}\right]\left(1 - \frac{f_0}{f}\right) \quad \text{and} \quad \sigma_c = V_f \cdot \frac{G_m}{1 - V_f}$$

with no initial deflection, in better agreement with [24] and [25].

Hahn [33] extended the microbuckling analysis of [6] to the final fracture of the fiber. The matrix was considered perfectly plastic, and failure was assumed to happen in 3 stages: 1- Fibers elastic microbuckling, 2- Matrix plastic yielding, 3- Fibers breaking. Because fibers buckle in phase, it assumes p=q=0 and $m=-A\tau_y$. The fiber breaking occurred at the location of maximum fiber curvature. This allowed a prediction for the kink width W as the distance between two maximum curvature points:

$$W = \pi\sqrt{\frac{E_f I}{\sigma_f A}}$$

This expression is in agreement with experimental data. The kink angle α could also be calculated, as equal to the maximum slope at the time of fiber fracture. It was however less than experimentally observed kink angles, which suggests that further fiber rotation occurs after fiber breaking, since predictions were made for the onset of fiber breaking.

Steif [34] considers the buckling of fibers in the shear mode, and thus takes p=q=0, and $m=a\tau$ due to shear stresses τ from the matrix at the fiber interface, where a is the fiber thickness. The main feature of this article is to take into account the weakness of the interface by requiring that τ be less than the interface shear strength τ_c. It thus can consider slipped and unslipped portions of the interface and their relative influence on the buckling load. A weak interface is found to give failure strains lower than the classical microbuckling strains.

Waas, Babcock and Knauss [35] studied the microbuckling of a fiber at a free edge. They first consider a single fiber bonded to a half-plane matrix foundation. Hence they took $p\neq0$, $q\neq0$, $m=p\cdot(h/2)$ where h is the fiber thickness. They found p and q from the elastic solution for the matrix, and then applied boundary conditions at the fiber/matrix

interface. They finally obtained the buckling strain and wavelength as the minimum of the strain with respect to the wavelength. They then studied the case where the matrix foundation is replaced by a composite. The predicted buckling strain remained higher than the shear mode from Rosen [23], while experimental buckling strain are lower. However, for low fiber volume fraction, the decay mode was preferred and a short wavelength predicted.

Steif [36] considered the buckling of a fiber of radius r with p=q=0 and $m=4\cdot r^2\cdot\tau$ due to a shear couple τ around the fiber. Taking the load P as along x gave $Q=-P\cdot\sin(\theta)$, and the following equilibrium equation in θ, angle of the fiber with the loading axis:

$$\frac{dM}{ds} + P\,sin(\theta) - 4r^2\tau = 0$$

This is the nonlinear equivalent of the buckling equation in [34]. The constitutive relations were:

$$M = EI\frac{d\theta}{ds} \qquad \text{and} \qquad \tau = \tau_c\, tanh\left(\frac{G\theta}{\tau_c}\right)$$

where G is the shear modulus of the elastic perfectly plastic composite with yielding at τ_c. The nonlinear constitutive equation was solved numerically. Failure was found to occur when the critical tensile strain of the fiber was reached. If a fiber offset of r was assumed, it was found that if one equates the half wavelength of the initial imperfection to the observed kink width, then the theoretical fiber-breaking strain agreed with the observed failure strain. This indicates that fiber breaking is a critical step in the formation of the kink band. The second part of [36] dealt with the kink formation. The first condition for the kink formation is the kink equilibrium. This equilibrium equation is the same equation

as the kink equilibrium equation in [4]. The second condition states that the energy of the kink configuration is less than the energy of the unkinked one. Plastic shearing in the kink was taken into account. This analysis predicted that α was slightly more than β.

Frost [37] used nonlinear strains and an energy method to find the buckling stress for fibers with initial curvature, along with a matrix shear strength failure criterion. The buckling equation was solved numerically. Nonlinear effects were significant only at short initial wavelengths.

Lo and Shim [26] predicted the compressive strength σ_c using the Timoshenko beam theory, thus taking into account shear effects. They used an energy method with p=q=m=0, and included the shear correction factor k'. The reference volume was a portion of buckled fibers of length l. Minimization of the total potential energy lead to the following expression for σ_c:

$$\sigma_c = \frac{k'G_{12}}{1+\left(\frac{l}{\alpha\pi}\right)^2\left(\frac{k'AG_{12}}{E_{11}I}\right)}$$

where G_{12} was the composite shear modulus, E_{11} the composite longitudinal modulus, α a coefficient that allows for the boundary conditions on the portion of the fiber in the reference volume. For a rectangular reference volume element of length L, width w and thickness h, k'=2/3 and the authors obtained:

$$\sigma_c = \frac{G_{12}}{\frac{3}{2}+12\left(\frac{L}{\alpha\pi h}\right)^2\left(\frac{G_{12}}{E_{11}}\right)}$$

The only unknown was the ratio $(L/\alpha h)$. It should be determined from experiments, and must be independent of the materials. A ratio of 6 was arbitrarily chosen. It gave results below Rosen's [23], and agreed very well with experiments. When fiber misalignment is taken into account in E_{11}, the compressive strength also agrees with experiments.

Wilczynski [38] modeled the microbuckling of a single fiber on foundation submitted to a distributed normal force q=Kv. This gave a buckling load:

$$P_c = 2\sqrt{KE_f I}$$

By modeling elastic deformation of the matrix due to the fiber movement, he found:

$$K = \frac{8\pi}{(1+\nu)^2} E_m \quad \text{for plane stress, and:} \qquad K = 8\pi\left(\frac{1-\nu}{1+\nu}\right) E_m \quad \text{for plane strain.}$$

This gave the fiber buckling stress:

$$\sigma_c = \sqrt{8E_m E_{fa}\left(\frac{1-\nu}{1+\nu}\right)} \qquad \text{where} \qquad E_{fa} = \frac{E_f}{1+8\left(a_i/d\right)^2}$$

is the apparent modulus of the buckled fiber, a_i its initial amplitude and d its diameter.

Xu and Reifsnider [39] modeled the microbuckling of a single square fiber of side b on foundation submitted to a distributed normal force q=Kv, and a couple m due to shear forces τ: $m = \tau \cdot b^2$. This gave a buckling load:

$$P_c = 2\sqrt{KE_f I} + G_m b^2$$

and a half buckling wavelength:

$$\lambda = \pi\left(\frac{E_f I}{K}\right)^{\frac{1}{4}}$$

which is the same as in [6]. The coefficient K was found by calculating the elastic stresses in the composite in the transverse direction under a transverse sinusoidal displacement (due to the bending of the fibers). This gave:

$$K = \frac{2\pi E_T}{1+\nu_{LT}}$$

and ultimately the fiber buckling stress:

$$\sigma_c = \sqrt{\frac{2\pi}{3}\frac{E_T E_f}{1+\nu_{LT}}} + G_m$$

Chung and Weitsmann [24,40] modeled the microbuckling of a representative volume of width (2c) made of a fiber and the matrix between fibers (layered medium) [24]. Fibers had initial waviness and deformed in the shear mode. The normal force q=q(x,c) was due to the matrix and the distributed moment $m=-2c\tau^m$ due to the shear stress τ^m in the matrix. They obtained Rosen's result when the matrix was linear in shear. When the matrix was bilinear in shear, the critical load was found numerically. In [40] the theory was extended to the case of a Timoshenko beam instead of a Euler beam. The Timoshenko beam includes shear deformations of the fiber $\gamma^f=v_{,x}-\psi$, where ψ is the independent cross-section rotation (for a Euler beam $\gamma^f=0$) and $v_{,x}$ is the derivative of v with respect to x. The coupled nonlinear differential equations in ψ and v were solved

numerically. Numerical results showed that γ^f becomes discontinuous at some points along the fiber past the buckling load. This approach had therefore the capability to model kink formation.

Häberle and Matthews [41] considered the microbuckling of plies with initial waviness f_0 with p=q=0 and $m=2\Delta y\cdot\tau$ where (Δy) is the width of a fiber and the surrounding nonlinear matrix. This gave an equation similar to [6] for the buckling stress but without the V_f coefficient and with K=0:

$$\sigma_c = \left[G_{LT} + \frac{EI}{A}\left(\frac{\pi}{l}\right)^2\right]\left(1 - \frac{f_0}{f}\right)$$

Neglecting the bending term and the initial waviness,

$$\sigma_c = \frac{G_{LT}\cdot\gamma}{\gamma + \phi_0}$$

where γ is the shear strain and ϕ_0 the maximum initial fiber angle. This is the Budiansky result [47] if γ is the shear yield strain. If $f_0 = 0$, we get Rosen's result [23].

Zhang and Latour [42] studied the microbuckling of two fibers of radius r in a matrix with p=0, $q=2\sigma_y$, and $m=2r\tau_{xy}$. The stresses σ_y and τ_{xy} were found by solving the problem of an elastic matrix between two fibers. The new aspect of this work was to allow for different deformation amplitudes of the two fibers: A and $(k\cdot A)$ with $-1 \le k \le 1$. The compressive stress σ_c was an involved expression of the buckling wavelength α and was minimized with respect to α. It is interesting to note that the compressive stress decreased from k=-1 (extension mode) to k=1 (shear mode), thus predicting that the shear mode is preferred. This is consistent with kink band failure. Results also showed that the

microbuckling half-wavelength was infinite when k=1 (as in Rosen analysis [23]), but decreased very fast to the experimentally observed kink band widths at k=0.999. This is consistent with kink band formation since in a real composite, we will never have k=1, due to nonuniform fiber distribution and edge effects. A finite element analysis was also performed on two fibers, and gave similar results. These results were consistent with [6], at least for low fiber volume fractions.

Effendi, Barrau and Guedra [10] modeled the microbuckling of a rectangular fiber of height h_f on foundation. Experiments showed that the compressive stress-strain curves were elastic nonlinear almost up to failure. They also showed that the width of the kink band that ultimately formed was half the buckling wavelength. The microbuckling was modeled with $m = -\tau_{LT} \cdot h_f / V_f$, $\tau_{LT} = (v - v_0)_{,x} \cdot G_m / (1 - V_f)$, p = 0, and q = k(v-$v_0$), where v and v_0 are the final and initial deflections of amplitudes f and f_0 respectively. The critical stress was given by letting f go to infinity:

$$\sigma_c = \frac{G_m}{1 - V_f} + EI \frac{V_f}{h_f} \left(\frac{\pi}{l} \right)^2 + k \frac{V_f}{h_f} \left(\frac{l}{\pi} \right)^2$$

If one neglects the second and third terms, Rosen's results [23] are obtained.

Sadowsky, Pu and Hussain [43] considered the microbuckling of a single fiber in a 3-D matrix. The approach was thus similar to [27], but more general since p, q, and m were all non-zero. Displacements were assumed continuous at the fiber/matrix interface. Eventually p, q, and m were connected to the elasticity solution (expressed in terms of Bessel functions) and the buckling equation was solved to come up with an expression for the buckling load. No comparison was made with experiments.

Davis [44] considered the microbuckling of fibers in the shear mode. He assumed that the fibers had an initial deflection and modeled the composite as a Timoshenko beam made up of alternating fiber and matrix layers. Since nonlinear behavior of the layers was considered, equations were solved incrementally. They allow the calculation of in-plane shear stresses in between fibers (which lead to delamination), as well as the critical buckling load for shear instability. Predictions agreed with experiments on boron/epoxy tubes.

Karayaka and Setihoglu [45] found experimentally that for unidirectional composites, a more ductile matrix favors failure by kinking. This is in agreement with common belief that the matrix plays a central role in the kinking process owing to the large fiber rotation.

Mueller et al. [46] made an interesting investigation of the influence of the relative position of fibers on the compression mode by studying the compression of two model polyamide fibers embedded in a transparent silicone matrix. They found that co-operative (in the same plane) microbuckling in the shear mode occurred below a certain distance (equal in this case to 10 fiber diameters), thus confirming the essential role played by fiber stress field interactions.

2.2.2 Existing kinking theories:

Budiansky [47] modeled the formation of a kink band using a plastic microbuckling theory (elastic perfectly plastic body) with no fiber bending. He obtained the compressive stress:

$$\sigma_c = \frac{k^*}{\phi_0 + \gamma_Y} \qquad \text{with} \quad k^* = k\sqrt{1+(\sigma_T/k)^2 \tan^2(\beta)}$$

where k is the composite shear yield strength, σ_T is the tensile transverse composite yield strength, γ_Y is the composite shear yield strain, and ϕ_0 is the initial fiber misalignment angle. β is the kink band angle. However k* is minimum (and then equal to k) for β=0, which is not the experimentally observed kink band angle. Then, when taking into account the elastic inextensible deformation of a fiber, he obtained the following partial differential equation for the transverse displacements v:

$$(G-\sigma)v_{,xx} + E_T v_{,yy} = \sigma v_{0,xx}$$

where G is the composite shear modulus and v_0 the initial imperfection. Considering the extreme cases of a short-wave and a long-wave imperfection along the edge of a half-plane, the direction of maximum curvature gives in each case the angle β. The domain of β thus obtained was:

$$\left(\sqrt{2}-1\right)\sqrt{\frac{G}{E_T}\left(1-\frac{\sigma_c}{G}\right)} \le \tan\beta \le \sqrt{\frac{G}{E_T}\left(1-\frac{\sigma_c}{G}\right)}$$

This gave $12° \le \beta \le 27°$ for E_T=2G and $15° \le \beta \le 35°$ for E_T=4G. All observed experimental values for β fell within this range.

Budiansky then predicted the kink band width W (see also Soutis [2]) using a couple stress theory. The relation giving W was:

$$\left(\frac{d_f}{W}\right)^3 + \varepsilon_f\left(\frac{4}{\pi}\right)^2 \cdot \left(\frac{d_f}{W}\right) - \frac{2k}{V_f E_f}\left(\frac{4}{\pi}\right)^3 = 0$$

where ε_f is the strain to failure, d_f is the fiber diameter and E_f is the fiber modulus. For perfectly brittle fibers he obtained:

$$\frac{W}{d_f} = \frac{\pi}{4}\left(\frac{V_f E_f}{2k}\right)^{1/3}$$

This gave typical value for W on the order of $(10 \cdot d_f)$, in agreement with experimental values.

Fleck and Budiansky [4] first derived equilibrium equations for a kink band in order to calculate the shear strain-kink angle relationship, and the buckling load in the case of elastic microbuckling. The predicted kink boundary angle, β, was still 0°, in disagreement with experimental observations. This ruled out elastic microbuckling in favor of irreversible plastic microbuckling[20]. An elastic perfectly plastic matrix was then assumed. The buckling load was found using an arbitrary quadratic yield criterion, and the equation for the buckling stress derived in [47] was obtained. An energy balance was then used to model the steady-state propagation of the existing kink band. The energy balance contained a toughness term representing the energy dissipated in delamination with off-axis plies. It predicted a kink band angle β in the range 45°-75°, much larger than the 10°-30° experimental values. Fiber bending was not included in the theory, so the kink band width W could not be predicted.

Budiansky and Fleck [48] extended the analysis of [4] by considering an elastic-plastic matrix with strain hardening. A scheme similar to [4] (equilibrium of the kink band and quadratic yield criterion) was used, combined with the deformation theory of plasticity, a plastic strain hardening law, and the Ramberg-Osgood relation. They found that strain-hardening hardly modified the value of the kinking stress compared to perfect

plasticity. Fiber bending was still not included in the theory. Neglecting fiber extensibility in the theory had little effect upon the kinking response.

Slaughter and Fleck [49] improved the analysis of [48] thanks to the use of a couple stress model, which takes into account fiber bending stiffness. Their theory uses kinematics closely related to those in [50]. Couple stresses (distributed moments m in the fiber due to bending stiffness) appeared in the equilibrium relations. Assuming that the fibers were linear elastic inextensible circular beams, they obtained a linear constitutive law linking m and $\phi_{,x}$. The other constitutive equation linked the effective shear stress and strain through a Ramberg-Osgood relation that also contained the composite shear yield stress and strain. The same quadratic yield criterion and effective stress as in [48] were used. These equations lead to a second-order nonlinear differential equation for ϕ with the applied compressive stress as a parameter. The maximum value of the stress when ϕ varies was interpreted as the microbuckling stress. They found values 10% to 50% higher than the kinking stress (where fiber bending stiffness is neglected).

Fleck, Deng and Budiansky [51] extended the analysis of [49] with the aim to predict the kink band width by taking into account the fiber bending stiffness through the couple stress theory. They obtained the same differential equation in ϕ as in [49] and solved it numerically. The fiber fracture criterion was then formulated assuming that fibers on the kink band boundaries fail in bending. The kink band width W was given by the fiber fracture criteria and calculated numerically by iteration. The amplitude or the wavelength of the initial imperfection had little influence on W, but the fiber bending resistance had a significant influence. Prediction of W was between 10 and 15 fiber diameters, in agreement with experimental values [20].

Fleck and Shu [52] extended the analysis done in [51] by considering kinks of finite length. They did so within the framework of a polar theory (Cosserat theory) which allowed for the modeling of a kink band microrotation. A FEA code based on this theory was developed. The theory yields values for the predicted strength between those of Rosen [23] and Fleck, Deng and Budiansky [51].

Slaughter and Fleck [53] extended the analysis of [48] to the case of a viscoelastic matrix. The matrix outside the kink band behaved elastically. Both the standard linear viscoelastic case and the logarithmically creeping cases were considered. Depending on the ratio of the composite shear modulus to the shear viscosity, it was found that viscoelastic microbuckling may occur before or after plastic microbuckling.

Moran and Shih [8], Liu and Shih [54], and Moran, Liu and Shih [55] used a video coupled to a microscope to film the initiation and propagation of a kink band in a notched unidirectional graphite/thermoplastic composite. Only in-plane deformation occurred because the specimen was fully clamped between two plates, one of which had a transparent window for the video. This approach allowed them to observe in real time the formation process of a kink. They observed that the kink first formed by instability, with fiber rotation and plastic shearing of the matrix (incipient kinking). The kink then propagated while fibers in the kink kept on rotating. At large matrix shear strains, the fibers locked-up at a given angle, allegedly due to stiffening of the matrix. Further compression of the specimen occurred then by steady broadening of the kink band, as the bends in the fibers moved away from each other. This band broadening was believed to be the most energy favorable deformation mode at this stage. The final band width was set when the fibers snapped. Energy balance during steady state band broadening lead to the following relation between the applied stress σ and the kink band angle β:

$$\sigma = \frac{1}{2\sin^2\beta}\left[\tau_y\left(2\tan\beta - \frac{\gamma_y}{2}\right) + \frac{1}{2}G_s(2\tan\beta - \gamma_s)^2\right]$$

The shape of the shear stress-strain relation was based on PEEK data which is linear from zero to τ_y with slope G, constant up to γ_s, and linear beyond γ_s with slope G_s. Minimizing σ with respect to β gave β and σ. The theory predicted a kink band boundary angle β between 18° and 24° in agreement with experiments. Using β in the equation above gives the kink band broadening stress σ. Assuming that initial kinking occurred when the resolved shear stress in the fiber direction reached the composite shear yield stress lead to the same equation as [47] for the kinking stress.

Kyriakides et al. [56] studied kinking in graphite/thermoplastic composite tubes. Failure was catastrophic, with the formation of multiple kink bands at β around 15°. A FEA modeling of a composite was done assuming initial fiber imperfections and using the deformation theory of plasticity. It showed rotation and broadening of the kink band, this being defined as the region between points of maximum curvature. The FEA study was therefore in agreement with results of [8,54,55] and supported the hypothesis that kinking is ultimately a localization process initiated by microbuckling instability. FEA predictions for the compressive stress were in agreement with experiments, but predictions for β were lower than experimental results.

Shapery [50] chose to model a single composite ply using damage mechanics. He introduced an internal state variable (ISV) S, defined as the tangent area under the ply stress-strain curve. Nonlinearity of the matrix was included in the model. One empirical relation linking two material coefficients was used. Equilibrium equations for the kink band were then expressed using large strain kinematics of wavy fibers. The waviness was due either to initial misalignment or to microbuckling. Boundary conditions were

formulated and equations solved numerically. He concluded that owing to kinked fibers inducing rotation of fibers at the tip of the kink band, the kink propagation stress was lower than the kink initiation stress. A kink boundary angle β of 17° was predicted using the criterion of maximum shear strain in the kink band. His calculations showed that kink bands would form less easily at free surfaces because local stresses (along wavy fibers) were lower at free surfaces, hence β higher, and the fiber fracture stress also higher. This was, however, in contradiction with the experimental fact that fiber fractures initiate at free edges.

The damage mechanics approach was also used by Barbero and Tomblin [57]. The shear response of the composite (obtained from torsion experiments on glass fiber reinforced rods) was modeled by a hyperbolic tangent. This, and an adequate representative volume element, served as the basis for the derivation of an imperfection sensitivity curve that linked buckling stress and initial fiber misalignment. This analytical relation was obtained from the principle of total potential energy. Fiber misalignments were observed experimentally and fitted with a Gaussian distribution, and the damage variable was defined as the area of buckled fibers at a given load level. There was reasonably good agreement between theoretical predictions and test data.

Lankford [21] claimed that the fiber-matrix interface plays a key role in kinking initiation. Indeed, experiments by Madhukar and Drzal [58] had shown that the compressive stress increased with interface strength, and surmised that experimentally observed broomed fracture surfaces was a sign of extensive fiber matrix debonding. Lankford then concluded that debonding had to occur before buckling instability, otherwise the fiber-matrix interface would have no influence upon kinking. He then asserted that debonding was due to fiber fracture in bending, since acoustic emission started well before catastrophic failure, thus indicating that fiber fractures had occurred.

This pre-kinking fiber fracture hypothesis was also supported by SEM pictures showing fibers breaking ahead of kink tips. This theory contradicts plastic buckling as preceding kink formation. It also suggests that the kink propagates like a crack and that the crack-bridging model developed by Sutcliffe and Fleck [59] was relevant.

Chaudhuri, Xie and Garala [60] investigated kink propagation in a different way. They modeled kink instability by considering in a classical fracture mechanics framework the propagation of the tip of a fiber wedge into a matrix medium. The wedge angle was therefore the kink orientation angle, α.

2.3 Cross-ply specimens

Kominar et al. [61] performed experiments on unidirectional and cross-ply $(0/90)_{8s}$ carbon/thermoplastic composites to investigate the occurrence of in-plane and out-of-plane kinking. Microscopic examination revealed out-of-plane kinking of the 0° plies in cross-ply laminates. Failure by out-of-plane kinking was most likely favored by the location of 0° plies as surface plies. Fiber fracture by bending was clearly displayed, as in [2]. Failure of the 0° plies in the cross-ply laminate occurred at higher ply compression stress than in the unidirectional composite, indicating support of the 0° plies by the 90° plies.

Tadjbakhsh and Wang [12] modeled each lamina in the cross-ply composite as alternating layers of fibers and matrix, each fiber being a rectangular strip of the same width as the ply and of the same area as the total fibers area in the ply. Within each ply, the stiffness variation between fibers and matrix was modeled by Fourier series with a half-wavelength equal to the distance between fibers. Their approach was thus similar to

[32]. The variations of the stiffness through the thickness were modeled by Fourier series with a half-wavelength equal to the ply thickness. The composite was subjected to a biaxial compression.

Even though it deals with a tube and not a plate, the work of Chaudhuri [62] has its place in our review of the kinking process. He studied the compressive failure of cross-ply thick section tubes with N axial (0°) plies and one transversal (90°) ply, both experimentally and analytically. Initial out-of-plane imperfections in the 0° ply were assumed. The main interest of this work lies in its improvement of the analysis of [47]. By using the same partial differential equation for the elastic inextensible deformation of a fiber but by considering a half-sine imperfection (which models a kink band), Chaudhuri obtained a relation between β and the critical compressive stress σ_c. By combining this relation with a minimum energy principle (giving σ_c), he derived the following expression for β, where γ_{fu} is the ultimate shear strain of a fiber and ϕ_0 the initial misalignment angle:

$$tan\beta = \sqrt{\frac{G}{E_T}\left(\frac{\phi_0}{\phi_0 + \gamma_{fu}}\right)}$$

For ϕ_0 on the order of 2°-3°, the above relation gave $\beta = 30° \pm 2°$, in agreement with experimental data.

2.4 Multidirectional specimens

Previous experiments show that the topology of fracture surfaces is complex [2], [63] and obviously involves several failure mechanisms. A review of articles on compression fracture is surveyed below. While the present work deals only with static fracture, we have also included in this section a review of the few existing studies on

compression fatigue. The sequence of failure mechanisms is likely to be different for static loading and fatigue, especially due to the different response of the matrix, but it appeared relevant to cover here the fatigue of multidirectional specimens because the present work could serve as the basis for a theory of fatigue failure.

2.4.1 Static loading

Hong and Kim performed experiments and FEA studies on multidirectional laminates without [64] and with [65] 0° plies. They concluded that the shear components of interlaminar stresses played a prominent role in the delamination process.

Soutis et al. [66] and Soutis and Fleck [67] performed experiments on unidirectional and $[(\pm 45/0_2)_3]_s$ graphite/epoxy composites with a central hole. The stress-strain curves exhibited nonlinearity. Scanning electron microscope pictures clearly showed that the initial failure mode was fibers microbuckling at the edge of the hole, as in [9,18], followed by delamination. Because of the stress gradient (due to the presence of the hole), the kink propagated initially in a stable manner. The kink propagation was modeled in the framework of fracture mechanics (see also [59]). The strain to failure for 0° specimens and quasi-isotropic specimens was found to be the same, which suggested that the mechanism of failure in axial plies was not affected by neighboring plies. Other experiments however revealed a difference [14,17,18].

Sohi, Hahn and Williams [17] obtained higher failure strains for quasi-isotropic composites $[45/0/-45/90]_{3s}$ than for unidirectional composites. They surmised that this was due to a better lateral support of the 0° plies by the off-axis plies. Experiments indicated that in-plane kinking in 0° plies occurs first, as in [19]. In some instances,

several kinks occurred simultaneously. They suggested that delamination occurred then due to the movement of the 0° plies during kinking and their subsequent failure, which reduced their support to neighboring plies. Compressive stress-strain curves were elastic nonlinear, as in [10]. Compressive strength was found to increase with matrix modulus.

Swanson [14] proposed a theory for microbuckling in multidirectional laminates taking into account the interlaminar stresses due to neighboring plies. An initial fiber waviness v_0 was assumed. The in-plane microbuckling induced an in-plane shear τ_{xy} which results in a distributed moment m on the fibers. The interlaminar shear τ_{yz} resulted in a distributed normal force $q = A \cdot \tau_{yz,z}$ where A is the fiber area, $\tau_{yz,z}$ is the derivative of τ_{yz} with respect to z, and where τ_{yz} has been linearized with respect to z. The variation of τ_{yz} with z was found by minimizing the total strain energy. The beam equilibrium equation for the fiber was then:

$$EI\frac{d^2(v - v_0)}{dx^2} + q + \frac{dm}{ds} + P\frac{d^2v}{dx^2} = 0$$

Ultimately, Swanson obtained a relation between the axial compressive force P and the amplitude v of the in-plane displacement. A failure criterion, either the bending of the fibers or the shear of the matrix then gave the critical failure load. However this model allowed for the effect of angled-plies on in-plane kinking only in a global manner through the extension stiffness matrix. In addition, edge-effects were not incorporated in the model. Tests were performed on tubular specimens. The compressive strain was found to be higher for multidirectional specimens than for unidirectional specimens, in agreement with the theory. Delamination failure was not included in the failure criteria.

Waas et al. [9] did an experimental study of multidirectional specimens with a hole in compression. In-plane kinking of 0° plies was the initial failure mode and occurred at the hole surface. Real time photography showed that once kinking has occurred, it triggered delamination in neighboring plies when the load was increased. In specimens with a proportion of 0° plies 40% or higher, the final failure load was about 5% higher than the microbuckling initiation load. This finding was in agreement with [18].

Guynn, Bradley and Ochoa [18] did an experimental study of the influence of neighboring plies on the microbuckling of 0° plies. Specimens with two circular notches on the sides and layups $[(\pm\theta/0_2)_3/\pm\theta/0]_s$ with θ = 15°, 45°, 75°, or 90° were tested. In order to investigate the influence of the free surface on the microbuckling of the 0° plies, the layup $[(0_2/\pm45°)_3/0/\pm45°]_s$, where 0° and 45° plies have been inverted, was also tested. Results show that the microbuckling strain ε as a function of θ is, from lowest to highest: $\varepsilon(15°)$, $\varepsilon(90°)$, $\varepsilon(75°)$, and $\varepsilon(45°)$. The least support was therefore provided by the 15° plies, and the most support by the 45° plies. Results also showed a 10% decrease in ε when the 0° are shifted from an interior to a surface position. When the global strain concentration factors were taken into account in order to allow for the influence of the notch, microbuckling strains all became of the same range.

Shuart [15] proposed a theory to predict the compressive stress of multidirectional and angle-ply laminates based on the out-of-plane buckling of plies of various orientations in a laminate. He modeled a ply of arbitrary orientation as a central fiber-plate surrounded by two matrix-foundations whose respective thicknesses match the actual fiber and matrix volume fractions. The fiber-plate obeyed the Kirchoff plate assumptions, i.e. the transverse normal strains ε_z, transverse shear strains γ_{xz} and γ_{xz} and the transverse normal stresses σ_z were neglected. The matrix-foundations were linear elastic and carried the interlaminar strains. The total potential energy for a ply was minimized to obtain the ply

equations. These equations were then solved numerically in two cases: linear analysis (no initial waviness of the fiber-plates) and nonlinear analysis (initial waviness of the fiber-plates and non-linear strain measures). Several failure criteria were then applied to predict laminate failure: interlaminar failure of the matrix, and matrix shearing between fibers within a ply. Interlaminar failure was found to occur in angle-ply laminates $[+\theta/-\theta]_{ns}$ for fiber angles θ below 15°.

Shuart [13] extended the study of angle-ply laminates done in [15] by including a third failure mode, matrix compression, which would be relevant at fiber angles θ above 75°. Predictions for the compressive stress over the whole range of θ were in agreement with experiments on $[+\theta/-\theta]_{ns}$ laminates.

Drapier et al. [16] proposed a global approach in an attempt to model the deformation-structure coupling by taking into account the loading induced boundary conditions and the stacking sequence. Plies were oriented at either 0°, 90°, or ±45°.

2.4.2 Fatigue loading

Harris and Morris [68] tested quasi-isotropic notched and unnotched specimens in compression at a stress ratio R=10 and a frequency f=10 Hz. Two different layups with the same ply distribution were investigated, one with tensile interlaminar normal stresses σ_z when in compression (layup (1): $[90/45/0/-45]_{ns}$), the other one with compressive interlaminar normal stresses (layup (2) :$[45/0/-45/90]_{ns}$). Unnotched specimens were tested around 400 MPa in fatigue. Edge delamination was observed and it was found that specimens with layup (1) delaminated faster than laminates with layup (2). The interlaminar shear stress τ_{zx} seemed to be the dominant interlaminar stress, as

delaminations formed where it was maximum, i.e. at the (0/-45) interface. Failure occurred before $5 \cdot 10^4$ cycles for 16-ply specimens.

Schulte [69] performed fatigue tests on unidirectional, cross-ply, and multidirectional $[0_2/\pm45/0_2/\pm45/90]_s$ composites at various stress ratios R equal to 0.1, -1, -0.5, and 10. Only the last case was therefore compression-compression fatigue. The observed damage modes were kinking in 0° plies followed by delamination. There was no evidence of edge delamination in compression-compression fatigue. Stiffness variation with the number of cycles in symmetric tension-compression fatigue showed an initial drop for $E_{tensile}$ followed by a plateau, while $E_{compressive}$ showed no initial drop but remained at a plateau. Both stiffnesses then dropped dramatically at about the same number of cycles.

Komorowski et al. [70] performed experiments in fatigue that suggested interaction between out-of-plane kinking and edge delamination. Indeed, delamination appeared in the last 10% of the fatigue life, and then triggered out-of-plane microbuckling of the fibers in the delaminated areas. Edge delamination had also been observed in a similar study by Komorowski et al. [71]. For two laminates with identical ply composition but different layups ($[45/-45/0_2/90/0_2/-45/45]_{ns}$ and $[90/0/45/0/45/0/-45/0/-45]_{ns}$), the laminate with the 0° plies closer to the surface had a much lower fatigue life. This fact had also been observed at high-temperature fatigue [63]. The authors surmised that the position of the 0° plies closer to the surface triggered an earlier delamination. Interlaminar stresses were calculated by FEA and a failure code (MRLife6™ [70]) was used to predict fatigue failure: it used a Paris law and an approximate equation linking the strain energy release rate and the elastic moduli of intact and delaminated composites [72]. The code correctly predicted that delamination in fatigue occurred in the interfaces where the interlaminar stress τ_{zx} was maximum, in agreement with [68].

2.5 Free-edge delamination

Free-edge delamination phenomenon under tensile loading has been studied since the 1970's, thanks to the pioneering work of Pagano [53], Pagano and Pipes [73,74], Pagano and Soni [75]. The existence of interlaminar strains (and consequently stresses) had been proven experimentally by Herakovich, Post and co-workers using Moiré interferometry [76]. Classical laminated plate theory (CLT) cannot take into account the interlaminar stresses (σ_z, τ_{zx}, τ_{zy}) since the Kirchoff assumptions imply that each layer is in a state of plane stress [77]. Interlaminar stresses are clearly an edge phenomenon and arise from stress free requirements at the laminate edges. They are restricted to a boundary layer. If x is the loading direction, y the width direction and z the thickness direction, then equilibrium of top or bottom plies requires interlaminar shear stresses τ_{zx} to balance the shear stresses τ_{xy}, interlaminar shear stresses τ_{zy} to balance the normal stresses σ_y, and interlaminar normal stresses σ_z to balance the shear stresses τ_{zy} (moment equilibrium), as shown in Figure 4. The curve in Figure 4 shows the variation of σ_z as a function of y. The change of sign of σ_z results in a moment that balances the moment due to the shear stress τ_{zy}. Even assuming that stresses and strains are independent of the axial coordinate x (a reasonable assumption based on Saint-Venant principle), the partial differential equations of elasticity for the free-edge problem do not have a closed form [73]. Hence all the above articles from Pagano and co-authors calculated interlaminar stresses numerically, either by finite differences of the elasticity equations, or by FEA. In the following works by other authors, interlaminar stresses are also obtained by various numerical methods: Galerkin's method with Legendre's polynomial [78], modified Rayleigh-Ritz method [79], nonlinear FEA [80,81], 3-D FEA with the so-called slice method [82], and complex stress potentials [83]. The effectiveness of finite elements is

however impaired by a mesh sensitivity of the interlaminar stresses at the free edges [82]. Herakovich [84] and Joo and Sun [85] predicted the propensity for delamination by linking phenomenologically the mismatches in Poisson's ratios and coefficients of mutual influence between plies, but this method only gave qualitative results. Therefore, coming

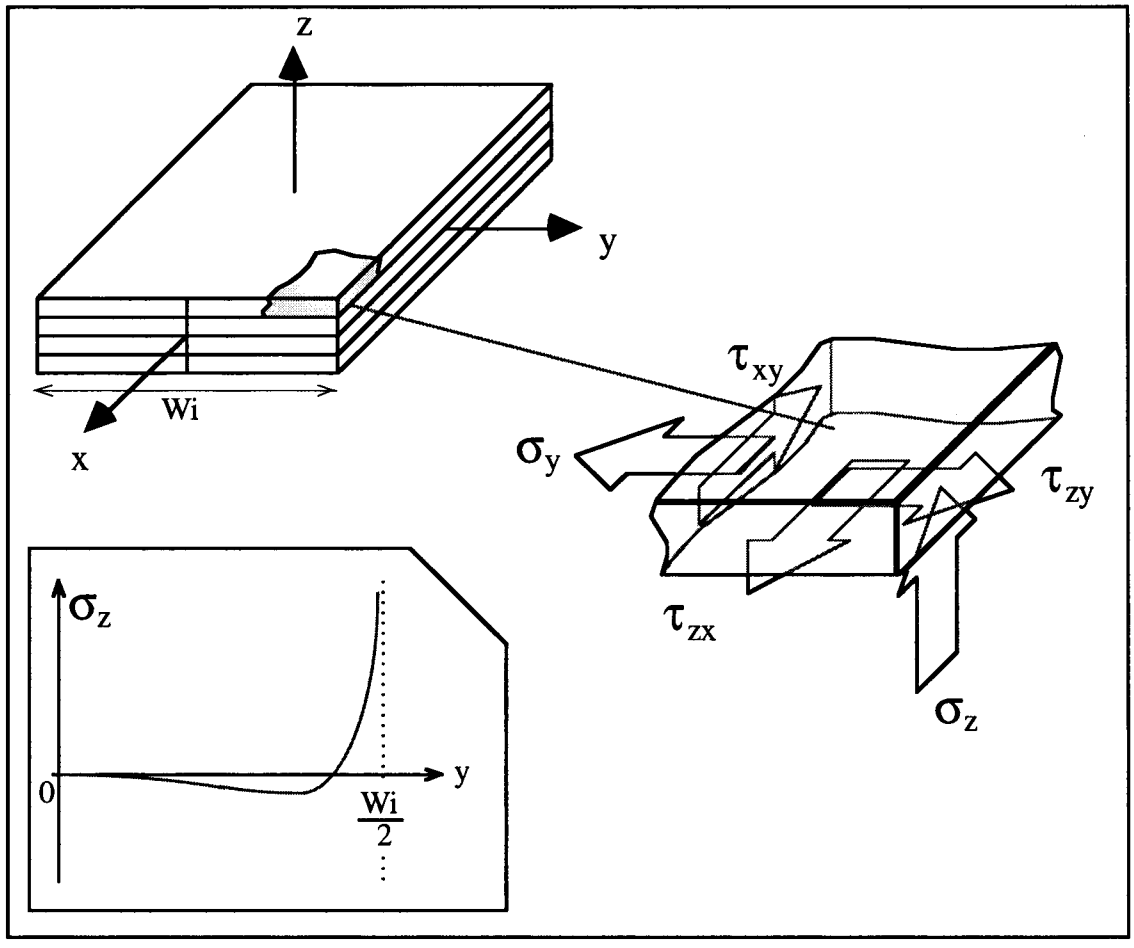

Figure 4. Interlaminar stresses

up with an analytical solution to the free-edge problem in laminates required approximations. Hsu and Herakovich [86] propose a perturbation solution (homogenization procedure) with an interior solution and a boundary layer, but their procedure is practically applicable only to bidirectional laminates. Tang's boundary layer theory [87] gave all three interlaminar stresses, but his solution did not fully satisfy the displacement continuity conditions. Whitney [88] used a phenomenological method, and

matched in-plane and interlaminar stresses computed numerically with mathematical expressions that satisfy equilibrium equations and boundary conditions but not the compatibility equations. Puppo and Evensen [89] modeled a two-layer laminate by two anisotropic layers separated by an isotropic layer where interlaminar shear stresses developed. A state of generalized plane stress is assumed for each anisotropic layer, and consequently there is no interlaminar normal stress. As formulated in their paper, the theory could only model a four-layer symmetrical laminate. They apply it to a $[\theta,-\theta]_s$ laminate. Their choice of the isotropic layer thickness was somewhat arbitrary.

The issue of the singularity of two of the interlaminar stresses (τ_{zx} and σ_z) at the free-edge is ubiquitous throughout most of the above articles, since FEA indicates infinite interlaminar stresses at the free-edge. The existence of a singularity originates from the solution to the problem of two bonded dissimilar layers. Indeed, the elasticity solution obtained using Lekhnitskii's stress potential [90] gave a weakly singular stress field at the intersection of the interlayer plane and the free-edge [91,92,93]. The alleged singularity does not, of course, exist. That this is the case is obvious on purely physical grounds: a stress singularity implies either a zero geometrical length or infinite displacements. The singularity is a mathematical artifact that arises from the artificial discontinuity in material constants at the layer interface introduced in the modeling process. This fact was recognized by Herakovich *et al* [76], Pagano [94], and Loo [95].

All of the above references dealt with laminate strips in tensile loading. The solution is analogous under compressive loading by performing a mere sign reversal of the stresses. Indeed free edge delamination in compression loading has been observed experimentally [64,65,96,97]. In [64], a 3-D FEA study of edge delamination in compression was also undertaken, and agreed with experiments.

(3) THEORY

3.1 Overview

The focus of this work is to develop a theory that predicts the failure strain of multidirectional composites in compression. Tackling this problem requires making several assumptions based on previous experimental studies and problem familiarity.

The laminates are assumed to be symmetrical. This allows the set-up of equilibrium equations (1), as explained later. This assumption is not a restricting one since laminates used in structural components are always symmetrical, except in a few very specific applications.

All previous experiments [17-19] on multidirectional composites with 0° plies have shown that in-plane microbuckling of 0° fibers is the initial failure mode. Out-of-plane microbuckling seems also to play a role in the failure of cross-ply specimens (made up of 0° and 90° plies) [61]. In addition, it is reasonable to assume that for un-notched laminates under static loading the failure of a 0° ply will trigger a failure chain reaction in remaining plies that will be catastrophic and that will lead to final failure of the whole laminate instantaneously. This would be especially true for laminates containing a significant percentage of 0° plies, such as the ones that were tested in this work (43%). These considerations lead us to formulate a failure theory for laminates that hinges on in-plane microbuckling failure of 0° fibers.

Previous experiments have also hinted at an influence of the initial angle θ of the plies adjacent to the 0° plies [18]. The only way the angle θ could have an influence on the microbuckling strain of 0° fibers is through interactions at the interface between these angled-plies and the 0° plies. It is therefore reasonable to incorporate in the theory the interlaminar stresses that will be created at these interfaces. These stresses will indeed depend on the angle θ. Now among the interlaminar stresses σ_z, τ_{zy} and τ_{zx}, only shear stresses τ_{zy} and τ_{zx} could influence the in-plane movement of the 0° fibers.

Finally, the above experiments have also shown that the microbuckling of 0° fibers always starts at the edges of the specimens. This is intuitive because fiber foundation support is reduced there. But furthermore FEA studies on straight composite specimens under tension clearly show that interlaminar stresses are close to zero in the central portion of the specimen and become significant only in a thin boundary layer near the edges where they display an exponential behavior [80-82]. Under compressive loading, these stresses would be equal but opposite. It is therefore physically sound that in the theory we will develop, interlaminar stresses should be maximum at (or very near) the edges of the specimen. We note that none of the previous theories for compression failure of multidirectional composites, while they considered interlaminar stresses, incorporated free-edge effects [12,14,15]. Instead, interlaminar stresses were calculated to be maximum in the center of the laminate [15]. This fact tends to distance these theories from physical observations.

The first part of our theory will therefore be the calculation of the interlaminar shear stresses τ_{zy} and τ_{zx} for any layup. The second part will incorporate these stresses into a general microbuckling equation for a 0° fiber located at the edge of a 0° ply. In order to complete the theory, it remains to formulate a failure criterion that governs fiber

failure. In parallel, we will also investigate matrix failure, either interlaminar, or in-between fibers inside a 0° ply. The third part of the theory will cover these topics.

3.2 Interlaminar edge stresses

3.2.1 General case ($\theta \neq 90°$)

The assessment of interlaminar stresses is indeed beyond the scope of classical laminated plate theory (CLT) since this is based on the Kirchoff plate assumptions. Ideally, the full 3-D problem should be solved. Unfortunately, as mentioned in Chapter 2, the partial differential equations giving the 3-D stress field in a laminate submitted to uniform traction (or compression) do not have a closed-form solution, even for a displacement field independent of x (the loading direction). In order to develop a comprehensive analytical theory for the compression failure of laminates, it was desirable to be able to calculate analytically the interlaminar stresses, and especially their magnitude at the free-edge. This could not be done by FEA analysis owing to the mesh sensitivity [82]. Based on the assumptions outlined above, we note that we are however only interested in the interlaminar shear stresses τ_{zy} and τ_{zx}. This leads us then to base our theory on the work done by Puppo and Evensen [89], whose theory gave interlaminar shear stresses. An additional reason behind this choice is the following argument based on physical grounds: we have seen in Chapter 2 that the free-edge interlaminar stress singularity was a mathematical outcome due to the artificial discontinuity in mechanical properties. In fact, a fiber at an angle θ_k in ply (k) will be separated from a fiber at an angle θ_{k+1} in ply (k+1) by a thin layer of matrix. It is therefore rational in our theory to

incorporate the thickness of these inter-ply matrix layers. This modeling approach is indeed the one used in [89], as it was in [15].

As formulated in [89], the theory could however only be applied to symmetrical laminates comprised of a total of 4 layers. Extending it to laminates with any number of layers required modifying the equilibrium equations. We will now detail this first step, as well as cover the kinematics of the problem.

Any ply in the laminate is replaced by an equivalent ply made up of a two parts: a central anisotropic plate that has the mechanical properties of the original ply, and two layers of thickness e that surround this plate. The two layers are made of the matrix material and are isotropic. The total thickness of a ply is, in each case, equal to h. The thickness e would typically be on the order of a fiber diameter, as estimated from microscopic observation. Figure 5 illustrates this modeling. The matrix layers between the anisotropic plates will carry the interlaminar stresses. While considering that only

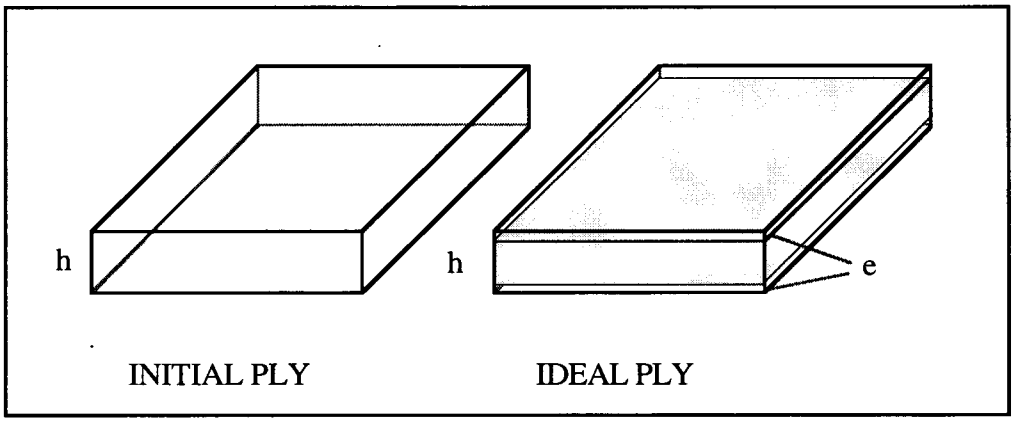

Figure 5. Modeling of a laminate ply

these matrix layers (and not the anisotropic plates) carry the interlaminar stresses is a simplifying assumption (in fact the interlaminar shear stresses vary accross the thickness [76]), it renders the boundary value problem mathematically tractable. Furthermore we

note that when applying this theory to a 4 layer (±45°) angle-ply laminate, Puppo and Evensen obtained results in agreement with FEA results [89].

Let us consider a symmetrical laminate made up of 2N plies. A given ply k ($1 \leq k \leq N$) has a thickness h_k and its fibers make an angle θ_k with the loading direction x. The width direction is y and the thickness direction is z, as shown in Figure 6. The plate has a width equal to Wi and a length L. The interlaminar normal stress σ_z is neglected. This is a

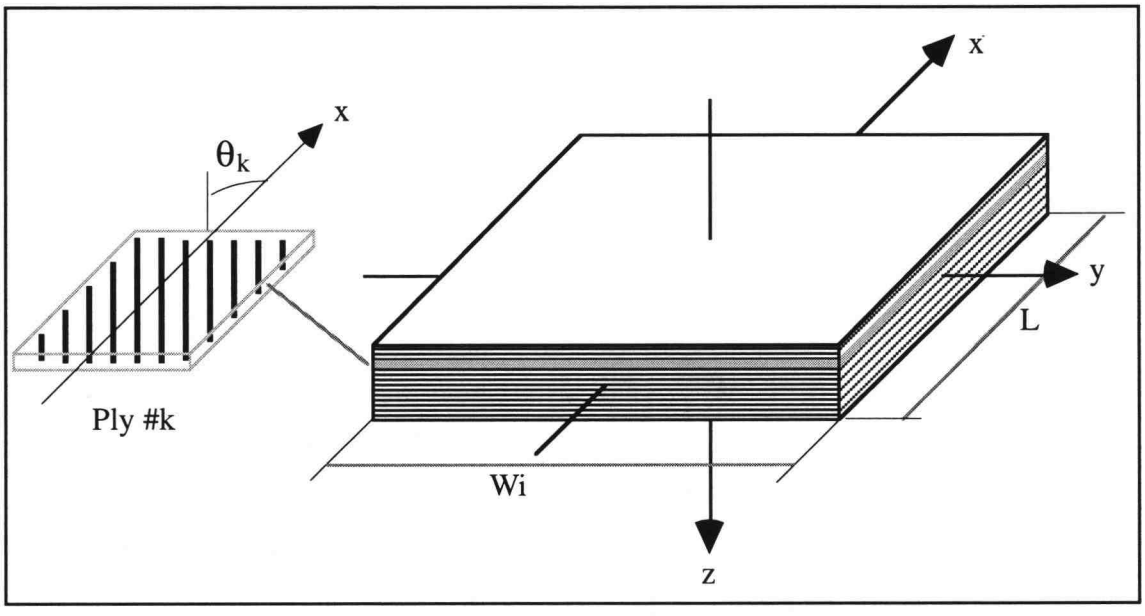

Figure 6. Laminate dimensions

fairly reasonable assumption because normal stresses are normal to the movement of the 0° fibers when they buckle in-plane. They should therefore not have an influence upon the in-plane microbuckling of the 0° fibers. The matrix layers will thus develop only shear stresses as illustrated in Figure 7.

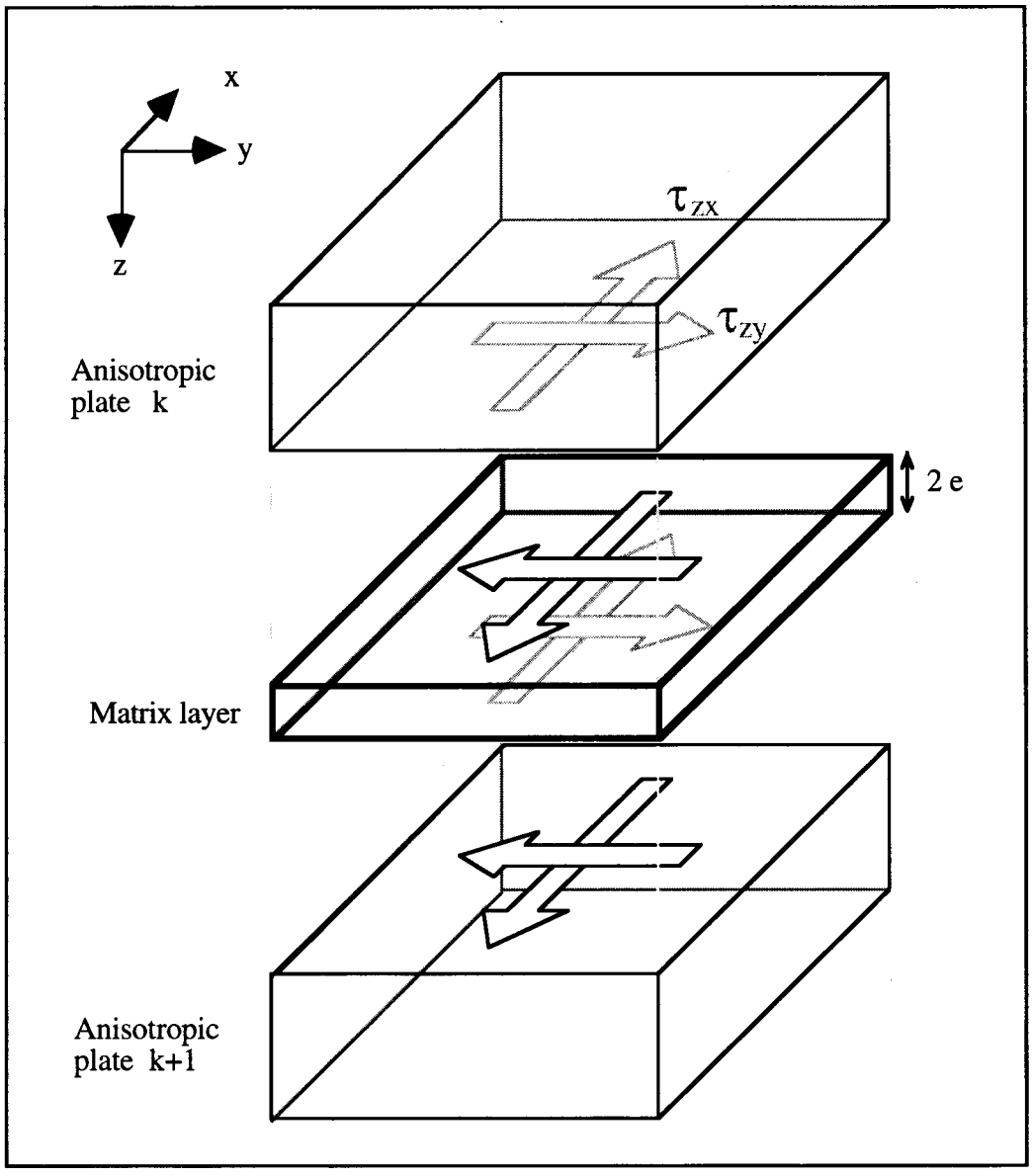

Figure 7. Inter-ply matrix layer and interlaminar shear stresses

Furthermore we consider that the displacements u_k, v_k (in the x and y directions respectively) of each plate k are the thickness averages of the actual values. Therefore, in the general case of a laminate with 2N plies, we modify the equilibrium equations of [89] as follows:

For the ply k = 1 (top ply):

$$\begin{cases} \dfrac{\partial \sigma_x^{(1)}}{\partial x} + \dfrac{\partial \tau_{xy}^{(1)}}{\partial y} - \dfrac{\tau_{zx}^{(1)}}{h_1} = 0 \\ \dfrac{\partial \tau_{xy}^{(1)}}{\partial x} + \dfrac{\partial \sigma_y^{(1)}}{\partial y} - \dfrac{\tau_{zy}^{(1)}}{h_1} = 0 \end{cases} \tag{1a}$$

For ply k, $2 \le k \le N\text{-}1$:

$$\begin{cases} \dfrac{\partial \sigma_x^{(k)}}{\partial x} + \dfrac{\partial \tau_{xy}^{(k)}}{\partial y} - \dfrac{\tau_{zx}^{(k)}}{h_k} + \dfrac{\tau_{zx}^{(k-1)}}{h_k} = 0 \\ \dfrac{\partial \tau_{xy}^{(k)}}{\partial x} + \dfrac{\partial \sigma_y^{(k)}}{\partial y} - \dfrac{\tau_{zy}^{(k)}}{h_k} + \dfrac{\tau_{zy}^{(k-1)}}{h_k} = 0 \end{cases} \tag{1b}$$

For the ply k = N (middle ply):

$$\begin{cases} \dfrac{\partial \sigma_x^{(N)}}{\partial x} + \dfrac{\partial \tau_{xy}^{(N)}}{\partial y} + \dfrac{\tau_{zx}^{(N-1)}}{h_N} = 0 \\ \dfrac{\partial \tau_{xy}^{(N)}}{\partial x} + \dfrac{\partial \sigma_y^{(N)}}{\partial y} + \dfrac{\tau_{zy}^{(N-1)}}{h_N} = 0 \end{cases} \tag{1c}$$

In (1a), (1b), (1c) and all the equations that follow, subscripts refer to the ply number. The shear stresses in the matrix layer (k) between plies (k) and (k+1) are $\tau_{zx}^{(k)}$ and $\tau_{zy}^{(k)}$, $1 \le k \le N\text{-}1$. When N=2, only equilibrium equations (1a) and (1c) remain, and they are identical to equations (1) in the Puppo and Evensen paper. When N is equal or greater than 3, the new equilibrium equations (1b), which include the action of both top and bottom matrix layers on a given ply, must be used. Now the laminate being symmetrical, we only need to treat the upper half (layers 1 to N). We point out here that laminate symmetry is a necessary assumption for the validity of equations (1). Indeed, equations (1) imply that interlaminar shear stresses are acting on the middle of each ply, whereas in fact they act on the top and bottom faces of the plies. This is an acceptable approximation as long as warping of the laminate is prevented, as will be the case for a symmetrical laminate. The shear stresses in the matrix layer (k) are then:

$$\begin{cases} \tau_{zx}^{(k)} = G_m\left[\dfrac{\partial u}{\partial z}+\dfrac{\partial w}{\partial x}\right] \approx \dfrac{G_m}{2e}\left(u_k - u_{k+1}\right) \\ \tau_{zy}^{(k)} = G_m\left[\dfrac{\partial v}{\partial z}+\dfrac{\partial w}{\partial y}\right] \approx \dfrac{G_m}{2e}\left(v_k - v_{k+1}\right) \end{cases} \quad \text{where } G_m \text{ is the matrix shear stiffness.} \quad (2)$$

The stresses σ_x, σ_y, and τ_{xy} in a ply k, $1 \le k \le N\text{-}1$ are related to the strains ε_x, ε_y, and γ_{xy} by the constitutive equations from the CLT theory [77]:

$$\begin{bmatrix} \sigma_x \\ \sigma_y \\ \tau_{xy} \end{bmatrix}_{(k)} = \begin{bmatrix} \overline{Q}_{11} & \overline{Q}_{12} & \overline{Q}_{16} \\ \overline{Q}_{12} & \overline{Q}_{22} & \overline{Q}_{26} \\ \overline{Q}_{16} & \overline{Q}_{26} & \overline{Q}_{66} \end{bmatrix}_{(k)} \cdot \begin{bmatrix} \varepsilon_x \\ \varepsilon_y \\ \gamma_{xy} \end{bmatrix}_{(k)} \quad (3)$$

with the transformation formulas [77]:

$$\overline{Q}_{11} = Q_{11}\cos^4\theta + 2\left(Q_{12}+2Q_{66}\right)\sin^2\theta\cdot\cos^2\theta + Q_{22}\sin^4\theta \quad (4a)$$

$$\overline{Q}_{12} = \left(Q_{11}+Q_{22}-4Q_{66}\right)\sin^2\theta\cdot\cos^2\theta + Q_{12}\left(\sin^4\theta+\cos^4\theta\right) \quad (4b)$$

$$\overline{Q}_{22} = Q_{11}\sin^4\theta + 2\left(Q_{12}+2Q_{66}\right)\sin^2\theta\cdot\cos^2\theta + Q_{22}\cos^4\theta \quad (4c)$$

$$\overline{Q}_{16} = \left(Q_{11}-Q_{12}-2Q_{66}\right)\sin\theta\cdot\cos^3\theta + \left(Q_{12}-Q_{22}+2Q_{66}\right)\sin^3\theta\cdot\cos\theta \quad (4d)$$

$$\overline{Q}_{26} = \left(Q_{11}-Q_{12}-2Q_{66}\right)\sin^3\theta\cdot\cos\theta + \left(Q_{12}-Q_{22}+2Q_{66}\right)\sin\theta\cdot\cos^3\theta \quad (4e)$$

$$\overline{Q}_{66} = \left(Q_{11}+Q_{22}-2Q_{12}-2Q_{66}\right)\sin^2\theta\cdot\cos^2\theta + Q_{66}\left(\sin^4\theta+\cos^4\theta\right) \quad (4f)$$

where the index k was dropped for simplicity.

The ply stiffness matrix in the principal directions Q in plane stress is linked to the fiber and matrix elastic constants by [77]:

$$Q=\begin{bmatrix} \dfrac{E_1}{1-\nu_{12}\nu_{21}} & \dfrac{E_2\nu_{12}}{1-\nu_{12}\nu_{21}} & 0 \\ \dfrac{E_2\nu_{12}}{1-\nu_{12}\nu_{21}} & \dfrac{E_2}{1-\nu_{12}\nu_{21}} & 0 \\ 0 & 0 & G \end{bmatrix} \quad \text{with} \quad \begin{cases} E_1 = E_f V_f + E_m(1-V_f) \\ E_2 = \dfrac{E_f E_m}{E_m V_f + E_f(1-V_f)} \\ G = \dfrac{G_m}{1-V_f} \quad \text{and} \quad \nu_{21} = \nu_{12}\dfrac{E_2}{E_1} \end{cases} \tag{5}$$

where E_f is the fiber stiffness, E_m is the matrix stiffness, and ν_{12} is Poisson's ratio.

Replacing equations (2) and (3) into the equilibrium equations (1) leads to the following equilibrium equations for the displacements:

$$\left[\overline{Q}_{11}^{(k)}\frac{\partial^2}{\partial x^2}+2\overline{Q}_{16}^{(k)}\frac{\partial^2}{\partial x\partial y}+\overline{Q}_{66}^{(k)}\frac{\partial^2}{\partial y^2}\right]u_k + \left[\overline{Q}_{16}^{(k)}\frac{\partial^2}{\partial x^2}+\left(\overline{Q}_{12}^{(k)}+\overline{Q}_{66}^{(k)}\right)\frac{\partial^2}{\partial x\partial y}+\overline{Q}_{26}^{(k)}\frac{\partial^2}{\partial y^2}\right]v_k+\frac{G_m}{2eh_k}\left(u_{k+1}-2u_k+u_{k-1}\right)=0 \tag{6a}$$

$$\left[\overline{Q}_{16}^{(k)}\frac{\partial^2}{\partial x^2}+\left(\overline{Q}_{12}^{(k)}+\overline{Q}_{66}^{(k)}\right)\frac{\partial^2}{\partial x\partial y}+\overline{Q}_{26}^{(k)}\frac{\partial^2}{\partial y^2}\right]u_k + \left[\overline{Q}_{66}^{(k)}\frac{\partial^2}{\partial x^2}+2\overline{Q}_{26}^{(k)}\frac{\partial^2}{\partial x\partial y}+\overline{Q}_{22}^{(k)}\frac{\partial^2}{\partial y^2}\right]v_k+\frac{G_m}{2eh_k}\left(v_{k+1}-2v_k+v_{k-1}\right)=0 \tag{6b}$$

Equations (6a) and (6b) are valid for $2 \le k \le N-1$.

For k = 1 and k = N, we have instead the equilibrium equations:

For k = 1:

$$\left[\overline{Q}_{11}^{(1)}\frac{\partial^2}{\partial x^2}+2\overline{Q}_{16}^{(1)}\frac{\partial^2}{\partial x\partial y}+\overline{Q}_{66}^{(1)}\frac{\partial^2}{\partial y^2}\right]u_1 + \left[\overline{Q}_{16}^{(1)}\frac{\partial^2}{\partial x^2}+\left(\overline{Q}_{12}^{(1)}+\overline{Q}_{66}^{(1)}\right)\frac{\partial^2}{\partial x\partial y}+\overline{Q}_{26}^{(1)}\frac{\partial^2}{\partial y^2}\right]v_1+\frac{G_m}{2eh_1}\left(u_2-u_1\right)=0 \tag{7a}$$

$$\left[\overline{Q}_{16}^{(1)}\frac{\partial^2}{\partial x^2}+\left(\overline{Q}_{12}^{(1)}+\overline{Q}_{66}^{(1)}\right)\frac{\partial^2}{\partial x\partial y}+\overline{Q}_{26}^{(1)}\frac{\partial^2}{\partial y^2}\right]u_1$$
$$+\left[\overline{Q}_{66}^{(1)}\frac{\partial^2}{\partial x^2}+2\overline{Q}_{26}^{(1)}\frac{\partial^2}{\partial x\partial y}+\overline{Q}_{22}^{(1)}\frac{\partial^2}{\partial y^2}\right]v_1+\frac{G_m}{2eh_1}\left(v_2-v_1\right)=0 \qquad (7b)$$

and for k = N:

$$\left[\overline{Q}_{11}^{(N)}\frac{\partial^2}{\partial x^2}+2\overline{Q}_{16}^{(N)}\frac{\partial^2}{\partial x\partial y}+\overline{Q}_{66}^{(N)}\frac{\partial^2}{\partial y^2}\right]u_N$$
$$+\left[\overline{Q}_{16}^{(N)}\frac{\partial^2}{\partial x^2}+\left(\overline{Q}_{12}^{(N)}+\overline{Q}_{66}^{(N)}\right)\frac{\partial^2}{\partial x\partial y}+\overline{Q}_{26}^{(N)}\frac{\partial^2}{\partial y^2}\right]v_N+\frac{G_m}{2eh_N}\left(u_{N-1}-u_N\right)=0 \qquad (8a)$$

$$\left[\overline{Q}_{16}^{(N)}\frac{\partial^2}{\partial x^2}+\left(\overline{Q}_{12}^{(N)}+\overline{Q}_{66}^{(N)}\right)\frac{\partial^2}{\partial x\partial y}+\overline{Q}_{26}^{(N)}\frac{\partial^2}{\partial y^2}\right]u_N$$
$$+\left[\overline{Q}_{66}^{(N)}\frac{\partial^2}{\partial x^2}+2\overline{Q}_{26}^{(N)}\frac{\partial^2}{\partial x\partial y}+\overline{Q}_{22}^{(N)}\frac{\partial^2}{\partial y^2}\right]v_N+\frac{G_m}{2eh_N}\left(v_{N-1}-v_N\right)=0 \qquad (8b)$$

We first solve the problem in the case of an infinitely wide laminate, that is Wi tends to infinity. For an applied uniform compression of amplitude u_a ($u_a < 0$) in the x direction, the boundary conditions are:

$$\begin{cases} u_k = +\dfrac{u_a}{2}, \quad v_k = 0 \qquad \text{at} \quad x = +\dfrac{L}{2} \\ u_k = -\dfrac{u_a}{2}, \quad v_k = 0 \qquad \text{at} \quad x = -\dfrac{L}{2} \end{cases} \qquad \forall k / 1 \le k \le N \qquad (9)$$

It is straightforward to verify that the displacements $u_k = \dfrac{u_a}{L}x$, $v_k = 0$ satisfy the boundary conditions (9) and the equilibrium equations (6a), (6b), (7a), (7b), (8a), (8b). The solution is therefore, for any ply k:

$$\begin{cases} \sigma_x^{(k)} = \overline{Q}_{11}^{(k)} \cdot \left(\frac{u_a}{L}\right) \\ \sigma_y^{(k)} = \overline{Q}_{12}^{(k)} \cdot \left(\frac{u_a}{L}\right) \end{cases} \qquad \begin{cases} \tau_{xy}^{(k)} = \overline{Q}_{16}^{(k)} \cdot \left(\frac{u_a}{L}\right) \\ \tau_{zx}^{(k)} = \tau_{zy}^{(k)} = 0 \end{cases} \qquad 1 \le k \le N \qquad (10)$$

Now actually the laminate has a finite width Wi. In the above solution, valid for an infinite laminate, normal stresses p_k and shear stresses t_k exist on the cross-sections located at $y = \pm Wi/2$ as illustrated in Figure 8:

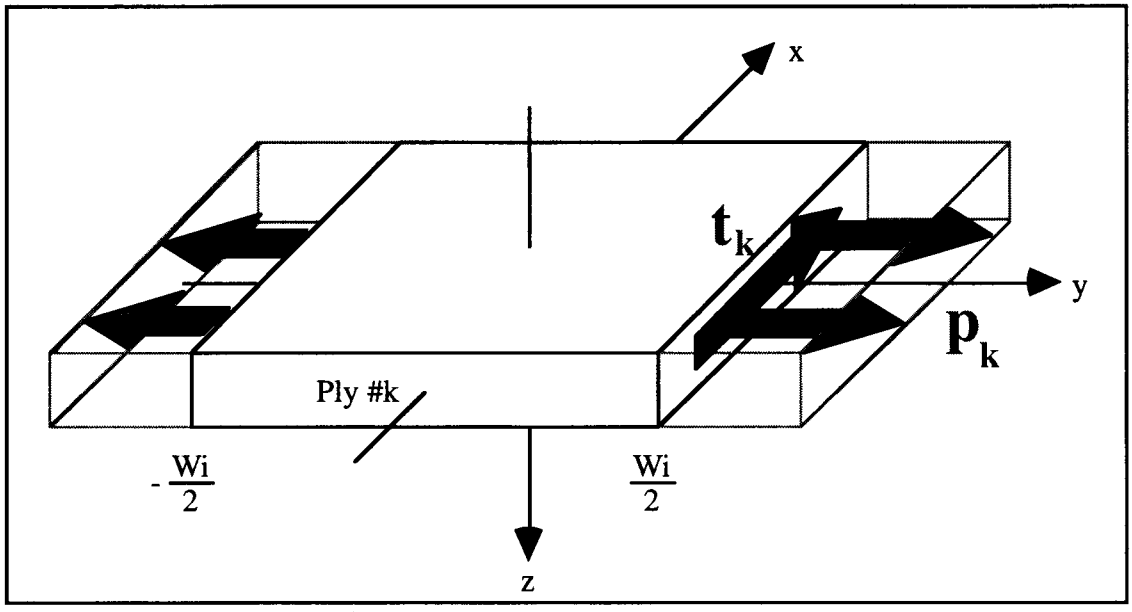

Figure 8. Boundary stresses

The stresses created are, from solution (10):

$$p_k = \overline{Q}_{12}^{(k)} \cdot \left(\frac{u_a}{L}\right) \quad \text{and} \quad t_k = \overline{Q}_{16}^{(k)} \cdot \left(\frac{u_a}{L}\right) \quad \text{on ply (k).} \qquad (11)$$

In order to obtain the solution for a finite laminate of width Wi, we then have to apply the opposite of stresses p_k and t_k at $y = \pm Wi/2$ to cancel these. The final solution for a laminate of width Wi under uniform compression will therefore be the superposition

of the solution for an infinitely wide laminate under uniform compression (solution (10)) and the solution for a laminate under no compression but subjected to stresses $(-p_k)$ and $(-t_k)$ at $y = \pm Wi/2$ as given by equation (11). Let us now solve this latter problem. The boundary conditions are then:

$$\text{At } y = \frac{Wi}{2}: \quad \sigma_y^{(k)} = -p_k \quad \text{and} \quad \tau_{xy}^{(k)} = -t_k \quad \text{for } 1 \le k \le N \tag{12a}$$

$$\text{At } y = -\frac{Wi}{2}: \quad \sigma_y^{(k)} = -p_k \quad \text{and} \quad \tau_{xy}^{(k)} = -t_k \quad \text{for } 2 \le k \le N \tag{12b}$$

$$\text{At } y = 0: \quad u_1 = 0 \quad \text{and} \quad v_1 = 0 \tag{12c}$$

We note that we have added condition (12c) on the displacements in order to eliminate rigid translations of the laminate.

We are therefore looking for a solution to equilibrium equations (6a), (6b), (7a), (7b), (8a) and (8b) with the boundary conditions (12a), (12b) and (12c). Since the solution is independent of x, we choose a displacement solution of the form:

$$\begin{cases} u_k(y) = A^{(k)} e^{ry} \\ v_k(y) = B^{(k)} e^{ry} \end{cases} \qquad \text{for } 1 \le k \le N \tag{13}$$

The number e in equations (13), (18), (19), (45) and (46) is Néper's number. In all other equations, it is the thickness of the matrix interlayer.

Replacing (13) into the equilibrium equations (6a), (6b), (7a), (7b), (8a) and (8b) gives us a system of 2N equations for the 2N unknowns $\{A^{(k)}, B^{(k)}\}$, $1 \le k \le N$. These equations are the following:

For k = 1:

$$\left[\overline{Q}_{66}^{(1)}\, r^2 - \frac{G_m}{2eh_1}\right] A^{(1)} + \left[\frac{G_m}{2eh_1}\right] A^{(2)} + \left[\overline{Q}_{26}^{(1)}\, r^2\right] B^{(1)} = 0 \tag{14a}$$

$$\left[\overline{Q}_{26}^{(1)}\, r^2\right] A^{(1)} + \left[\overline{Q}_{22}^{(1)}\, r^2 - \frac{G_m}{2eh_1}\right] B^{(1)} + \left[\frac{G_m}{2eh_1}\right] B^{(2)} = 0 \tag{14b}$$

For $2 \le k \le N\text{-}1$:

$$\left[\overline{Q}_{66}^{(k)}\, r^2 - \frac{G_m}{2eh_k}\right] A^{(k)} + \left[\frac{G_m}{2eh_k}\right] A^{(k+1)} + \left[\frac{G_m}{2eh_k}\right] A^{(k-1)} + \left[\overline{Q}_{26}^{(k)}\, r^2\right] B^{(k)} = 0 \tag{14c}$$

$$\left[\overline{Q}_{26}^{(k)}\, r^2\right] A^{(1)} + \left[\overline{Q}_{22}^{(k)}\, r^2 - \frac{G_m}{eh_k}\right] B^{(k)} + \left[\frac{G_m}{2eh_k}\right] B^{(k+1)} + \left[\frac{G_m}{2eh_k}\right] B^{(k-1)} = 0 \tag{14d}$$

For k = N:

$$\left[\overline{Q}_{66}^{(N)}\, r^2 - \frac{G_m}{2eh_N}\right] A^{(N)} + \left[\frac{G_m}{2eh_N}\right] A^{(N-1)} + \left[\overline{Q}_{26}^{(N)}\, r^2\right] B^{(N)} = 0 \tag{14e}$$

$$\left[\overline{Q}_{26}^{(N)}\, r^2\right] A^{(N)} + \left[\overline{Q}_{22}^{(N)}\, r^2 - \frac{G_m}{2eh_N}\right] B^{(N)} + \left[\frac{G_m}{2eh_N}\right] B^{(N-1)} = 0 \tag{14f}$$

The system made up of the 2N homogeneous equations (14a), (14b), (14c), (14d), (14e) and (14f) has a non-trivial solution if and only if its determinant is zero. This condition will give us the 4N roots r. Since only squares of the roots r_i appear in the determinant, we will use from now on the notation:

$$\rho = r^2 \tag{15}$$

The 2N roots ρ are the solution to equation (16):

$$
\begin{vmatrix}
Q_{66}^{(1)}\rho & & & & & & & & & \\
-\frac{G_m}{2eh_1} & Q_{26}^{(1)}\rho & \frac{G_m}{2eh_1} & 0 & \cdots & \cdots & 0 & 0 & 0 & 0 \\
Q_{26}^{(1)}\rho & Q_{22}^{(1)}\rho & & & & & & & & \\
 & -\frac{G_m}{2eh_1} & 0 & \frac{G_m}{2eh_1} & 0 & \cdots & \cdots & 0 & 0 & 0 \\
\frac{G_m}{2eh_2} & 0 & Q_{66}^{(2)}\rho & Q_{26}^{(2)}\rho & \frac{G_m}{2eh_2} & 0 & \cdots & \cdots & 0 & 0 \\
 & & -\frac{G_m}{eh_2} & & & & & & & \\
0 & \frac{G_m}{2eh_2} & Q_{26}^{(2)}\rho & Q_{22}^{(2)}\rho & 0 & \frac{G_m}{2eh_2} & 0 & \cdots & \cdots & 0 \\
 & & & -\frac{G_m}{eh_2} & & & & & & \\
0 & \ddots & \ddots & \ddots & \ddots & \ddots & \ddots & \ddots & \ddots & \vdots \\
\vdots & \ddots & \ddots & \ddots & \ddots & \ddots & \ddots & \ddots & \ddots & 0 \\
 & & & & & & Q_{66}^{(N-1)}\rho & & & \\
0 & \cdots & \cdots & 0 & \frac{G_m}{2eh_{N-1}} & 0 & -\frac{G_m}{eh_{N-1}} & Q_{26}^{(N-1)}\rho & \frac{G_m}{2eh_{N-1}} & 0 \\
 & & & & & & & Q_{22}^{(N-1)}\rho & & \\
0 & 0 & \cdots & \cdots & 0 & \frac{G_m}{2eh_{N-1}} & Q_{26}^{(N-1)}\rho & -\frac{G_m}{eh_{N-1}} & 0 & \frac{G_m}{2eh_{N-1}} \\
 & & & & & & & & Q_{66}^{(N)}\rho & \\
0 & 0 & 0 & \cdots & \cdots & 0 & \frac{G_m}{2eh_N} & 0 & -\frac{G_m}{2eh_N} & Q_{26}^{(N)}\rho \\
 & & & & & & & & & Q_{22}^{(N)}\rho \\
0 & 0 & 0 & 0 & \cdots & \cdots & 0 & \frac{G_m}{2eh_N} & Q_{26}^{(N)}\rho & -\frac{G_m}{2eh_N}
\end{vmatrix} = 0
$$

Two of the 2N roots are zero and correspond to solutions of the form:

$$
\begin{cases} u_k = A_{2N-1}^{(k)}\, y + A_{2N}^{(k)} \\ v_k = B_{2N-1}^{(k)}\, y + B_{2N}^{(k)} \end{cases} \qquad \text{for } 1 \le k \le N \tag{17}
$$

The presence of a double zero root was to be expected since it corresponds to a rigid translation and rotation of a ply.

We recall that from the definition of ρ, to each root ρ correspond two conjugate roots $\left(\sqrt{\rho}, -\sqrt{\rho}\right)$. The remaining (2N-2) roots are real and correspond then to solutions of the form:

$$\begin{cases} u_k = \sum_{i=1}^{2N-2} \left(A_i^{(k)} \, e^{\sqrt{\rho_i}\, y} + \overline{A}_i^{(k)} \, e^{-\sqrt{\rho_i}\, y} \right) \\ v_k = \sum_{i=1}^{2N-2} \left(B_i^{(k)} \, e^{\sqrt{\rho_i}\, y} + \overline{B}_i^{(k)} \, e^{-\sqrt{\rho_i}\, y} \right) \end{cases} \quad \text{for } 1 \le k \le N \qquad (18)$$

where the new coefficients $\overline{A}_i^{(k)}$, $\overline{B}_i^{(k)}$ correspond to the negative roots.

Combining solutions (17) and (18), the total solution to the problem is therefore:

$$\begin{cases} u_k = \sum_{i=1}^{2N-2} \left(A_i^{(k)} \, e^{\sqrt{\rho_i}\, y} + \overline{A}_i^{(k)} \, e^{-\sqrt{\rho_i}\, y} \right) + A_{2N-1}^{(k)} \, y + A_{2N}^{(k)} \\ v_k = \sum_{i=1}^{2N-2} \left(B_i^{(k)} \, e^{\sqrt{\rho_i}\, y} + \overline{B}_i^{(k)} \, e^{-\sqrt{\rho_i}\, y} \right) + B_{2N-1}^{(k)} \, y + B_{2N}^{(k)} \end{cases} \quad \text{for } 1 \le k \le N \qquad (19)$$

For later convenience, we can rewrite solution (19) as a sum of hyperbolic functions, while keeping the same notation for the coefficients $A_i^{(k)}$, $B_i^{(k)}$, $\overline{A}_i^{(k)}$, $\overline{B}_i^{(k)}$. We have therefore:

$$\begin{cases} u_k = \sum_{i=1}^{2N-2} \left(A_i^{(k)} \, sinh\left(\sqrt{\rho_i}\, y\right) + \overline{A}_i^{(k)} \, cosh\left(\sqrt{\rho_i}\, y\right) \right) + A_{2N-1}^{(k)} \, y + A_{2N}^{(k)} \\ v_k = \sum_{i=1}^{2N-2} \left(B_i^{(k)} \, sinh\left(\sqrt{\rho_i}\, y\right) + \overline{B}_i^{(k)} \, cosh\left(\sqrt{\rho_i}\, y\right) \right) + B_{2N-1}^{(k)} \, y + B_{2N}^{(k)} \end{cases} \quad \text{for } 1 \le k \le N \qquad (20)$$

For each root ρ_i, $1 \le i \le 2N-2$, we can express the coefficients $A_i^{(k)}$ (for $2 \le k \le N$) and $B_i^{(k)}$ (for $1 \le k \le N$) as a function of $A_i^{(1)}$ using any (2N-1) equations of the 2N equations

(14a), (14b), (14c), (14d), (14e) and (14f). The relations between these coefficients are then of the form:

$$\begin{cases} A_i^{(k)} = \left(FacA_i^{(k)}\right) \cdot A_i^{(1)} & \text{for } 2 \le k \le N \\ B_i^{(k)} = \left(FacB_i^{(k)}\right) \cdot A_i^{(1)} & \text{for } 1 \le k \le N \end{cases} \quad \text{for } 1 \le i \le 2N\text{-}2 \tag{21}$$

which defines the factors $\left(FacA_i^{(k)},\ FacB_i^{(k)}\right)$.

Similarly, we can express the coefficients $\overline{A}_i^{(k)}$ (for $2 \le k \le N$) and $\overline{B}_i^{(k)}$ (for $1 \le k \le N$) as a function of $\overline{A}_i^{(1)}$ using the same (2N-1) equations among the 2N equations (14a), (14b), (14c), (14d), (14e) and (14f). These relations will of course be identical to relations (21), and are given below:

$$\begin{cases} \overline{A}_i^{(k)} = \left(FacA_i^{(k)}\right) \cdot \overline{A}_i^{(1)} & \text{for } 2 \le k \le N \\ \overline{B}_i^{(k)} = \left(FacB_i^{(k)}\right) \cdot \overline{A}_i^{(1)} & \text{for } 1 \le k \le N \end{cases} \quad \text{for } 1 \le i \le 2N\text{-}2 \tag{22}$$

We now have (8N-4) unknowns:

$$\left(A_i^{(1)},\ \overline{A}_i^{(1)}\right) \qquad \text{for } 1 \le i \le 2N\text{-}2,$$

$$\text{and} \quad \left(A_{2N-1}^{(k)},\ A_{2N}^{(k)},\ B_{2N-1}^{(k)},\ B_{2N}^{(k)}\right) \qquad \text{for } 1 \le k \le N.$$

Now replacing u_k and v_k into the partial differential equations (6a), (6b), (7a), (7b), (8a) and (8b), we see that, for the double zero roots, we have:

$$\text{For } k = 1: \quad \begin{cases} \left(A_{2N-1}^{(2)}\, y + A_{2N}^{(2)}\right) - \left(A_{2N-1}^{(1)}\, y + A_{2N}^{(1)}\right) = 0 \\ \left(B_{2N-1}^{(2)}\, y + B_{2N}^{(2)}\right) - \left(B_{2N-1}^{(1)}\, y + B_{2N}^{(1)}\right) = 0 \end{cases} \tag{23a}$$

For $2 \le k \le N\text{-}1$:
$$\begin{cases} \left(A_{2N-1}^{(k+1)}\, y + A_{2N}^{(k+1)}\right) - 2\left(A_{2N-1}^{(k)}\, y + A_{2N}^{(k)}\right) + \left(A_{2N-1}^{(k-1)}\, y + A_{2N}^{(k-1)}\right) = 0 \\ \left(B_{2N-1}^{(k+1)}\, y + B_{2N}^{(k+1)}\right) - 2\left(B_{2N-1}^{(k)}\, y + B_{2N}^{(k)}\right) + \left(B_{2N-1}^{(k-1)}\, y + B_{2N}^{(k-1)}\right) = 0 \end{cases} \tag{23b}$$

For $k = N$:
$$\begin{cases} \left(A_{2N-1}^{(N)}\, y + A_{2N}^{(N)}\right) - \left(A_{2N-1}^{(N-1)}\, y + A_{2N}^{(N-1)}\right) = 0 \\ \left(B_{2N-1}^{(N)}\, y + B_{2N}^{(N)}\right) - \left(B_{2N-1}^{(N-1)}\, y + B_{2N}^{(N-1)}\right) = 0 \end{cases} \tag{23c}$$

which gives:

$$A_{2N-1}^{(k)} = A_{2N-1}^{(1)}, \quad A_{2N}^{(k)} = A_{2N}^{(1)}, \quad B_{2N-1}^{(k)} = B_{2N-1}^{(1)}, \quad B_{2N}^{(k)} = B_{2N}^{(1)} \quad \text{for } 2 \le k \le N \tag{24}$$

We therefore end up with 4N unknowns for 4N boundary conditions (12a), (12b), (12c):

$$\left(A_i^{(1)}, \overline{A}_i^{(1)}\right) \quad \text{for } 1 \le i \le 2N\text{-}2, \quad \text{and} \quad \left(A_{2N-1}^{(1)}, A_{2N}^{(1)}, B_{2N-1}^{(1)}, B_{2N}^{(1)}\right)$$

We can rearrange these boundary conditions as follows:

$$\begin{cases} \sigma_y^{(k)}\left(\dfrac{Wi}{2}\right) + \sigma_y^{(k)}\left(-\dfrac{Wi}{2}\right) = -2p_k \\ \tau_{xy}^{(k)}\left(\dfrac{Wi}{2}\right) + \tau_{xy}^{(k)}\left(-\dfrac{Wi}{2}\right) = -2t_k \end{cases} \quad \text{for } 2 \le k \le N \tag{25a}$$

$$\begin{cases} \sigma_y^{(k)}\left(\dfrac{Wi}{2}\right) - \sigma_y^{(k)}\left(-\dfrac{Wi}{2}\right) = 0 \\ \tau_{xy}^{(k)}\left(\dfrac{Wi}{2}\right) - \tau_{xy}^{(k)}\left(-\dfrac{Wi}{2}\right) = 0 \end{cases} \quad \text{for } 2 \le k \le N \tag{25b}$$

$$\sigma_y^{(1)}\left(\frac{Wi}{2}\right) = -p_1, \qquad \tau_{xy}^{(1)}\left(\frac{Wi}{2}\right) = -t_1 \tag{25c}$$

$$u_1(0) = 0, \qquad v_1(0) = 0 \tag{25d}$$

The coefficients $\left(A_{2N}^{(1)}, B_{2N}^{(1)}\right)$ are given by the boundary conditions (25d) and do not appear in the other boundary conditions which contain only derivatives of the displacements. Hence we have (4N-2) unknowns:

$$\left(A_i^{(1)}, \overline{A}_i^{(1)}\right) \quad \text{for } 1 \le i \le 2N\text{-}2, \quad \text{and} \quad \left(A_{2N-1}^{(1)}, B_{2N-1}^{(1)}\right)$$

for (4N-2) boundary conditions (25a), (25b), (25c).

Now from the constitutive equations (3), we have:

$$\begin{cases} \sigma_y^{(k)} = \overline{Q}_{22}^{(k)} \dfrac{\partial v_k}{\partial y} + \overline{Q}_{26}^{(k)} \dfrac{\partial u_k}{\partial y} \\ \tau_{xy}^{(k)} = \overline{Q}_{26}^{(k)} \dfrac{\partial v_k}{\partial y} + \overline{Q}_{66}^{(k)} \dfrac{\partial u_k}{\partial y} \end{cases} \qquad \text{for } 1 \le k \le N \tag{26}$$

Replacing (26) into the boundary conditions (25b) gives:

$$\begin{cases} \overline{Q}_{22}^{(k)} \left(\left. \dfrac{\partial v_k}{\partial y} \right]_{\frac{w_i}{2}} - \left. \dfrac{\partial v_k}{\partial y} \right]_{-\frac{w_i}{2}} \right) + \overline{Q}_{26}^{(k)} \left(\left. \dfrac{\partial u_k}{\partial y} \right]_{\frac{w_i}{2}} - \left. \dfrac{\partial u_k}{\partial y} \right]_{-\frac{w_i}{2}} \right) = 0 \\ \overline{Q}_{26}^{(k)} \left(\left. \dfrac{\partial v_k}{\partial y} \right]_{\frac{w_i}{2}} - \left. \dfrac{\partial v_k}{\partial y} \right]_{-\frac{w_i}{2}} \right) + \overline{Q}_{66}^{(k)} \left(\left. \dfrac{\partial u_k}{\partial y} \right]_{\frac{w_i}{2}} - \left. \dfrac{\partial u_k}{\partial y} \right]_{-\frac{w_i}{2}} \right) = 0 \end{cases} \tag{27}$$

Replacing the solutions (20) for the displacements u_k and v_k into (27) gives:

$$\begin{cases} \overline{Q}_{22}^{(k)}\left(\sum_{i=1}^{2N-2}\sqrt{\rho_i}\,\overline{B}_i^{(k)}\,sinh\left(\sqrt{\rho_i}\,\frac{Wi}{2}\right)\right)+\overline{Q}_{26}^{(k)}\left(\sum_{i=1}^{2N-2}\sqrt{\rho_i}\,\overline{A}_i^{(k)}\,sinh\left(\sqrt{\rho_i}\,\frac{Wi}{2}\right)\right)=0 \\ \overline{Q}_{26}^{(k)}\left(\sum_{i=1}^{2N-2}\sqrt{\rho_i}\,\overline{B}_i^{(k)}\,sinh\left(\sqrt{\rho_i}\,\frac{Wi}{2}\right)\right)+\overline{Q}_{66}^{(k)}\left(\sum_{i=1}^{2N-2}\sqrt{\rho_i}\,\overline{A}_i^{(k)}\,sinh\left(\sqrt{\rho_i}\,\frac{Wi}{2}\right)\right)=0 \end{cases} \quad (28)$$

which are valid for $2 \le k \le N$. Now using the relations (23) we can replace the coefficients $\overline{A}_i^{(k)}$ and $\overline{B}_i^{(k)}$ by their expressions as a functions of the sole coefficients $\overline{A}_i^{(1)}$ into the equations (28). We obtain:

$$\begin{cases} \sum_{i=1}^{2N-2}\left(\overline{Q}_{22}^{(k)}\,FacB_i^{(k)}+\overline{Q}_{26}^{(k)}\,FacA_i^{(k)}\right)\sqrt{\rho_i}\,sinh\left(\sqrt{\rho_i}\,\frac{Wi}{2}\right)\cdot\overline{A}_i^{(1)}=0 \\ \sum_{i=1}^{2N-2}\left(\overline{Q}_{26}^{(k)}\,FacB_i^{(k)}+\overline{Q}_{66}^{(k)}\,FacA_i^{(k)}\right)\sqrt{\rho_i}\,sinh\left(\sqrt{\rho_i}\,\frac{Wi}{2}\right)\cdot\overline{A}_i^{(1)}=0 \end{cases} \quad \text{for } 2 \le k \le N \quad (29)$$

Hence we end up with a system of (2N-2) homogeneous equations for the (2N-2) unknowns $\overline{A}_i^{(1)}$. Therefore these coefficients are identically zero, and we have:

$$\overline{A}_i^{(1)} = 0 \qquad \forall i \quad (30)$$

Using equations (30) and (21) into the equations (20) for the displacements u_k and v_k we obtain the new expressions for the displacements:

$$\begin{cases} u_k = \sum_{i=1}^{2N-2}\left(FacA_i^{(k)}\right)sinh\left(\sqrt{\rho_i}\,y\right)\cdot A_i^{(1)}+A_{2N-1}^{(1)}\cdot y+A_{2N}^{(1)} \\ v_k = \sum_{i=1}^{2N-2}\left(FacB_i^{(k)}\right)sinh\left(\sqrt{\rho_i}\,y\right)\cdot A_i^{(1)}+B_{2N-1}^{(1)}\cdot y+B_{2N}^{(1)} \end{cases} \quad \text{for } 1 \le k \le N \quad (31)$$

We note that there now remains only the 2N unknowns $A_i^{(1)}$ for $1 \le i \le 2N\text{-}2$, and $\left(A_{2N-1}^{(1)}, B_{2N-1}^{(1)}\right)$. The set of 2N equations (25a) and (25c) will allow us to find these remaining unknowns. Replacing (31), (26) and (21) into (25a), we obtain:

$$\begin{cases} \displaystyle\sum_{i=1}^{2N-2} \left(\overline{Q}_{22}^{(k)}\, FacB_i^{(k)} + \overline{Q}_{26}^{(k)}\, FacA_i^{(k)}\right)\sqrt{\rho_i}\, cosh\left(\sqrt{\rho_i}\,\frac{Wi}{2}\right)\cdot A_i^{(1)} \\ \qquad\qquad + \overline{Q}_{22}^{(k)}\cdot B_{2N-1}^{(1)} + \overline{Q}_{26}^{(k)}\cdot A_{2N-1}^{(1)} = -p_k \\ \displaystyle\sum_{i=1}^{2N-2} \left(\overline{Q}_{26}^{(k)}\, FacB_i^{(k)} + \overline{Q}_{66}^{(k)}\, FacA_i^{(k)}\right)\sqrt{\rho_i}\, cosh\left(\sqrt{\rho_i}\,\frac{Wi}{2}\right)\cdot A_i^{(1)} \\ \qquad\qquad + \overline{Q}_{26}^{(k)}\cdot B_{2N-1}^{(1)} + \overline{Q}_{66}^{(k)}\cdot A_{2N-1}^{(1)} = -t_k \end{cases} \quad \text{for } 2 \le k \le N \qquad (32)$$

Now replacing (31), (26) and (21) into (25c), we obtain the coefficients $\left(A_{2N-1}^{(1)}, B_{2N-1}^{(1)}\right)$:

$$\begin{cases} A_{2N-1}^{(1)} = -\displaystyle\sum_{i=1}^{2N-2} \sqrt{\rho_i}\, cosh\left(\sqrt{\rho_i}\,\frac{Wi}{2}\right)\cdot A_i^{(1)} + \frac{p_1\overline{Q}_{26}^{(1)} - t_1\overline{Q}_{22}^{(1)}}{\overline{Q}_{22}^{(1)}\overline{Q}_{66}^{(1)} - \left(\overline{Q}_{26}^{(1)}\right)^2} \\ B_{2N-1}^{(1)} = -\displaystyle\sum_{i=1}^{2N-2} \sqrt{\rho_i}\, FacB_i^{(1)}\, cosh\left(\sqrt{\rho_i}\,\frac{Wi}{2}\right)\cdot A_i^{(1)} - \left(\frac{p_1\overline{Q}_{66}^{(1)} - t_1\overline{Q}_{26}^{(1)}}{\overline{Q}_{22}^{(1)}\overline{Q}_{66}^{(1)} - \left(\overline{Q}_{26}^{(1)}\right)^2}\right) \end{cases} \qquad (33)$$

Replacing (33) into (32) leads to the following system of (2N-2) equations for the (2N-2) unknowns $A_i^{(1)}$ with $1 \le i \le 2N\text{-}2$:

$$\begin{cases} \displaystyle\sum_{i=1}^{2N-2} \left[\overline{Q}_{22}^{(k)}\left(FacB_i^{(k)} - FacB_i^{(1)}\right) + \overline{Q}_{26}^{(k)}\left(FacA_i^{(k)} - 1\right)\right]\sqrt{\rho_i}\, cosh\left(\sqrt{\rho_i}\,\frac{Wi}{2}\right)\cdot A_i^{(1)} \\ \qquad = -p_k + \left(\frac{\overline{Q}_{22}^{(k)}\overline{Q}_{66}^{(1)} - \overline{Q}_{26}^{(k)}\overline{Q}_{26}^{(1)}}{\overline{Q}_{22}^{(1)}\overline{Q}_{66}^{(1)} - \left(\overline{Q}_{26}^{(1)}\right)^2}\right)p_1 + \left(\frac{\overline{Q}_{26}^{(k)}\overline{Q}_{22}^{(1)} - \overline{Q}_{22}^{(k)}\overline{Q}_{26}^{(1)}}{\overline{Q}_{22}^{(1)}\overline{Q}_{66}^{(1)} - \left(\overline{Q}_{26}^{(1)}\right)^2}\right)t_1 \\ \displaystyle\sum_{i=1}^{2N-2} \left[\overline{Q}_{26}^{(k)}\left(FacB_i^{(k)} - FacB_i^{(1)}\right) + \overline{Q}_{66}^{(k)}\left(FacA_i^{(k)} - 1\right)\right]\sqrt{\rho_i}\, cosh\left(\sqrt{\rho_i}\,\frac{Wi}{2}\right)\cdot A_i^{(1)} \\ \qquad = -t_k + \left(\frac{\overline{Q}_{26}^{(k)}\overline{Q}_{66}^{(1)} - \overline{Q}_{66}^{(k)}\overline{Q}_{26}^{(1)}}{\overline{Q}_{22}^{(1)}\overline{Q}_{66}^{(1)} - \left(\overline{Q}_{26}^{(1)}\right)^2}\right)p_1 + \left(\frac{\overline{Q}_{66}^{(k)}\overline{Q}_{22}^{(1)} - \overline{Q}_{26}^{(k)}\overline{Q}_{26}^{(1)}}{\overline{Q}_{22}^{(1)}\overline{Q}_{66}^{(1)} - \left(\overline{Q}_{26}^{(1)}\right)^2}\right)t_1 \end{cases} \qquad (34)$$

valid for $2 \le k \le N$. Now using relations (11), we can rewrite equations (34) under the following form:

$$\begin{cases} \sum_{i=1}^{2N-2} MM_i^{(k)} \cdot A_i^{(1)} = RR^{(k)} \cdot \left(\frac{u_a}{L}\right) \\ \sum_{i=1}^{2N-2} NN_i^{(k)} \cdot A_i^{(1)} = SS^{(k)} \cdot \left(\frac{u_a}{L}\right) \end{cases} \quad \text{for } 2 \le k \le N \tag{35}$$

with

$$MM_i^{(k)} = \left[\overline{Q}_{22}^{(k)}\left(FacB_i^{(k)} - FacB_i^{(1)}\right) + \overline{Q}_{26}^{(k)}\left(FacA_i^{(k)} - 1\right)\right]\sqrt{\rho_i}\, cosh\left(\sqrt{\rho_i}\,\frac{Wi}{2}\right) \tag{36}$$

$$NN_i^{(k)} = \left[\overline{Q}_{26}^{(k)}\left(FacB_i^{(k)} - FacB_i^{(1)}\right) + \overline{Q}_{66}^{(k)}\left(FacA_i^{(k)} - 1\right)\right]\sqrt{\rho_i}\, cosh\left(\sqrt{\rho_i}\,\frac{Wi}{2}\right) \tag{37}$$

$$RR^{(k)} = -\overline{Q}_{12}^{(k)} + \left(\frac{\overline{Q}_{22}^{(k)}\overline{Q}_{66}^{(1)} - \overline{Q}_{26}^{(k)}\overline{Q}_{26}^{(1)}}{\overline{Q}_{22}^{(1)}\overline{Q}_{66}^{(1)} - \left(\overline{Q}_{26}^{(1)}\right)^2}\right)\overline{Q}_{12}^{(1)} + \left(\frac{\overline{Q}_{26}^{(k)}\overline{Q}_{22}^{(1)} - \overline{Q}_{22}^{(k)}\overline{Q}_{26}^{(1)}}{\overline{Q}_{22}^{(1)}\overline{Q}_{66}^{(1)} - \left(\overline{Q}_{26}^{(1)}\right)^2}\right)\overline{Q}_{16}^{(1)} \tag{38}$$

$$SS^{(k)} = -\overline{Q}_{16}^{(k)} + \left(\frac{\overline{Q}_{26}^{(k)}\overline{Q}_{66}^{(1)} - \overline{Q}_{66}^{(k)}\overline{Q}_{26}^{(1)}}{\overline{Q}_{22}^{(1)}\overline{Q}_{66}^{(1)} - \left(\overline{Q}_{26}^{(1)}\right)^2}\right)\overline{Q}_{12}^{(1)} + \left(\frac{\overline{Q}_{66}^{(k)}\overline{Q}_{22}^{(1)} - \overline{Q}_{26}^{(k)}\overline{Q}_{26}^{(1)}}{\overline{Q}_{22}^{(1)}\overline{Q}_{66}^{(1)} - \left(\overline{Q}_{26}^{(1)}\right)^2}\right)\overline{Q}_{16}^{(1)} \tag{39}$$

valid for $2 \le k \le N$.

Solving the system (35) gives us the coefficients $A_i^{(1)}$.

The shear stresses τ_{zx} and τ_{zy} are then obtained by replacing the displacements u_k and v_k as given by (31) into equations (2). We obtain:

$$\begin{cases} \tau_{zx}^{(k)}(y) = \dfrac{G_m}{2e} \displaystyle\sum_{i=1}^{2N-2} A_i^{(1)} \left(FacA_i^{(k)} - FacA_i^{(k+1)} \right) sinh\left(\sqrt{\rho_i}\, y \right) \\ \tau_{zy}^{(k)}(y) = \dfrac{G_m}{2e} \displaystyle\sum_{i=1}^{2N-2} A_i^{(1)} \left(FacB_i^{(k)} - FacA_i^{(k+1)} \right) sinh\left(\sqrt{\rho_i}\, y \right) \end{cases} \quad \text{for } 1 \le k \le N\text{-}1 \qquad (40)$$

From (10), we recall that τ_{zx} and τ_{zy} were zero in the case of a laminate infinitely wide. The interlaminar shear stresses at an interface (k) between plies (k) and (k+1) in a laminate of width Wi submitted to a uniform compression are therefore given by equations (40).

We note that τ_{zx} and τ_{zy} are directly proportional to the amplitude u_a of the applied compressive displacement, since the coefficients $\left\{A_i^{(1)}\right\}$ are (see equations (35)). The stresses depend only upon the following parameters:

- The fiber and matrix elastic constants E_f, E_m, G_m, and ν_{12}.
- Geometrical lengths: the ply thicknesses h_k, the matrix layers thickness e, the specimen width (Wi).
- Angles: the ply angles θ_k.
- The fiber volume fraction V_f.

Indeed, the $\{\overline{Q}_{ij}\}$ are given by (4) and (5) and depend only upon the elastic constants E_f, E_m, G_m, ν_{12}, fiber volume fraction V_f, and the angles $\{\theta_k\}$. The roots $\{\rho_i\}$ are a solution of the determinant (16), hence a sole function of the $\{\overline{Q}_{ij}\}$, of G_m, of $\{h_k\}$, and of e. The coefficients $\left\{FacA_i^{(k)},\ FacB_i^{(k)}\right\}$, defined by (21) and (14), depend only upon the coefficients of equations (14), or equivalently the coefficients of matrix (16). These coefficients are a sole function of the $\{\overline{Q}_{ij}\}$, of G_m, of $\{h_k\}$, of e, and of the roots $\{\rho_i\}$. The coefficients $\left\{A_i^{(1)}\right\}$ are a solution of equations (35), hence a function of the coefficients $\left\{FacA_i^{(k)},\ FacB_i^{(k)}\right\}$, of the roots $\{\rho_i\}$, and of the width (Wi). Ultimately, the interlaminar stresses depend then upon E_f, E_m, G_m, ν_{12}, V_f, $\{\theta_k\}$, $\{h_k\}$, e, and Wi.

At any given interface, the shear stresses are indeed also a function of the laminate layup, and of the total number of plies 2N.

The various coefficients appearing in the above equations can be calculated by using mathematical computer packages (Maple V, Mathematica).

3.2.2 Special case of cross-ply laminates

Laminates that contains only 0° and 90° plies have to be treated separately. Indeed, in that case we have:

$$\overline{Q}_{16}^{(k)} = \overline{Q}_{26}^{(k)} = 0 \qquad \forall k$$

Equations (14a), (14b), (14c), (14d), (14e) and (14f) become then completely decoupled into N equations containing only coefficients $A^{(k)}$ and N equations containing only coefficients $B^{(k)}$.

The N equations containing coefficients $A^{(k)}$ are:

For k = 1:
$$\left[\overline{Q}_{66}^{(1)} r^2 - \frac{G_m}{2eh_1}\right] A^{(1)} + \left[\frac{G_m}{2eh_1}\right] A^{(2)} = 0 \qquad (41a)$$

For $2 \le k \le N-1$:
$$\left[\overline{Q}_{66}^{(k)} r^2 - \frac{G_m}{2eh_k}\right] A^{(k)} + \left[\frac{G_m}{2eh_k}\right] A^{(k+1)} + \left[\frac{G_m}{2eh_k}\right] A^{(k-1)} = 0 \qquad (41b)$$

For k = N:
$$\left[\overline{Q}_{66}^{(N)} r^2 - \frac{G_m}{2eh_N}\right] A^{(N)} + \left[\frac{G_m}{2eh_N}\right] A^{(N-1)} = 0 \qquad (41c)$$

and the N equations containing coefficients $B^{(k)}$ are:

For k = 1:
$$\left[\overline{Q}_{22}^{(1)} r^2 - \frac{G_m}{2eh_1}\right] B^{(1)} + \left[\frac{G_m}{2eh_1}\right] B^{(2)} = 0 \qquad (42a)$$

For $2 \le k \le N-1$:
$$\left[\overline{Q}_{22}^{(k)} r^2 - \frac{G_m}{eh_k}\right] B^{(k)} + \left[\frac{G_m}{2eh_k}\right] B^{(k+1)} + \left[\frac{G_m}{2eh_k}\right] B^{(k-1)} = 0 \qquad (42b)$$

For k = N:
$$\left[\overline{Q}_{22}^{(N)} r^2 - \frac{G_m}{2eh_N}\right] B^{(N)} + \left[\frac{G_m}{2eh_N}\right] B^{(N-1)} = 0 \qquad (42c)$$

After equations (13), we see that the solution to equations (41a), (41b), (41c) will give us the displacements u_k, and the solution to equations (42a), (42b), (42c) will give us the displacements v_k. We note that equations (41a), (41b), (41c) are identical to equations (42a), (42b), (42c) except for the $\overline{Q}_{66}^{(k)}$ which are replaced by the $\overline{Q}_{22}^{(k)}$. We can thus solve these two systems of equations separately. Each of them will have a non-trivial solution if and only if its determinant is zero. This will give us two sets of 2N roots r. Defining ρ as in equation (15), the N roots ρ corresponding to equations (41a), (41b), (41c) are then solutions to the following equation:

$$\begin{vmatrix}
Q_{66}^{(1)}\rho - \frac{G_m}{2eh_1} & \frac{G_m}{2eh_1} & 0 & \cdots & 0 & 0 \\
\frac{G_m}{2eh_2} & Q_{66}^{(2)}\rho - \frac{G_m}{eh_2} & \frac{G_m}{2eh_2} & 0 & \cdots & 0 \\
0 & \ddots & \ddots & \ddots & \ddots & \vdots \\
\vdots & \ddots & \ddots & \ddots & \ddots & 0 \\
0 & \cdots & 0 & \frac{G_m}{2eh_{N-1}} & Q_{66}^{(N)}\rho - \frac{G_m}{eh_{N-1}} & \frac{G_m}{2eh_{N-1}} \\
0 & 0 & \cdots & 0 & \frac{G_m}{2eh_N} & Q_{66}^{(N)}\rho - \frac{G_m}{2eh_N}
\end{vmatrix} = 0 \qquad (43)$$

The N roots ρ corresponding to equations (42a), (42b), (42c) are solutions to the following equation:

$$\begin{vmatrix} Q_{22}^{(1)}\rho - \frac{G_m}{2eh_1} & \frac{G_m}{2eh_1} & 0 & \cdots & 0 & 0 \\ \frac{G_m}{2eh_2} & Q_{22}^{(2)}\rho - \frac{G_m}{eh_2} & \frac{G_m}{2eh_2} & 0 & \cdots & 0 \\ 0 & \ddots & \ddots & \ddots & \ddots & \vdots \\ \vdots & \ddots & \ddots & \ddots & \ddots & 0 \\ 0 & \cdots & 0 & \frac{G_m}{2eh_{N-1}} & Q_{22}^{(N)}\rho - \frac{G_m}{eh_{N-1}} & \frac{G_m}{2eh_{N-1}} \\ 0 & 0 & \cdots & 0 & \frac{G_m}{2eh_N} & Q_{22}^{(N)}\rho - \frac{G_m}{2eh_N} \end{vmatrix} = 0 \qquad (44)$$

As expected, one of the roots of both (43) and (44) will be zero. The remaining 2 sets of (N-1) roots are real and correspond to solutions of the form:

$$\begin{cases} u_k = \sum_{i=1}^{N-1} \left(A_i^{(k)} e^{\sqrt{\rho_i}\, y} + \overline{A}_i^{(k)} e^{-\sqrt{\rho_i}\, y} \right) \\ v_k = \sum_{i=1}^{N-1} \left(B_i^{(k)} e^{\sqrt{\rho_{i+N-1}}\, y} + \overline{B}_i^{(k)} e^{-\sqrt{\rho_{i+N-1}}\, y} \right) \end{cases} \quad \text{for } 1 \le k \le N \qquad (45)$$

where the new coefficients $\overline{A}_i^{(k)}$, $\overline{B}_i^{(k)}$ correspond to the negative roots as discussed previously. We have designated the set $\{\rho_1, \ldots, \rho_{N-1}\}$ as the (N-1) non-zero roots of (43), and the set $\{\rho_N, \ldots, \rho_{2N-2}\}$ as the (N-1) non-zero roots of (44).

Combining zero and non-zero roots the total solution to the problem is therefore:

$$\begin{cases} u_k = \sum_{i=1}^{N-1} \left(A_i^{(k)} e^{\sqrt{\rho_i}\, y} + \overline{A}_i^{(k)} e^{-\sqrt{\rho_i}\, y} \right) + A_N^{(k)}\, y + A_{N+1}^{(k)} \\ v_k = \sum_{i=1}^{N-1} \left(B_i^{(k)} e^{\sqrt{\rho_{i+N-1}}\, y} + \overline{B}_i^{(k)} e^{-\sqrt{\rho_{i+N-1}}\, y} \right) + B_N^{(k)}\, y + B_{N+1}^{(k)} \end{cases} \quad \text{for } 1 \le k \le N \qquad (46)$$

We note that even though each system (41a), (41b), (41c) and (42a), (42b), (42c) has only one zero root, the solution to the actual initial problem must be obtained by solving the complete set of equations (41a), (41b), (41c), (42a), (42b), (42c). The determinant corresponding to this complete set, just like (16), has a double zero root. This double zero root gives us the linear solution for each of the displacement components. In fact, by permutation of the lines and columns in the determinant (16) where all the $\overline{Q}_{26}^{(k)}$ have been set to zero, it is easy to see that this determinant is the product of the two determinants (43) and (44).

As discussed previously, we can rewrite solution (46) as a sum of hyperbolic functions, while keeping the same notation for the coefficients $A_i^{(k)}$, $B_i^{(k)}$, $\overline{A}_i^{(k)}$, $\overline{B}_i^{(k)}$. We have therefore:

$$\begin{cases} u_k = \sum_{i=1}^{N-1} \left(A_i^{(k)} \, sinh\left(\sqrt{\rho_i}\, y\right) + \overline{A}_i^{(k)} \, cosh\left(\sqrt{\rho_i}\, y\right) \right) + A_N^{(k)} \, y + A_{N+1}^{(k)} \\ v_k = \sum_{i=1}^{N-1} \left(B_i^{(k)} \, sinh\left(\sqrt{\rho_{i+N-1}}\, y\right) + \overline{B}_i^{(k)} \, cosh\left(\sqrt{\rho_{i+N-1}}\, y\right) \right) + B_N^{(k)} \, y + B_{N+1}^{(k)} \end{cases} \quad \text{for } 1 \le k \le N \quad (47)$$

For each root ρ_i, $1 \le i \le N-1$, we can express the coefficients $A_i^{(k)}$ (for $2 \le k \le N$) as a function of $A_i^{(1)}$ using any (N-1) equations of the N equations (41a), (41b), (41c). Similarly, for each root ρ_i, $N \le i \le 2N-2$, we can express the coefficients $B_i^{(k)}$ (for $2 \le k \le N$) as a function of $B_i^{(1)}$ using any (N-1) equations of the N equations (42a), (42b), (42c). The relationships between these coefficients are then of the form:

$$\begin{cases} A_i^{(k)} = \left(FacA_i^{(k)} \right) \cdot A_i^{(1)} \\ B_i^{(k)} = \left(FacB_i^{(k)} \right) \cdot B_i^{(1)} \end{cases} \quad \text{for } 2 \le k \le N \text{ and for } 1 \le i \le N-1 \quad (48)$$

which defines the factors $\left(\text{FacA}_i^{(k)},\ \text{FacB}_i^{(k)}\right)$.

Similarly, we can express the coefficients $\overline{A}_i^{(k)}$ and $\overline{B}_i^{(k)}$ (for $2 \le k \le N$) as a function of $\overline{A}_i^{(1)}$ and $\overline{B}_i^{(1)}$ respectively using the same equations as in the case of $A_i^{(k)}$ and $B_i^{(k)}$. These relationships will of course be identical to (48), and are given below:

$$\begin{cases} \overline{A}_i^{(k)} = \left(\text{FacA}_i^{(k)}\right) \cdot \overline{A}_i^{(1)} \\ \overline{B}_i^{(k)} = \left(\text{FacB}_i^{(k)}\right) \cdot \overline{B}_i^{(1)} \end{cases} \quad \text{for} \quad 2 \le k \le N \quad \text{and for} \quad 1 \le i \le N\text{-}1 \tag{49}$$

We now have (8N-4) unknowns:

$$\begin{aligned} & \left(A_i^{(1)},\ \overline{A}_i^{(1)},\ B_i^{(1)},\ \overline{B}_i^{(1)}\right) && \text{for } 1 \le i \le N\text{-}1, \\ \text{and} \quad & \left(A_N^{(k)},\ A_{N+1}^{(k)},\ B_N^{(k)},\ B_{N+1}^{(k)}\right) && \text{for } 1 \le k \le N. \end{aligned}$$

Now substituting u_k and v_k into the partial differential equations (6a), (6b), (7a), (7b), (8a) and (8b), we see that, for the double zero roots, we have:

For k = 1:
$$\begin{cases} \left(A_N^{(2)}\, y + A_{N+1}^{(2)}\right) - \left(A_N^{(1)}\, y + A_{N+1}^{(1)}\right) = 0 \\ \left(B_N^{(2)}\, y + B_{N+1}^{(2)}\right) - \left(B_N^{(1)}\, y + B_{N+1}^{(1)}\right) = 0 \end{cases} \tag{50a}$$

For $2 \le k \le N\text{-}1$:
$$\begin{cases} \left(A_N^{(k+1)}\, y + A_{N+1}^{(k+1)}\right) - 2\left(A_N^{(k)}\, y + A_{N+1}^{(k)}\right) + \left(A_N^{(k-1)}\, y + A_{N+1}^{(k-1)}\right) = 0 \\ \left(B_N^{(k+1)}\, y + B_{N+1}^{(k+1)}\right) - 2\left(B_N^{(k)}\, y + B_{N+1}^{(k)}\right) + \left(B_N^{(k-1)}\, y + B_{N+1}^{(k-1)}\right) = 0 \end{cases} \tag{50b}$$

For k = N:
$$\begin{cases} \left(A_N^{(N)}\, y + A_{N+1}^{(N)}\right) - \left(A_N^{(N-1)}\, y + A_{N+1}^{(N-1)}\right) = 0 \\ \left(B_N^{(N)}\, y + B_{N+1}^{(N)}\right) - \left(B_N^{(N-1)}\, y + B_{N+1}^{(N-1)}\right) = 0 \end{cases} \tag{50c}$$

which gives:

$$A_N^{(k)} = A_N^{(1)}, \quad A_{N+1}^{(k)} = A_{N+1}^{(1)}, \quad B_N^{(k)} = B_N^{(1)}, \quad B_{N+1}^{(k)} = B_{N+1}^{(1)} \qquad \text{for } 2 \le k \le N \quad (51)$$

We therefore end up with (4N) unknowns:

$$\left(A_i^{(1)}, \overline{A}_i^{(1)}, B_i^{(1)}, \overline{B}_i^{(1)}\right) \text{ for } 1 \le i \le N\text{-}1, \quad \text{and} \quad \left(A_N^{(1)}, A_{N+1}^{(1)}, B_N^{(1)}, B_{N+1}^{(1)}\right).$$

for 4N boundary conditions (12a), (12b), (12c). As discussed previously, we can rearrange these boundary conditions as in (25a), (25b), (25c), (25d), and we note that coefficients $\left(A_{N+1}^{(1)}, B_{N+1}^{(1)}\right)$ are given by the boundary conditions (25d) and do not appear in the other boundary conditions which contain only derivatives of the displacements. Hence we have (4N-2) unknowns:

$$\left(A_i^{(1)}, \overline{A}_i^{(1)}, B_i^{(1)}, \overline{B}_i^{(1)}\right) \text{ for } 1 \le i \le N\text{-}1, \quad \text{and} \quad \left(A_N^{(1)}, B_N^{(1)}\right).$$

for (4N-2) boundary conditions (25a), (25b), (25c).

Substituting (26) into the boundary conditions (25b) and using the fact that the $\overline{Q}_{26}^{(k)}$ are zero for any k, we obtain:

$$\begin{cases} \overline{Q}_{22}^{(k)} \left(\dfrac{\partial v_k}{\partial y}\Big]_{\frac{w_i}{2}} - \dfrac{\partial v_k}{\partial y}\Big]_{-\frac{w_i}{2}} \right) = 0 \\ \overline{Q}_{66}^{(k)} \left(\dfrac{\partial u_k}{\partial y}\Big]_{\frac{w_i}{2}} - \dfrac{\partial u_k}{\partial y}\Big]_{-\frac{w_i}{2}} \right) = 0 \end{cases} \qquad (52)$$

Substituting the solutions (47) for the displacements u_k and v_k into (52) gives:

$$\begin{cases} \overline{Q}_{22}^{(k)}\left(\sum_{i=1}^{N-1}\sqrt{\rho_{i+N-1}}\,\overline{B}_i^{(k)}\,sinh\left(\sqrt{\rho_{i+N-1}}\,\frac{Wi}{2}\right)\right)=0 \\ \overline{Q}_{66}^{(k)}\left(\sum_{i=1}^{N-1}\sqrt{\rho_i}\,\overline{A}_i^{(k)}\,sinh\left(\sqrt{\rho_i}\,\frac{Wi}{2}\right)\right)=0 \end{cases} \quad \text{for } 2\le k\le N \qquad (53)$$

Now using the relationships (49) we can substitute into the equations (53) the coefficients $\overline{A}_i^{(k)}$ and $\overline{B}_i^{(k)}$ by their expressions as a function of the coefficients $\overline{A}_i^{(1)}$ and $\overline{B}_i^{(1)}$ respectively. We obtain:

$$\begin{cases} \sum_{i=1}^{N-1}\left(\overline{Q}_{22}^{(k)}\,FacB_i^{(k)}\right)\sqrt{\rho_{i+N-1}}\,sinh\left(\sqrt{\rho_{i+N-1}}\,\frac{Wi}{2}\right)\cdot\overline{B}_i^{(1)}=0 \\ \sum_{i=1}^{N-1}\left(\overline{Q}_{66}^{(k)}\,FacA_i^{(k)}\right)\sqrt{\rho_i}\,sinh\left(\sqrt{\rho_i}\,\frac{Wi}{2}\right)\cdot\overline{A}_i^{(1)}=0 \end{cases} \quad \text{for } 2\le k\le N \qquad (54)$$

Hence, we end up with a system of (N-1) homogeneous equations for the (N-1) unknowns $\overline{A}_i^{(1)}$, and a system of (N-1) homogeneous equations for the (N-1) unknowns $\overline{B}_i^{(1)}$. Therefore these coefficients are identically zero, and we have:

$$\overline{A}_i^{(1)}=\overline{B}_i^{(1)}=0 \qquad \forall i \qquad (55)$$

Using equations (55) and (48) into the equations (47) for the displacements u_k and v_k we obtain the new expressions for the displacements:

$$\begin{cases} u_k=\sum_{i=1}^{N-1}\left(FacA_i^{(k)}\right)sinh\left(\sqrt{\rho_i}\,y\right)\cdot A_i^{(1)}+A_N^{(1)}\cdot y+A_{N+1}^{(1)} \\ v_k=\sum_{i=1}^{N-1}\left(FacB_i^{(k)}\right)sinh\left(\sqrt{\rho_{i+N-1}}\,y\right)\cdot B_i^{(1)}+B_N^{(1)}\cdot y+B_{N+1}^{(1)} \end{cases} \quad \text{for } 1\le k\le N \qquad (56)$$

We note that there now remain only the 2N unknowns $\left(A_i^{(1)}, B_i^{(1)}\right)$ for $1 \le i \le N\text{-}1$, and $\left(A_N^{(1)}, B_N^{(1)}\right)$. The set of 2N equations (25a) and (25c) will allow us to find these remaining unknowns. Replacing (56), (26) and (48) into (25a), and using the fact that the $\overline{Q}_{26}^{(k)}$ are zero for any k, we obtain:

$$\begin{cases} \sum_{i=1}^{N-1} \left(\overline{Q}_{22}^{(k)}\, FacB_i^{(k)}\right) \sqrt{\rho_{i+N-1}}\, cosh\left(\sqrt{\rho_{i+N-1}}\, \frac{Wi}{2}\right) \cdot A_i^{(1)} + \overline{Q}_{22}^{(k)} \cdot B_N^{(1)} = -p_k \\ \sum_{i=1}^{N-1} \left(\overline{Q}_{66}^{(k)}\, FacA_i^{(k)}\right) \sqrt{\rho_i}\, cosh\left(\sqrt{\rho_i}\, \frac{Wi}{2}\right) \cdot A_i^{(1)} + \overline{Q}_{66}^{(k)} \cdot A_N^{(1)} = -t_k \end{cases} \quad \text{for } 2 \le k \le N \quad (57)$$

Now substituting (56), (26) and (48) into (25c), and using again the fact that the $\overline{Q}_{26}^{(k)}$ are zero for any k, we obtain the coefficients $\left(A_N^{(1)}, B_N^{(1)}\right)$:

$$\begin{cases} A_N^{(1)} = -\sum_{i=1}^{N-1} \sqrt{\rho_i}\, cosh\left(\sqrt{\rho_i}\, \frac{Wi}{2}\right) \cdot A_i^{(1)} - \frac{t_1}{\overline{Q}_{66}^{(1)}} \\ B_N^{(1)} = -\sum_{i=1}^{N-1} \sqrt{\rho_{i+N-1}}\, cosh\left(\sqrt{\rho_{i+N-1}}\, \frac{Wi}{2}\right) \cdot B_i^{(1)} - \frac{p_1}{\overline{Q}_{22}^{(1)}} \end{cases} \quad (58)$$

Substituting (58) into (57) leads to the following system of (2N-2) equations for the (2N-2) unknowns $\left(A_i^{(1)}, B_i^{(1)}\right)$ with $1 \le i \le N\text{-}1$:

$$\begin{cases} \sum_{i=1}^{N-1} \overline{Q}_{22}^{(k)} \left(FacB_i^{(k)} - 1\right) \sqrt{\rho_{i+N-1}}\, cosh\left(\sqrt{\rho_{i+N-1}}\, \frac{Wi}{2}\right) \cdot B_i^{(1)} = -p_k + \left(\frac{\overline{Q}_{22}^{(k)}}{\overline{Q}_{22}^{(1)}}\right) p_1 \\ \sum_{i=1}^{N-1} \overline{Q}_{66}^{(k)} \left(FacA_i^{(k)} - 1\right) \sqrt{\rho_i}\, cosh\left(\sqrt{\rho_i}\, \frac{Wi}{2}\right) \cdot A_i^{(1)} = -t_k + \left(\frac{\overline{Q}_{66}^{(k)}}{\overline{Q}_{66}^{(1)}}\right) t_1 \end{cases} \quad (59)$$

valid for $2 \le k \le N$. Now using relations (11) and the fact that the $\overline{Q}_{16}^{(k)}$ are zero for any k, we can rewrite equations (59) in the following form:

$$\begin{cases} \sum_{i=1}^{N-1} MM_i^{(k)} \cdot B_i^{(1)} = RR^{(k)} \cdot \left(\frac{u_a}{L}\right) \\ \sum_{i=1}^{N-1} NN_i^{(k)} \cdot A_i^{(1)} = 0 \end{cases} \qquad \text{for } 2 \le k \le N \qquad (60)$$

with

$$MM_i^{(k)} = \overline{Q}_{22}^{(k)} \left(FacB_i^{(k)} - 1\right)\sqrt{\rho_{i+N-1}}\ cosh\left(\sqrt{\rho_{i+N-1}}\,\frac{Wi}{2}\right) \qquad (61)$$

$$NN_i^{(k)} = \overline{Q}_{66}^{(k)} \left(FacA_i^{(k)} - 1\right)\sqrt{\rho_i}\ cosh\left(\sqrt{\rho_i}\,\frac{Wi}{2}\right) \qquad (62)$$

$$RR^{(k)} = \frac{\overline{Q}_{22}^{(k)}\overline{Q}_{12}^{(1)} - \overline{Q}_{12}^{(k)}\overline{Q}_{22}^{(1)}}{\overline{Q}_{22}^{(1)}} \qquad (63)$$

valid for $2 \le k \le N$.

We see from the second set of equations (60) that all coefficients $A_i^{(1)}$ are zero. Solving the first set of equations (60) gives us the coefficients $B_i^{(1)}$.

The shear stresses τ_{zx} and τ_{zy} are then obtained by substituting the displacements u_k and v_k as given by (56) into equations (2). We obtain:

$$\begin{cases} \tau_{zx}^{(k)}(y) \equiv 0 \\ \tau_{zy}^{(k)}(y) = \frac{G_m}{2e} \sum_{i=1}^{N-1} B_i^{(1)} \left(FacB_i^{(k)} - FacB_i^{(k+1)}\right) sinh\left(\sqrt{\rho_{i+N-1}}\ y\right) \end{cases} \qquad \text{for } 1 \le k \le N\text{-}1 \qquad (64)$$

From (10), we recall that τ_{zx} and τ_{zy} were zero in the case of a laminate infinitely wide. The interlaminar shear stresses at an interface (k) between plies (k) and (k+1) in a

laminate of width Wi submitted to a uniform compression are therefore given by equations (64). We immediately notice that for a cross-ply laminate, the interlaminar shear stresses τ_{zx} are identically zero.

The shear stresses τ_{zx} and τ_{zy} along the width of a specimen can now be calculated at any interface by the method outlined above. The numerical procedure used to obtain these will be detailed in Chapter 6, when we treat the case of the $[\theta/-\theta/0_2/\theta/-\theta/0]_s$ laminate.

The second part of our theoretical work consists of incorporating the action of the adjacent angled-plies (by means of interlaminar shear stresses) on the 0° plies to come up with a general microbuckling equation for the 0° fibers. The next section is devoted to the derivation of this equation.

3.3 Microbuckling of 0° fibers

To derive an equation governing the microbuckling of the 0° fiber in a multidirectional laminate, we start from the general buckling equation for a beam on foundation. This equation was mentioned at the beginning of the literature review. The fiber is submitted to a buckling load P. The medium surrounding the fiber may act on it in three possible ways: through a distributed couple m, through a distributed axial force p in the fiber direction, and through a distributed transverse force q normal to the fiber. For convenience, we reproduce below (Figure 9) Figure 3 showing a fiber element and the various efforts acting on it. Q and M are respectively the shear force and moment acting at the fiber element sections. The fiber is initially along the x axis.

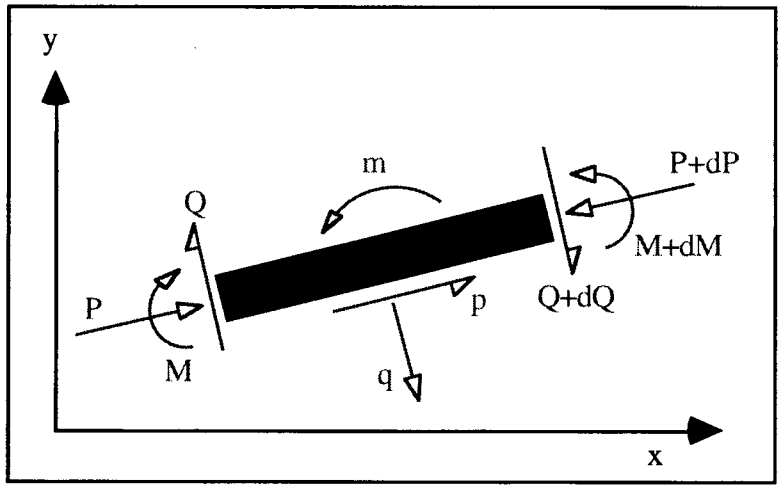

Figure 9. Fiber equilibrium

Both the fiber and the foundation are modeled as linear elastic isotropic materials. Assuming small deflections, the equilibrium equations for the fiber portion are:

$$\begin{cases} \text{Force equilibrium along y:} & q + \dfrac{dQ}{dx} + P\dfrac{d\omega}{dx} = 0 \\ \text{Force equilibrium along x:} & p - \dfrac{dP}{dx} + Q\dfrac{d\omega}{dx} = 0 \\ \text{Moment equilibrium:} & \dfrac{dM}{dx} - Q + m = 0 \end{cases} \tag{65}$$

where v is the amplitude of the fiber movement in the y direction, and ω is the slope of the deflected fiber axis defined by:

$$\omega = \frac{dv}{dx} \tag{66}$$

Differentiating the third equation (65) with respect to x and replacing it in the first equation to eliminate the shear, Q, we obtain:

$$\frac{d^2M}{dx^2} + q + \frac{dm}{dx} + P\frac{d^2v}{dx^2} = 0 \qquad (67)$$

It will be assumed throughout this work that the fiber has, prior to loading, the shape of a sine function $v_0(x)$ of amplitude V_0. Now if the effect of shearing deformation is neglected, the expression for the curvature of the axis of the beam is:

$$E_f I \frac{d^2(v - v_0)}{dx^2} = M \qquad (68)$$

where E_f is the fiber Young's modulus, and I the moment of inertia of the fiber. The carbon fibers are considered as circular and of constant radius r_f, in which case we have for the fiber area A_f and its moment of inertia I:

$$A_f = \pi r_f^2 \qquad \text{and} \qquad I = \pi \frac{r_f^4}{4} \qquad (69)$$

Substituting equation (68) into equation (67), we obtain:

$$E_f I \frac{d^4(v - v_0)}{dx^4} + q + \frac{dm}{dx} + P\frac{d^2v}{dx^2} = 0 \qquad (70)$$

The next step consists now in assessing the quantities m and q. For composites with a high volume fraction of fibers V_f (above 0.3), it is more energetically favorable for the fibers to deform in the shear mode rather than in the extension mode [23,46]. In the so-called extension mode the fibers deform out-of-phase, while they deform in-phase in the shear mode. Figure 10 illustrates these modes.

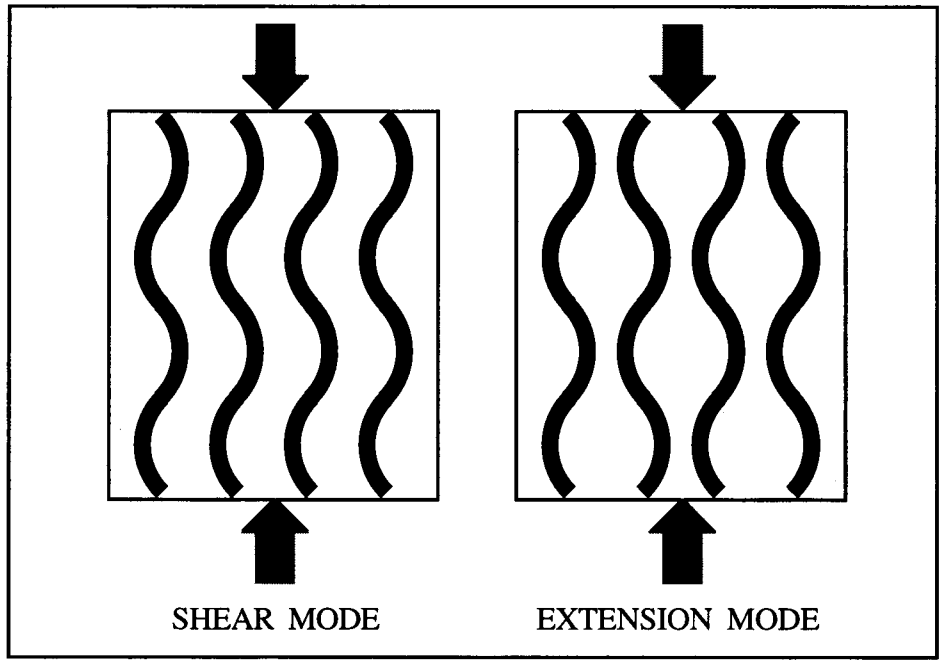

Figure 10. Fiber microbuckling: shear mode and extension mode

High performance composites have a fiber volume fraction well above 30%, typically around 55% - 70%. Hence we can assume that microbuckling of carbon fibers will always occur in the shear mode, as observed experimentally [8]. In this case, the rotation of the fibers that occurs when their amplitude increases is resisted by deformation of the surrounding matrix in shear. This resistance, therefore, may be adequately modeled as a distributed couple. We therefore seek to express the distributed couple m as a function of the fiber rotation and the matrix mechanical properties. The tensor representing the action of the matrix between the fibers is:

$$\overline{\overline{T}} = \begin{pmatrix} 0 & \tau_{xy} & 0 \\ \tau_{xy} & 0 & 0 \\ 0 & 0 & 0 \end{pmatrix} \tag{71}$$

The effort due to $\overline{\overline{T}}$ on the fiber surface is therefore the vector parallel to the fiber surface:

$$\overline{\overline{T}} \cdot \vec{n} = \begin{pmatrix} 0 & \tau_{xy} & 0 \\ \tau_{xy} & 0 & 0 \\ 0 & 0 & 0 \end{pmatrix} \cdot \begin{pmatrix} 0 \\ -sin\varphi \\ cos\varphi \end{pmatrix} = \begin{pmatrix} -\tau_{xy}\, sin\varphi \\ 0 \\ 0 \end{pmatrix} \tag{72}$$

where $\vec{n}$ is the normal to the fiber surface, as illustrated on Figure 11. A circle with a dot

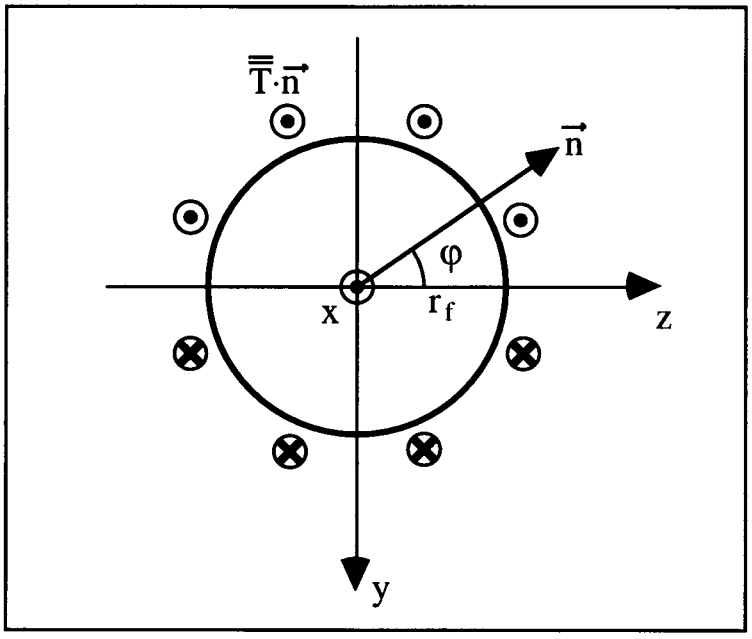

Figure 11. Tensor representing the action of the distributed couple m

indicates a vector out of the page, a circle with a cross indicates a vector into the page. The moment m about the z axis due to $\overline{\overline{T}}$ on the fiber is therefore:

$$m = -2 \int_0^{\pi} \left\| \overline{\overline{T}} \cdot \vec{n} \right\| (r_f\, sin\varphi) \cdot r_f\, d\varphi \tag{73}$$

Replacing (72) into (73) and integrating, we obtain [14]:

$$m = -(\pi\, r_f^2)\, \tau_{xy} = -A_f\, \tau_{xy} \tag{74}$$

Now the shear stress τ_{xy} is the shear strain γ_{xy} times the composite shear modulus G. Using G instead of the matrix shear modulus G_m allows us to incorporate the influence of the neighboring fibers. The shear strain γ_{xy} is the derivative of the amplitude v with respect to x. We thus finally obtain from (74):

$$m = -A_f G \frac{d(v - v_0)}{dx} = -A_f \frac{G_m}{1 - V_f} \frac{d(v - v_0)}{dx} \tag{75}$$

Replacing (75) into (70) gives us the microbuckling equation:

$$E_f I \frac{d^4(v - v_0)}{dx^4} + q - A_f \frac{G_m}{1 - V_f} \frac{d^2(v - v_0)}{dx^2} + P \frac{d^2 v}{dx^2} = 0 \tag{76}$$

We recall that the distributed force q represents the effect normal to the fiber.

We now go back to the study of interlaminar stresses completed in the previous section. Interlaminar shear stresses τ_{zy} will develop at the interface between a 0° ply and an adjacent angled-ply, in the interlaminar matrix region of thickness 2e. They will tend to push the fiber along the y direction. Figure 12 illustrates the case where τ_{zy} pushes toward y increasing.

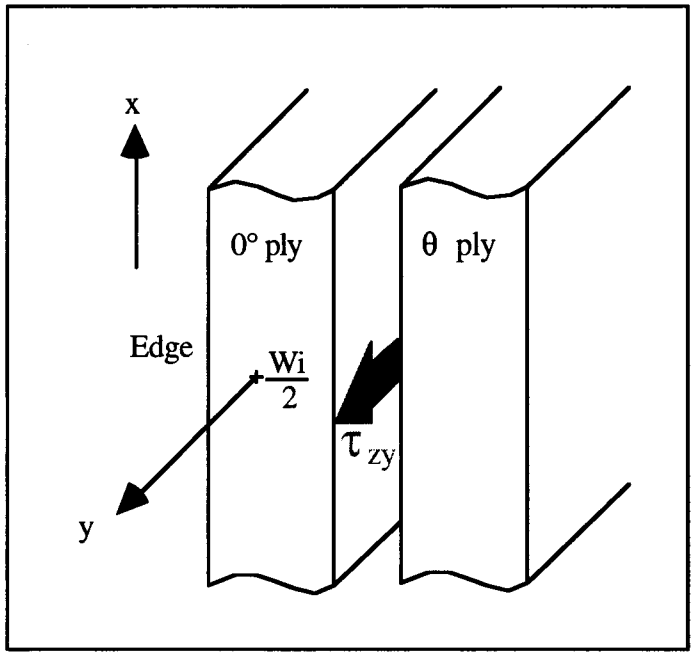

Figure 12. Interlaminar shear stress τ_{zy}

The interlaminar stress theory developed in the previous section calculates the average of displacements u and v in a given ply over the thickness of that ply. Therefore the actual shear stress distribution through the thickness of a ply is not known. It would however be unreasonable to expect to solve the actual stress distribution owing to the circular geometry of the fibers, and the fact that the spatial distribution of fibers in a 0° ply is not uniform. We will consider that 0° fibers at the ply interface experience the distributed force $\{\tau_{zy}(2r_f)\}$. Let us now consider a 0° fiber located at the edge of the ply as shown on Figure 13. Because τ_{zy} varies with y, the half of the fibers closest to the edge will be exposed to a distributed force different from the one experienced by the half of the fiber further away from the edge.

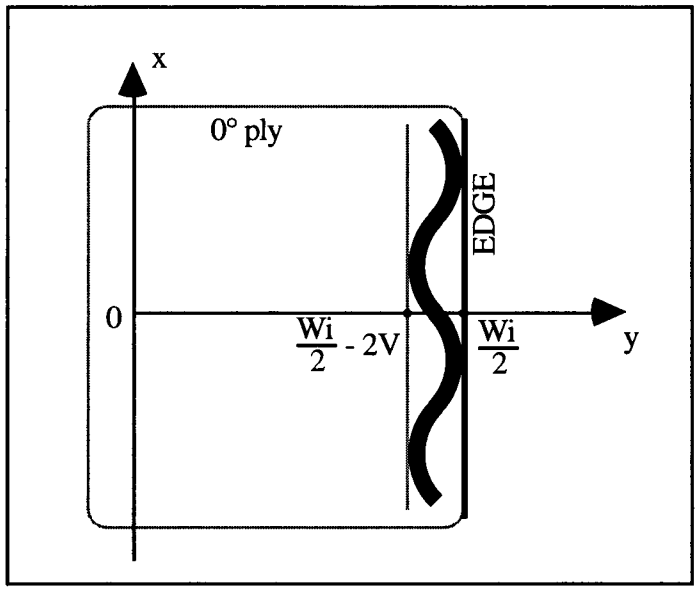

Figure 13. Edge fiber in a 0° ply

If the fiber waviness amplitude V is small enough, it is reasonable to assume that over the distance 2V the shear stress τ_{zy} will not change sign. The normal force q on the fiber therefore has a magnitude:

$$2r_f\left\{\tau_{zy}\left(y=\frac{Wi}{2}\right)-\tau_{zy}\left(y=\frac{Wi}{2}-2v\right)\right\}\approx 2r_f\left\{\left[\frac{d\tau_{zy}}{dy}\right]_{\frac{Wi}{2}}\right\}\cdot 2v \qquad (77)$$

The load P on one fiber is related to the stress $\sigma_{0°ply}$ on a 0° ply by:

$$P = A_f\left|\sigma_{0°fiber}\right| = \frac{A_f}{V_f}\left|\sigma_{0°ply}\right| \qquad (78)$$

Substituting (77) and (78) into (76) and recognizing that q will help the buckling process when the derivative of τ_{zy} is positive, we obtain a microbuckling equation for a 0° fiber located in a given 0° ply that takes into account the action from the angled-plies surrounding this 0° ply:

$$E_f I \frac{d^4(v-v_0)}{dx^4} - 2(2r_f)\left[\frac{d\tau_{zy}}{dy}\right]_{\frac{wi}{2}} v - A_f \frac{G_m}{1-V_f}\frac{d^2(v-v_0)}{dx^2} + \frac{A_f}{V_f}\left|\sigma_{0°ply}\right|\frac{d^2v}{dx^2} = 0 \qquad (79)$$

As a first approximation, we may consider that the shear stress τ_{zx} has no significant effect on the microbuckling of 0° fibers. Indeed, this stress is uniformly distributed on the fiber but in the loading direction, so its effect cancels out globally.

The solution to the homogeneous differential equation (79) is of the form:

$$v(x) = V \sin\left(\pi \frac{x}{\lambda}\right) \qquad (80)$$

with $$v_0(x) = V_0 \sin\left(\pi \frac{x}{\lambda}\right) \qquad \text{as previously assumed.} \qquad (81)$$

The length λ is the half-wavelength.

Replacing (80) and (81) into (79) gives us a non-linear relationship between the stress on a 0° ply and the amplitude V of buckling of a 0° fiber:

$$V = \frac{V_0}{1 - \dfrac{\dfrac{A_f}{V_f}\left|\sigma_{0°ply}\right| + 2(2r_f)\left[\dfrac{d\tau_{zy}}{dy}\right]_{\frac{wi}{2}}\left(\dfrac{\lambda}{\pi}\right)^2}{E_f I\left(\dfrac{\pi}{\lambda}\right)^2 + A_f \dfrac{G_m}{1-V_f}}} \qquad (82)$$

Equation (82) shows that the interlaminar shear stress τ_{zy} has the same effect as an increase in the applied stress $\sigma_{0°ply}$, thus resulting in a smaller denominator and consequently a larger microbuckling amplitude V. We note that the assumption that fibers have an initial waviness results in a continuous variation of the amplitude with the applied

stress rather than a bifurcation instability criterion. This assumption is physically justified since 0° fibers in a ply are never perfectly aligned with the loading direction. Angles measured in unidirectional plies before loading are typically in the range 2°-3° for various carbon fiber reinforced plastics [22].

In virtually all previous studies on microbuckling (Chapter 2) the buckling load was found as being the load at which $\lambda = \lambda_{critical}$, where $\lambda_{critical}$ is the wavelength that minimizes the buckling load. This approach however does not take into account the value of the initial wavelength λ_0 of the fiber, which nevertheless reflects the fiber and matrix properties. We thus propose a more physical approach by considering that the fiber buckling wavelength will be equal to λ_0. This is a reasonable assumption since a typical failure strain of less than 1% will result in an equivalent change in λ_0. The initial wavelength λ_0 will be measured before testing by microscopic observation of the specimens. The initial amplitude V_0 is related to λ_0 by the following equation:

$$max\left(\frac{dv_0}{dx}\right) = V_0\left(\frac{\pi}{\lambda_0}\right) = tan(\phi) \quad \Rightarrow \quad V_0 = \left(\frac{\lambda_0}{\pi}\right)\cdot tan(\phi) \tag{83}$$

where ϕ is the initial fiber misalignment angle.

The stress in a 0° ply is identical for all the 0° plies in the laminate and is related to the applied displacement u_a by the CLT theory as ((3) and (5)):

$$\sigma_{0°ply} = Q_{11}\left(\frac{u_a}{L}\right) \quad \text{with} \quad u_a < 0 \tag{84}$$

Eventually the 0° fiber buckling amplitude V in a given 0° ply in a laminate is therefore a function of the applied displacement through $\sigma_{0°ply}$ and τ_{zy}. τ_{zy} is a linear

function of u_a since after (40) they are a linear function of the coefficients $A_i^{(1)}$ and $B_i^{(1)}$ (equations (40) and (64) respectively) which themselves are solutions of linear systems with left-hand side proportional to u_a (equations (35) and (60) respectively). The amplitude V depends also upon the initial angles of all the angled-plies in the composite, and especially upon the angles of the two plies adjacent to the considered 0° ply. Indeed the amplitude V of a 0° fiber should be maximum at one of the two interfaces of the 0° ply where the slope of τ_{zy} is maximum . Finally it depends, through τ_{zy}, upon the general layup of the laminate.

Now because the fibers that buckle first are located at the edge of the specimen, the support provided to these fibers by the surrounding matrix will be less than in the case of interior fibers. Theoretical investigations of the influence of free surfaces upon buckling fibers show that the critical shortening for a fiber located close to the free surface (on the order of a few fiber diameters) is about 40% below the critical shortening for a fiber located away from the free surface [46]. Hence we choose to reduce the support provided by the matrix by 40%, which means multiplying the couple-stress term $\left\{A_f \cdot G_m/(1-V_f)\right\}$ by (0.6). The equation giving the microbuckling amplitude for an edge fiber is therefore, from equation (82):

$$V(u_a,\theta_k)=\frac{V_0}{1-\dfrac{\dfrac{A_f}{V_f}\left|\sigma_{0°ply}(u_a)\right|+2(2r_f)\cdot\left[\dfrac{d\tau_{zy}(u_a,\theta_k)}{dy}\right]_{\frac{w_i}{2}}\left(\dfrac{\lambda_0}{\pi}\right)^2}{E_f I\left(\dfrac{\pi}{\lambda_0}\right)^2+(0.6)\,A_f\dfrac{G_m}{1-V_f}}} \qquad (85)$$

where the index (k) refers to the ply number.

One possible objection to the above model is the fact that from equilibrium considerations, the interlaminar shear stress τ_{zy} is zero at the free-edge, and reaches a maximum very close to it (see for instance [80]). The present approximate theory puts this maximum exactly at the free edge. It is however reasonable to consider that these surface fibers have only a negligible effect upon the general buckling of the fibers that are located behind them and that they are under the influence of the wider interlaminar stress field given by equations (40) and (64). This validates our approach.

This concludes the derivation of our general microbuckling equation. In order to predict the failure of the laminate, it remains to formulate a fiber failure criterion. Actually, the present theory will be shown to allow us to investigate the propensity for laminate failure by delamination.

3.4 Failure criteria

3.4.1 Fiber failure

As mentioned in Chapter 2, experiments on multidirectional laminates indicate that in-plane kinking of 0° fibers is the initial failure mode and it leads to catastrophic failure of the whole laminate immediately or very shortly afterwards. A relevant laminate failure criterion that hinges on this observation is fiber failure in bending. Failure will occur when the tensile strain in the fiber ε_f reaches the fiber failure strain in tension ε_{tf}. The maximum tensile strain in the fiber occurs at the fiber surface and is the sum of a compressive component and a bending component. We have:

$$\varepsilon_f = -\frac{|\sigma_{0^\circ \text{fiber}}|}{E_f} + r_f \left(\frac{d^2V}{dx^2}\right) \tag{86}$$

Replacing equations (78) and (80) into (86), we obtain the criterion for fiber failure:

$$\varepsilon_f = -\frac{|\sigma_{0^\circ \text{ply}}|}{V_f E_f} + r_f \left(\frac{\pi}{\lambda_0}\right)^2 (V) = \varepsilon_{tf} \tag{87}$$

where $V(u_a,\theta_k)$ is given by (85). Equation (87) will yield a value for the critical applied displacement u_a. Dividing u_a by L will then give us the failure strain $\varepsilon_{failure}$.

3.4.2 Matrix failure (interlaminar failure)

Failure of the matrix may occur in two modes: the first one is interlaminar failure due to the interlaminar stresses. We choose a quadratic failure criterion:

$$\sqrt{(\tau_{zy})^2 + (\tau_{zx})^2} = \tau_f \tag{88}$$

where τ_f is the shear failure stress of the matrix. Since τ_{zx} and τ_{zy} depend upon the applied displacement u_a (see equations (35), (40), (60), (64)), equation (88) will yield a value for the critical applied displacement u_a. Dividing u_a by L will then give us the failure strain, $\varepsilon_{failure}$.

It must be kept in mind that this failure criterion is not conservative because it does not include the interlaminar normal stress σ_z which could play a role if the layup sequence is such that $\sigma_z > 0$: σ_z would then tend to peel off 0° plies from their neighboring plies.

3.4.3 Matrix failure (in-ply failure)

The second matrix failure mode is failure within a 0° ply due to shear stresses that develop in-between 0° fibers as a result of their in-phase buckling. The acting stress is then τ_{xy}, which is given by the relation:

$$max\{\tau_{xy}\} = G_m \cdot max\{\gamma_{xy}\} = G_m \cdot max\left\{\left[\frac{d(v - v_0)}{dx}\right]\right\} \tag{89}$$

Using equations (89) and (80), the failure criterion will then be:

$$G_m\left(\frac{\pi}{\lambda_0}\right)(V - V_0) = \tau_f \tag{90}$$

where $V(u_a,\theta_k)$ is given by (85). Equation (90) will yield a value for the critical applied displacement u_a. Dividing u_a by L will then give us the failure strain, $\varepsilon_{failure}$. We are now able to investigate analytically the failure in compression of a given laminate. In Chapter 6 we will apply the above theory to the case of the laminate $[\theta/-\theta/0_2/\theta/-\theta/0]_s$, then compare theoretical predictions with the results from compressive tests conducted on this laminate, for various values of the angle θ. These tests will now be covered in Chapter 4.

(4) EXPERIMENTS

4.1 Overview

For the same fiber and matrix, the interlaminar shear stresses depend upon various factors such as the ply angles, thicknesses, and layup. We chose to test our theory with a laminate whose only variable would be the angle of the off-axis plies. Varying the ply sequence would have resulted in highly discontinuous data not easily comparable owing to possible confounding variables (for example the position of the 0° plies with respect to the free surfaces). Varying the ply thicknesses (by stacking two or more plies together at each angle) would have resulted in different structure-deformation couplings and consequently would have affected the test results in a different manner. The easiest option to implement and test, and the one with the most wide-ranging and practical potential, was to vary the angles of the off-axis plies. For simplicity, all the off-axis plies had the same angle θ. The laminate $[\theta/-\theta/0_2/\theta/-\theta/0]_s$ was finally chosen to test the theory developed in Chapter 3 because its layup was identical (with two less $(\theta/-\theta/0_2)$ groups) to the one used in [18], which is to our knowledge the only systematic experimental study of the off-axis plies angle influence on the compressive failure strain. This would, therefore, give us an additional experimental reference point with which to compare qualitatively our own theoretical predictions and tests results. In order to have a set of data as complete as possible, the angle θ was varied from 10° to 90° in 10° intervals. The choice of a composite with 14 plies was a compromise between a specimen thick enough to prevent Euler buckling (see below) and with a number of plies as low as possible to minimize the computation time for theoretical predictions.

An additional series of tests was performed with a single 0° ply sandwiched between a transparent plastic. These tests were intended to observe the kinking process in a 0° ply as well as to provide extra insight into the propensity for out-of-plane buckling in specimens with a high angle θ. We will elaborate on these tests later in this chapter.

4.2 $[\theta/-\theta/0_2/\theta/-\theta/0]_s$ laminate

4.2.1 Specimens manufacturing

Composite plates were manufactured from a roll of AS4 fibers pre-impregnated with a thermoplastic (polyphenylene sulfide PPS). Plies were cut from the roll with a razor blade at the desired orientation. The plies (dimensions: 80mm x 100 mm) were then stacked in the sequence: $[\theta/-\theta/0_2/\theta/-\theta/0]_s$ with the angle θ varying from 10° to 90° in 10° intervals. The stacking sequence was the same for all the plates, only the value of the angle θ varied from one plate to another. The fourteen plies were then placed in a specially designed aluminum mold as shown on Figure 14. The mold was made of two plates, a male part and a female part. The purpose of the mold was to prevent flowing of the matrix to the sides during the high temperature phase of the processing. In order to allow for a limited amount of flowing and to accommodate the different coefficients of thermal expansion of the composite and the aluminum, a gap of 1 mm was left between each edge of the plate and the inside walls of the mold. The mold was placed between two aluminum plates containing internal heaters. The plates in turn were put between the platens of a press. A composite plate (dimensions: 82 mm x 100 mm) was then manufactured using the following process:

- Heating of the aluminum plates up to 320°C in 15 minutes with no pressure applied.
- Pressure applied (0.85 MPa) at 320°C for 15 minutes.
- Cooling of the aluminum plates down to room temperature under pressure.

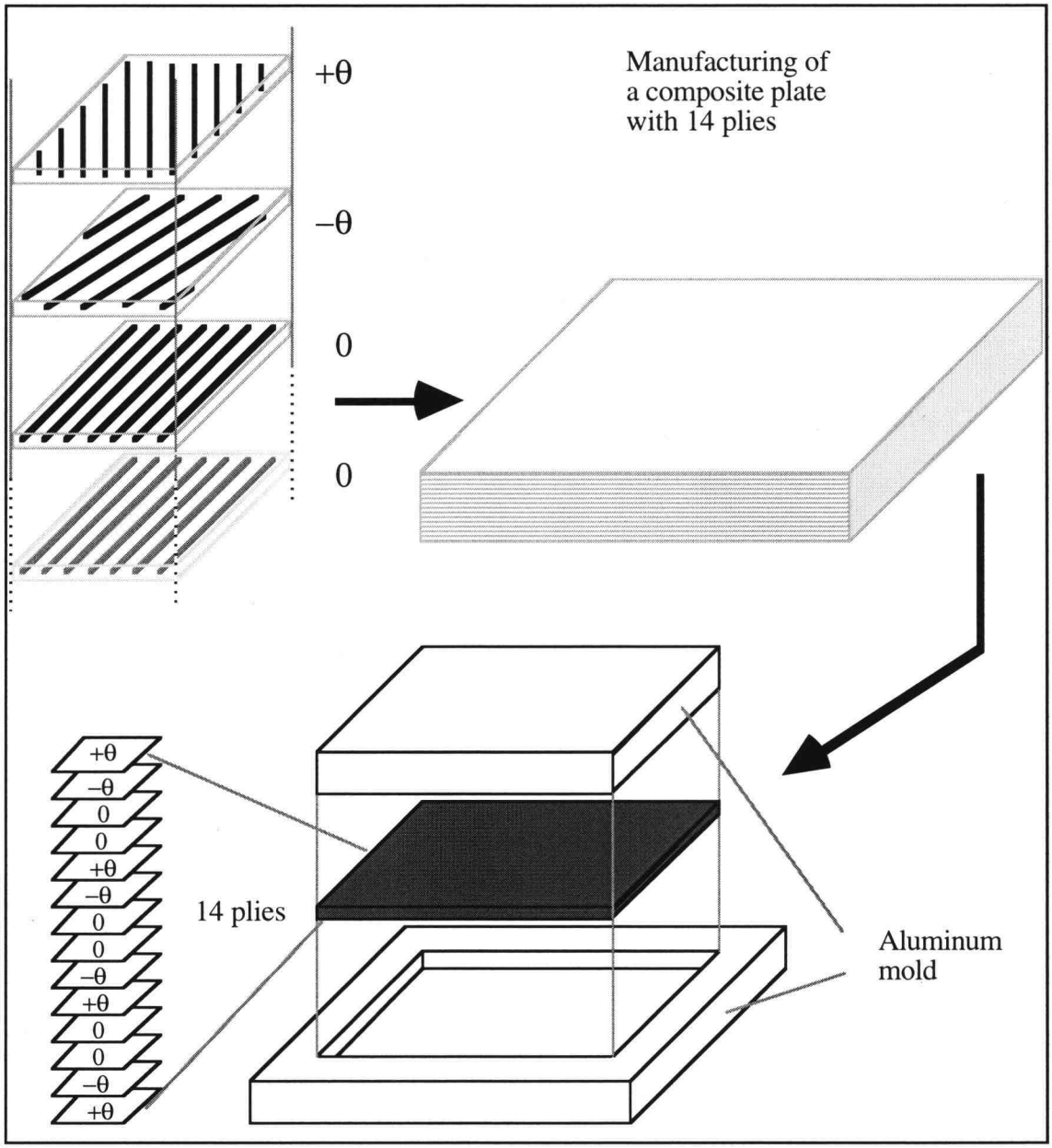

Figure 14. Ply stacking sequence in $[\theta/-\theta/0_2/\theta/-\theta/0]_s$ and plate manufacturing

Five specimens were then cut out of the center of the composite plate using a diamond-coated wheel. The specimen dimensions were the following:

Length: L = 80 mm Width: Wi = 12.7 mm Thickness: t = 1.7 mm

The fiber volume fraction V_f of the composite was 60%. Testing methodology is summarized in Figure 15.

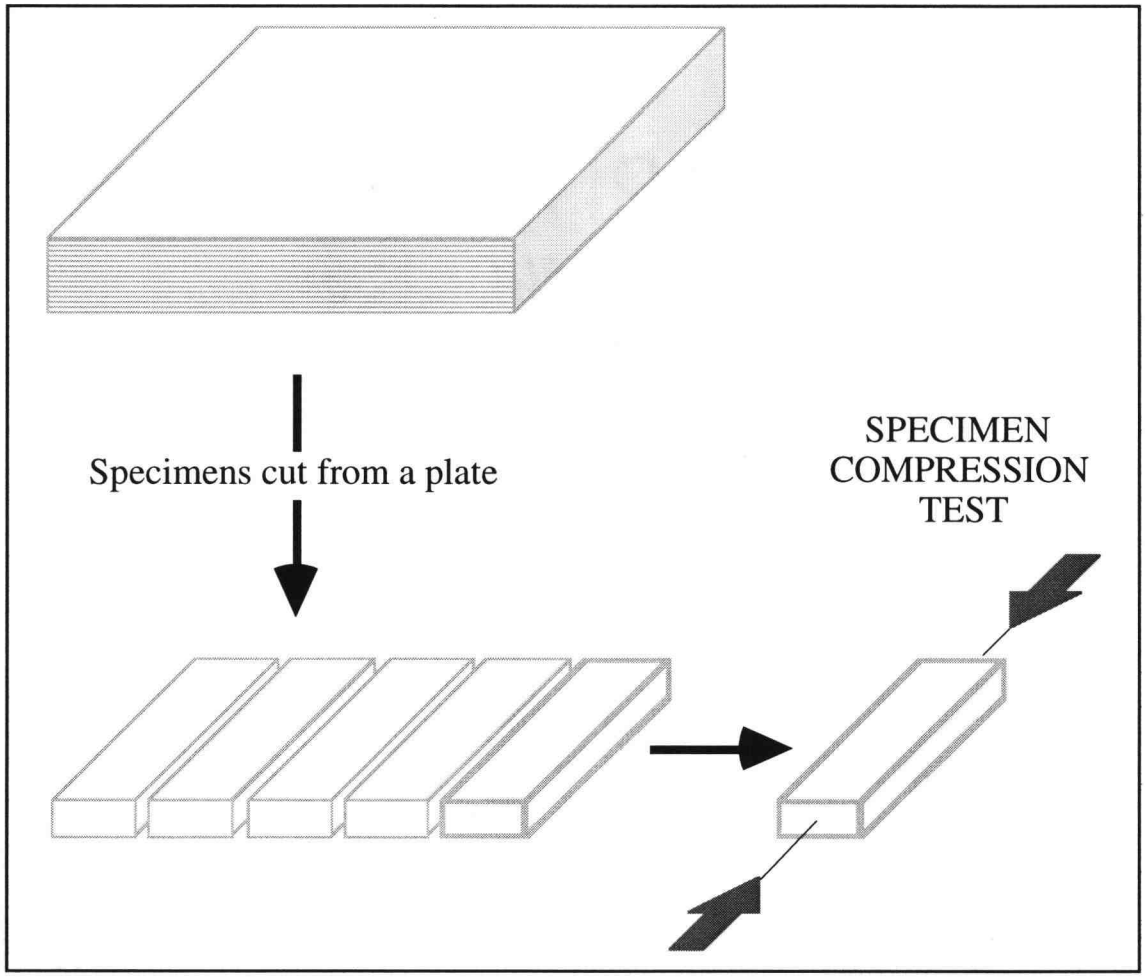

Figure 15. Testing methodology

4.2.2 Compression testing

Compression tests of composite materials are intrinsically more difficult to implement than tension tests. Compressive strength has been shown to be sensitive to the loading mechanism [99]. In addition, gross Euler buckling and crushing of the ends of the specimen must be avoided during loading. For these reasons, tabs must be glued at the top and bottom on each side of the specimen. They leave a central section of the specimen free, and failure should occur in this central region. Due to the large number of specimens prepared for testing (6 specimens for each of the 9 angles = 54 specimens) we chose to use two pairs of jigs to clamp the top and bottom of the specimen. Figure 16 is

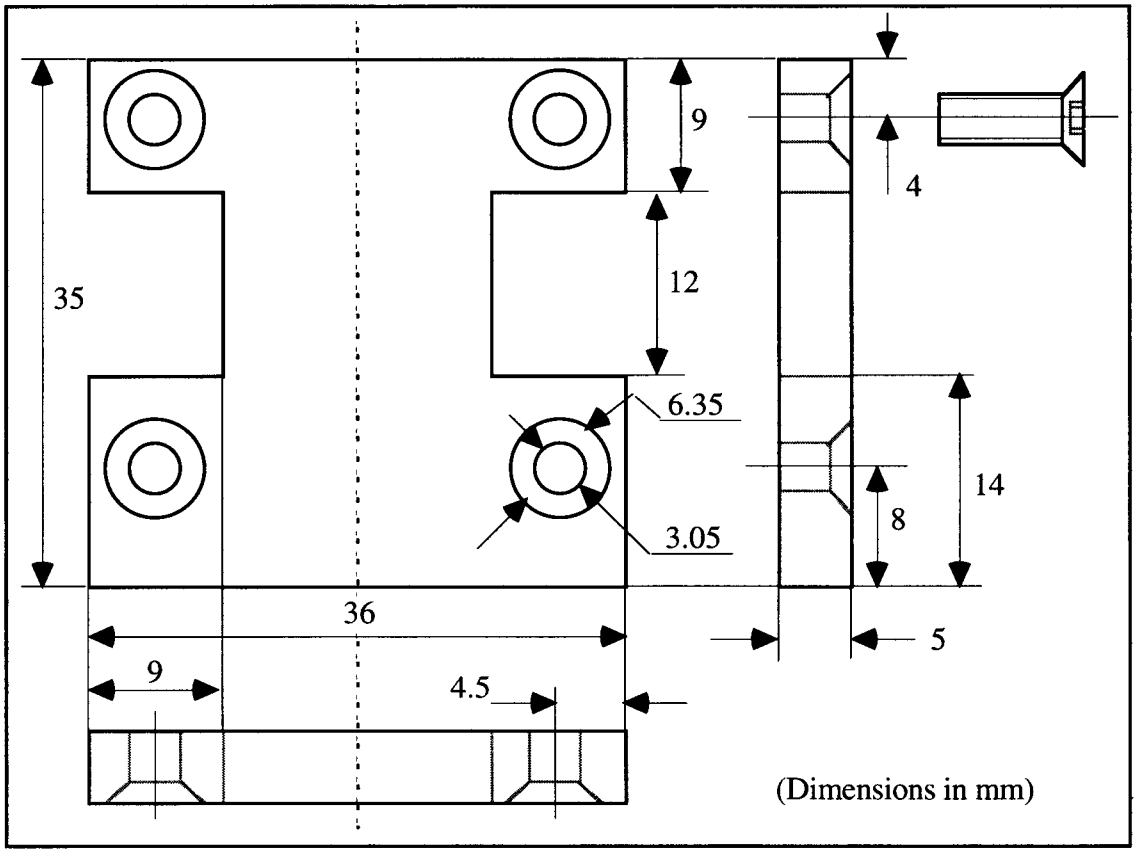

Figure 16. Jigs used to clamp the top and bottom ends of specimens

a detailed drawing of one of the four jigs used. Using jigs allowed fast and convenient replacement of a specimen just tested by the next specimen without having to manufacture fiberglass tabs for each specimen. The jigs were made out of steel for adequate restraint of the specimen during loading. Their design was similar but not identical to the design of jigs used in [61]. The major modification was the use of non-protruding screws to fasten the jigs together. This was necessary owing to the fact that the jigs had to slide freely in the compression test fixture. Indeed, special fixtures must be used for compression tests in order to obtain proper axial loading of the specimen. The Boeing modified ASTM D695 compression fixture was used for this purpose. The jigs were all identical except for the fact that two jigs had four partly conical holes to accommodate the screws heads (as on Figure 16), and two jigs had four threaded through-holes for the screws. Figure 17 shows the positioning of the specimen in the jigs, and Figure 18 the global positioning of the specimen plus jigs in the compression fixture.

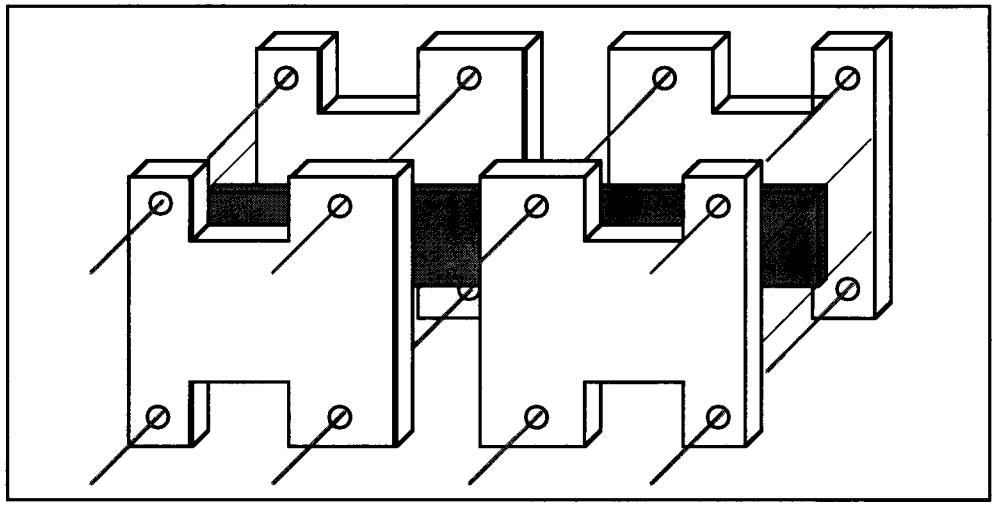

Figure 17. Positioning of the specimen in the jigs

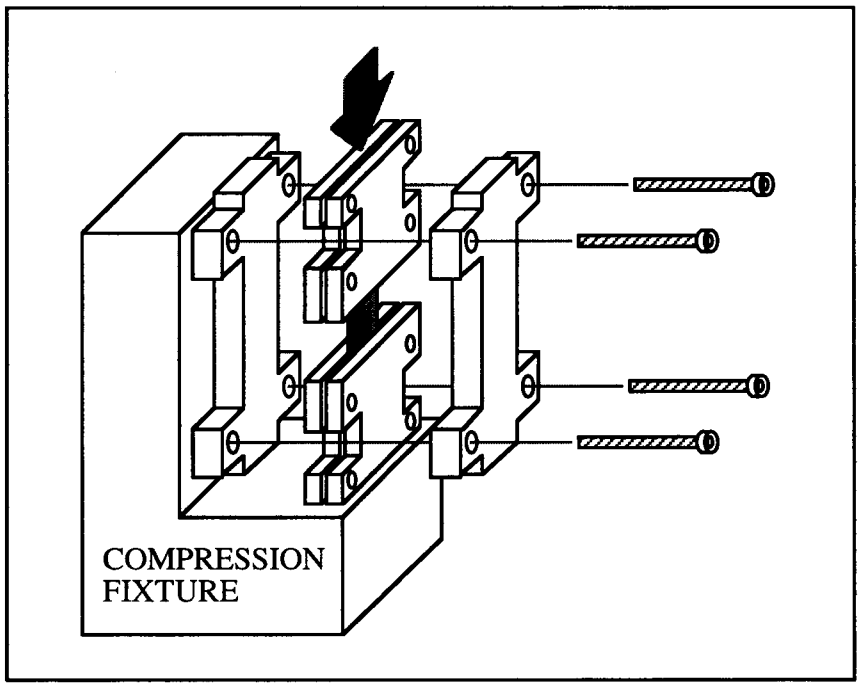

Figure 18. Positioning of the specimen in the compression fixture

The gage-length, g, was chosen small enough to avoid Euler buckling of the central section of the specimen, yet large enough to allow for strain-gages to be placed in the central section. In order to avoid Euler buckling, the compressive strength of the material σ_c must be less than the Euler buckling stress σ_e:

$$\sigma_c \leq \sigma_e = \left(\frac{2}{3}\right)\frac{c\pi^2 E}{12\left(\frac{g}{t}\right)^2} \tag{91}$$

where E is the material's stiffness

g is the gage-length

t is the thickness of the specimen

c is a coefficient varying from 1 (simply supported) to 4 (clamped)

the coefficient (2/3) is to allow for shear effect due to anisotropy.

In our case we obtain (for a 0° specimen and with c=2.5) a value of σ_e around 3 GPa, which is more than twice the compressive strength. Euler buckling was therefore avoided.

In order to obtain a good axial loading, two steel plates with spherical dimples and a steel ball in between them were placed on the top of the jigs and specimen. Strain-gages were glued on both sides of each specimen in order to monitor possible bending during loading. The strain-gages were connected to strain indicators and the strain read in real time. All tests were performed on a Instron 4505 at the speed of 0.05 mm/min., and data (load and cross-head displacement) were acquired using the "Labview" software on a Macintosh SE. The very low test speed was chosen in an attempt to observe in-plane microbuckling of fibers at the edge of the specimens in real time using a stereo microscope in a manner similar to [18]. Because specimens were unnotched, the location of fracture along the gage-length could not be predicted, unlike in [18] where notched specimens were used. It was therefore necessary to have the whole gage-length in the field of view, and the magnification was consequently limited to X15. However examination of the edge of three of the specimens in real time did not reveal any damage up to final failure, which happened catastrophically.

The jigs were clamped manually on the specimens using an Allen wrench. Tight clamping was necessary in order to prevent failure out of the gage section. Most specimens then broke in the middle.

We considered that the microbuckling strain and the final failure strain were identical. This assumption is justified by the fact that for straight specimens, failure is catastrophic. In [9] and [18], final failure was occurring about 5% above the microbuckling initiation strain. This was due to the presence of the hole. Failure was not

catastrophic because the kink propagates from the high stress hole/notch surface to a lower stress region. Its propagation is therefore stable, and load must be further increased to drive the kink through the whole width. In the case of a straight specimen, the stress field across the width is almost uniform, and therefore the kink propagates almost instantly.

Results from the these tests will be presented in Chapter 5.

4.3 Single-ply specimens

In order to study further the mechanism of in-plane kinking and out-of-plane kinking in AS4/PPS, we performed additional experiments on specimens made up of a single 0° ply embedded in a transparent acrylic thermoplastic (acrylic). The purpose of these tests was two-fold: first to verify that a 0° ply of AS4/PPS failed in compression by kinking, and second to study the propensity for out-of-plane kinking versus in-plane kinking. The use of a transparent material allowed direct observation of the failure process. Acrylic was chosen over polycarbonate because its modulus of elasticity was slightly higher, and because microscopic view of the 0° ply through the acrylic was clearer.

Samples were prepared by gluing a single ply of AS4/PPS in between two acrylic specimens with an acrylic cement. Dimensions of an acrylic specimen were 81 mm x 12.7 mm x 2.8 mm. A first set of three samples was manufactured by letting them cure under a 10 kg weight for 24 hours. The bonding was found to be poor, with gaps before loading between the plastic and the ply. A second set of three samples was prepared by pressing each sample at 1 Mpa (higher pressure cracked the acrylic) for 30 seconds, and then

leaving the three samples under a 20 kg weight for 24 hours. The bonding was then satisfactory, with no gaps between the plastic and the ply. Tests showed that the fibers adhered well to the plastic, because broken fibers stuck to the plastic upon strain recovery after testing.

To avoid gross Euler buckling, the specimen was slightly clamped in the same compression fixture as used previously (tighter clamping resulted in undesirable friction between the specimen and the fixture). Figure 19 shows this set up. The loading speed was 1mm/min.

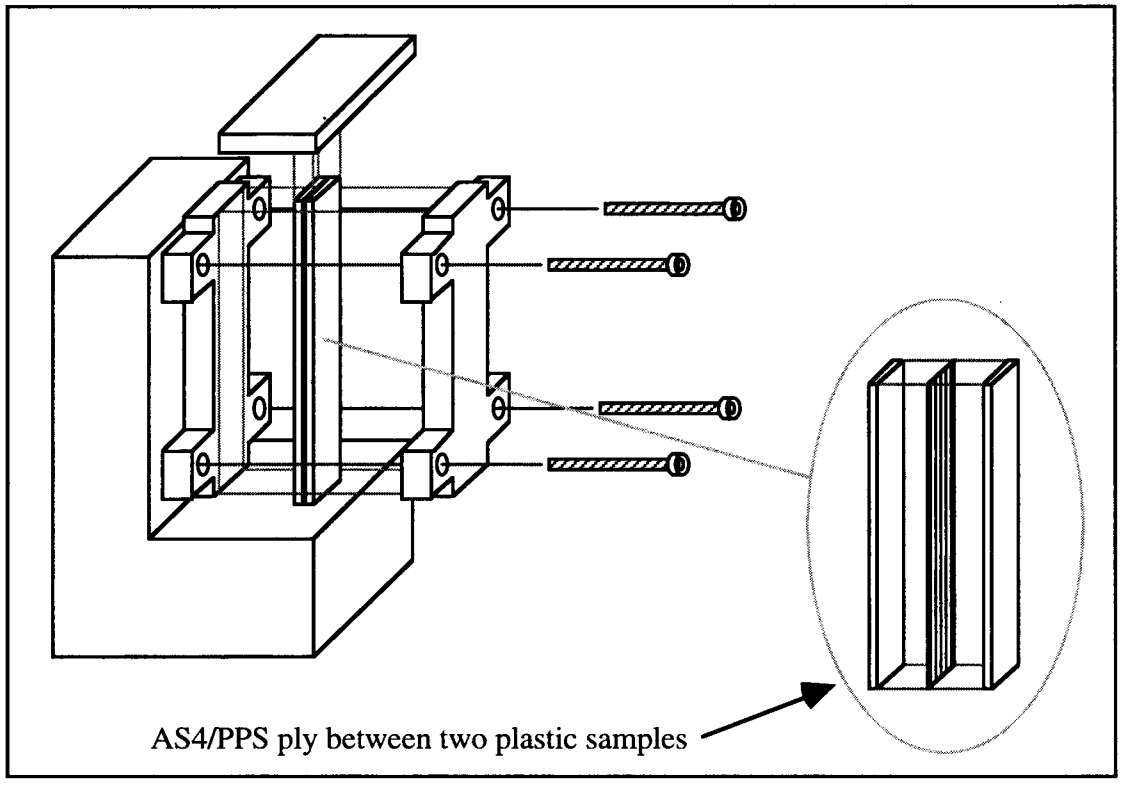

Figure 19. Single-ply sandwich specimen in compression fixture

We also performed compression tests on unidirectional 90° AS4/PPS samples. The purpose of these tests was to correlate the propensity for out-of-plane microbuckling with the stiffness of the medium surrounding the 0° ply. These last samples were

manufactured from 8 hand-laid plies of pre-impregnated roll at a temperature of 320°C and a pressure of 0.5 Mpa for 10 minutes, using the same aluminum mold as for the multidirectional laminate. Three samples were cut from this plate and tested. Their width and length were the same as for the acrylic/(AS4/PPS)/acrylic sandwich specimens.

(5) EXPERIMENTAL RESULTS

5.1 $[\theta/-\theta/0_2/\theta/-\theta/0]_s$ laminate

The results obtained are presented in Figure 20 as a graph of the failure strain as a function of the angle θ. Each cross-hair corresponds to a specimen successfully tested.

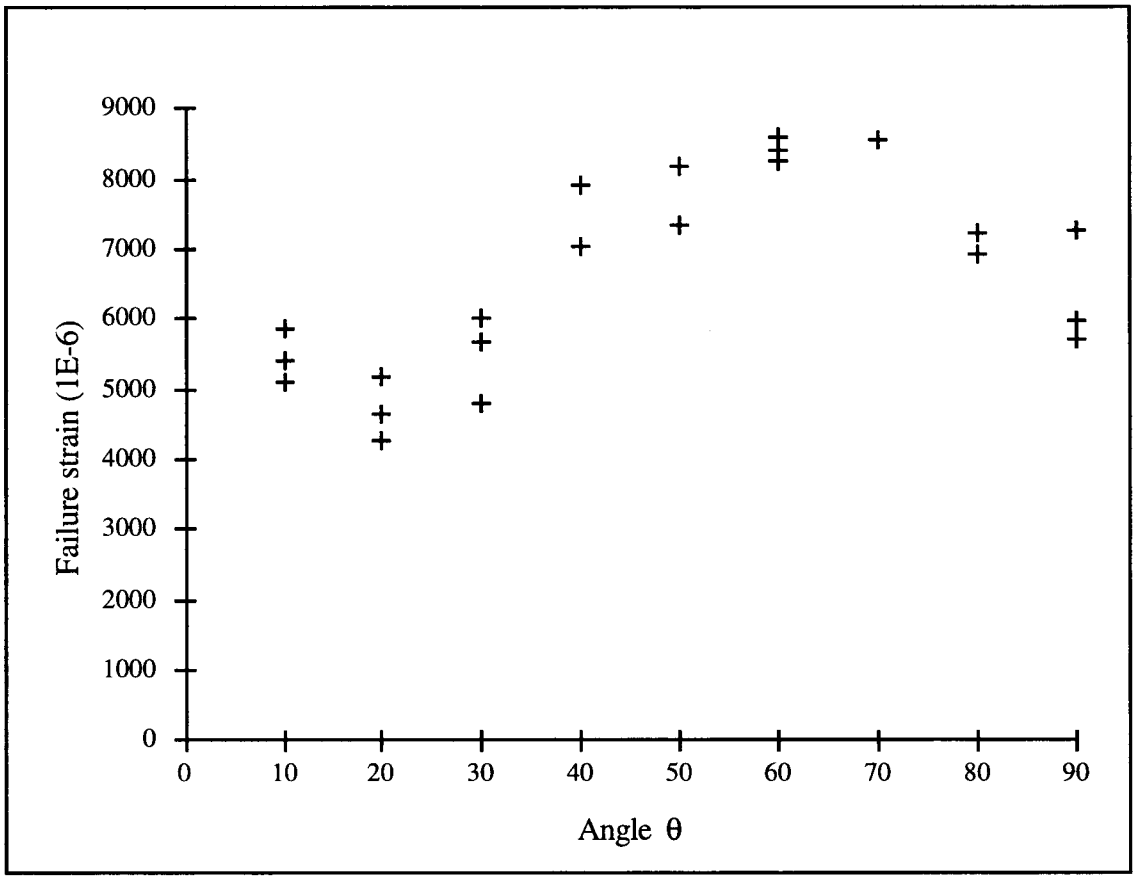

Figure 20. Failure strains obtained from experiments

Most of the samples broke as expected in the central gage section in a catastrophic manner. The stress-strain curves exhibited similar features at all angles. There was little

sign of non-linearity, except possibly just before fracture. Selected stress-strain curves are shown in Appendix A. On some specimens microscopic examination of the edge revealed broken fibers protruding in the y direction. This was an indication of the occurrence of in-plane kinking. However the catastrophic nature of the failure and subsequent interpenetrating of plies prevented us from concluding whether in-plane kinking had occurred first. It is nonetheless relevant to note that in some instances the specimens failed non-catastrophically out of the gage section: when this happened, failure was by in-plane kinking. A crack was heard, corresponding to the breaking of fibers, and the test was stopped immediately. Because of the restraint from the jigs, further failure was prevented and microscopic examination was possible. Figure 21 clearly displays this event in the side 0_2 ply (plies 3 and 4). It shows 0° fibers that had buckled in-plane. The dark zone corresponds to a region of the 0° ply that is out of focus owing to fibers having buckled in-plane (out of the page). Similar pictures may be found in [9]. A few specimens broke prematurely by global ply delamination. We surmise that this was due to non-uniform flowing of the matrix and consequently improper bonding of the plies during the manufacturing process. When such a premature failure happened, the results were discarded. It was necessary to manufacture a second plate at $\theta = 50°$ because all specimens from the initial plate at $\theta = 50°$ broke prematurely.

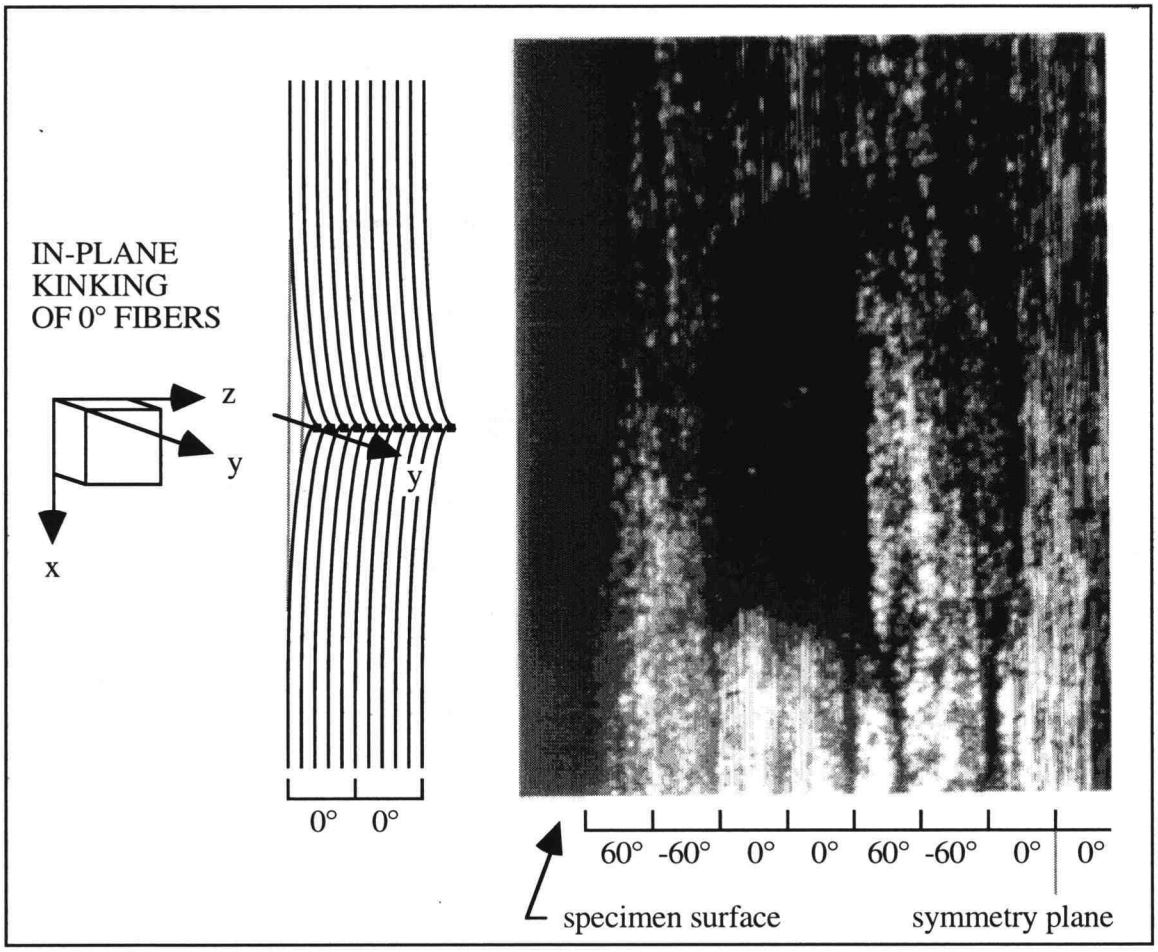

Figure 21. Edge view of an in-plane kink (dark zone) (sample with θ=60°, X50)

5.2 Single-ply specimens

Upon loading, samples failed by catastrophic propagation of a crack across the width. Subsequent increase of the load resulted in appearance of other cracks at various locations on the sample, either totally or partially through the width. Microscopic examination of the samples revealed that near the edges these cracks had inclined portions, which were in-plane kinks, at an angle of $\beta = 20°$. This value of β was in agreement with previous studies [4-8,17]. The rest of the cracks were made of fibers that broke by bending out of the ply plane. Figure 22 shows the various failure mechanisms.

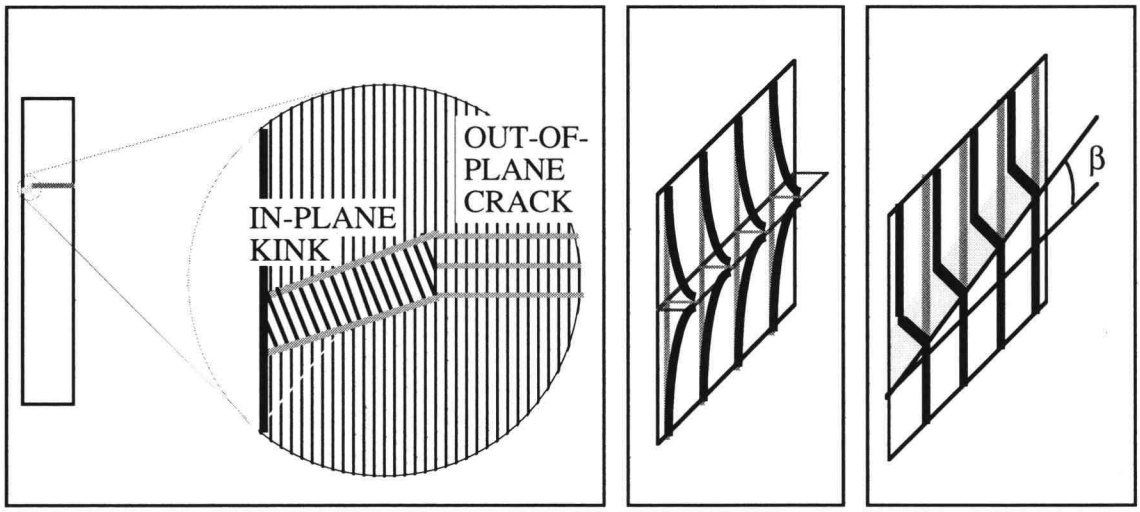

Figure 22. Failure mechanism in single-ply sandwich specimen. (a) Typical crack — Thick lines indicate location of breakage of fibers. (b) Out-of-plane crack. (c) In-plane kink and kink band angle β. (Gray lines in (b) and (c) are the fibers initial positions).

Figure 23 is a photograph of an in-plane kink in one of the AS4/PPS plies. The kink band boundaries, where fibers are broken, are clearly visible. The angle β of the kink boundaries relative to the perpendicular to the loading axis is about 20°. On the right of the photograph one sees that only the top kink boundary is defined. The bottom right kink boundary is not formed because fibers there have not yet broken. The observed failure cracks are therefore a combination of out-of-plane and in-plane kinks. In all cases, the cracks initiate at the edges. This confirms the critical role played by edges in the compressive behavior of composites. It also shows that in-plane kinking is typically an edge phenomenon, and will tend to occur before out-of-plane kinking. Only one previous study of a single ply embedded in transparent plastic had, to our knowledge, been conducted [100]. A single ply was cast in epoxy and tested in compression. It revealed out-of-plane bending and kinking of the fibers. However the authors did not mention in-plane kinks at all or report whether they had observed in-plane kinks.

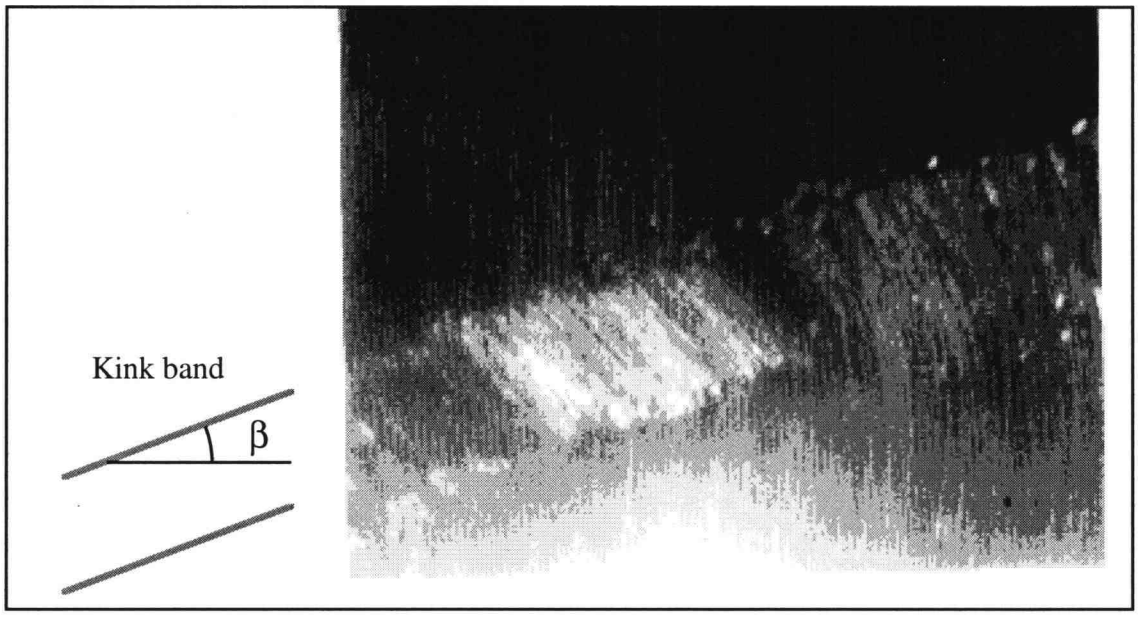

Figure 23. In-plane kink (acrylic/AS4-PPS sample, X100)

In theory, buckling should occur in the plane having the lowest bending stiffness [22]. In-plane buckling will be favored at the edges of the specimen owing to the lesser support at the free-edge. In the central section of the specimen, the out-of-plane bending of the fibers will be favored owing to the lower stiffness of the acrylic compared to that of the adjacent fibers within the ply. This through-the-thickness motion is therefore correlated with the stiffness of the medium surrounding the ply and the fibers. In the case of the Acrylic/AS4-PPS/Acrylic sample, it is the stiffness of the plastic itself. In the case of a AS4-PPS 0° ply inside a laminate, it is the transverse stiffness of the composite. In order to test this assumption, we performed compressive tests on the acrylic alone and on a unidirectional 90° AS4/PPS specimen and measured their compressive moduli. The compressive stress-strain curves of the acrylic are given in Figure 24.

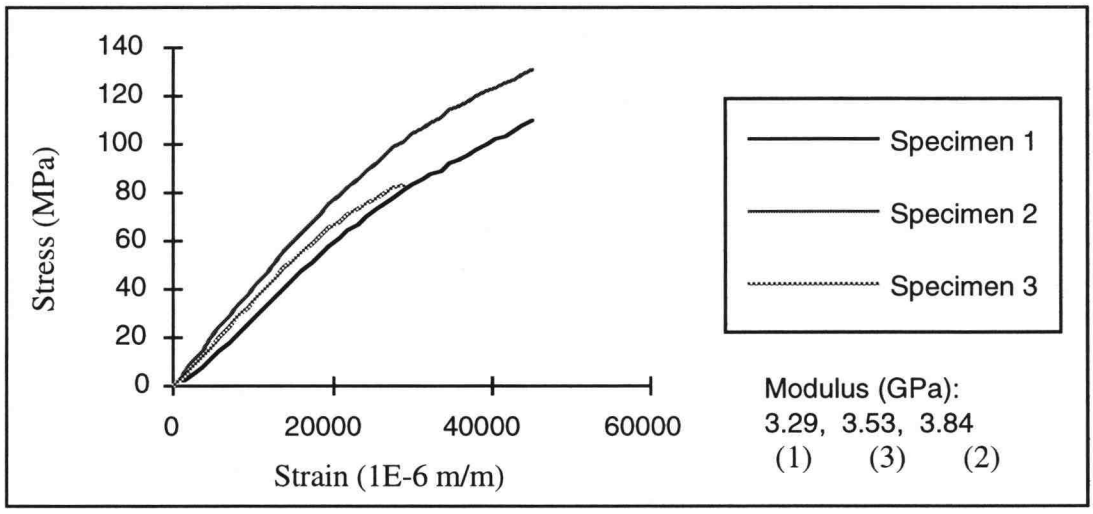

Figure 24. Compressive stiffness of the acrylic

The transverse compressive stress-strain curves of the composite are given in Figure 25. The respective moduli are compared in Figure 26. We note that the acrylic has indeed a compressive stiffness lower (43%) than the transverse compressive stiffness of the composite. This is an indication that our modeling of the high angle behavior based on the bending stiffnesses of the outer plies is correct.

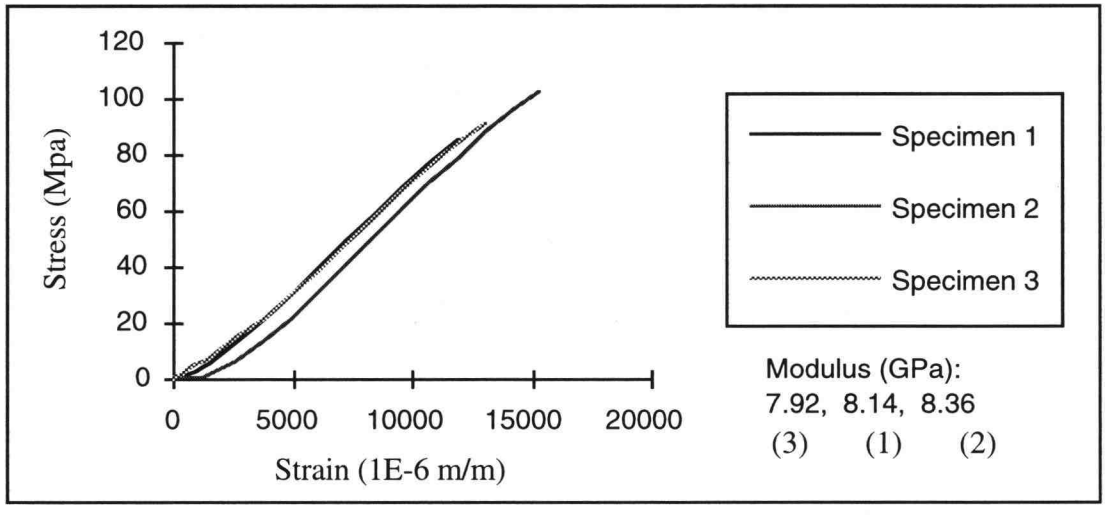

Figure 25. Transverse compressive stiffness of the composite

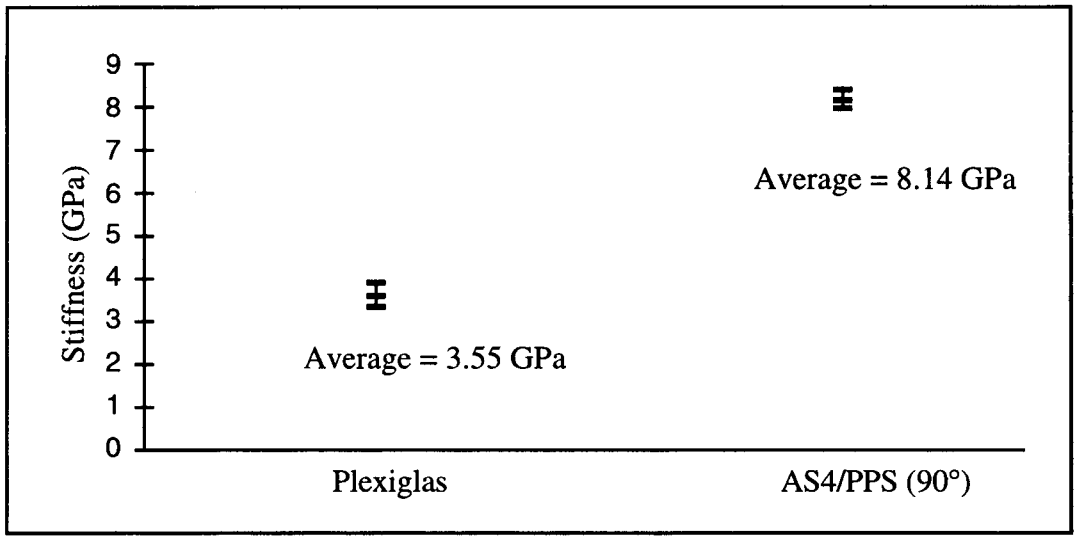

Figure 26. Comparison of the acrylic and AS4/PPS (90°) stiffnesses

(6) ANALYSIS

6.1 Theoretical predictions for the $[\theta/-\theta/0_2/\theta/-\theta/0]_s$ laminate

We apply the theory of Chapter 3 to the laminate $[\theta/-\theta/0_2/\theta/-\theta/0]_s$ made up of AS4/PPS plies. The properties of the AS4 fibers were taken from [14]:

$$E_f = 214 \text{ GPa}$$
$$\varepsilon_{tf} = 0.014 \quad \text{(tensile strain to failure)}$$
$$r_f = 3.5 \cdot 10^{-6} \text{ m}$$

The properties of the PPS matrix were obtained directly from the manufacturer:

$$E_m = 3.4 \text{ GPa}$$
$$G_m = 1.3 \text{ GPa}$$
$$\tau_f = 80 \text{ GPa} \quad \text{(shear failure stress)}$$

Because the shear failure stress was not available, the tensile strength was used as an estimate. The Poisson's ratio was taken as $\nu_{12} = 0.3$.

The dimensions of each specimen were:

Length: L = 80 mm

Width: Wi = 12.7 mm

Thickness: t = 1.7 mm

Ply thickness: h = t/14 = 0.123 mm

The thickness, e, of the matrix layer was chosen equal to h/10, that is between one and two fiber diameters.

The calculation of the interlaminar stresses was done using the symbolic software package "Maple V" (Release 3). A high numerical accuracy turned out to be essential in order to obtain correct results. For the above laminate we had N = 6 (the 0_2 ply was counted as one), and therefore ten non-zero roots ρ_i (equation (16)) These were on the order of 10^8 m^{-1} with slopes at the roots on the order of 10^{100}. Owing to the factors $\left\{cosh\left(\sqrt{\rho_i} \cdot Wi/2\right)\right\}$ in the system of simultaneous algebraic equations (system (35)), a high number of significant figures (30) was required in order to come up with accurate and converging numerical results.

The computer program written in "Maple V" is self explanatory and is given in Appendix B, both for the multidirectional and the cross-ply laminates. The running time on PC (Pentium 100MHz) was less than 15 minutes. For a given angle θ, the program calculates the shear stresses τ_{zx} and τ_{zy} as a function of y and of the applied displacement u_a at any interface. Because the 0_2 ply is counted as a single ply of double thickness, the interfaces were numbered as follows (corresponding interfaces are in dark on the layup):

Interface 1 $[\theta/-\theta/0_2/\theta/-\theta/0]_S$

Interface 2 $[\theta/-\theta/0_2/\theta/-\theta/0]_S$

Interface 3 $[\theta/-\theta/0_2/\theta/-\theta/0]_S$

Interface 4 $[\theta/-\theta/0_2/\theta/-\theta/0]_S$

Interface 5 $[\theta/-\theta/0_2/\theta/-\theta/0]_S$

The interfaces we are interested in are the ones bordering a 0° ply, that is interfaces 2, 3, and 5. The curves $\tau_{zx}(y)$ and $\tau_{zy}(y)$ are given in Appendix C for selected values of θ, and for u_a equal to 10^{-3} m. Only a half laminate is shown since the shear stresses are odd in y. The chosen value of u_a gives a strain on the order of the failure strain of the composite. Because the shear stresses are directly proportional to u_a, a different value of u_a will only affect the amplitude of the curves, not their shape. The curves show that the shear stresses are very small in the central region and increase sharply in a boundary region near the edge of the laminate, as expected. Ultimately we are interested in the value of τ_{zx} and τ_{zy} at the edge (y = Wi/2). Figure 27 summarizes the results and gives the

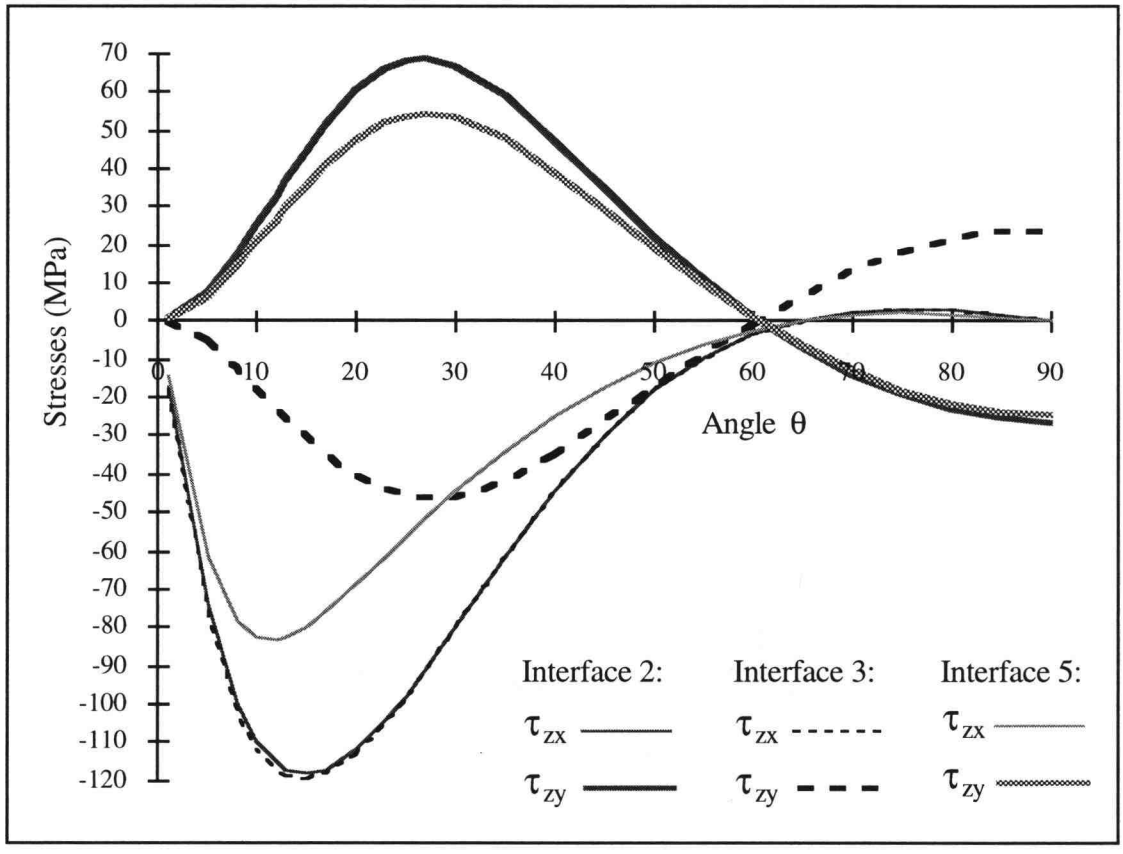

Figure 27. Maximum interlaminar shear stresses τ_{zx} and τ_{zy} at (Wi/2) as a function of θ (at interfaces 2, 3 and 5)

values of τ_{zx} and τ_{zy} at the edge for the three interfaces 2, 3 and 5. When θ tends to 90°, the shear stresses given by equations (40) tend to the shear stresses given by equations

(64) for the special case $\theta = 90°$, as they should. We note that the amplitude of the shear stresses is maximum around $\theta = 20°$, and minimum around $\theta = 60°$. This finding suggests that for any laminate there is a theoretical range of angles (here between 55° and 70°) for which shear stresses are almost zero. The microbuckling amplitude V should therefore be minimum in this range, for a given applied displacement u_a. Consequently the strain to failure should be maximum in this range, as verified on Figure (20). It is interesting to note that FEA studies of angle-ply $[\theta/-\theta]_s$ laminates had shown that the interlaminar stress τ_{zx} was also minimum around $\theta = 60°$ [73].

It is useful at this point to investigate the kinematics of interlaminar displacements. Equation (2) shows that shear stresses τ_{zx} and τ_{zy} at any interface (k) are proportional to and have the same sign as the difference in displacements between ply (k) and ply (k+1).

$$(\text{Shear stress}) \propto \{[\text{Displacement ply \#(k)}] - [\text{Displacement ply \#(k+1)}]\} \qquad (92)$$

Figure 28 shows the displacements corresponding to the angles θ below 60°, based on the signs of the shear stresses and equation (92).

We see that a positive τ_{zy} at interfaces 2 and 5 (and a negative τ_{zy} at interface 3) corresponds to an effort from angled-plies to push the 0° fibers towards the edge of the ply. Since τ_{zy} and its derivative have the same sign, we see that below $\theta = 60°$, the interlaminar shear stresses τ_{zy} promote the microbuckling of all 0° fibers (Equation (85)).

Above $\theta = 60°$ the signs in Figure 28 are reversed, hence the derivative of τ_{zy} is negative, and consequently the interlaminar shear stresses τ_{zy} hinder the microbuckling of all 0° fibers.

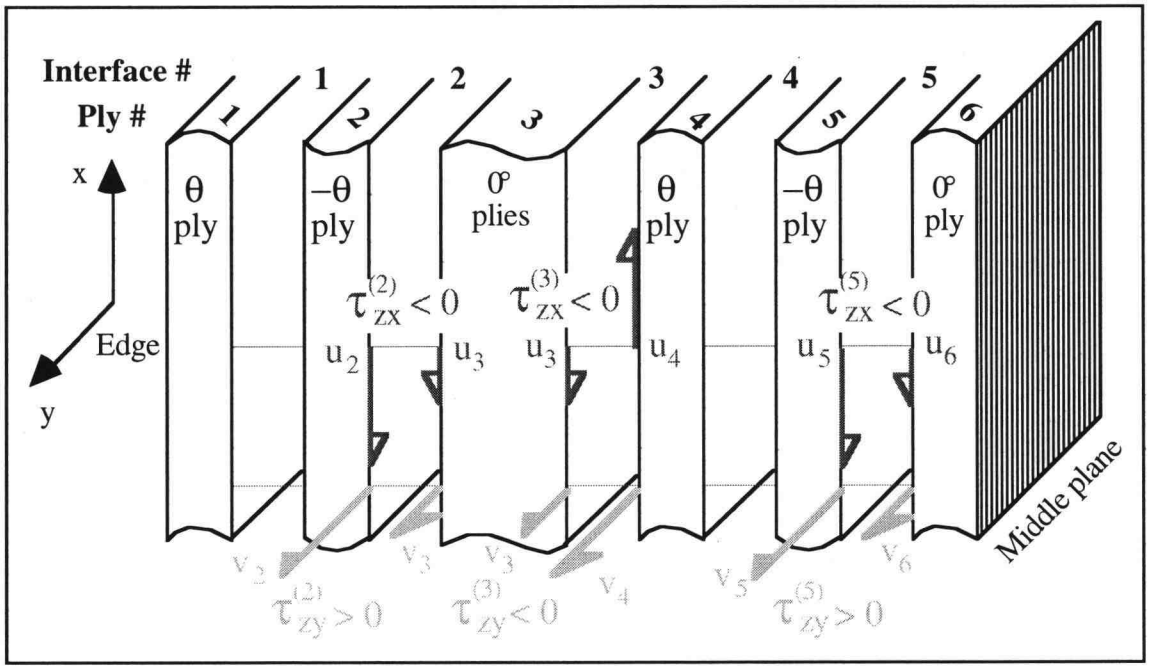

Figure 28. Interlaminar shear stresses and ply kinematics (for $\theta < 60°$)

The 0° fiber buckling amplitude, V, and of the fiber maximum tensile strain, ε_f, were then calculated using equations (85) and (87) respectively. The composite predicted failure strain was evaluated as the ratio of the applied displacement u_a corresponding to the fiber maximum tensile strain ε_f being equal to the fiber failure tensile strain ε_{tf}, divided by L. These calculations were done with the mathematical software "Mathcad 5+". The calculations were done at interface 2 since it is the interface where τ_{zy} (and its derivative) are maximum.

The predicted curves are given in the next section and compared with the experimental results.

In the present form, our theory could be applied to any laminate for the prediction of microbuckling failure. The "Maple V" program could be easily modified for this purpose. As an example, we include in Appendix D a "Maple V" program that calculates the failure strain for any 8 ply symmetrical laminate $[\theta_1, \theta_2, \theta_3, \theta_4]_s$. The angles

$\{\theta_i\}_{i=1..4}$ are specified as inputs. The program gives numerical values for the case $[45/-45/0/90]_s$. The program could also be used to estimate interlaminar shear stresses at any interface, in compression as well as in tension, simply by specifying in the program the interface k and the applied displacement u_a.

6.2 Comparison between experimental results and theoretical predictions

Results from experiments on the multidirectional samples are shown in Figure 29, along with predictions from our theory. The graph also displays the curves for matrix failure, both within a 0° ply and at the interface. We recall that the in-plane kinking failure, interlaminar matrix failure and in-ply matrix failure were governed by criteria (86), (87), and (88) respectively. Only predictions corresponding to interface 2 are shown, since interlaminar stresses are maximum there. We notice that there is a good agreement between the theory and the experiments below $\theta = 60°$. In particular, the theory correctly predicts the presence of a minimum failure strain around $\theta = 25°$. This shows that shear stresses are the central mechanism involved in the in-plane kinking of the edge fibers below $\theta = 60°$, and it validates our theoretical approach. We further note that these results are qualitatively and quantitatively in agreement with experimental results obtained in [18] with the same layup, the same fibers and a thermoplastic matrix with similar properties. The study of the curves showing matrix failure give some additional insight into the failure mechanisms taking place. We note that the curve predicting interlaminar failure is well above both the curve predicting fiber microbuckling and the tests results. This implies that the microbuckling of the 0° fibers located at the edge, and consequently of the other 0° fibers, precedes interlaminar failure. We recall that interlaminar normal stresses σ_z were not taken into account in the failure criterion (equation (88)), and consequently

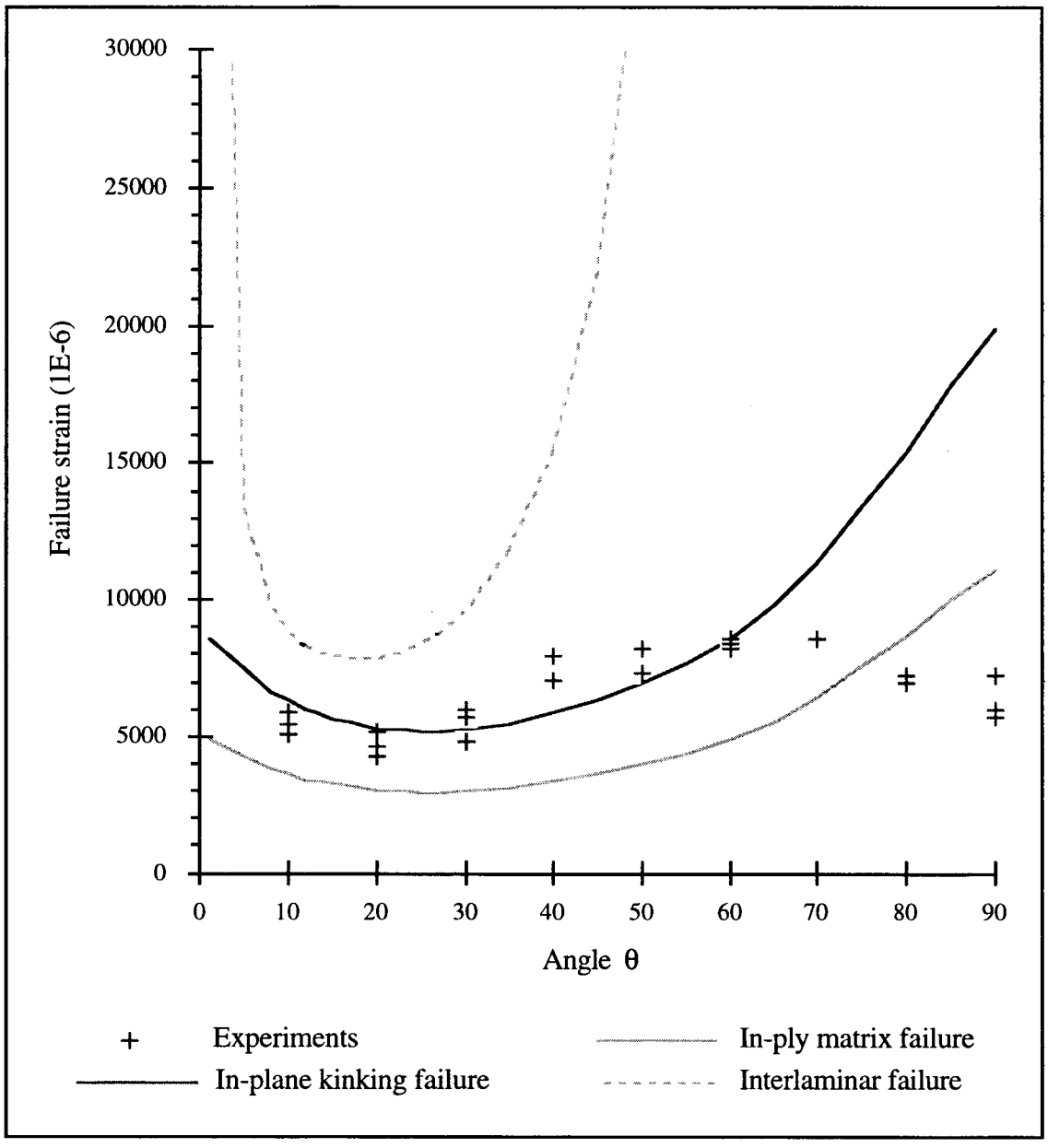

Figure 29. Failure strains: theoretical predictions and experimental results

the strain for interlaminar failure predicted by our theory would in general be conservative. However the interlaminar failure strain must still be higher than the microbuckling failure strain because curves on Figure 29 are in agreement with experiments with a similar layup [18], the latter showing that microbuckling was the initial failure mode.

The curve predicting shear failure of the matrix between fibers inside a 0° ply is, on the contrary, below the curve predicting fiber microbuckling and the tests results (except possibly above $\theta = 80°$ for the tests). This indicates that the matrix fails in shear in-between the 0° fibers before the fibers fail in bending. This is in agreement with previous experimental results which showed matrix cracking in between 0° fibers [59]. In fact, the significant fiber rotations that occur during microbuckling and kinking [8] will cause plastic yielding of the matrix. Plasticity and non-linear shear behavior were not considered in this work because the matrix was modeled as linear elastic.

There remains however a discrepancy between the predictions from the theory and experimental results at high angles, $\theta > 60°$. While the theory predicts a failure strain that keeps on increasing with θ, tests show a decrease in failure strain beyond $\theta = 70°$. We will see later in this chapter that our theory provides nevertheless a physical insight into this phenomenon. We will indicate what is then the most likely mechanism at work, and we will show how our theory could then be succinctly modified to give an estimate of the failure strain in good agreement with the test data.

6.3 Parametric study

In order to investigate the influence of variations in the stiffness of the composite upon the failure strain, we performed two parametric analyses. In the first one the fiber modulus E_f is varied from (E_f-10%) to (E_f+10%) and the other parameters are left constant. In the second one the matrix moduli E_m and G_m are varied from (E_m-10%) and (G_m-10%) to (E_m+10%) and (G_m+10%) respectively, and the other parameters are left constant. The corresponding strain to failure variations are shown on Figures 30 and 31 respectively.

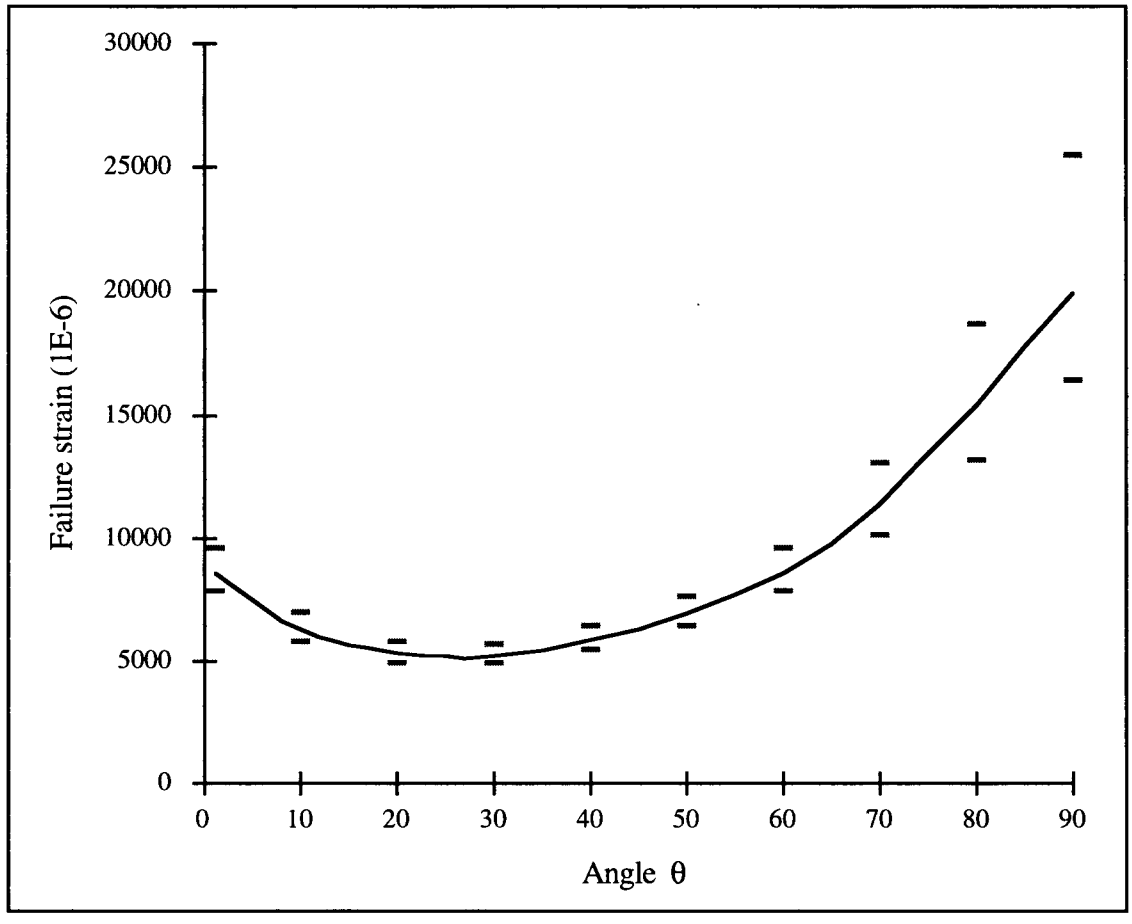

Figure 30. Failure strain intervals (based on in-plane kinking model) corresponding to a ±10% variation in the fiber modulus E_f

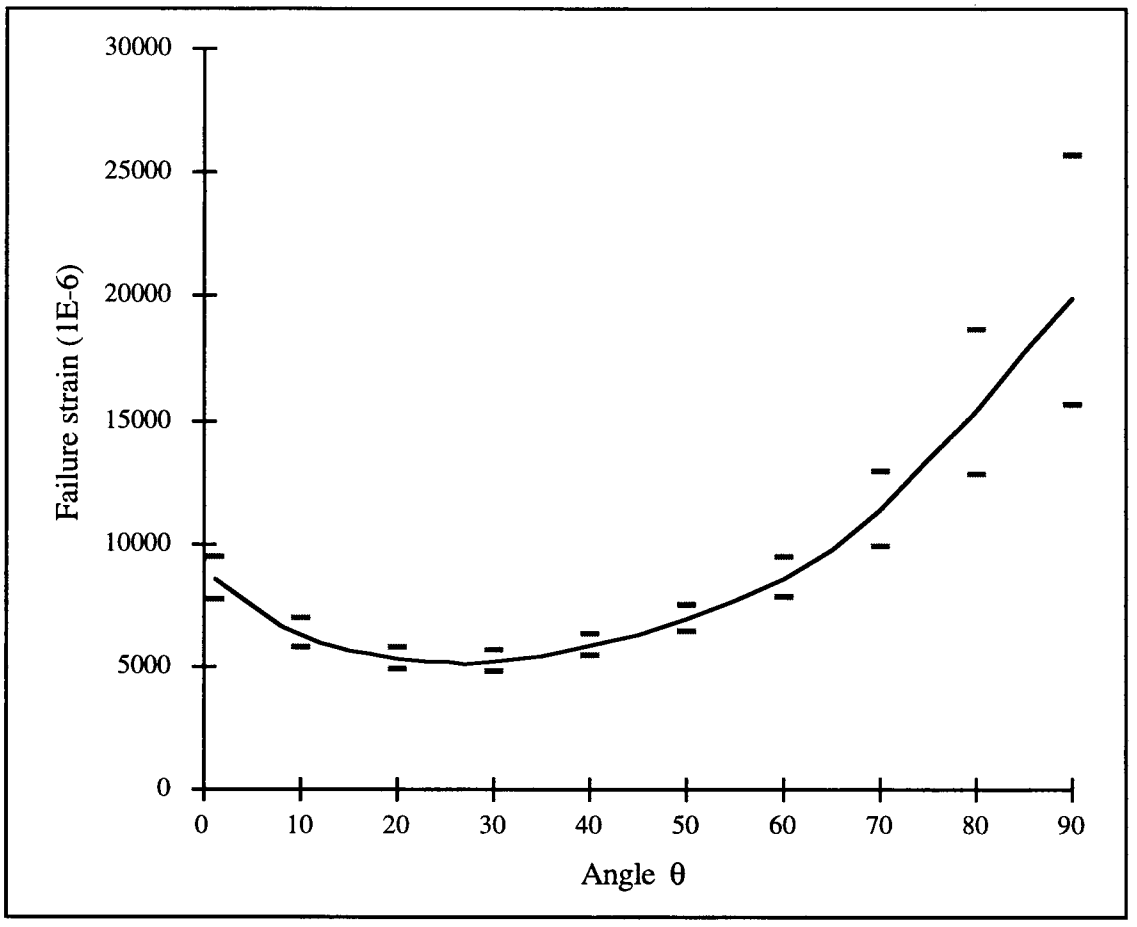

Figure 31. Failure strain intervals (based on in-plane kinking model) corresponding to a ±10% variation in the matrix moduli E_m and G_m

We note that the failure strain variations are of the same magnitude in both cases. This indicates that fiber properties and matrix properties have a similar influence upon the failure process, at least in the elastic regime. The variations are between ±7% and ±10% for angles θ below 60°, where the theory is in agreement with experiments. The intrinsic statistical distribution of fiber and matrix mechanical properties should therefore give a correlated statistical distribution for the failure strain. Only beyond θ=70° do the stiffness variations yield failure strain variations in excess of 10%. These variations increase with θ and reach (+21%; -27%) at θ=90°.

6.4 Statistical study

A specimen with off-axis plies at a given angle θ cannot strictly be considered statistically independent from another specimen at the same angle because they come from the same plate. In addition, the manufacturing process of the plates introduces confounding variables such as the position of the specimen in the plate (closer to the plate edges or to the plate center). Therefore we limit our statistical analysis to a curve fitting procedure on the experimental data. It turns out that the best fit is given by a fourth degree polynomial in θ, as shown on Figure 32.

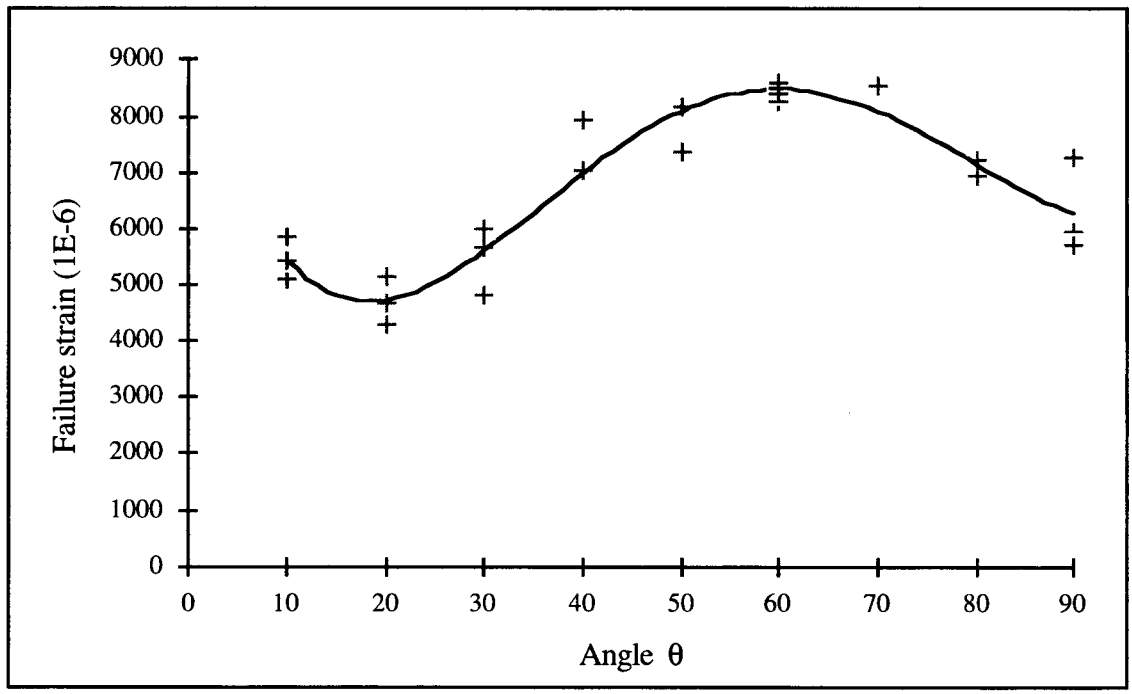

Figure 32. Curve fitting of experimental data

This fourth degree polynomial is:

$$(0.001436)\cdot\theta^4 - (0.3299)\cdot\theta^3 + (24.257)\cdot\theta^2 - (590.64)\cdot\theta + (9243.3)$$

The coefficient of determination R^2 (equal to the ratio of the residuals sum of squares to the corrected sum of squares) is equal to 0.88. Almost 90% of the variation in the experimental data could therefore be accounted for by the model (fitting curve). This is an informal indication of the presence of a minimum strain around $\theta = 20°$ and a maximum around $\theta = 60°$.

6.5 The high angle case ($\theta > 60°$)

We recall from our theoretical predictions in Chapter 6 that above $\theta = 60°$ the interlaminar shear stress τ_{zy} and the derivative of τ_{zy} with respect to y are negative (see Figure 28). Hence the interlaminar shear stresses τ_{zy} tend to push the fibers toward the center of the specimen, and consequently to hinder the microbuckling of 0° fibers over the whole specimen width, the effect being more severe at the edges. We will therefore assume that the 0° fibers may then buckle out-of-plane, that is through the thickness (z direction). The intuitive argument behind this assumption is the following: the out-of-plane movement of the 0° fibers will cause bending of the surface (θ/-θ) plies. The resistance to the movement of the 0° fibers will thus be proportional to the bending stiffness of the surface (θ/-θ) plies. Because the bending stiffness of (θ/-θ) plies is minimum at θ=90° and increases as θ decreases to 0°, the out-of-plane buckling amplitude of a 0° fiber should decrease with θ and consequently the strain to failure $\varepsilon_{failure}$ should increase as θ decreases from 90°. Physically, we will also recall that out-of-plane kinking of 0° fibers had been observed in cross-ply composites [61], which is a clue that out-of-plane buckling could occur at angles θ close to 90°. In order to give a quantitative aspect to this analysis and prove that out-of-plane buckling is the favored failure mode at high angles θ, an estimation of the strain to failure due to out-of-plane buckling of the 0° fibers may be quantified as follows:

We model the surface plies (θ/-θ) as a cantilever beam of thickness (2.h) and width (Wi). that is subjected to a distributed lateral load q'. From the geometry of the loading and the top and bottom jigs, we consider that this beam is a cantilever beam of length g. This is illustrated on Figure 33.

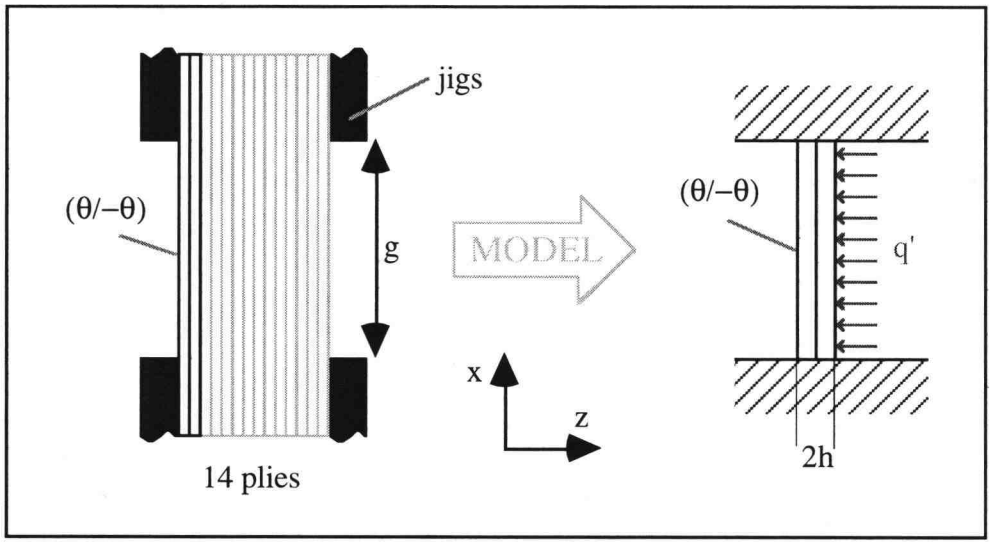

Figure 33. Modeling of out-of-plane buckling of 0° plies

From Timoshenko [101], the middle (maximum) bending amplitude δ of the beam is:

$$\delta = \frac{q' g^4}{384 E_b I_b} \tag{93}$$

where E_b is the longitudinal stiffness of the (θ/-θ) beam and I_b its moment of inertia. The stiffness E_b depends on θ and is given by:

$$E_b(\theta) = \frac{\overline{Q}_{11}(\theta)\cdot h + \overline{Q}_{11}(-\theta)\cdot h}{2\,h} = \overline{Q}_{11}(\theta) \tag{94}$$

with $\overline{Q}_{11}(\theta)$ given by equation (4a).

The moment of inertia I_b is:

$$I_b = \frac{(Wi)\cdot(2h)^3}{12} = \frac{2}{3}(Wi)\cdot h^3 \tag{95}$$

Now the deflection δ is the maximum W of the out-of-plane buckling amplitude w of the 0° fibers given by:

$$w(x) = W\, sin\left(\pi\frac{x}{\lambda_0}\right) \tag{96}$$

The initial amplitude w_0 will be:

$$w_0(x) = W_0\, sin\left(\pi\frac{x}{\lambda_0}\right) \tag{97}$$

with W_0 equal to V_0 given by equation (83). For mathematical simplicity, we will assume that the load q' is actually proportional to the amplitude w and distributed along the 0° fiber. Using equations (93), (94) and the above assumption, we have therefore:

$$q'(\theta) = \frac{384\,\overline{Q}_{11}(\theta)\,I_b}{g^4}\cdot w \tag{98}$$

Owing to experimentally observed out-of-plane kinking, we can assume that out-of-plane microbuckling occurs in the shear mode. Hence we may use equation (79), substituting w and w_0 for v and v_0, and replacing q by q' as given by equation (98). We thus obtain the following out-of-plane microbuckling equation:

$$E_f I\frac{d^4(w-w_0)}{dx^4} + \frac{384\,\overline{Q}_{11}(\theta)\,I_b}{g^4}\cdot w - A_f\frac{G_m}{1-V_f}\frac{d^2(w-w_0)}{dx^2} + \frac{A_f}{V_f}\left|\sigma_{0°ply}\right|\frac{d^2w}{dx^2} = 0 \tag{99}$$

We note that the sign in front of the normal load q' in equation (99) is opposite to the one in front of q in equation (79). This is because the normal loads are now hindering the buckling of the 0° fibers. Replacing equations (96) and (97) into (99), we then derive the following relationship between W, u_a, and θ, in the same way equation (85) for $V(u_a,\theta)$ had been obtained:

$$W(u_a,\theta)=\frac{W_0}{1-\dfrac{\dfrac{A_f}{V_f}\left|\sigma_{0°ply}(u_a)\right|-\dfrac{384\,\bar{Q}_{11}(\theta)\,I_b}{g^4}\left(\dfrac{\lambda_0}{\pi}\right)^2}{E_f I\left(\dfrac{\pi}{\lambda_0}\right)^2+A_f\dfrac{G_m}{1-V_f}}} \tag{100}$$

Now the actual distributed force q' on one 0° fiber is less than q' given by equation (98). Indeed, we may expect that several and possibly all fibers along the width will buckle out-of-plane. The distributed force q' should therefore be divided by the number of rows of fibers buckling out-of-plane. On the other hand, we have not taken into account the additional resistance to buckling that arises from the fact that the (θ/-θ) surface plies are not isolated, but bound to the remaining plies by the matrix interlayers. This would contribute to increase the value of q'. We therefore introduce a correction coefficient C_{corr} in the expression for q', with $0 < C_{corr} < 1$. Equation (100) becomes then:

$$W(u_a,\theta)=\frac{W_0}{1-\dfrac{\dfrac{A_f}{V_f}\left|\sigma_{0°ply}(u_a)\right|-C_{corr}\left(\dfrac{384\,\bar{Q}_{11}(\theta)\,I_b}{g^4}\right)\cdot\left(\dfrac{\lambda_0}{\pi}\right)^2}{E_f I\left(\dfrac{\pi}{\lambda_0}\right)^2+A_f\dfrac{G_m}{1-V_f}}} \tag{101}$$

For a correction coefficient equal to 0.25, equation (101) yields predictions for the buckling strain (using equation (27) with W instead of V) which are well above

experimental values in the angle range $\theta > 60°$, as shown on Figure 34. This indicates that the matrix offers actually a less than ideal support to the buckling fibers. We may therefore model the reduced matrix support by introducing a coefficient of reduction C_{red} smaller than 1 and modifying equation (101) as follows:

$$W(u_a,\theta) = \frac{W_0}{1 - \dfrac{\dfrac{A_f}{V_f}\left|\sigma_{0°ply}(u_a)\right| - C_{corr}\left(\dfrac{384\,\bar{Q}_{11}(\theta)\,I_b}{g^4}\right)\cdot\left(\dfrac{\lambda_0}{\pi}\right)^2}{E_f I\left(\dfrac{\pi}{\lambda_0}\right)^2 + A_f\dfrac{G_m}{1-V_f}C_{red}}} \qquad (102)$$

Arbitrarily choosing C_{red} equal to $^1/_3$ yields results in agreement with experimental values, as shown on Figure 34. The rationale behind this choice is the fact that matrix failure (by yielding or microcracking) around the buckling fibers occurs before fiber breakage (see Figure 29). Consequently, the support provided by the matrix to the fibers is increasingly reduced, thus suggesting a coefficient C_{red} closer to zero. Estimating the actual value of C_{red} would require calculating the three dimensional stress field around the fibers, a task obviously quite complex owing to the geometry and the non-uniform packing of the fibers. Figure 35 summarizes experimental results and theoretical predictions for in-plane and out-of-plane fiber microbuckling.

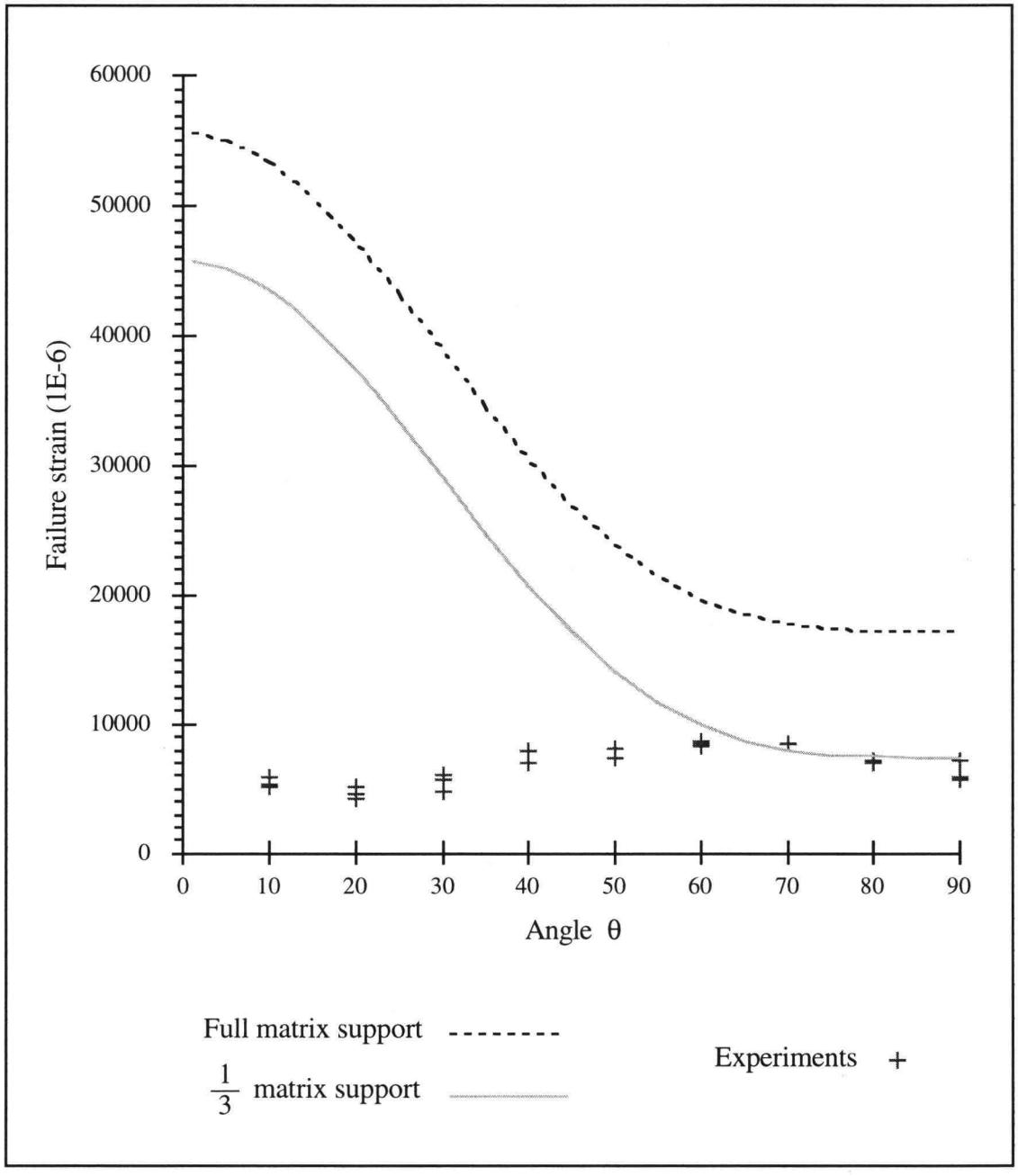

Figure 34. Out-of-plane buckling theoretical predictions and experimental results

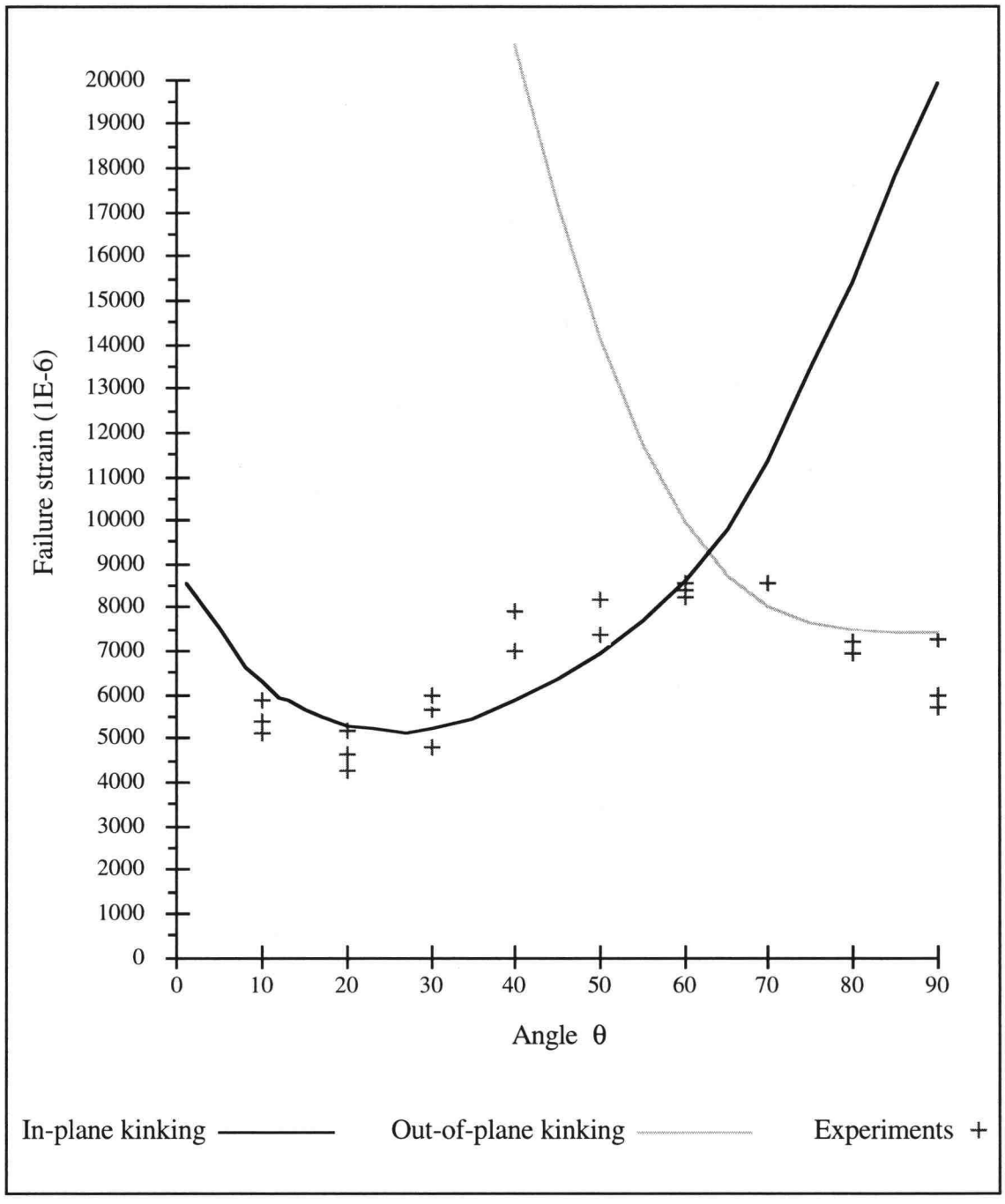

Figure 35. In-plane buckling and out-of-plane buckling theoretical predictions and experimental results

Our series of tests on single ply specimens show that 0° AS4/PPS plies fail in compression by kinking, and thus indicates that kinking is indeed the failure mechanism of 0° plies in the multidirectional specimens. Moreover, results from these tests shed some

additional light on the behavior of our multidirectional specimens when the angle θ is greater than 60°

We first note that experimental results support the claim that buckling occurs in the direction with the lowest compressive stiffness. Indeed the acrylic is half as stiff as the transverse composite and out-of-plane buckling, toward the acrylic, is favored over in-plane buckling, in the transverse direction of the composite. This is in qualitative agreement with our theoretical predictions which show that out-of-plane buckling occurs more easily when the surrounding medium has a lower bending stiffness.

Second, experiments show the critical role played by the free-edge in the promotion of in-plane kinking. Indeed, in the vicinity of the edges of the specimens, in-plane kinking becomes energetically more favorable than out-of-plane kinking, and occurs with an angle β around 20°.

(7) CONCLUSIONS

7.1 Summary

The present investigation has focused on the development of a new theory for the prediction of compressive failure strains in multidirectional GFRP laminates, and its experimental validation. In order to summarize this body of theoretical and experimental work, the essential features of this investigation and the results obtained will be highlighted below, as well as the relevant conclusions that may be inferred from these results.

- The theory comprised two stages: in the first stage a new theory is developed for the determination of interlaminar shear stresses at the free-edge of a multidirectional composite. This theory is based on the concept of matrix layers in between plies. It could be applied to any layup, with reasonable computation times. As such it constituted an enticing alternative to the FEA calculation of interlaminar stresses, since FEA results are prone to mesh sensitivity. The interlaminar stresses depend upon the fiber and matrix properties, specimen geometry, ply sequences, and ply orientation.

  In a second stage a new analytical solution is developed for the strain to failure of 0° fibers in a multidirectional composite. It is derived from a general buckling equation for a fiber on foundation in the plane of the 0° ply. This solution incorporates the interlaminar stresses determined in the first stage of the theory, namely the transverse shear stresses τ_{zy}. The developed solution is thus the first one to take into account

interlaminar edge stresses. The physical justification behind this approach is the observed experimental fact that in-plane microbuckling of 0° fibers starts at the edges of specimens.

- The theory allowed calculation of the 0° fibers strain to failure using the fiber tensile failure strain as a criterion. The composite strain to failure is taken as the 0° fibers strain to failure. This is a reasonable assumption for straight specimens based on the fact that failure is then catastrophic or almost catastrophic after the onset of edge 0° fibers microbuckling. The strain to failure of 0° fibers is therefore ultimately a function of the fiber and matrix properties, specimen geometry, ply sequences, and ply orientations.

- In addition, the theory allows direct calculation of the applied strains that cause matrix shear failure either in between plies (interlaminar matrix failure) or in between fibers within a 0° ply (in-ply matrix failure). It predicts that 0° fiber failure in bending precedes interlaminar matrix failure. Even though the interlaminar matrix failure criterion was possibly conservative (owing to its not taking into account interlaminar normal stresses), this prediction is in agreement with experimental observations showing fiber microbuckling preceding interlaminar failure. The theory also predicts that in-ply matrix failure preceded 0° fiber failure, again in agreement with large matrix shear strains accompanying observed fiber rotations in kink bands.

- Specimens with the layup $[\theta/-\theta/0_2/\theta/-\theta/0]_s$ with various values of the angle θ between 10° and 90° were manufactured, and compression tests were performed. The strain to failure of each specimen was recorded and compared with experimental predictions as a function of the angle θ. The experimental strain to failure is found to decrease from θ=10° to θ=20°, increase between θ=20° and θ=60°, and decrease again

up to θ=90°. There is a very good qualitative and quantitative agreement between theory and experiments for angles θ between 10° and 60°.

- In an attempt to explain experimental data above θ=60°, the above theory is then modified to model out-of-plane buckling of 0° fibers by evaluating the restraint due to adjacent plies on the through-the-thickness movement of 0° fibers. Theoretical predictions are then in good agreement with experimental data.

- Further compression tests are conducted on single 0° ply embedded in acrylic. They reveal that in-plane kink bands of 0° fibers formed at the specimen edges, and that out-of-plane microbuckling of 0° fibers occurs in the central region of the specimens. This confirmed that in a laminate in-plane kinking was the failure mechanism of 0° fibers located at the edge, and that out-of-plane microbuckling would be promoted when the laminate had off-axis plies with higher angle fibers.

In conclusion, we have proposed and built a new comprehensive theory for predicting compression failure in multidirectional laminates. Contrary to existing theories, our theory is physically sound because it incorporates previous experimental observations, and focuses on fiber failure at the specimen edges. It is also in agreement with observed features of compression failure in multidirectional laminates. Experiments validate our theoretical approach, and confirm the critical role played by interlaminar shear stresses at the free-edges. In addition, our theory explains the propensity for out-of-plane buckling of 0° fibers when surrounded with high-angle off-axis plies, phenomena that had been observed in cross-ply laminates.

7.2 Recommendations for further studies

The theory laid out in the present work could serve as a stepping stone for numerous further investigations into the compression behavior of multidirectional laminates. Below are suggested directions for future research which we believe would shed light on this topic.

- Improve the theory to include a calculation of the normal interlaminar stresses σ_z. This would allow incorporation of the normal stresses in the interlaminar matrix failure criterion (88), for instance as follows (where σ_f is the matrix failure strain in tension):

$$\left(\frac{\tau_{zy}}{\tau_f}\right)^2+\left(\frac{\tau_{zx}}{\tau_f}\right)^2+\left(\frac{\sigma_z}{\sigma_f}\right)^2=1$$

  It would ultimately yield better estimates for the applied strain at which interlaminar failure occurs. In the case of layups with high positive normal interlaminar stresses, interlaminar matrix failure could occur prior to in-plane kinking of 0° fibers.

- Incorporate in the theory a more systematic and comprehensive model for the propensity for out-of-plane kinking, including the case where 0° plies are outside plies.

- Model fibers as Timoshenko beams, thereby taking into account shear effects. This would allow the modeling of the formation of kink bands because strain discontinuities could then be directly incorporated in the theory.

- Incorporate in the theory the fiber/matrix interface. This would allow including in the theory the possibility of regions of fiber/matrix relative slipping by considering strength of the fiber/matrix interface and an associated slipping criteria.

- Include in the theory the plastic behavior of the matrix.

- Improve the assessment of the onset of microbuckling/kinking by taking into account stress concentrations due to the 3-D nature of the stress field around the 0° fibers. A study of hexagonal arrays of fibers revealed significant stress concentrations [102].

- Extend the present theory to incorporate the influence of the temperature upon the compression behavior of multidirectional laminates. High temperature studies in compression are still rare, even though state-of-the-art practical applications of composites will require high temperature resistance. Such a theoretical approach could usefully be complemented by tests at elevated temperature on specimens.

- Improve upon the theory by taking into account the fact that in-ply matrix failure (by yielding or microcracking) around the buckling fibers occurs before fiber breakage (see Figure 29). At the onset of matrix failure, the support from the matrix to the fibers would be correspondingly reduced. A further increase of the compressive strain would then yield a larger increase in the fiber curvature, further damaging the matrix and therefore reducing its support to the fibers, until final fiber failure.

- The present theory, valid for static loading, could serve as a guide for the build-up of a theory to model compressive fatigue behavior of multidirectional composites, an active area of research. The incorporation of interlaminar stresses in a theoretical model, as done herein, should be an essential feature of any fatigue theory owing to

the fatigue behavior of the matrix. The weakening support of the matrix to 0° fibers as the number of cycles increases could be incorporated in the in-plane microbuckling equation. This would lead to a criterion for in-plane kinking where the number of cycles would be a parameter.

BIBLIOGRAPHY

[1] Soutis C., Turkmen D., Applied Composite Materials **2**, p.327 (1995)

[2] Soutis C., Composites Science & Technology **42**, p.373 (1991)

[3] Bazhenov S., Kozey V., J. Materials Science **26** p.2677 (1991)

[4] Fleck N., Budiansky B., *1990 IUTAM Symposium* , p.235 (1990)

[5] Evans A., Adler W., Acta Metallurgica 26, p.725 (1978)

[6] Hahn T., Williams J., ASTM STP 893, p.115 (1986)

[7] Weaver C., Williams J., J. Materials Science **10**, p.1323 (1975)

[8] Moran P., Shih C., Soc. Engineering Science 32nd Meeting, p.383 (1995)

[9] Waas A.*et al.*, Int. J. Solids & Structures **26**, n°9, p.1071 (1990)

[10] Effendi R., Barrau J., Guedra D., Composite Structures **31**, n°2, p.87 (1995)

[11] Curtis P., Gates J., Molyneux C., Composites **22**, n°5, p.363 (1991)

[12] Tadjbakhsh I., Wang Y., Int. J. Solids & Structures **29**, n°24, p.3169 (1992)

[13] Shuart M., AIAA J. **27**, n°9, p.1274 (1989)

[14] Swanson S., J. Engineering Materials & Technology **114**, p.8 (1992)

[15] Shuart M., NASA Technical Memorandum 87640 (1985)

[16] Drapier S. *et al.*, J. Composites Science & Technology **56**, p.861 (1996)

[17] Sohi M., Hahn H., Williams J., ASTM STP 937, p.37 (1987)

[18] Guynn E., Bradley W., Ochoa O., J. Composite Materials **26**, p.1617 (1992)

[19] Wung E., Chaterjee S., J. Composite Materials **26**, n°13, p.1885 (1992)

[20] Jelf P., Fleck N., J. Composite Materials **26**, n°18 p.2706 (1992)

[21] Lankford J., J. Materials Science **30**, p.4343 (1995)

[22] Schultheisz C., Waas A., Progress in Aerospace Science **32**, pp.1-78 (1996)

[23] Rosen B., *Fiber Composite Materials*, ASM Seminar, p.37 (1964)

[24] Chung I., Weitsman Y., Int. J. Solids & Structures **31**, n°18, p.2519 (1994)

[25] Bazhenov S., Kozey V., J. Materials Science **26**, p.6764 (1991)

[26] Lo K., Chim E., J. Reinforced Plastics & Composites **11**, p.838 (1992)

[27] Herrmann R., Mason W., Chan S., J. Composite Materials **1**, p.212 (1967)

[28] Darby M., Kanellopoulos V., J. Physics D **20**, p.298 (1987)

[29] Taggart D., 8th Int. Conf. on Composite Materials, 35-D-1 (1991)

[30] Lagoudas D., Saleh A., J. Composite Materials **27**, n°1, p.83 (1993)

[31] Lagoudas D., Saleh A., 8th Int. Conf. on Composite Materials, 35-E-1 (1991)

[32] Lagoudas D., Tadsbakhsh I., Fares N., J. Applied Mechanics **58**, p.473 (1991)

[33] Hahn H., 6th Int. Conf. on Composite Materials, vol.1, p.269 (1987)

[34] Steif P., J. Composite Materials **22**, p.818 (1988)

[35] Waas A., Babcock C., Knauss W., J. Applied Mechanics **57**, p.138 (1990)

[36] Steif P.A., Int. J. Solids & Structures **26**, n°5-6, p.563 (1990)

[37] Frost S., J. Composite Materials **26**, n°8, p.1151 (1992)

[38] Wilczynski A., Composite Science & Technology **45**, p.37 (1992)

[39] Xu Y., Reifsnider K., J. Composite Materials **27**, n°6, p.572 (1993)

[40] Chung I., Weitsman Y., Int. J. Solids & Structures 32, n°16, p.2329 (1995)

[41] Häberle J., Matthews F., J. Composite Materials **28**, n°17, p.1618 (1994)

[42] Zhang G., Latour R., J. Composites Science & Technology **51**, p.95 (1994)

[43] Sadowsky M., Pu S., Hussain M., J. Applied Mechanics **34**, p.1011 (1967)

[44] Davis J., ASTM STP 580, p.364 (1975)

[45] Karayaka M., Sehitoglu H., J. Composite Materials **30**, n°10, p.1150 (1996)

[46] Mueller et al., J. Materials Science **31**, p.2247 (1996)

[47] Budiansky B., Computers & Structures 16, n°1-4, p.3 (1983)

[48] Budiansky B., Fleck N., J. Mechanics & Physics of Solids **41**, n°1,p.183 (1993)

[49] Slaughter W., Fleck L., J. Mechanics & Physics of Solids **42**, n°11,p.1743 (1994)

[50] Schapery R., Int. J. Solids & Structures **32**, n°6-7, p.739 (1995)

[51] Fleck N., Deng L., Budiansky B., J. Applied Mechanics **62**, p.329 (1995)

[52] Fleck N., Shu J., J. Mechanics & Physics of solids **43**, n°12, p.1887 (1995)

[53] Slaughter W., Fleck N., J. Applied Mechanics **60**, p.802 (1993)

[54] Liu X., Shih C., Soc. Engineering Science 32nd Meeting, p.333 (1995)

[55] Moran P., Liu X., Shih C., Acta Metallurg. et Materialia **43**, n°8, p.2943 (1995)

[56] Kyriakides S. *et al.*, Int. J. Solids & Structures **32**, n°6-7, p.689 (1995)

[57] Barbero E., Tomblin J., Int. J. Solids & Structures **33**, n°29, p.4379 (1996)

[58] Madhukar M., Drzal L., J. Composite Materials **26**, p.310 (1992)

[59] Sutcliffe M., Fleck L., Acta Metallurgica et Materialia **42**, n°7, p.2219 (1994)

[60] Chaudhuri R., Xie M., Garala H., J. Composite Materials **30**, n°6, p.672 (1996)

[61] Kominar V. *et al.*, J. Materials Science **30**, p. 2620 (1995)

[62] Chaudhuri R., J. Composite Materials **25**, p.1244 (1991)

[63] Berbinau P., Wolff E., 10th Int. Conf. on Composite Materials, v.1,p.609 (1995)

[64] Hong C., Kim D., 8th Int. Conf. on Composite Materials, 28-D-1 (1991)

[65] Kim D., Hong C., Composites Science & Technology **43**, p.147 (1992)

[66] Soutis C. *et al.*, J. Composite Materials **25**, p.1476 (1991)

[67] Soutis C., Fleck N., J. Composite Materials **24**, p.536 (1990)

[68] Harris C., Morris D., ASTM STP 864, p.153 (1985)

[69] Schulte K., ASTM STP 1185, p.278 (1994)

[70] Komorowski J. *et al.*, ASTM STP 1230, p.249 (1995)

[71] Komorowski *et al.*, 9th Int. Conf. on Composite Materials, vol.6, p.597 (1993)

[72] O'Brien T.K., ASTM STP 775, p.140 (1982)

[73] Pipes R., Pagano N., J. Composite Materials **4**, p.538 (1970)

[74] Pipes R., Pagano N., J. Composite Materials **5**, p.50 (1971)

[75] Pagano N., Soni S., Int. J. Solids & Structures **19**, n°3, p.207 (1983)

[76] Herakovich C. *et al, NASA-VPI Interim Report 46* (1984)

[77] Jones R., *Mechanics of Composite Materials*, p.210, Ed. Taylor & Francis (1975)

[78] Wang J., Dickson J., J. Composite Materials **12**, p.390 (1978)

[79] Bar-Joseph P., Pian T., J. Composite Materials **15**, p.225 (1981)

[80] Gu Q., Reddy J., Int. J. Non-linear Mechanics **27**, n°1, P.27 (1992)

[81] Schellekens J., De Borst R., Composite Structures **28**, p.357 (1994)

[82] Lessard L. *et al*, Int. J. Solids & Structures **33**, n°15, p.2243 (1996)

[83] Wang S., Choi I., J. Applied Mechanics **49**, p.549 (1982)

[84] Herakovich C., J. Composite Materials **15**, p.336 (1981)

[85] Joo J., Sun C., J. Composite Materials **26**, n°10, p.1510 (1992)

[86] Hsu P., Herakovich C., ASTM STP 617, p.296 (1977)

[87] Tang S., Levy S., J. Composite Materials **9**, p.41 (1975)

[88] Whitney J., ASTM STP 521, p.167 (1973)

[89] Puppo A., Evensen H., J. Composite Materials **4**, p.204 (1970)

[90] Lekhnitskii S., *Theory of Elasticity of an Anisotropic Body*, Ed. Holden (1963)

[91] Wang S., Choi I., J. Applied Mechanics **49**, p.541 (1982)

[92] Zwiers R., Ting T., Spilker R., J. Applied Mechanics **49**, p.561 (1982)

[93] Huang T., Chen W., Int. J. Solids & Structures **31**, n°22, p.3139 (1994)

[94] Pagano N., Rybicky E., J. Composite Materials **8**, p.214 (1974)

[95] Loo T., Int. Symp. on Composite Materials & Structures, Beijing, p.801 (1986)

[96] Wang A., *Interlaminar Response of Composite Materials*, p.93, Ed. Pagano (1989)

[97] Wang A., *Interlaminar Response of Composite Materials*, p.141, Ed. Pagano (1989)

[98] Lapusta Y., 11th European Conf. on Fracture, p.1633 (1996)

[99] Adams D., Odom E., J. Composite Materials **25**, p.774 (1991)

[100] Ha J., Nairn J., SAMPE Quarterly, p.29 (April 1992)

[101] Timoshenko S., Gere J.,*Theory of Elastic Stability*, p.9,Ed. McGraw-Hill (1961)

[102] Xu S., Weitsman Y., Composites Science & Technology **56**, p.1113 (1996)

APPENDICES

APPENDIX A

Compressive stress-strain curves
for the laminate $[\theta/-\theta/0_2/\theta/-\theta/0]_s$
for selected values of θ.

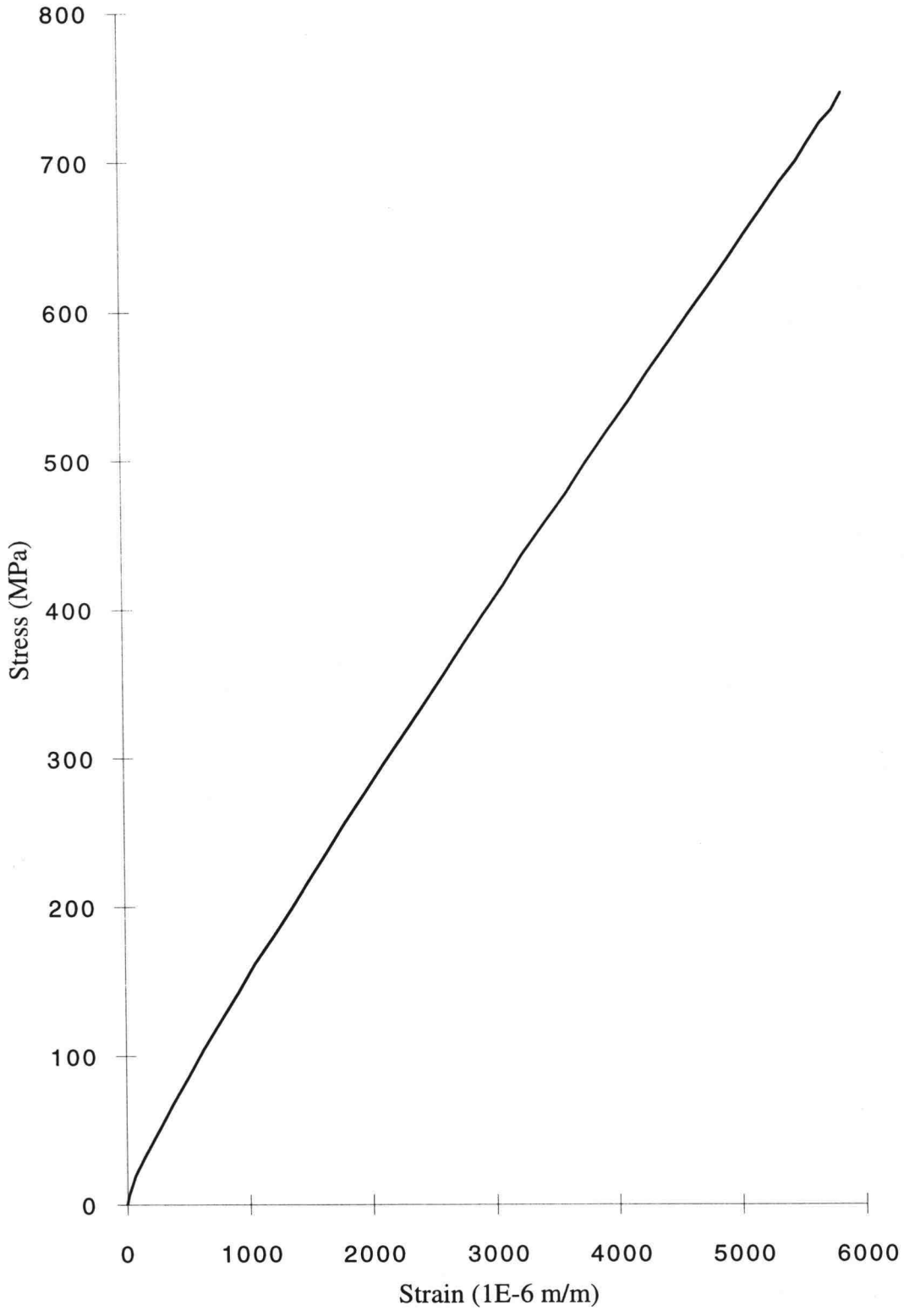

Figure A.1: Experimental stress-strain curve ($\theta = 10°$)

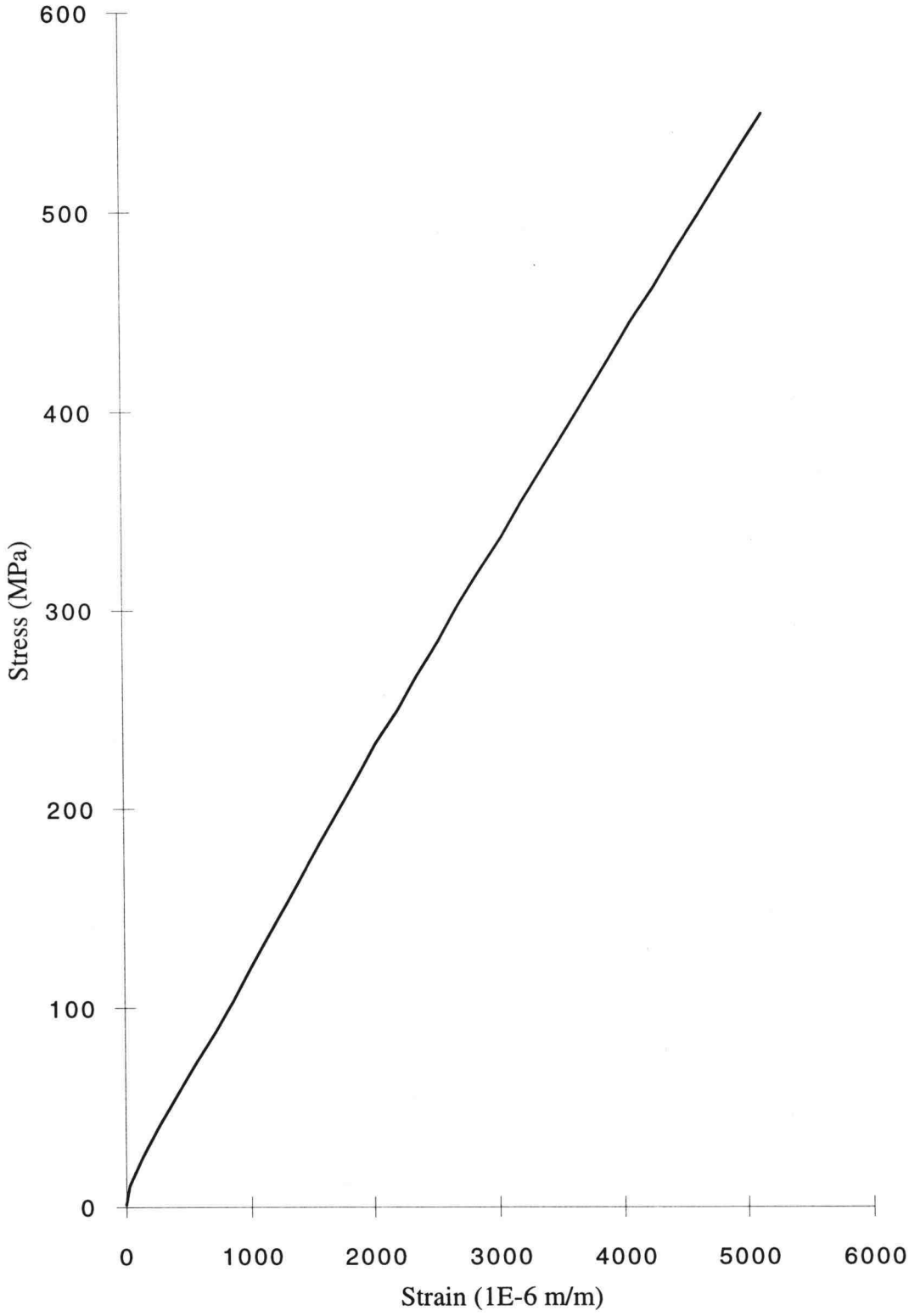

Figure A.2: Experimental stress-strain curve ($\theta = 20°$)

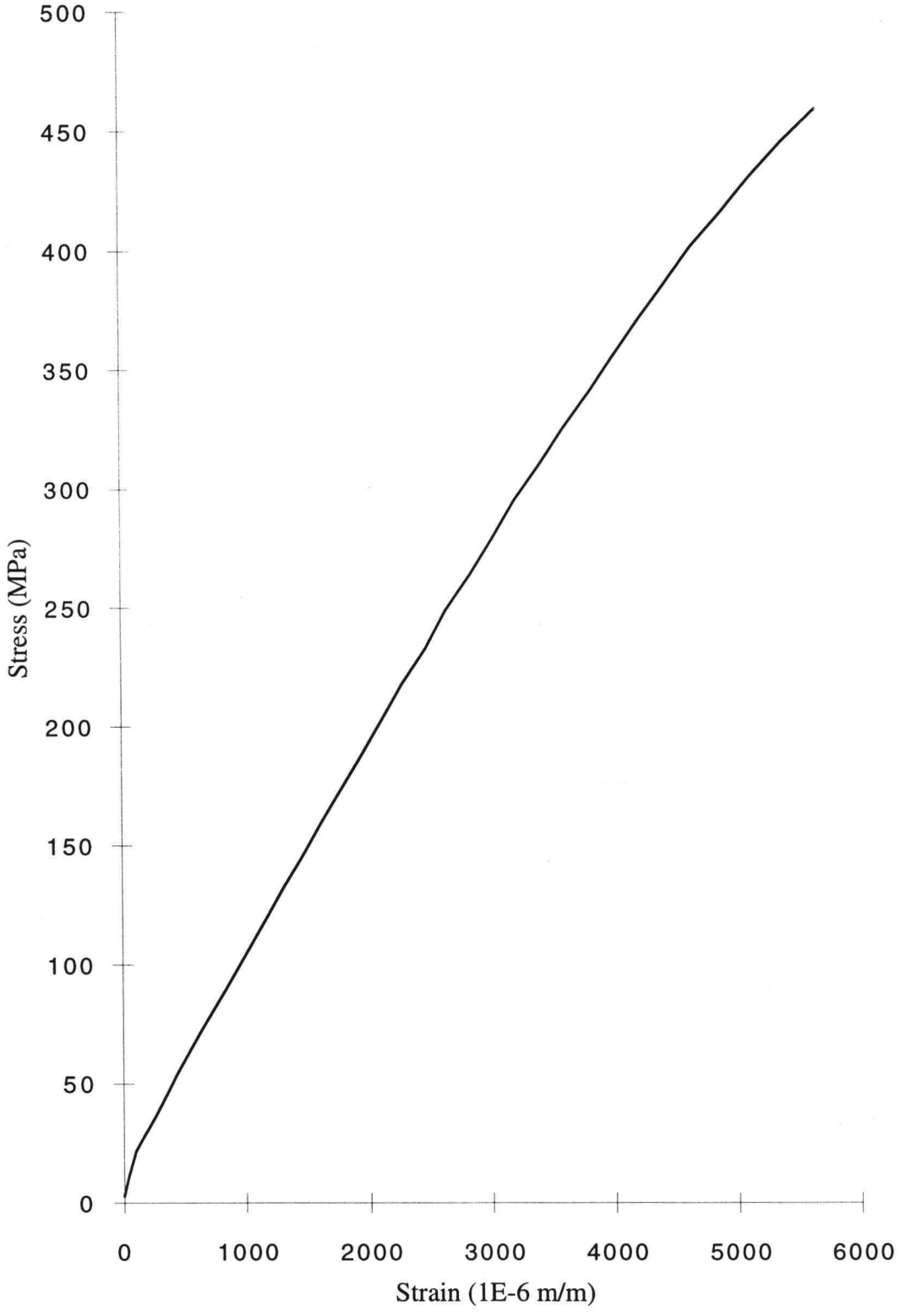

Figure A.3: Experimental stress-strain curve ($\theta = 30°$)

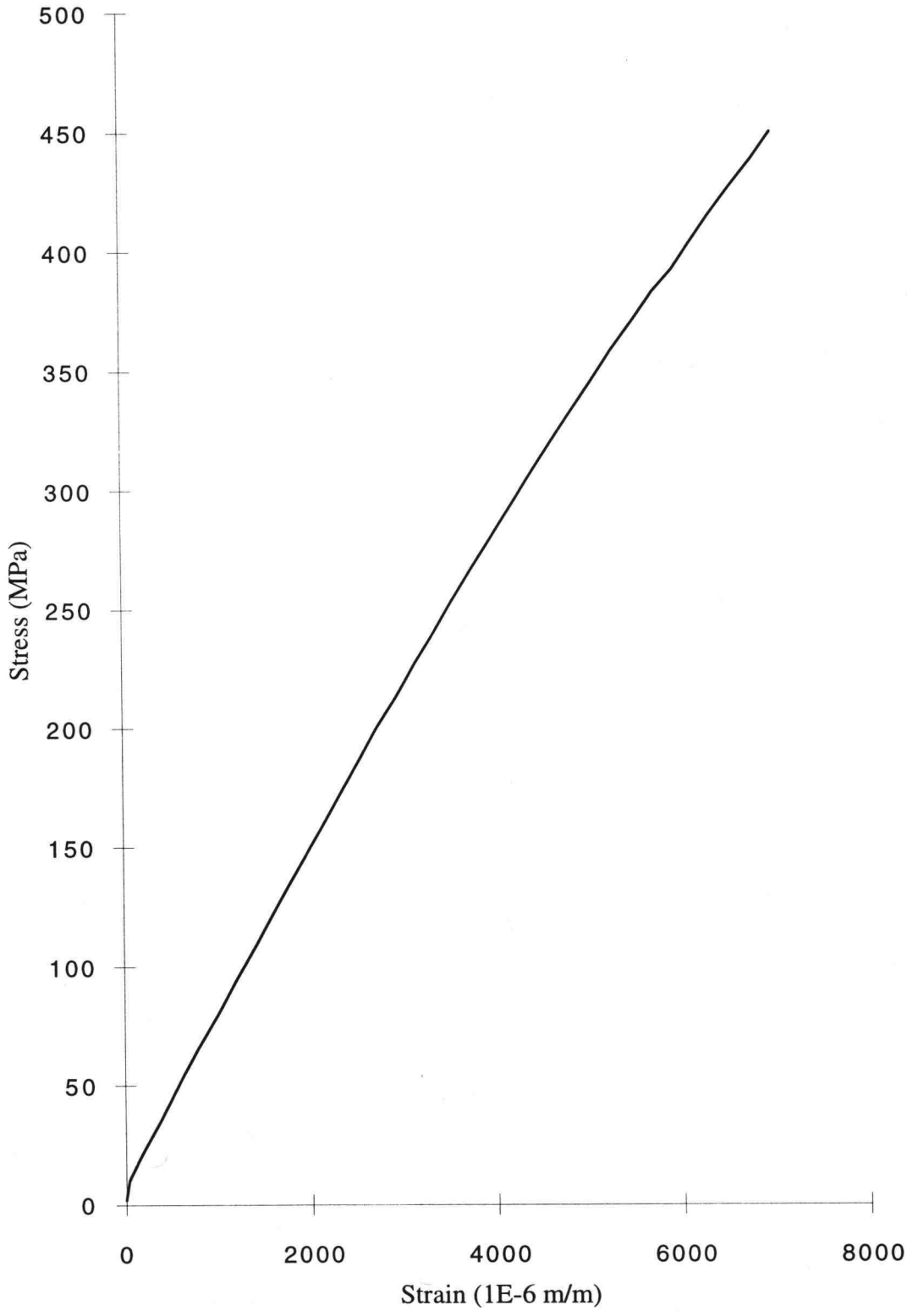

Figure A.4: Experimental stress-strain curve ($\theta = 40°$)

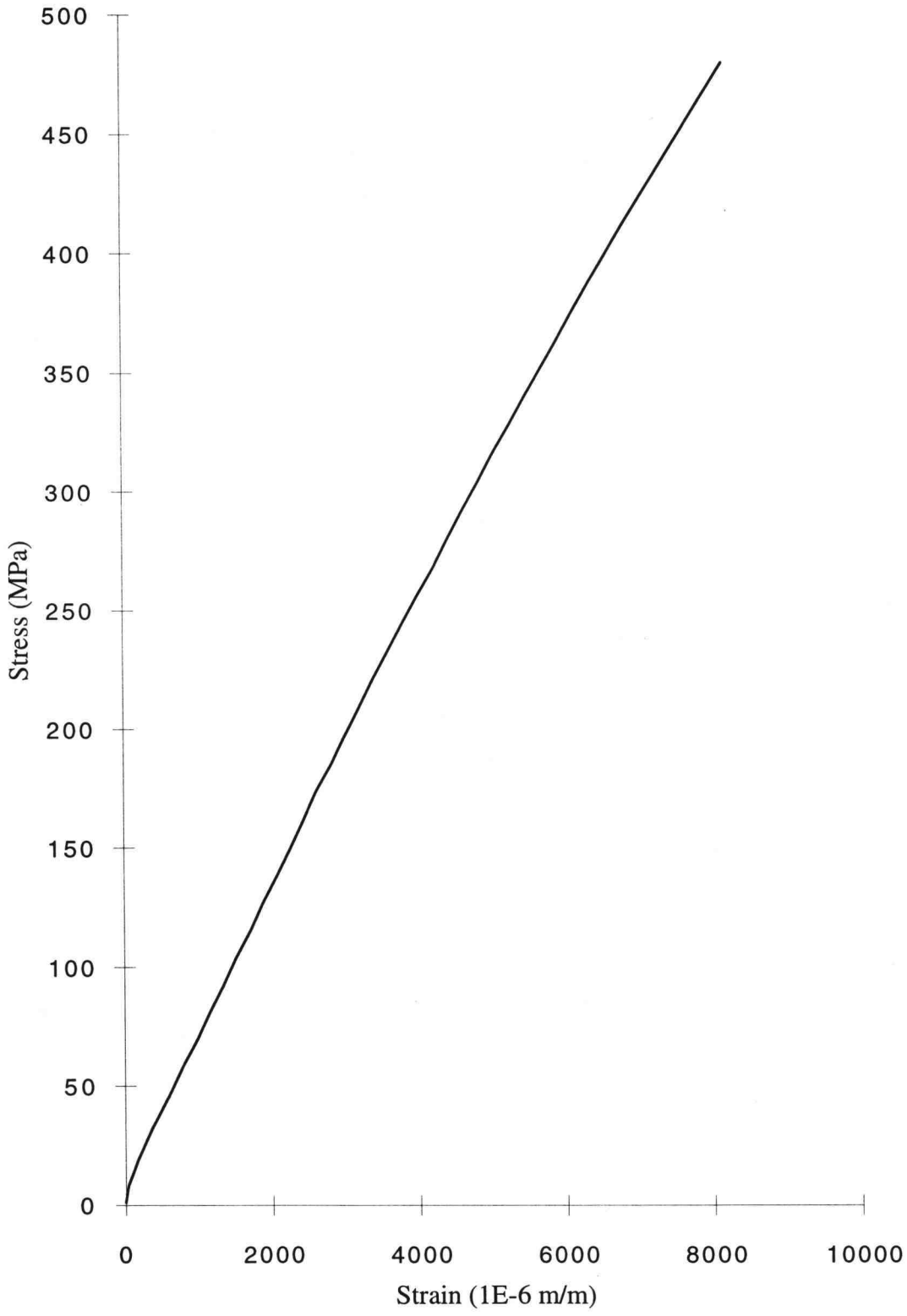

Figure A.5: Experimental stress-strain curve ($\theta = 50°$)

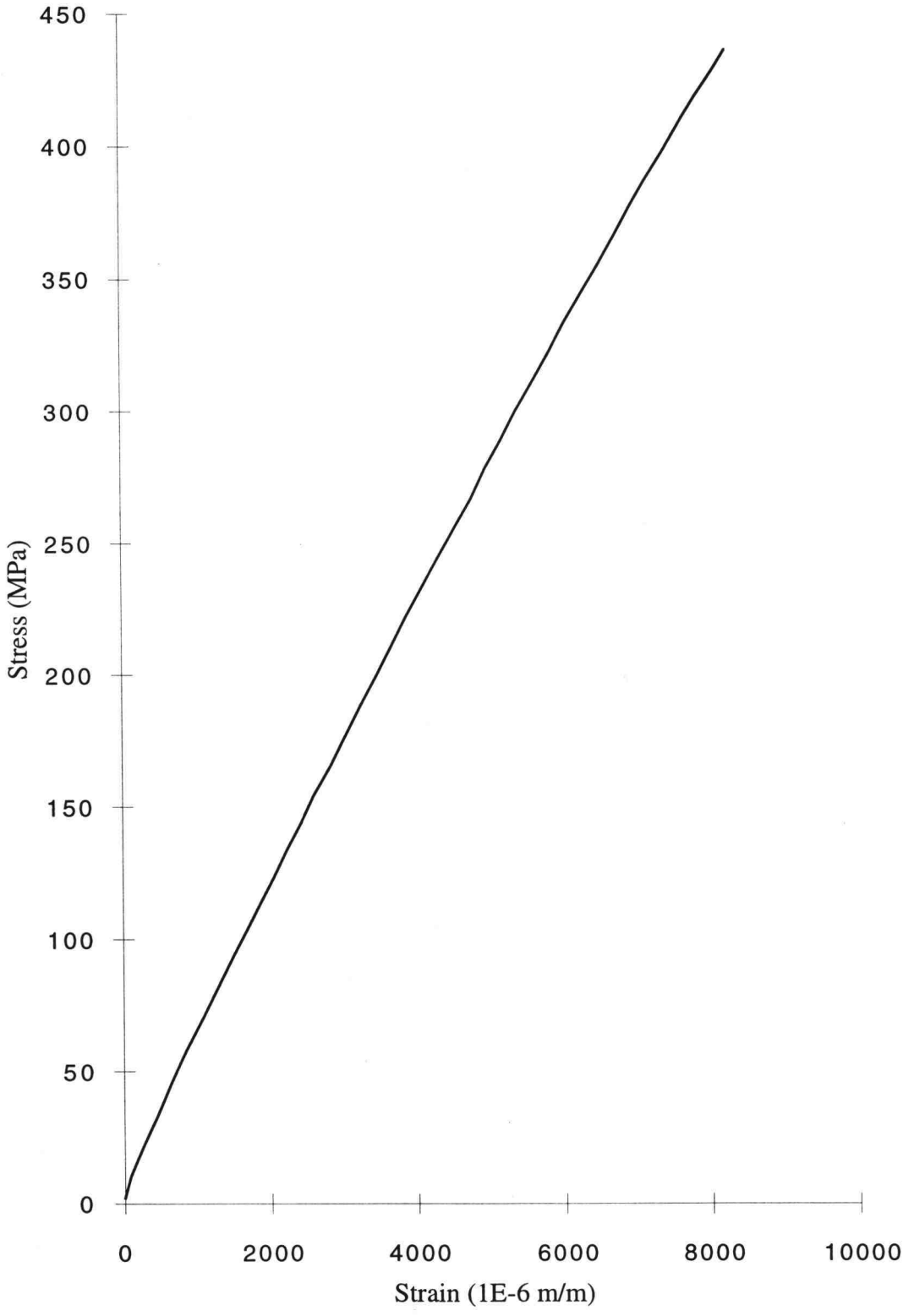

Figure A.6: Experimental stress-strain curve ($\theta = 60°$)

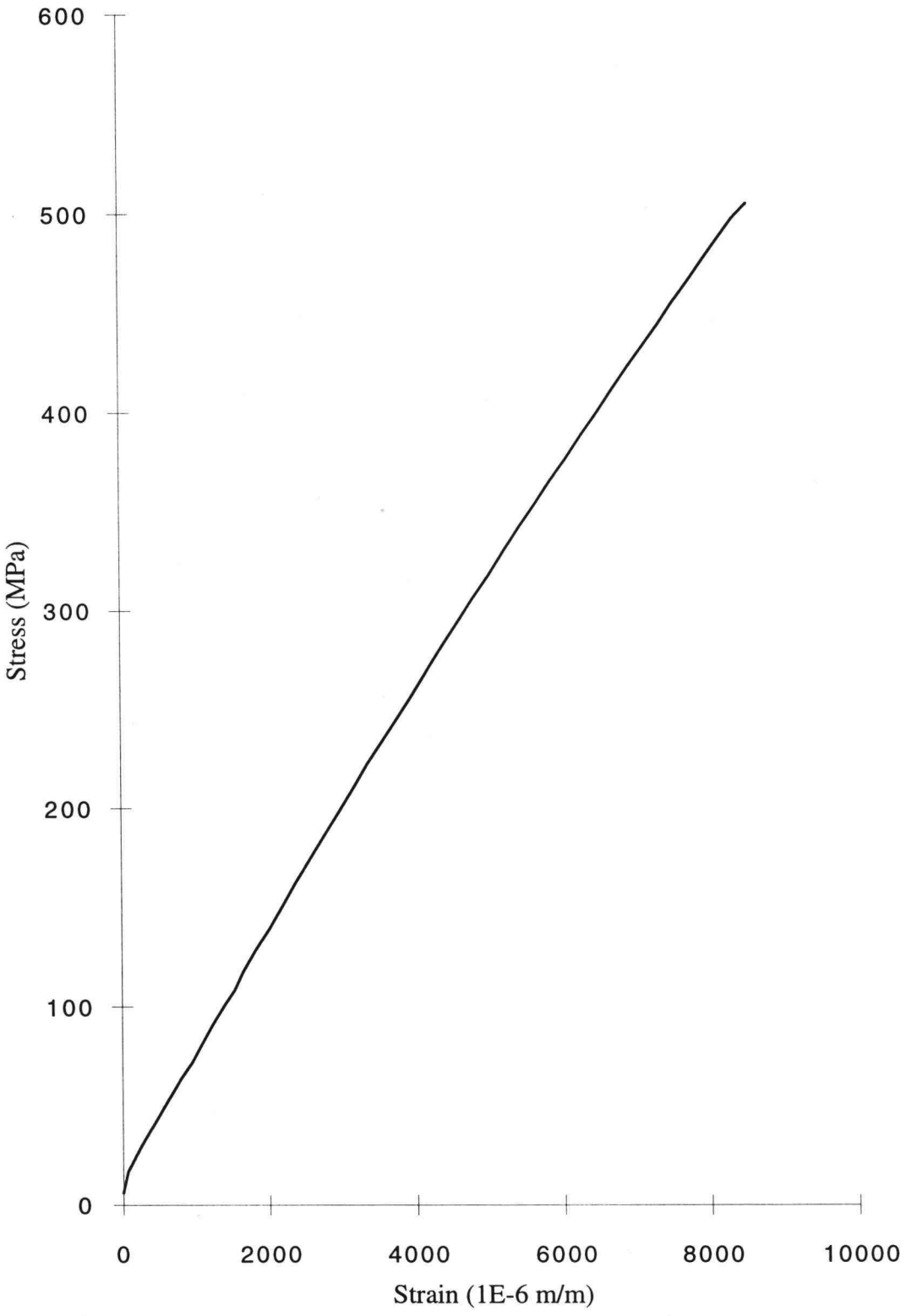

Figure A.7: Experimental stress-strain curve ($\theta = 70°$)

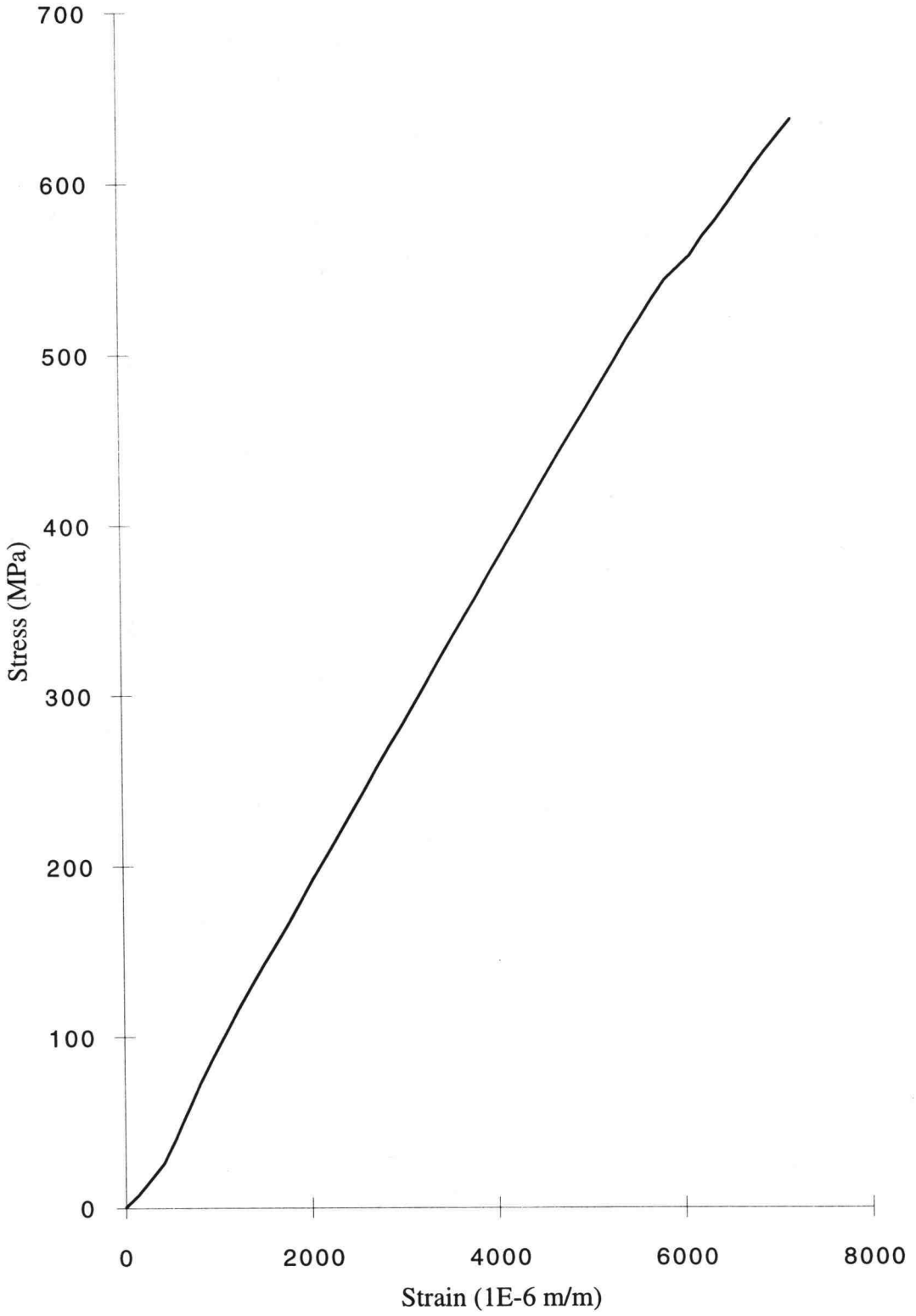

Figure A.8: Experimental stress-strain curve ($\theta = 80°$)

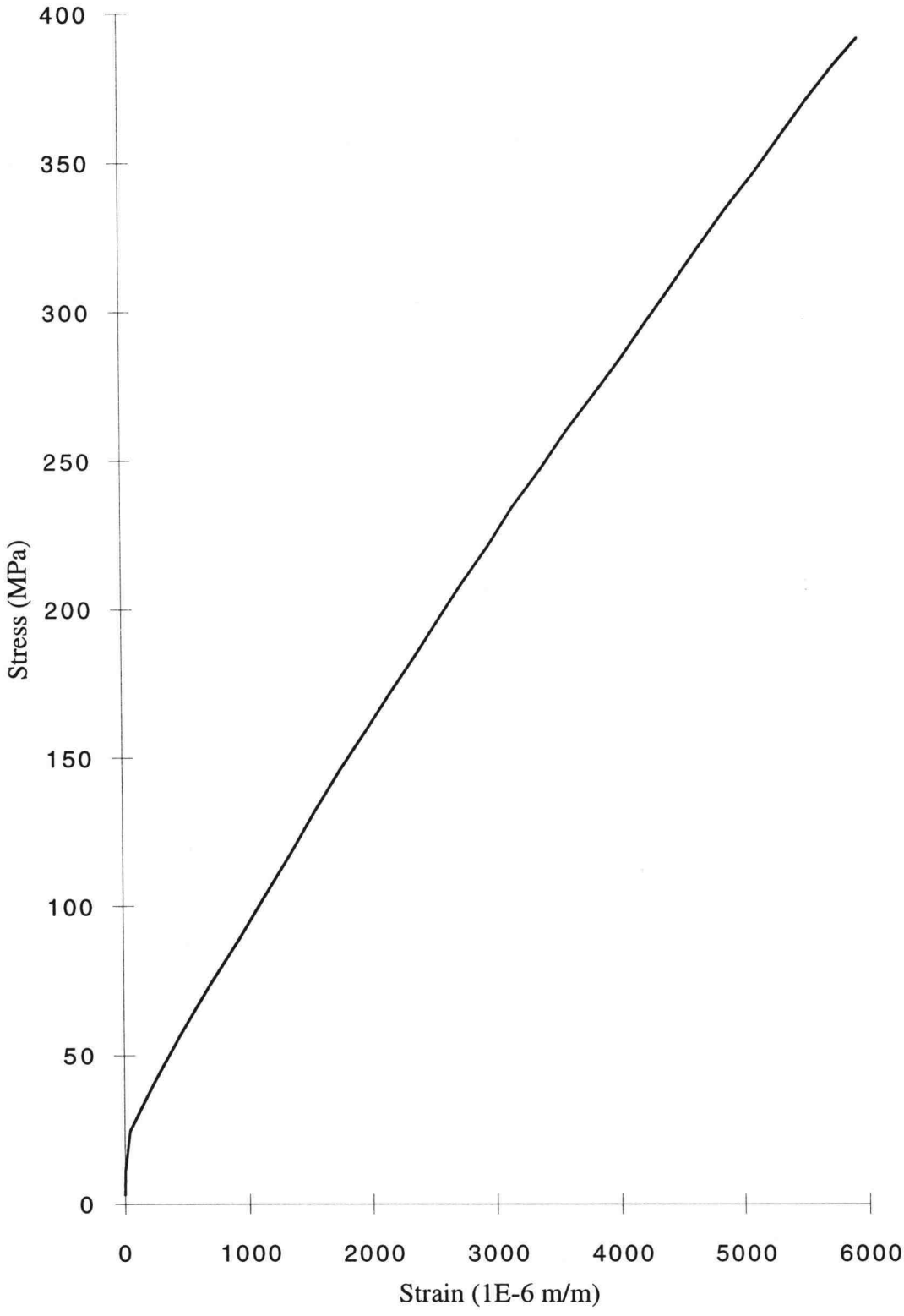

Figure A.9: Experimental stress-strain curve ($\theta = 90°$)

APPENDIX B

Program "Maple V" for the calculation
of interlaminar stresses τ_{zx} and τ_{zy}
for the laminate $[\theta/-\theta/0_2/\theta/-\theta/0]_s$

CALCULATION OF INTERLAMINAR SHEAR STRESSES FOR [theta/-theta/0/0/theta/-theta/0]s.

All quantities are in S.I. units, except stiffnesses which are in GPa. Final shear stresses are in Pa.

```
> Ef:=214:

> Em:=34*10^(-1):

> Gm:=13*10^(-1):

> nu12:=3*10^(-1):

> Vf:=6*10^(-1):

> E1:=Ef*Vf + Em*(1-Vf):

> E2:=Ef*Em/(Vf*Em + (1-Vf)*Ef):

> G:=Gm/(1-Vf):

> nu21:=nu12*E2/E1:

> e:=123*10^(-7):

> h:=123*10^(-6):

> L:=8*10^(-2):

> Wi:=127*10^(-4):
```

All calculations performed with an accuracy of "Digits" given below:

```
> Digits:=30:

> Q:=array([ [E1/(1-nu12*nu21), E2*nu12/(1-nu12*nu21),0], [E2*nu12/(1-nu12*n
> u21), E2/(1-nu12*nu21),0], [0,0,G] ]):

> Qb:=array(1..3,1..3):

> Qb[1,1]:=Q[1,1]*((cos(the/180*Pi))^4)+(2*Q[1,2]+4*Q[3,3])*((cos(the/180*Pi))^
> 2)*((sin(the/180*Pi))^2)+Q[2,2]*((sin(the/180*Pi))^4):

> Qb[1,2]:=(Q[1,1]+Q[2,2]- 4*Q[3,3])*((cos(the/180*Pi))^2)*((sin(the/180*Pi))^2)+
```

```
> Q[1,2]*(((sin(the/180*Pi))^4)+((cos(the/180*Pi))^4)):

> Qb[2,2]:=Q[1,1]*((sin(the/180*Pi))^4)+(2*Q[1,2]+4*Q[3,3])*((cos(the/180*Pi))^
> 2)*((sin(the/180*Pi))^2)+Q[2,2]*((cos(the/180*Pi))^4):

> Qb[1,3]:=(Q[1,1]- Q[1,2]- 2*Q[3,3])*(sin(the/180*Pi))*((cos(the/180*Pi))^3)+(Q[
> 1,2]- Q[2,2]+2*Q[3,3])*((sin(the/180*Pi))^3)*(cos(the/180*Pi)):

> Qb[2,3]:=(Q[1,1]- Q[1,2]- 2*Q[3,3])*((sin(the/180*Pi))^3)*(cos(the/180*Pi))+(Q[
> 1,2]- Q[2,2]+2*Q[3,3])*(sin(the/180*Pi))*((cos(the/180*Pi))^3):

> Qb[3,3]:=(Q[1,1]+Q[2,2]- 2*Q[1,2]- 2*Q[3,3])*((sin(the/180*Pi))^2)*((cos(the/18
> 0*Pi))^2)+Q[3,3]*(((sin(the/180*Pi))^4)+((cos(the/180*Pi))^4)):

> H:=array([Gm/(2*e*h),Gm/(2*e*h),Gm/(4*e*h),Gm/(2*e*h),Gm/(2*e*h),Gm/(2
> *e*h)]):

> AA:=array([ [Qb[3,3]*rho-H[1], Qb[2,3]*rho, H[1], 0, 0, 0, 0, 0, 0, 0, 0, 0],  [Qb[2
> ,3]*rho, Qb[2,2]*rho-H[1], 0, H[1], 0, 0, 0, 0, 0, 0, 0, 0], [H[2], 0, Qb[3,3]*rho-2*
> H[2], -Qb[2,3]*rho, H[2], 0, 0, 0, 0, 0, 0, 0], [0, H[2], -Qb[2,3]*rho, Qb[2,2]*rho-2
> *H[2], 0, H[2], 0, 0, 0, 0, 0, 0, 0],  [0, 0, H[3], 0, Q[3,3]*rho-2*H[3], 0, H[3], 0, 0, 0, 0
> , 0], [0, 0, 0, H[3], 0, Q[2,2]*rho-2*H[3], 0, H[3], 0, 0, 0, 0], [0, 0, 0, 0, H[4], 0, Qb[
> 3,3]*rho-2*H[4], Qb[2,3]*rho, H[4], 0, 0, 0], [0, 0, 0, 0, 0, H[4], Qb[2,3]*rho, Qb[
> 2,2]*rho-2*H[4], 0, H[4], 0, 0], [0, 0, 0, 0, 0, 0, H[5], 0, Qb[3,3]*rho-2*H[5], -Qb[
> 2,3]*rho, H[5], 0], [0, 0, 0, 0, 0, 0, 0, H[5], -Qb[2,3]*rho, Qb[2,2]*rho-2*H[5], 0,
> H[5]], [0, 0, 0, 0, 0, 0, 0, 0, H[6], 0, Q[3,3]*rho-H[6], 0], [0, 0, 0, 0, 0, 0, 0, 0, 0, H[6
> ], 0, Q[2,2]*rho-H[6]] ]):

> with(linalg):
  Warning: new definition for   norm
  Warning: new definition for   trace

> detAA:=det(AA):

  Calculation of all roots and coefficients for a given theta given below by
  "angletheta"

> angletheta:=50:

> detAAang:=subs(the=angletheta,detAA):


> rang := fsolve(detAAang=0,rho,fulldigits):
```

```
> rhos:=vector( [ rang[3], rang[4], rang[5], rang[6], rang[7], rang[8],  rang[9], ran
> g[10], rang[11], rang[12] ] ):

> Identity:=array([ [1, 0, 0], [0, 1, 0], [0, 0, 1] ]):

> Qb[2,1]:=Qb[1,2]:

> Qb[3,1]:=Qb[1,3]:

> Qb[3,2]:=Qb[2,3]:

> Qbm[1,1]:=Qb[1,1]:

> Qbm[1,2]:=Qb[1,2]:

> Qbm[2,2]:=Qb[2,2]:

> Qbm[3,3]:=Qb[3,3]:

> Qbm[1,3]:=- Qb[1,3]:

> Qbm[2,3]:=- Qb[2,3]:

> Qbm[2,1]:=Qbm[1,2]:

> Qbm[3,1]:=Qbm[1,3]:

> Qbm[3,2]:=Qbm[2,3]:


> the:=angletheta:

> R1:=array(1..3,1..3): for m to 3 do for n to 3 do R1[m,n]:=evalf(Qb[m,n]*rhos[i]
> - H[1]*Identity[m,n]) od od:

> R2:=array(1..3,1..3): for m to 3 do for n to 3 do R2[m,n]:=evalf(Qbm[m,n]*rhos[
> i] - 2*H[2]*Identity[m,n]) od od:

> R3:=array(1..3,1..3): for m to 3 do for n to 3 do R3[m,n]:=evalf(Q[m,n]*rhos[i] -
> 2*H[3]*Identity[m,n]) od od:

> R4:=array(1..3,1..3): for m to 3 do for n to 3 do R4[m,n]:=evalf(Qb[m,n]*rhos[i]
> - 2*H[4]*Identity[m,n]) od od:
```

```
> R5:=array(1..3,1..3): for m to 3 do for n to 3 do R5[m,n]:=evalf(Qbm[m,n]*rhos[
> i] - 2*H[5]*Identity[m,n]) od od:

> R6:=array(1..3,1..3): for m to 3 do for n to 3 do R6[m,n]:=evalf(Q[m,n]*rhos[i] -
> H[6]*Identity[m,n]) od od:

> eq1:=R133*A1+H[1]*A2+R123*B1=0:

> eq2:=R123*A1+R122*B1+H[1]*B2=0:

> eq3:=R233*A2+H[2]*A3+H[2]*A1+R223*B2=0:

> eq4:=R223*A2+R222*B2+H[2]*B3+H[2]*B1=0:

> eq5:=R333*A3+H[3]*A4+H[3]*A2+R323*B3=0:

> eq6:=R323*A3+R322*B3+H[3]*B4+H[3]*B2=0:

> eq7:=R433*A4+H[4]*A5+H[4]*A3+R423*B4=0:

> eq8:=R423*A4+R422*B4+H[4]*B5+H[4]*B3=0:

> eq9:=R533*A5+H[5]*A6+H[5]*A4+R523*B5=0:

> eq10:=R523*A5+R522*B5+H[5]*B6+H[5]*B4=0:

> eq11:=R633*A6+H[6]*A5+R623*B6=0:

> A1:='A1': A2:='A2': A3:='A3': A4:='A4': A5:='A5': A6:='A6': B1:='B1': B2
> :='B2': B3:='B3': B4:='B4': B5:='B5': B6:='B6':


> Z:=solve( {eq1,eq2,eq3,eq4,eq5,eq6,eq7,eq8,eq9,eq10,eq11}, {A2,A3,A4,A5,A6,B
> 1,B2,B3,B4,B5,B6} ):

> assign (Z):

> FacA2:=subs(R122=R1[2,2], R222=R2[2,2], R322=R3[2,2], R422=R4[2,2], R522
> =R5[2,2], R123=R1[2,3], R223=R2[2,3], R323=R3[2,3], R423=R4[2,3],R523=R5[
> 2,3], R623=R6[2,3], R133=R1[3,3], R233=R2[3,3], R333=R3[3,3],R433=R4[3,3],
> R533=R5[3,3], R633=R6[3,3], A1=1, A2):

> FacA3:=subs(R122=R1[2,2], R222=R2[2,2], R322=R3[2,2], R422=R4[2,2],R522=
```

```
> R5[2,2], R123=R1[2,3], R223=R2[2,3], R323=R3[2,3], R423=R4[2,3],R523=R5[2,
> 3], R623=R6[2,3], R133=R1[3,3], R233=R2[3,3], R333=R3[3,3],R433=R4[3,3], R
> 533=R5[3,3], R633=R6[3,3], A1=1, A3):

> FacA4:=subs(R122=R1[2,2], R222=R2[2,2], R322=R3[2,2], R422=R4[2,2],R522=
> R5[2,2], R123=R1[2,3], R223=R2[2,3], R323=R3[2,3], R423=R4[2,3],R523=R5[2,
> 3], R623=R6[2,3], R133=R1[3,3], R233=R2[3,3], R333=R3[3,3],R433=R4[3,3], R
> 533=R5[3,3], R633=R6[3,3], A1=1, A4):

> FacA5:=subs(R122=R1[2,2], R222=R2[2,2], R322=R3[2,2], R422=R4[2,2],R522=
> R5[2,2], R123=R1[2,3], R223=R2[2,3], R323=R3[2,3], R423=R4[2,3],R523=R5[2,
> 3], R623=R6[2,3], R133=R1[3,3], R233=R2[3,3], R333=R3[3,3],R433=R4[3,3], R
> 533=R5[3,3], R633=R6[3,3], A1=1, A5):

> FacA6:=subs(R122=R1[2,2], R222=R2[2,2], R322=R3[2,2], R422=R4[2,2],R522=
> R5[2,2], R123=R1[2,3], R223=R2[2,3], R323=R3[2,3], R423=R4[2,3],R523=R5[2,
> 3], R623=R6[2,3], R133=R1[3,3], R233=R2[3,3], R333=R3[3,3],R433=R4[3,3], R
> 533=R5[3,3], R633=R6[3,3], A1=1, A6):

> FacB1:=subs(R122=R1[2,2], R222=R2[2,2], R322=R3[2,2], R422=R4[2,2],R522=
> R5[2,2], R123=R1[2,3], R223=R2[2,3], R323=R3[2,3], R423=R4[2,3],R523=R5[2,
> 3], R623=R6[2,3], R133=R1[3,3], R233=R2[3,3], R333=R3[3,3],R433=R4[3,3], R
> 533=R5[3,3], R633=R6[3,3], A1=1, B1):

> FacB2:=subs(R122=R1[2,2], R222=R2[2,2], R322=R3[2,2], R422=R4[2,2],R522=
> R5[2,2], R123=R1[2,3], R223=R2[2,3], R323=R3[2,3], R423=R4[2,3],R523=R5[2,
> 3], R623=R6[2,3], R133=R1[3,3], R233=R2[3,3], R333=R3[3,3],R433=R4[3,3], R
> 533=R5[3,3], R633=R6[3,3], A1=1, B2):

> FacB3:=subs(R122=R1[2,2], R222=R2[2,2], R322=R3[2,2], R422=R4[2,2],R522=
> R5[2,2], R123=R1[2,3], R223=R2[2,3], R323=R3[2,3], R423=R4[2,3],R523=R5[2,
> 3], R623=R6[2,3], R133=R1[3,3], R233=R2[3,3], R333=R3[3,3],R433=R4[3,3], R
> 533=R5[3,3], R633=R6[3,3], A1=1, B3):

> FacB4:=subs(R122=R1[2,2], R222=R2[2,2], R322=R3[2,2], R422=R4[2,2],R522=
> R5[2,2], R123=R1[2,3], R223=R2[2,3], R323=R3[2,3], R423=R4[2,3],R523=R5[2,
> 3], R623=R6[2,3], R133=R1[3,3], R233=R2[3,3], R333=R3[3,3],R433=R4[3,3], R
> 533=R5[3,3], R633=R6[3,3], A1=1, B4):

> FacB5:=subs(R122=R1[2,2], R222=R2[2,2], R322=R3[2,2], R422=R4[2,2],R522=
> R5[2,2], R123=R1[2,3], R223=R2[2,3], R323=R3[2,3], R423=R4[2,3],R523=R5[2,
> 3], R623=R6[2,3], R133=R1[3,3], R233=R2[3,3], R333=R3[3,3],R433=R4[3,3], R
> 533=R5[3,3], R633=R6[3,3], A1=1, B5):
```

```
> FacB6:=subs(R122=R1[2,2], R222=R2[2,2], R322=R3[2,2], R422=R4[2,2],R522=
> R5[2,2], R123=R1[2,3], R223=R2[2,3], R323=R3[2,3], R423=R4[2,3],R523=R5[2,
> 3], R623=R6[2,3], R133=R1[3,3], R233=R2[3,3], R333=R3[3,3],R433=R4[3,3], R
> 533=R5[3,3], R633=R6[3,3], A1=1, B6):

> eq12:=R122*A1-R122=0:

> ZZ:=solve( {eq12}, {A1} ):

> assign (ZZ):

> FacA1:=subs(R122=R1[2,2], A1):


> MM21:=subs( i=1, ( Qbm[2,2]*(FacB2-FacB1)+Qbm[2,3]*(FacA2-FacA1) )*sqrt
> ( rhos[i] )*cosh( sqrt( rhos[i] )*Wi/2 )):

> MM31:=subs( i=1, ( Q[2,2]*(FacB3-FacB1)+Q[2,3]*(FacA3-FacA1) )*sqrt( rhos[
> i] )*cosh( sqrt( rhos[i] )*Wi/2 )):

> MM41:=subs( i=1, ( Qb[2,2]*(FacB4-FacB1)+Qb[2,3]*(FacA4-FacA1) )*sqrt( rh
> os[i] )*cosh( sqrt( rhos[i] )*Wi/2 )):

> MM51:=subs(i=1, ( Qbm[2,2]*(FacB5-FacB1)+Qbm[2,3]*(FacA5-FacA1) )*sqrt(
>  rhos[i] )*cosh( sqrt( rhos[i] )*Wi/2 )):

> MM61:=subs( i=1, ( Q[2,2]*(FacB6-FacB1)+Q[2,3]*(FacA6-FacA1) )*sqrt( rhos[
> i] )*cosh( sqrt( rhos[i] )*Wi/2 )):

> MM22:=subs( i=2, ( Qbm[2,2]*(FacB2-FacB1)+Qbm[2,3]*(FacA2-FacA1) )*sqrt
> ( rhos[i] )*cosh( sqrt( rhos[i] )*Wi/2 )):

> MM32:=subs( i=2, ( Q[2,2]*(FacB3-FacB1)+Q[2,3]*(FacA3-FacA1) )*sqrt( rhos[
> i] )*cosh( sqrt( rhos[i] )*Wi/2 )):

> MM42:=subs( i=2, ( Qb[2,2]*(FacB4-FacB1)+Qb[2,3]*(FacA4-FacA1) )*sqrt( rh
> os[i] )*cosh( sqrt( rhos[i] )*Wi/2 )):

> MM52:=subs( i=2, ( Qbm[2,2]*(FacB5-FacB1)+Qbm[2,3]*(FacA5-FacA1) )*sqrt
> ( rhos[i] )*cosh( sqrt( rhos[i] )*Wi/2 )):

> MM62:=subs( i=2, ( Q[2,2]*(FacB6-FacB1)+Q[2,3]*(FacA6-FacA1) )*sqrt( rhos[
> i] )*cosh( sqrt( rhos[i] )*Wi/2 )):
```

```
> MM23:=subs( i=3, ( Qbm[2,2]*(FacB2-FacB1)+Qbm[2,3]*(FacA2-FacA1) )*sqrt
> ( rhos[i] )*cosh( sqrt( rhos[i] )*Wi/2 )):

> MM33:=subs( i=3, ( Q[2,2]*(FacB3-FacB1)+Q[2,3]*(FacA3-FacA1) )*sqrt( rhos[
> i] )*cosh( sqrt( rhos[i] )*Wi/2 )):

> MM43:=subs( i=3, ( Qb[2,2]*(FacB4-FacB1)+Qb[2,3]*(FacA4-FacA1) )*sqrt( rh
> os[i] )*cosh( sqrt( rhos[i] )*Wi/2 )):

> MM53:=subs( i=3, ( Qbm[2,2]*(FacB5-FacB1)+Qbm[2,3]*(FacA5-FacA1) )*sqrt
> ( rhos[i] )*cosh( sqrt( rhos[i] )*Wi/2 )):

> MM63:=subs( i=3, ( Q[2,2]*(FacB6-FacB1)+Q[2,3]*(FacA6-FacA1) )*sqrt( rhos[
> i] )*cosh( sqrt( rhos[i] )*Wi/2 )):

> MM24:=subs( i=4, ( Qbm[2,2]*(FacB2-FacB1)+Qbm[2,3]*(FacA2-FacA1) )*sqrt
> ( rhos[i] )*cosh( sqrt( rhos[i] )*Wi/2 )):

> MM34:=subs( i=4, ( Q[2,2]*(FacB3-FacB1)+Q[2,3]*(FacA3-FacA1) )*sqrt( rhos[
> i] )*cosh( sqrt( rhos[i] )*Wi/2 )):

> MM44:=subs( i=4, ( Qb[2,2]*(FacB4-FacB1)+Qb[2,3]*(FacA4-FacA1) )*sqrt( rh
> os[i] )*cosh( sqrt( rhos[i] )*Wi/2 )):

> MM54:=subs( i=4, ( Qbm[2,2]*(FacB5-FacB1)+Qbm[2,3]*(FacA5-FacA1) )*sqrt
> ( rhos[i] )*cosh( sqrt( rhos[i] )*Wi/2 )):

> MM64:=subs( i=4, ( Q[2,2]*(FacB6-FacB1)+Q[2,3]*(FacA6-FacA1) )*sqrt( rhos[
> i] )*cosh( sqrt( rhos[i] )*Wi/2 )):

> MM25:=subs( i=5, ( Qbm[2,2]*(FacB2-FacB1)+Qbm[2,3]*(FacA2-FacA1) )*sqrt
> ( rhos[i] )*cosh( sqrt( rhos[i] )*Wi/2 )):

> MM35:=subs( i=5, ( Q[2,2]*(FacB3-FacB1)+Q[2,3]*(FacA3-FacA1) )*sqrt( rhos[
> i] )*cosh( sqrt( rhos[i] )*Wi/2 )):

> MM45:=subs( i=5, ( Qb[2,2]*(FacB4-FacB1)+Qb[2,3]*(FacA4-FacA1) )*sqrt( rh
> os[i] )*cosh( sqrt( rhos[i] )*Wi/2 )):

> MM55:=subs( i=5, ( Qbm[2,2]*(FacB5-FacB1)+Qbm[2,3]*(FacA5-FacA1) )*sqrt
> ( rhos[i] )*cosh( sqrt( rhos[i] )*Wi/2 )):

> MM65:=subs( i=5, ( Q[2,2]*(FacB6-FacB1)+Q[2,3]*(FacA6-FacA1) )*sqrt( rhos[
> i] )*cosh( sqrt( rhos[i] )*Wi/2 )):
```

```
> MM26:=subs( i=6, ( Qbm[2,2]*(FacB2-FacB1)+Qbm[2,3]*(FacA2-FacA1) )*sqrt
> ( rhos[i] )*cosh( sqrt( rhos[i] )*Wi/2 )):

> MM36:=subs( i=6, ( Q[2,2]*(FacB3-FacB1)+Q[2,3]*(FacA3-FacA1) )*sqrt( rhos[
> i] )*cosh( sqrt( rhos[i] )*Wi/2 )):

> MM46:=subs( i=6, ( Qb[2,2]*(FacB4-FacB1)+Qb[2,3]*(FacA4-FacA1) )*sqrt( rh
> os[i] )*cosh( sqrt( rhos[i] )*Wi/2 )):

> MM56:=subs( i=6, ( Qbm[2,2]*(FacB5-FacB1)+Qbm[2,3]*(FacA5-FacA1) )*sqrt
> ( rhos[i] )*cosh( sqrt( rhos[i] )*Wi/2 )):

> MM66:=subs( i=6, ( Q[2,2]*(FacB6-FacB1)+Q[2,3]*(FacA6-FacA1) )*sqrt( rhos[
> i] )*cosh( sqrt( rhos[i] )*Wi/2 )):

> MM27:=subs( i=7, ( Qbm[2,2]*(FacB2-FacB1)+Qbm[2,3]*(FacA2-FacA1) )*sqrt
> ( rhos[i] )*cosh( sqrt( rhos[i] )*Wi/2 )):

> MM37:=subs( i=7, ( Q[2,2]*(FacB3-FacB1)+Q[2,3]*(FacA3-FacA1) )*sqrt( rhos[
> i] )*cosh( sqrt( rhos[i] )*Wi/2 )):

> MM47:=subs( i=7, ( Qb[2,2]*(FacB4-FacB1)+Qb[2,3]*(FacA4-FacA1) )*sqrt( rh
> os[i] )*cosh( sqrt( rhos[i] )*Wi/2 )):

> MM57:=subs( i=7, ( Qbm[2,2]*(FacB5-FacB1)+Qbm[2,3]*(FacA5-FacA1) )*sqrt
> ( rhos[i] )*cosh( sqrt( rhos[i] )*Wi/2 )):

> MM67:=subs( i=7, ( Q[2,2]*(FacB6-FacB1)+Q[2,3]*(FacA6-FacA1) )*sqrt( rhos[
> i] )*cosh( sqrt( rhos[i] )*Wi/2 )):

> MM28:=subs( i=8, ( Qbm[2,2]*(FacB2-FacB1)+Qbm[2,3]*(FacA2-FacA1) )*sqrt
> ( rhos[i] )*cosh( sqrt( rhos[i] )*Wi/2 )):

> MM38:=subs( i=8, ( Q[2,2]*(FacB3-FacB1)+Q[2,3]*(FacA3-FacA1) )*sqrt( rhos[
> i] )*cosh( sqrt( rhos[i] )*Wi/2 )):

> MM48:=subs( i=8, ( Qb[2,2]*(FacB4-FacB1)+Qb[2,3]*(FacA4-FacA1) )*sqrt( rh
> os[i] )*cosh( sqrt( rhos[i] )*Wi/2 )):

> MM58:=subs( i=8, ( Qbm[2,2]*(FacB5-FacB1)+Qbm[2,3]*(FacA5-FacA1) )*sqrt
> ( rhos[i] )*cosh( sqrt( rhos[i] )*Wi/2 )):

> MM68:=subs( i=8, ( Q[2,2]*(FacB6-FacB1)+Q[2,3]*(FacA6-FacA1) )*sqrt( rhos[
```

```
> i] )*cosh( sqrt( rhos[i] )*Wi/2 )):

> MM29:=subs( i=9, ( Qbm[2,2]*(FacB2-FacB1)+Qbm[2,3]*(FacA2-FacA1) )*sqrt
> ( rhos[i] )*cosh( sqrt( rhos[i] )*Wi/2 )):

> MM39:=subs( i=9, ( Q[2,2]*(FacB3-FacB1)+Q[2,3]*(FacA3-FacA1) )*sqrt( rhos[
> i] )*cosh( sqrt( rhos[i] )*Wi/2 )):

> MM49:=subs( i=9, ( Qb[2,2]*(FacB4-FacB1)+Qb[2,3]*(FacA4-FacA1) )*sqrt( rh
> os[i] )*cosh( sqrt( rhos[i] )*Wi/2 )):

> MM59:=subs( i=9, ( Qbm[2,2]*(FacB5-FacB1)+Qbm[2,3]*(FacA5-FacA1) )*sqrt
> ( rhos[i] )*cosh( sqrt( rhos[i] )*Wi/2 )):

> MM69:=subs( i=9, ( Q[2,2]*(FacB6-FacB1)+Q[2,3]*(FacA6-FacA1) )*sqrt( rhos[
> i] )*cosh( sqrt( rhos[i] )*Wi/2 )):

> MM210:=subs( i=10, ( Qbm[2,2]*(FacB2-FacB1)+Qbm[2,3]*(FacA2-FacA1) )*s
> qrt( rhos[i] )*cosh( sqrt( rhos[i] )*Wi/2 )):

> MM310:=subs( i=10, ( Q[2,2]*(FacB3-FacB1)+Q[2,3]*(FacA3-FacA1) )*sqrt( rh
> os[i] )*cosh( sqrt( rhos[i] )*Wi/2 )):

> MM410:=subs( i=10, ( Qb[2,2]*(FacB4-FacB1)+Qb[2,3]*(FacA4-FacA1) )*sqrt(
> rhos[i] )*cosh( sqrt( rhos[i] )*Wi/2 )):

> MM510:=subs( i=10, ( Qbm[2,2]*(FacB5-FacB1)+Qbm[2,3]*(FacA5-FacA1) )*s
> qrt( rhos[i] )*cosh( sqrt( rhos[i] )*Wi/2 )):

> MM610:=subs( i=10, ( Q[2,2]*(FacB6-FacB1)+Q[2,3]*(FacA6-FacA1) )*sqrt( rh
> os[i] )*cosh( sqrt( rhos[i] )*Wi/2 )):

> NN21:=subs( i=1, ( Qbm[2,3]*(FacB2-FacB1)+Qbm[3,3]*(FacA2-FacA1) )*sqrt(
> rhos[i] )*cosh( sqrt( rhos[i] )*Wi/2 )):

> NN31:=subs( i=1, ( Q[2,3]*(FacB3-FacB1)+Q[3,3]*(FacA3-FacA1) )*sqrt( rhos[i
> ] )*cosh( sqrt( rhos[i] )*Wi/2 )):

> NN41:=subs( i=1, ( Qb[2,3]*(FacB4-FacB1)+Qb[3,3]*(FacA4-FacA1) )*sqrt( rho
> s[i] )*cosh( sqrt( rhos[i] )*Wi/2 )):

> NN51:=subs( i=1, ( Qbm[2,3]*(FacB5-FacB1)+Qbm[3,3]*(FacA5-FacA1) )*sqrt(
> rhos[i] )*cosh( sqrt( rhos[i] )*Wi/2 )):
```

```
> NN61:=subs( i=1, ( Q[2,3]*(FacB6-FacB1)+Q[3,3]*(FacA6-FacA1) )*sqrt( rhos[i
> ] )*cosh( sqrt( rhos[i] )*Wi/2 )):

> NN22:=subs( i=2, ( Qbm[2,3]*(FacB2-FacB1)+Qbm[3,3]*(FacA2-FacA1) )*sqrt(
> rhos[i] )*cosh( sqrt( rhos[i] )*Wi/2 )):

> NN32:=subs( i=2, ( Q[2,3]*(FacB3-FacB1)+Q[3,3]*(FacA3-FacA1) )*sqrt( rhos[i
> ] )*cosh( sqrt( rhos[i] )*Wi/2 )):

> NN42:=subs( i=2, ( Qb[2,3]*(FacB4-FacB1)+Qb[3,3]*(FacA4-FacA1) )*sqrt( rho
> s[i] )*cosh( sqrt( rhos[i] )*Wi/2 )):

> NN52:=subs( i=2, ( Qbm[2,3]*(FacB5-FacB1)+Qbm[3,3]*(FacA5-FacA1) )*sqrt(
> rhos[i] )*cosh( sqrt( rhos[i] )*Wi/2 )):

> NN62:=subs( i=2, ( Q[2,3]*(FacB6-FacB1)+Q[3,3]*(FacA6-FacA1) )*sqrt( rhos[i
> ] )*cosh( sqrt( rhos[i] )*Wi/2 )):

> NN23:=subs( i=3, ( Qbm[2,3]*(FacB2-FacB1)+Qbm[3,3]*(FacA2-FacA1) )*sqrt(
> rhos[i] )*cosh( sqrt( rhos[i] )*Wi/2 )):

> NN33:=subs( i=3, ( Q[2,3]*(FacB3-FacB1)+Q[3,3]*(FacA3-FacA1) )*sqrt( rhos[i
> ] )*cosh( sqrt( rhos[i] )*Wi/2 )):

> NN43:=subs( i=3, ( Qb[2,3]*(FacB4-FacB1)+Qb[3,3]*(FacA4-FacA1) )*sqrt( rho
> s[i] )*cosh( sqrt( rhos[i] )*Wi/2 )):

> NN53:=subs( i=3, ( Qbm[2,3]*(FacB5-FacB1)+Qbm[3,3]*(FacA5-FacA1) )*sqrt(
> rhos[i] )*cosh( sqrt( rhos[i] )*Wi/2 )):

> NN63:=subs( i=3, ( Q[2,3]*(FacB6-FacB1)+Q[3,3]*(FacA6-FacA1) )*sqrt( rhos[i
> ] )*cosh( sqrt( rhos[i] )*Wi/2 )):

> NN24:=subs( i=4, ( Qbm[2,3]*(FacB2-FacB1)+Qbm[3,3]*(FacA2-FacA1) )*sqrt(
> rhos[i] )*cosh( sqrt( rhos[i] )*Wi/2 )):

> NN34:=subs( i=4, ( Q[2,3]*(FacB3-FacB1)+Q[3,3]*(FacA3-FacA1) )*sqrt( rhos[i
> ] )*cosh( sqrt( rhos[i] )*Wi/2 )):

> NN44:=subs( i=4, ( Qb[2,3]*(FacB4-FacB1)+Qb[3,3]*(FacA4-FacA1) )*sqrt( rho
> s[i] )*cosh( sqrt( rhos[i] )*Wi/2 )):

> NN54:=subs( i=4, ( Qbm[2,3]*(FacB5-FacB1)+Qbm[3,3]*(FacA5-FacA1) )*sqrt(
> rhos[i] )*cosh( sqrt( rhos[i] )*Wi/2 )):
```

```
> NN64:=subs( i=4, ( Q[2,3]*(FacB6-FacB1)+Q[3,3]*(FacA6-FacA1) )*sqrt( rhos[i
> ] )*cosh( sqrt( rhos[i] )*Wi/2 )):

> NN25:=subs( i=5, ( Qbm[2,3]*(FacB2-FacB1)+Qbm[3,3]*(FacA2-FacA1) )*sqrt(
> rhos[i] )*cosh( sqrt( rhos[i] )*Wi/2 )):

> NN35:=subs( i=5, ( Q[2,3]*(FacB3-FacB1)+Q[3,3]*(FacA3-FacA1) )*sqrt( rhos[i
> ] )*cosh( sqrt( rhos[i] )*Wi/2 )):

> NN45:=subs( i=5, ( Qb[2,3]*(FacB4-FacB1)+Qb[3,3]*(FacA4-FacA1) )*sqrt( rho
> s[i] )*cosh( sqrt( rhos[i] )*Wi/2 )):

> NN55:=subs( i=5, ( Qbm[2,3]*(FacB5-FacB1)+Qbm[3,3]*(FacA5-FacA1) )*sqrt(
> rhos[i] )*cosh( sqrt( rhos[i] )*Wi/2 )):

> NN65:=subs( i=5, ( Q[2,3]*(FacB6-FacB1)+Q[3,3]*(FacA6-FacA1) )*sqrt( rhos[i
> ] )*cosh( sqrt( rhos[i] )*Wi/2 )):

> NN26:=subs( i=6, ( Qbm[2,3]*(FacB2-FacB1)+Qbm[3,3]*(FacA2-FacA1) )*sqrt(
> rhos[i] )*cosh( sqrt( rhos[i] )*Wi/2 )):

> NN36:=subs( i=6, ( Q[2,3]*(FacB3-FacB1)+Q[3,3]*(FacA3-FacA1) )*sqrt( rhos[i
> ] )*cosh( sqrt( rhos[i] )*Wi/2 )):

> NN46:=subs( i=6, ( Qb[2,3]*(FacB4-FacB1)+Qb[3,3]*(FacA4-FacA1) )*sqrt( rho
> s[i] )*cosh( sqrt( rhos[i] )*Wi/2 )):

> NN56:=subs( i=6, ( Qbm[2,3]*(FacB5-FacB1)+Qbm[3,3]*(FacA5-FacA1) )*sqrt(
> rhos[i] )*cosh( sqrt( rhos[i] )*Wi/2 )):

> NN66:=subs( i=6, ( Q[2,3]*(FacB6-FacB1)+Q[3,3]*(FacA6-FacA1) )*sqrt( rhos[i
> ] )*cosh( sqrt( rhos[i] )*Wi/2 )):

> NN27:=subs( i=7, ( Qbm[2,3]*(FacB2-FacB1)+Qbm[3,3]*(FacA2-FacA1) )*sqrt(
> rhos[i] )*cosh( sqrt( rhos[i] )*Wi/2 )):

> NN37:=subs( i=7, ( Q[2,3]*(FacB3-FacB1)+Q[3,3]*(FacA3-FacA1) )*sqrt( rhos[i
> ] )*cosh( sqrt( rhos[i] )*Wi/2 )):

> NN47:=subs( i=7, ( Qb[2,3]*(FacB4-FacB1)+Qb[3,3]*(FacA4-FacA1) )*sqrt( rho
> s[i] )*cosh( sqrt( rhos[i] )*Wi/2 )):

> NN57:=subs( i=7, ( Qbm[2,3]*(FacB5-FacB1)+Qbm[3,3]*(FacA5-FacA1) )*sqrt(
```

```
> rhos[i] )*cosh( sqrt( rhos[i] )*Wi/2 )):

> NN67:=subs( i=7, ( Q[2,3]*(FacB6-FacB1)+Q[3,3]*(FacA6-FacA1) )*sqrt( rhos[i
> ] )*cosh( sqrt( rhos[i] )*Wi/2 )):

> NN28:=subs(i=8, ( Qbm[2,3]*(FacB2-FacB1)+Qbm[3,3]*(FacA2-FacA1) )*sqrt(
> rhos[i] )*cosh( sqrt( rhos[i] )*Wi/2 )):

> NN38:=subs( i=8, ( Q[2,3]*(FacB3-FacB1)+Q[3,3]*(FacA3-FacA1) )*sqrt( rhos[i
> ] )*cosh( sqrt( rhos[i] )*Wi/2 )):

> NN48:=subs( i=8, ( Qb[2,3]*(FacB4-FacB1)+Qb[3,3]*(FacA4-FacA1) )*sqrt( rho
> s[i] )*cosh( sqrt( rhos[i] )*Wi/2 )):

> NN58:=subs( i=8, ( Qbm[2,3]*(FacB5-FacB1)+Qbm[3,3]*(FacA5-FacA1) )*sqrt(
> rhos[i] )*cosh( sqrt( rhos[i] )*Wi/2 )):

> NN68:=subs( i=8, ( Q[2,3]*(FacB6-FacB1)+Q[3,3]*(FacA6-FacA1) )*sqrt( rhos[i
> ] )*cosh( sqrt( rhos[i] )*Wi/2 )):

> NN29:=subs(i=9, ( Qbm[2,3]*(FacB2-FacB1)+Qbm[3,3]*(FacA2-FacA1) )*sqrt(
> rhos[i] )*cosh( sqrt( rhos[i] )*Wi/2 )):

> NN39:=subs(i=9, ( Q[2,3]*(FacB3-FacB1)+Q[3,3]*(FacA3-FacA1) )*sqrt( rhos[i]
>  )*cosh( sqrt( rhos[i] )*Wi/2 )):

> NN49:=subs( i=9, ( Qb[2,3]*(FacB4-FacB1)+Qb[3,3]*(FacA4-FacA1) )*sqrt( rho
> s[i] )*cosh( sqrt( rhos[i] )*Wi/2 )):

> NN59:=subs( i=9, ( Qbm[2,3]*(FacB5-FacB1)+Qbm[3,3]*(FacA5-FacA1) )*sqrt(
> rhos[i] )*cosh( sqrt( rhos[i] )*Wi/2 )):

> NN69:=subs( i=9, ( Q[2,3]*(FacB6-FacB1)+Q[3,3]*(FacA6-FacA1) )*sqrt( rhos[i
> ] )*cosh( sqrt( rhos[i] )*Wi/2 )):

> NN210:=subs( i=10, ( Qbm[2,3]*(FacB2-FacB1)+Qbm[3,3]*(FacA2-FacA1) )*sq
> rt( rhos[i] )*cosh( sqrt( rhos[i] )*Wi/2 )):

> NN310:=subs( i=10, ( Q[2,3]*(FacB3-FacB1)+Q[3,3]*(FacA3-FacA1) )*sqrt( rho
> s[i] )*cosh( sqrt( rhos[i] )*Wi/2 )):

> NN410:=subs( i=10, ( Qb[2,3]*(FacB4-FacB1)+Qb[3,3]*(FacA4-FacA1) )*sqrt( r
> hos[i] )*cosh( sqrt( rhos[i] )*Wi/2 )):
```

```
> NN510:=subs( i=10, ( Qbm[2,3]*(FacB5-FacB1)+Qbm[3,3]*(FacA5-FacA1) )*sq
> rt( rhos[i] )*cosh( sqrt( rhos[i] )*Wi/2 )):

> NN610:=subs( i=10, ( Q[2,3]*(FacB6-FacB1)+Q[3,3]*(FacA6-FacA1) )*sqrt( rho
> s[i] )*cosh( sqrt( rhos[i] )*Wi/2 )):

> RR2:=Qb[1,2]*(Qbm[2,2]*Qb[3,3] - Qbm[2,3]*Qb[2,3])/(Qb[2,2]*Qb[3,3] - Qb[2
> ,3]*Qb[2,3]) - Qbm[1,2] + Qb[1,3]*(Qbm[2,3]*Qb[2,2] - Qbm[2,2]*Qb[2,3])/(Qb[
> 2,2]*Qb[3,3] - Qb[2,3]*Qb[2,3]):

> RR3:=Qb[1,2]*(Q[2,2]*Qb[3,3] - Q[2,3]*Qb[2,3])/(Qb[2,2]*Qb[3,3] - Qb[2,3]*Q
> b[2,3]) - Q[1,2] + Qb[1,3]*(Q[2,3]*Qb[2,2] - Q[2,2]*Qb[2,3])/(Qb[2,2]*Qb[3,3] -
> Qb[2,3]*Qb[2,3]):

> RR4:=Qb[1,2]*(Qb[2,2]*Qb[3,3] - Qb[2,3]*Qb[2,3])/(Qb[2,2]*Qb[3,3] - Qb[2,3]*
> Qb[2,3]) - Qb[1,2] + Qb[1,3]*(Qb[2,3]*Qb[2,2] - Qb[2,2]*Qb[2,3])/(Qb[2,2]*Qb[
> 3,3] - Qb[2,3]*Qb[2,3]):

> RR5:=Qb[1,2]*(Qbm[2,2]*Qb[3,3] - Qbm[2,3]*Qb[2,3])/(Qb[2,2]*Qb[3,3] - Qb[2
> ,3]*Qb[2,3]) - Qbm[1,2] + Qb[1,3]*(Qbm[2,3]*Qb[2,2] - Qbm[2,2]*Qb[2,3])/(Qb[
> 2,2]*Qb[3,3] - Qb[2,3]*Qb[2,3]):

> RR6:=Qb[1,2]*(Q[2,2]*Qb[3,3] - Q[2,3]*Qb[2,3])/(Qb[2,2]*Qb[3,3] - Qb[2,3]*Q
> b[2,3]) - Q[1,2] + Qb[1,3]*(Q[2,3]*Qb[2,2] - Q[2,2]*Qb[2,3])/(Qb[2,2]*Qb[3,3] -
> Qb[2,3]*Qb[2,3]):

> SS2:=Qb[1,2]*(Qbm[2,3]*Qb[3,3] - Qbm[3,3]*Qb[2,3])/(Qb[2,2]*Qb[3,3] - Qb[2,
> 3]*Qb[2,3]) - Qbm[1,3] + Qb[1,3]*(Qbm[3,3]*Qb[2,2] - Qbm[2,3]*Qb[2,3])/(Qb[
> 2,2]*Qb[3,3] - Qb[2,3]*Qb[2,3]):

> SS3:=Qb[1,2]*(Q[2,3]*Qb[3,3] - Q[3,3]*Qb[2,3])/(Qb[2,2]*Qb[3,3] - Qb[2,3]*Qb
> [2,3]) - Q[1,3] + Qb[1,3]*(Q[3,3]*Qb[2,2] - Q[2,3]*Qb[2,3])/(Qb[2,2]*Qb[3,3] - Q
> b[2,3]*Qb[2,3]):

> SS4:=Qb[1,2]*(Qb[2,3]*Qb[3,3] - Qb[3,3]*Qb[2,3])/(Qb[2,2]*Qb[3,3] - Qb[2,3]*
> Qb[2,3]) - Qb[1,3] + Qb[1,3]*(Qb[3,3]*Qb[2,2] - Qb[2,3]*Qb[2,3])/(Qb[2,2]*Qb[
> 3,3] - Qb[2,3]*Qb[2,3]):

> SS5:=Qb[1,2]*(Qbm[2,3]*Qb[3,3] - Qbm[3,3]*Qb[2,3])/(Qb[2,2]*Qb[3,3] - Qb[2,
> 3]*Qb[2,3]) - Qbm[1,3] + Qb[1,3]*(Qbm[3,3]*Qb[2,2] - Qbm[2,3]*Qb[2,3])/(Qb[
> 2,2]*Qb[3,3] - Qb[2,3]*Qb[2,3]):

> SS6:=Qb[1,2]*(Q[2,3]*Qb[3,3] - Q[3,3]*Qb[2,3])/(Qb[2,2]*Qb[3,3] - Qb[2,3]*Qb
> [2,3]) - Q[1,3] + Qb[1,3]*(Q[3,3]*Qb[2,2] - Q[2,3]*Qb[2,3])/(Qb[2,2]*Qb[3,3] - Q
```

```
> b[2,3]*Qb[2,3]):

> eq21:=MM21*At1+MM22*At2+MM23*At3+MM24*At4+MM25*At5+MM26*
> At6+MM27*At7+MM28*At8+MM29*At9+MM210*At10=RR2:

> eq22:=MM31*At1+MM32*At2+MM33*At3+MM34*At4+MM35*At5+MM36*
> At6+MM37*At7+MM38*At8+MM39*At9+MM310*At10=RR3:

> eq23:=MM41*At1+MM42*At2+MM43*At3+MM44*At4+MM45*At5+MM46*
> At6+MM47*At7+MM48*At8+MM49*At9+MM410*At10=RR4:

> eq24:=MM51*At1+MM52*At2+MM53*At3+MM54*At4+MM55*At5+MM56*
> At6+MM57*At7+MM58*At8+MM59*At9+MM510*At10=RR5:

> eq25:=MM61*At1+MM62*At2+MM63*At3+MM64*At4+MM65*At5+MM66*
> At6+MM67*At7+MM68*At8+MM69*At9+MM610*At10=RR6:

> eq26:=NN21*At1+NN22*At2+NN23*At3+NN24*At4+NN25*At5+NN26*At6+N
> N27*At7+NN28*At8+NN29*At9+NN210*At10=SS2:

> eq27:=NN31*At1+NN32*At2+NN33*At3+NN34*At4+NN35*At5+NN36*At6+N
> N37*At7+NN38*At8+NN39*At9+NN310*At10=SS3:

> eq28:=NN41*At1+NN42*At2+NN43*At3+NN44*At4+NN45*At5+NN46*At6+N
> N47*At7+NN48*At8+NN49*At9+NN410*At10=SS4:

> eq29:=NN51*At1+NN52*At2+NN53*At3+NN54*At4+NN55*At5+NN56*At6+N
> N57*At7+NN58*At8+NN59*At9+NN510*At10=SS5:

> eq30:=NN61*At1+NN62*At2+NN63*At3+NN64*At4+NN65*At5+NN66*At6+N
> N67*At7+NN68*At8+NN69*At9+NN610*At10=SS6:

> At1:='At1': At2:='At2': At3:='At3': At4:='At4': At5:='At5': At6:='At6': At7:='A
> t7': At8:='At8': At9:='At9': At10:='At10':

> At:=solve( {eq21,eq22,eq23,eq24,eq25,eq26,eq27,eq28,eq29,eq30},{At1,At2,At3,
> At4,At5,At6,At7,At8,At9,At10} ):

> assign (At):

> Atf:=vector( [At1,At2,At3,At4,At5,At6,At7,At8,At9,At10] ):

> FacA:=vector( [1, FacA2, FacA3, FacA4, FacA5, FacA6] ):
```

```
> FacB:=vector( [FacB1, FacB2, FacB3, FacB4, FacB5, FacB6] ):
```

Definition of shear stresses at the interface k (between ply 'k' and ply 'k+1'):

```
> k:=2:

> ua:=-1*10^(-3):

> Tauzx:=(ua/L)*(Gm/(2*e))*( Atf[1]*(subs(i=1, FacA[k]-FacA[k+1]))*sinh( sqrt(
> rhos[1] )*y ) +Atf[2]*(subs(i=2, FacA[k]-FacA[k+1]))*sinh( sqrt( rhos[2] )*y ) +
> Atf[3]*(subs(i=3, FacA[k]-FacA[k+1]))*sinh( sqrt( rhos[3] )*y ) +Atf[4]*(subs(i=
> 4, FacA[k]-FacA[k+1]))*sinh( sqrt( rhos[4] )*y ) +Atf[5]*(subs(i=5, FacA[k]-Fac
> A[k+1]))*sinh( sqrt( rhos[5] )*y ) +Atf[6]*(subs(i=6, FacA[k]-FacA[k+1]))*sinh(
> sqrt( rhos[6] )*y ) +Atf[7]*(subs(i=7, FacA[k]-FacA[k+1]))*sinh( sqrt( rhos[7] )*
> y ) +Atf[8]*(subs(i=8, FacA[k]-FacA[k+1]))*sinh( sqrt( rhos[8] )*y ) +Atf[9]*(su
> bs(i=9, FacA[k]-FacA[k+1]))*sinh( sqrt( rhos[9] )*y ) +Atf[10]*(subs(i=10, FacA
> [k]-FacA[k+1]))*sinh( sqrt( rhos[10] )*y ) ):

>  Tauzy:=(ua/L)*(Gm/(2*e))*( Atf[1]*(subs(i=1, FacB[k]-FacB[k+1]))*sinh( sqrt(
> rhos[1] )*y ) +Atf[2]*(subs(i=2, FacB[k]-FacB[k+1]))*sinh( sqrt( rhos[2] )*y ) +A
> tf[3]*(subs(i=3, FacB[k]-FacB[k+1]))*sinh( sqrt( rhos[3] )*y ) +Atf[4]*(subs(i=4,
> FacB[k]-FacB[k+1]))*sinh( sqrt( rhos[4] )*y ) +Atf[5]*(subs(i=5, FacB[k]-FacB[
> k+1]))*sinh( sqrt( rhos[5] )*y ) +Atf[6]*(subs(i=6, FacB[k]-FacB[k+1]))*sinh( sq
> rt( rhos[6] )*y ) +Atf[7]*(subs(i=7, FacB[k]-FacB[k+1]))*sinh( sqrt( rhos[7] )*y )
>  +Atf[8]*(subs(i=8, FacB[k]-FacB[k+1]))*sinh( sqrt( rhos[8] )*y ) +Atf[9]*(subs(i
> =9, FacB[k]-FacB[k+1]))*sinh( sqrt( rhos[9] )*y ) +Atf[10]*(subs(i=10, FacB[k]-
> FacB[k+1]))*sinh( sqrt( rhos[10] )*y ) ):


> val:=subs(y=Wi/2,Tauzy*10^9):

> Digits:=10:

> val;
```

$$-.2431958723\ 10^{8}$$

```
> plot({Tauzx*10^9,Tauzy*10^9},y=0..Wi/2);

> the;
```

$$50$$

```
>
```

SPECIAL CASE OF theta=90*.

```
> Ef:=214:

> Em:=34*10^(-1):

> Gm:=13*10^(-1):

> nu12:=3*10^(-1):

> Vf:=6*10^(-1):

> E1:=Ef*Vf + Em*(1-Vf):

> E2:=Ef*Em/(Vf*Em + (1-Vf)*Ef):

> G:=Gm/(1-Vf):

> nu21:=nu12*E2/E1:

> e:=123*10^(-7):

> h:=123*10^(-6):

> L:=8*10^(-2):

> Wi:=127*10^(-4):

> Q:=array([ [E1/(1-nu12*nu21), E2*nu12/(1-nu12*nu21),0], [E2*nu12/(1-nu12*n
> u21), E2/(1-nu12*nu21),0], [0,0,G] ]):


> Qb:=array(1..3,1..3):

> Qb[1,1]:=Q[2,2]:

> Qb[1,2]:=Q[1,2]:

> Qb[2,2]:=Q[1,1]:

> Qb[1,3]:=0:

> Qb[2,3]:=0:
```

```
> Qb[3,3]:=Q[3,3]:

> H:=array([ Gm/(4*e*h),Gm/(4*e*h),Gm/(4*e*h),Gm/(2*e*h) ]):

> f:'f': f:=rho-> ((Qb[2,2]*Q[2,2])^2)*(rho^3) - ( Qb[2,2]*(H[4]+2*H[2])+Q[2,2]*(
> H[1]+2*H[3]) )*Qb[2,2]*Q[2,2]*(rho^2) + (Qb[2,2]*Q[2,2]*(H[1]*H[2]+H[3]*H[
> 4]+H[1]*H[4]+3*H[2]*H[3])+2*H[2]*H[4]*(Qb[2,2]^2)+2*H[1]*H[3]*(Q[2,2]^2
> ) )*rho - ( Qb[2,2]*(H[2]*H[3]*H[4]+H[1]*H[2]*H[4])+Q[2,2]*(H[1]*H[3]*H[4]
> +H[1]*H[2]*H[3]) ):

> plot(f(rho), rho=5.1*10^7..5.5*10^7):

> Digits:=30:


> eq1:= ((Qb[2,2]*Q[2,2])^2)*(rho^3) - ( Qb[2,2]*(H[4]+2*H[2])+Q[2,2]*(H[1]+2*
> H[3]) )*Qb[2,2]*Q[2,2]*(rho^2)+( Qb[2,2]*Q[2,2]*(H[1]*H[2]+H[3]*H[4]+H[1]*
> H[4]+3*H[2]*H[3])+2*H[2]*H[4]*(Qb[2,2]^2)+2*H[1]*H[3]*(Q[2,2]^2) )*rho - (
>  Qb[2,2]*(H[2]*H[3]*H[4]+H[1]*H[2]*H[4])+Q[2,2]*(H[1]*H[3]*H[4]+H[1]*H[
> 2]*H[3]) )=0:

> with(linalg):
  Warning: new definition for   norm
  Warning: new definition for   trace

> rhos:=fsolve(eq1,rho,fulldigits):

> Identity:=array([ [1, 0, 0], [0, 1, 0], [0, 0, 1] ]):

> Qb[2,1]:=Qb[1,2]:

> Qb[3,1]:=Qb[1,3]:

> Qb[3,2]:=Qb[2,3]:



> R1:=array(1..3,1..3): for m to 3 do for n to 3 do R1[m,n]:=evalf(Qb[m,n]*rhos[i]
> - H[1]*Identity[m,n]) od od:

> R2:=array(1..3,1..3): for m to 3 do for n to 3 do R2[m,n]:=evalf(Q[m,n]*rhos[i] -
> 2*H[2]*Identity[m,n]) od od:

> R3:=array(1..3,1..3): for m to 3 do for n to 3 do R3[m,n]:=evalf(Qb[m,n]*rhos[i]
```

```
> - 2*H[3]*Identity[m,n]) od od:

> FacB2:= -R1[2,2]/H[1]:

> FacB3:= -1 + R2[2,2]*R1[2,2]/(H[1]*H[2]):

> FacB4:=R1[2,2]/H[1] + R3[2,2]/H[3] - R3[2,2]*R2[2,2]*R1[2,2]/(H[1]*H[2]*H[3]
> ):

> MM21:=subs(i=1, (FacB2-1)*sqrt(rhos[i])*cosh( sqrt(rhos[i])*Wi/2 )):

> MM31:=subs(i=1, (FacB3-1)*sqrt(rhos[i])*cosh( sqrt(rhos[i])*Wi/2 )):

> MM41:=subs(i=1, (FacB4-1)*sqrt(rhos[i])*cosh( sqrt(rhos[i])*Wi/2 )):

> MM22:=subs(i=2, (FacB2-1)*sqrt(rhos[i])*cosh( sqrt(rhos[i])*Wi/2 )):

> MM32:=subs(i=2, (FacB3-1)*sqrt(rhos[i])*cosh( sqrt(rhos[i])*Wi/2 )):

> MM42:=subs(i=2, (FacB4-1)*sqrt(rhos[i])*cosh( sqrt(rhos[i])*Wi/2 )):

> MM23:=subs(i=3, (FacB2-1)*sqrt(rhos[i])*cosh( sqrt(rhos[i])*Wi/2 )):

> MM33:=subs(i=3, (FacB3-1)*sqrt(rhos[i])*cosh( sqrt(rhos[i])*Wi/2 )):

> MM43:=subs(i=3, (FacB4-1)*sqrt(rhos[i])*cosh( sqrt(rhos[i])*Wi/2 )):

> RR2:=(Q[2,2]*Qb[1,2] - Qb[2,2]*Q[1,2])/(Q[2,2]*Qb[2,2]):

> RR3:=(Qb[2,2]*Qb[1,2] - Qb[2,2]*Qb[1,2])/(Q[2,2]*Qb[2,2]):

> RR4:=(Q[2,2]*Qb[1,2] - Qb[2,2]*Q[1,2])/(Q[2,2]*Qb[2,2]):

> eq21:=MM21*Bt1+MM22*Bt2+MM23*Bt3=RR2:

> eq22:=MM31*Bt1+MM32*Bt2+MM33*Bt3=RR3:

> eq23:=MM41*Bt1+MM42*Bt2+MM43*Bt3=RR4:

> Bt1:='Bt1': Bt2:='Bt2': Bt3:='Bt3':

> Bt:=solve( {eq21,eq22,eq23}, {Bt1,Bt2,Bt3} ):
```

```
> assign (Bt):

> Btf:=vector( [Bt1,Bt2,Bt3] ):

> FacB:=vector( [1, FacB2, FacB3,FacB4] ):

  Definition of shear stresses at the interface  k
  (for the angle defined in "angletheta"):

> k:=1:

> ua:=-1*10^(-3):

>  Tauzy:=(ua/L)*(Gm/(2*e))*( Btf[1]*(subs(i=1, FacB[k]-FacB[k+1]))*sinh( sqrt(
> rhos[1] )*y ) + Btf[2]*(subs(i=2, FacB[k]-FacB[k+1]))*sinh( sqrt( rhos[2] )*y ) +
> Btf[3]*(subs(i=3, FacB[k]-FacB[k+1]))*sinh( sqrt( rhos[3] )*y ) ):


> Digits:=10:

> val:=subs(y=Wi/2,Tauzy*10^9):

> val;

                                -.2713002983 10^8

> plot({0,Tauzy*10^9},y=0..Wi/2);

>
```

APPENDIX C

Curves τ_{zx} and τ_{zy} as a function of y

at interfaces 2,3, and 5

for the laminate $[\theta/-\theta/0_2/\theta/-\theta/0]_s$

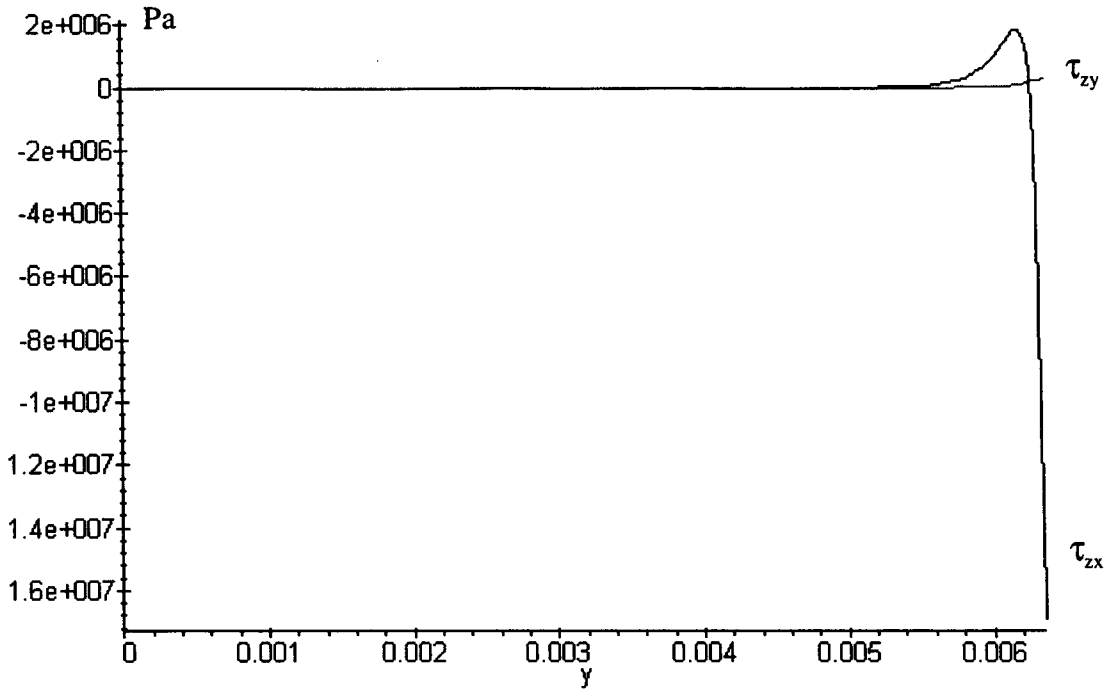

Figure C.1: Plots of τ_{zx} and τ_{zy} as a function of y $(0 < y < Wi/2)$ for u_a=-10^{-3} m. (Angle $\theta = 1^{o}$, Interface 2)

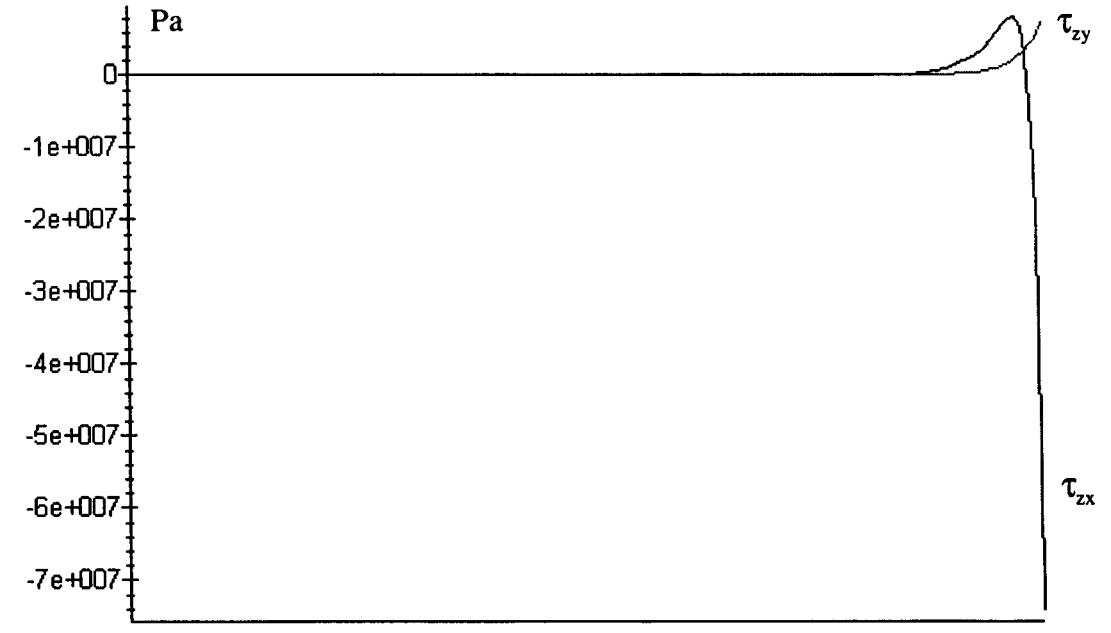

Figure C.2: Plots of τ_{zx} and τ_{zy} as a function of y $(0 < y < Wi/2)$ for u_a=-10^{-3} m. (Angle $\theta = 5^{o}$, Interface 2)

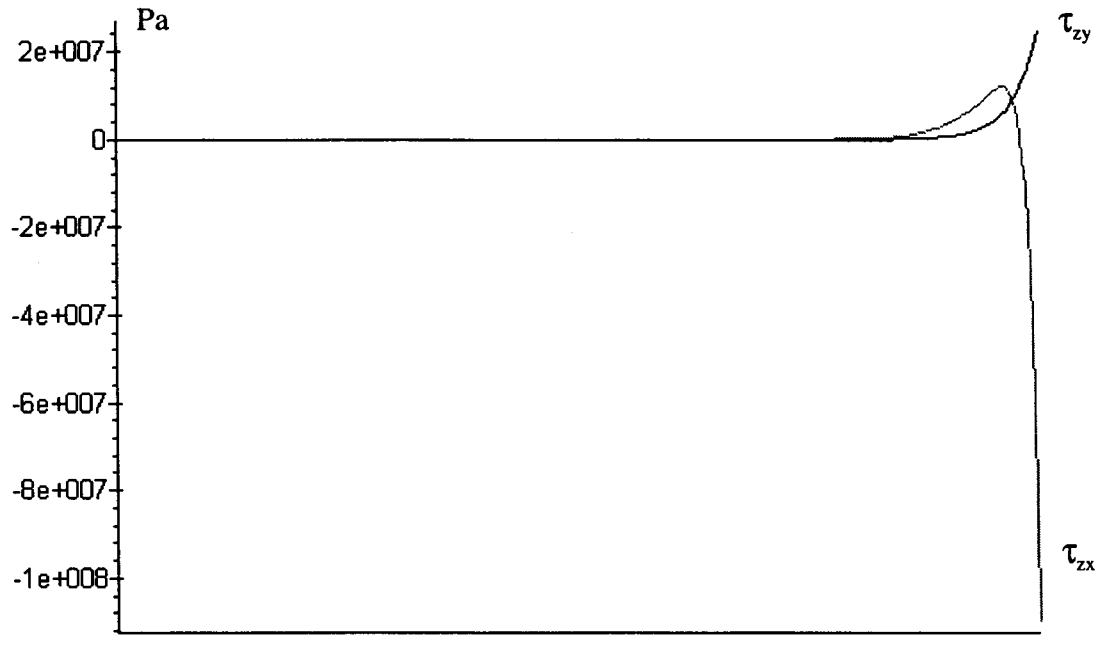

Figure C.3: Plots of τ_{zx} and τ_{zy} as a function of y $(0 < y < Wi/2)$ for u_a=-10^{-3} m. (Angle $\theta = 10^{o}$, Interface 2)

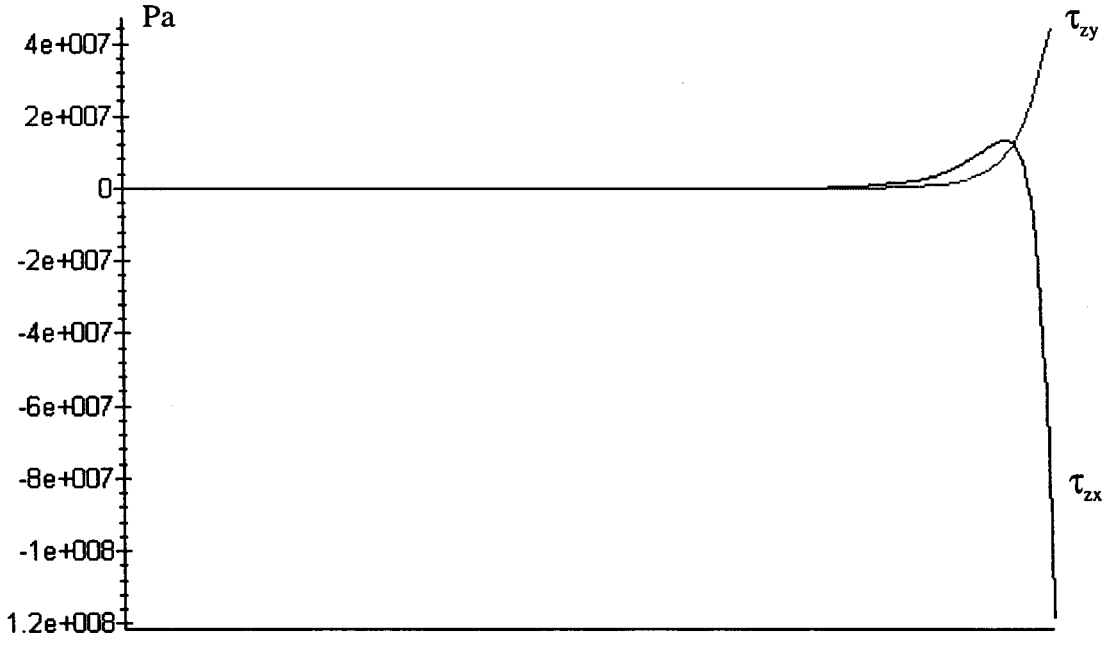

Figure C.4: Plots of τ_{zx} and τ_{zy} as a function of y $(0 < y < Wi/2)$ for u_a=-10^{-3} m. (Angle $\theta = 15^{o}$, Interface 2)

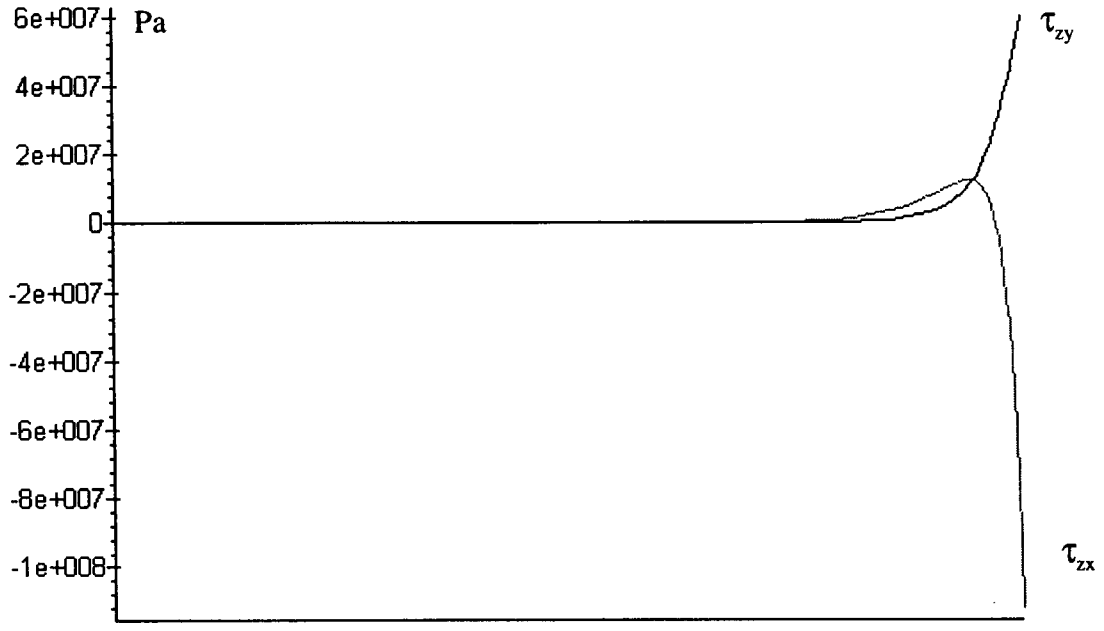

Figure C.5: Plots of τ_{zx} and τ_{zy} as a function of y $(0 < y < Wi/2)$ for u_a=-10^{-3} m. (Angle $\theta = 20^{o}$, Interface 2)

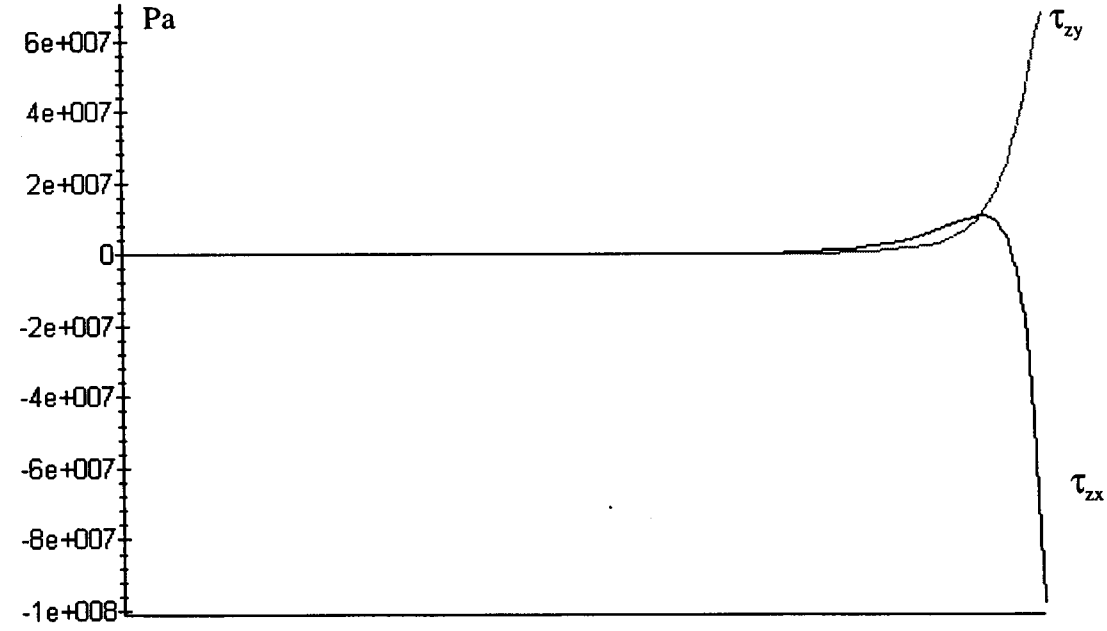

Figure C.6: Plots of τ_{zx} and τ_{zy} as a function of y $(0 < y < Wi/2)$ for u_a=-10^{-3} m. (Angle $\theta = 25^{o}$, Interface 2)

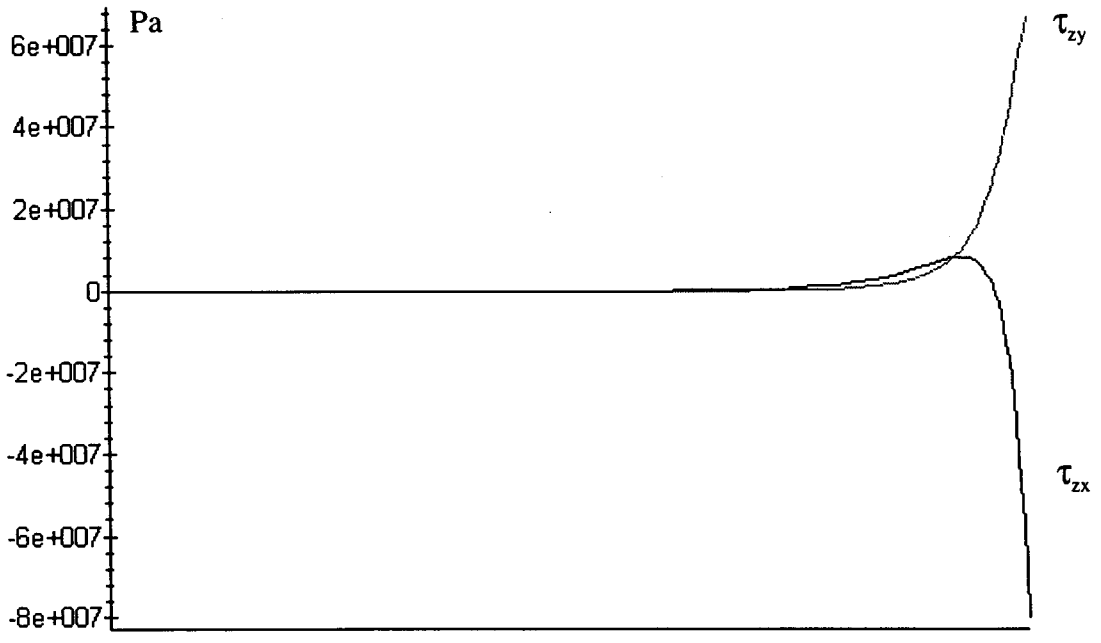

Figure C.7: Plots of τ_{zx} and τ_{zy} as a function of y $(0 < y < Wi/2)$ for u_a=-10^{-3} m. (Angle $\theta = 30^{o}$, Interface 2)

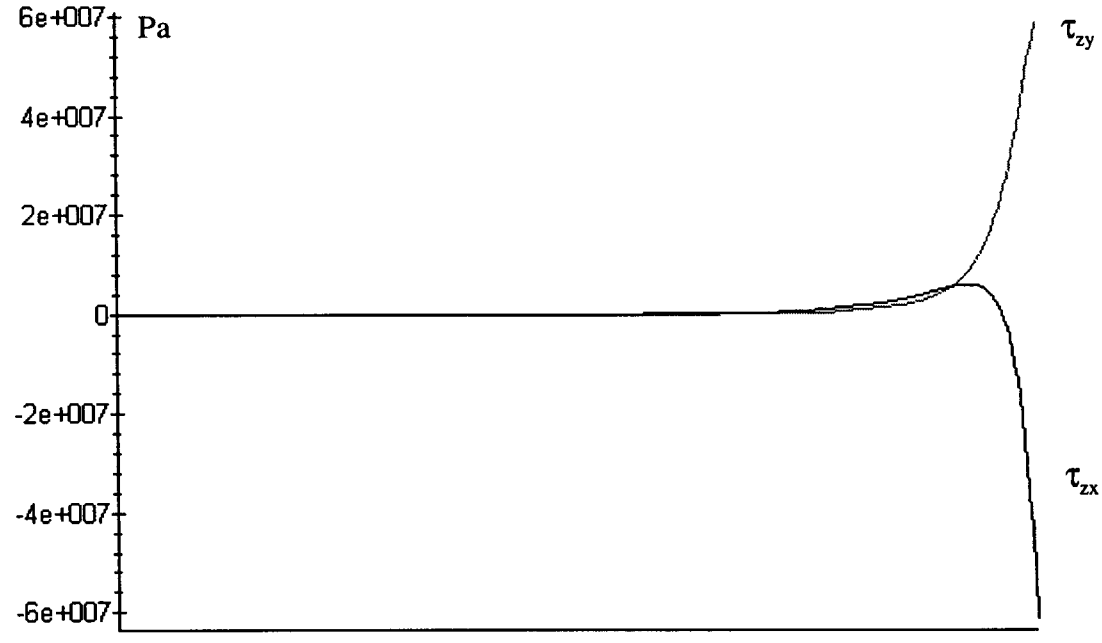

Figure C.8: Plots of τ_{zx} and τ_{zy} as a function of y $(0 < y < Wi/2)$ for u_a=-10^{-3} m. (Angle $\theta = 35^{o}$, Interface 2)

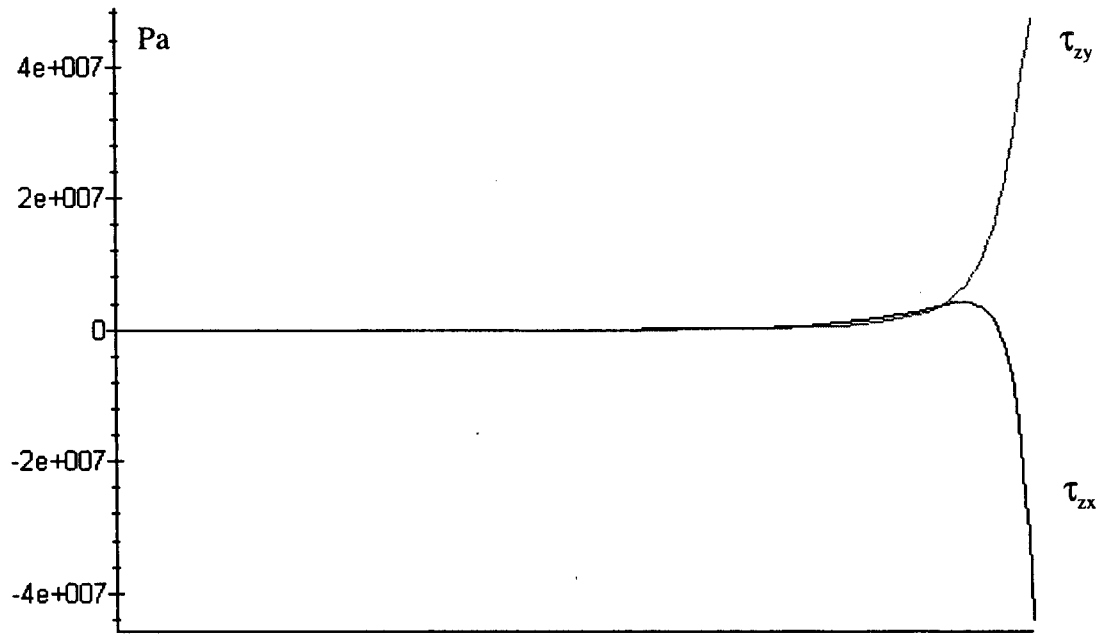

Figure C.9: Plots of τ_{zx} and τ_{zy} as a function of y $(0 < y < Wi/2)$ for u_a=-10^{-3} m. (Angle $\theta = 40^{o}$, Interface 2)

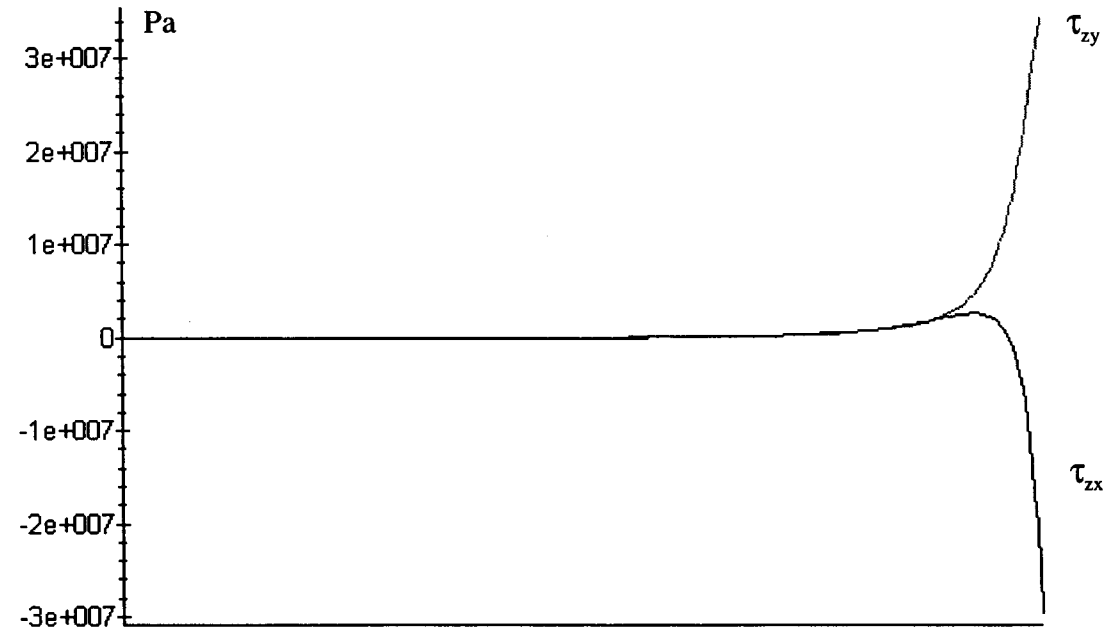

Figure C.10: Plots of τ_{zx} and τ_{zy} as a function of y $(0 < y < Wi/2)$ for u_a=-10^{-3} m. (Angle $\theta = 45^{o}$, Interface 2)

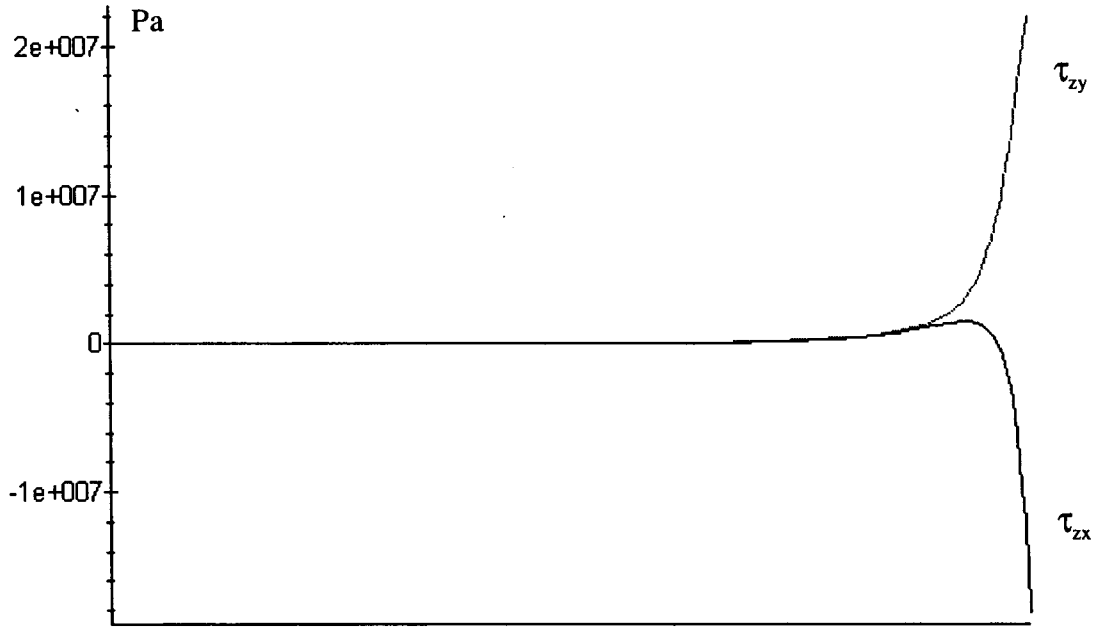

Figure C.11: Plots of τ_{zx} and τ_{zy} as a function of y $(0 < y < Wi/2)$ for u_a=-10^{-3} m. (Angle $\theta = 50^{o}$, Interface 2)

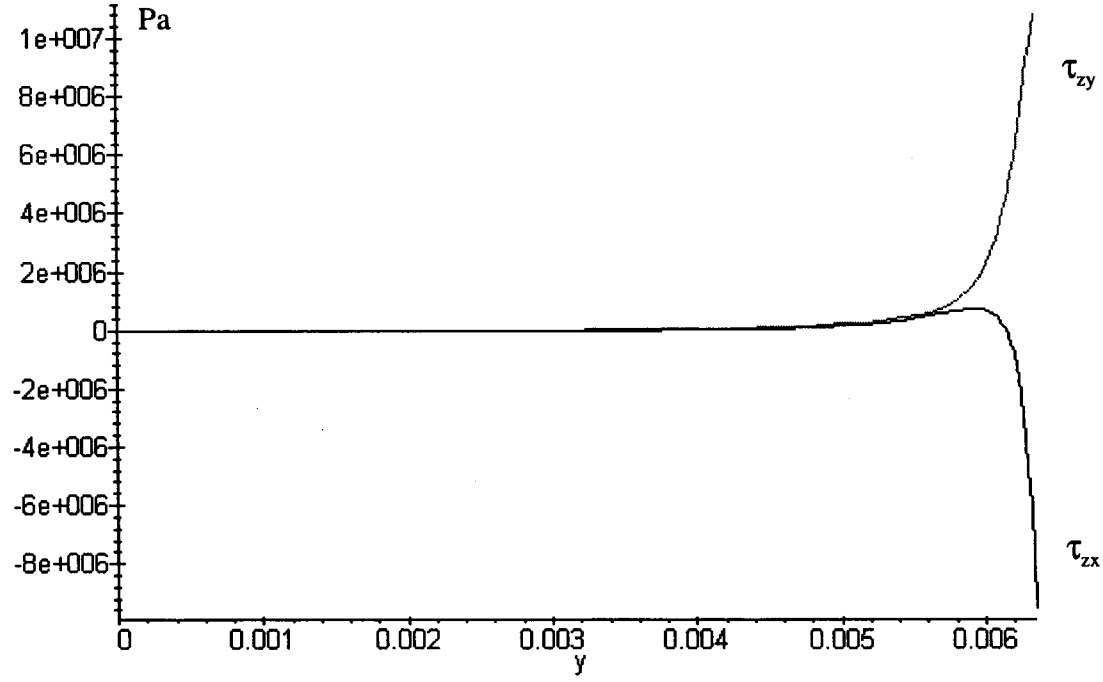

Figure C.12: Plots of τ_{zx} and τ_{zy} as a function of y $(0 < y < Wi/2)$ for u_a=-10^{-3} m. (Angle $\theta = 55^{o}$, Interface 2)

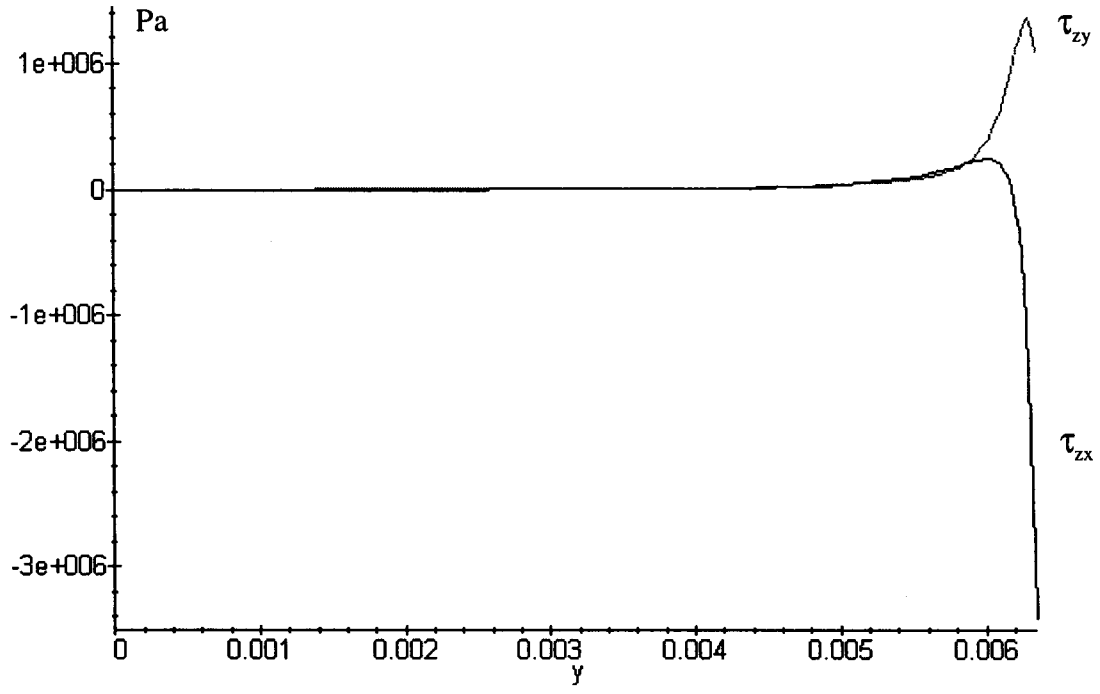

Figure C.13: Plots of τ_{zx} and τ_{zy} as a function of y $(0 < y < Wi/2)$ for u_a=-10^{-3} m. (Angle $\theta = 60^{o}$, Interface 2)

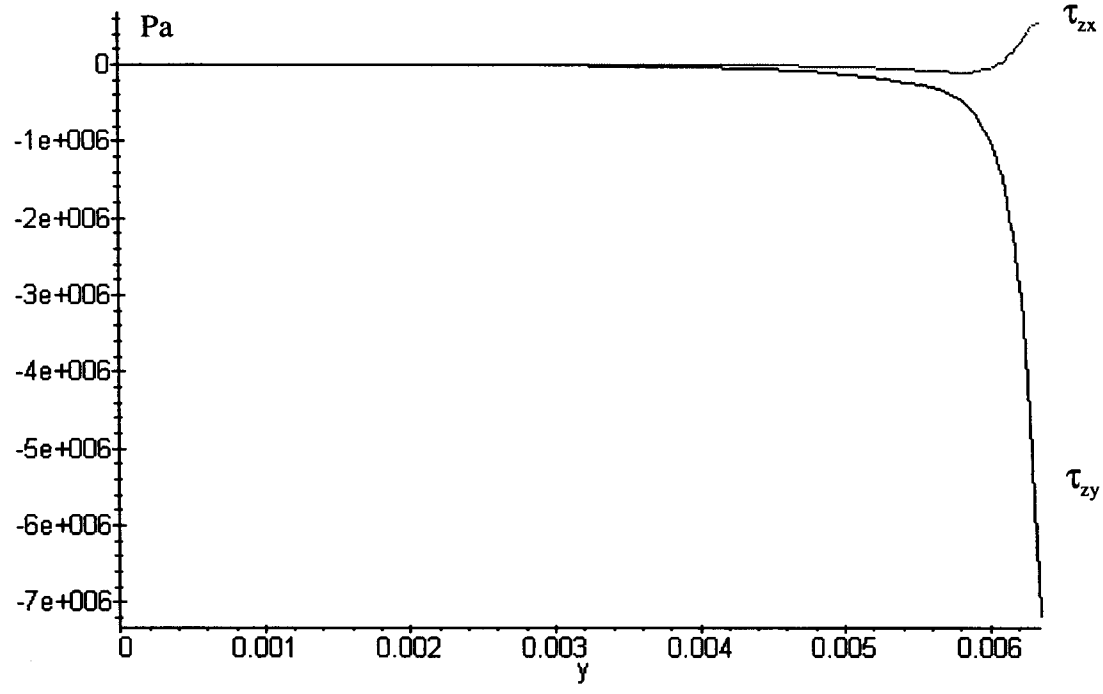

Figure C.14: Plots of τ_{zx} and τ_{zy} as a function of y $(0 < y < Wi/2)$ for u_a=-10^{-3} m. (Angle $\theta = 65^{o}$, Interface 2)

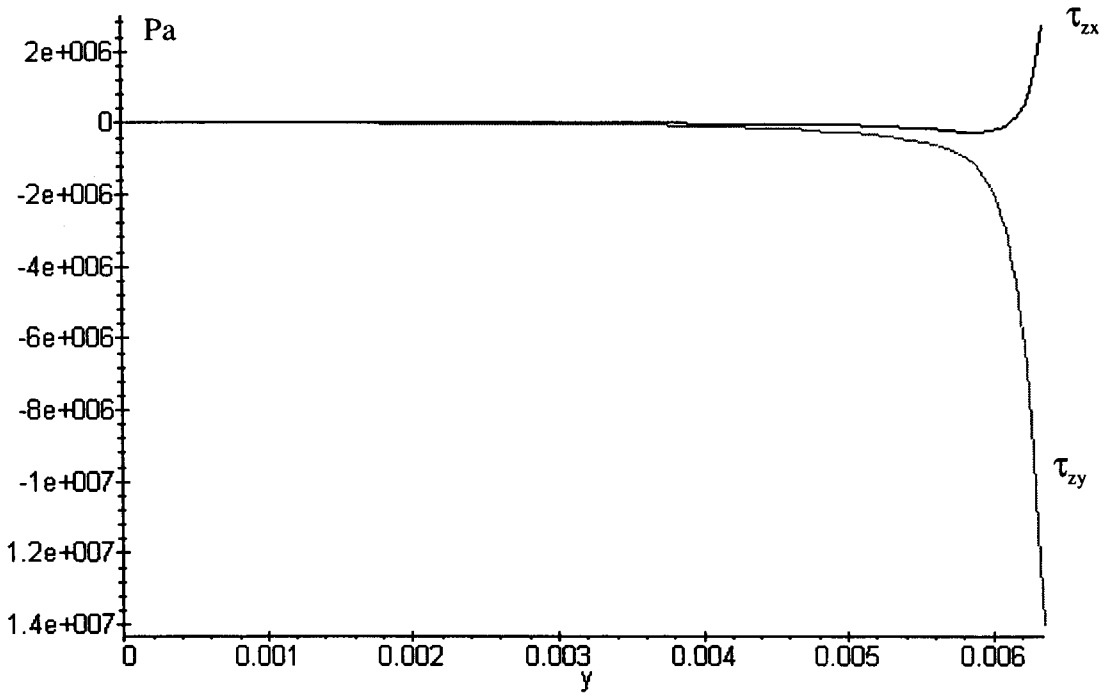

Figure C.15: Plots of τ_{zx} and τ_{zy} as a function of y $(0 < y < Wi/2)$ for u_a=-10^{-3} m. (Angle $\theta = 70^{o}$, Interface 2)

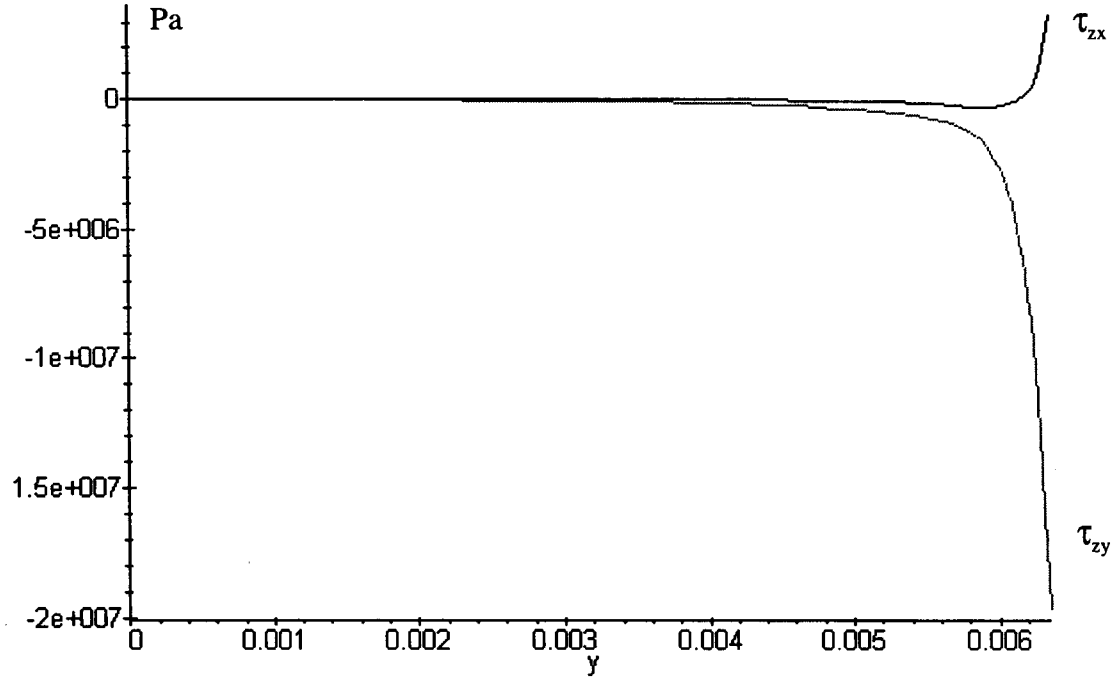

Figure C.16: Plots of τ_{zx} and τ_{zy} as a function of y $(0 < y < Wi/2)$ for u_a=-10^{-3} m. (Angle $\theta = 75^{o}$, Interface 2)

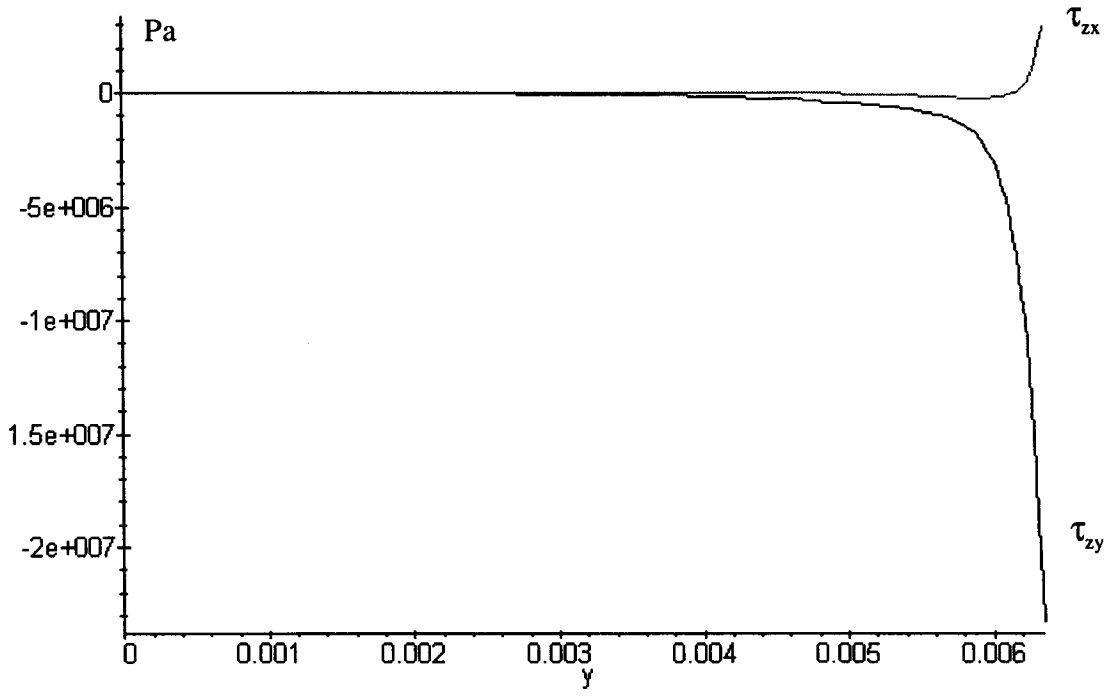

Figure C.17: Plots of τ_{zx} and τ_{zy} as a function of y $(0 < y < Wi/2)$ for u_a=-10^{-3} m. (Angle $\theta = 80^o$, Interface 2)

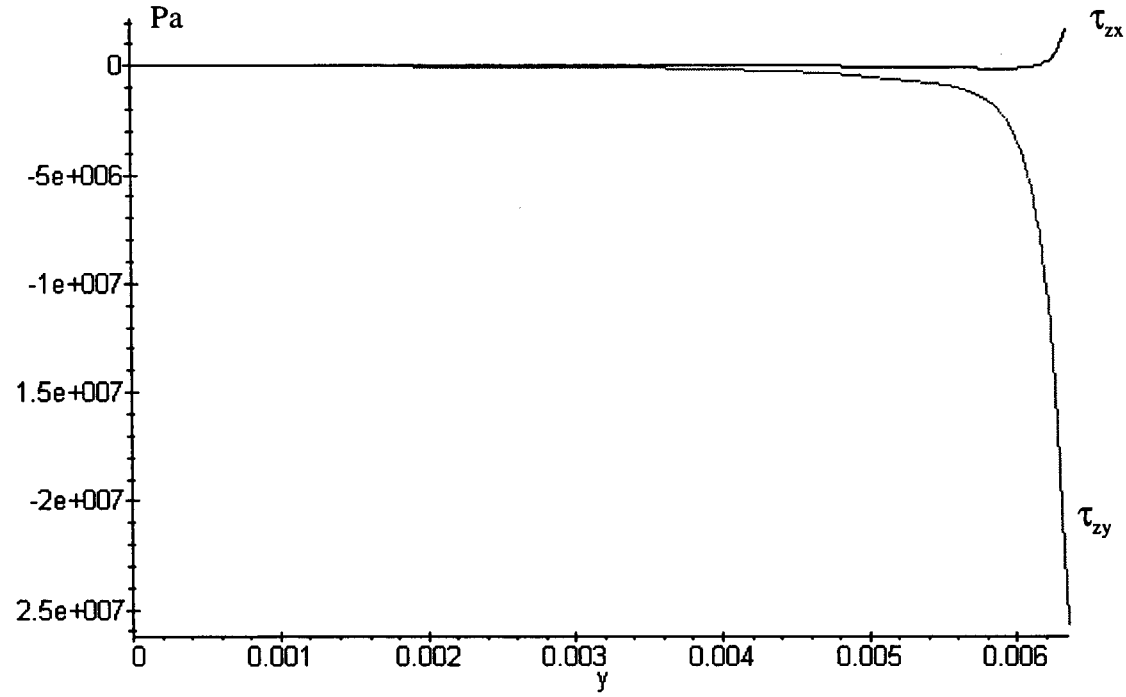

Figure C.18: Plots of τ_{zx} and τ_{zy} as a function of y $(0 < y < Wi/2)$ for u_a=-10^{-3} m. (Angle $\theta = 85^o$, Interface 2)

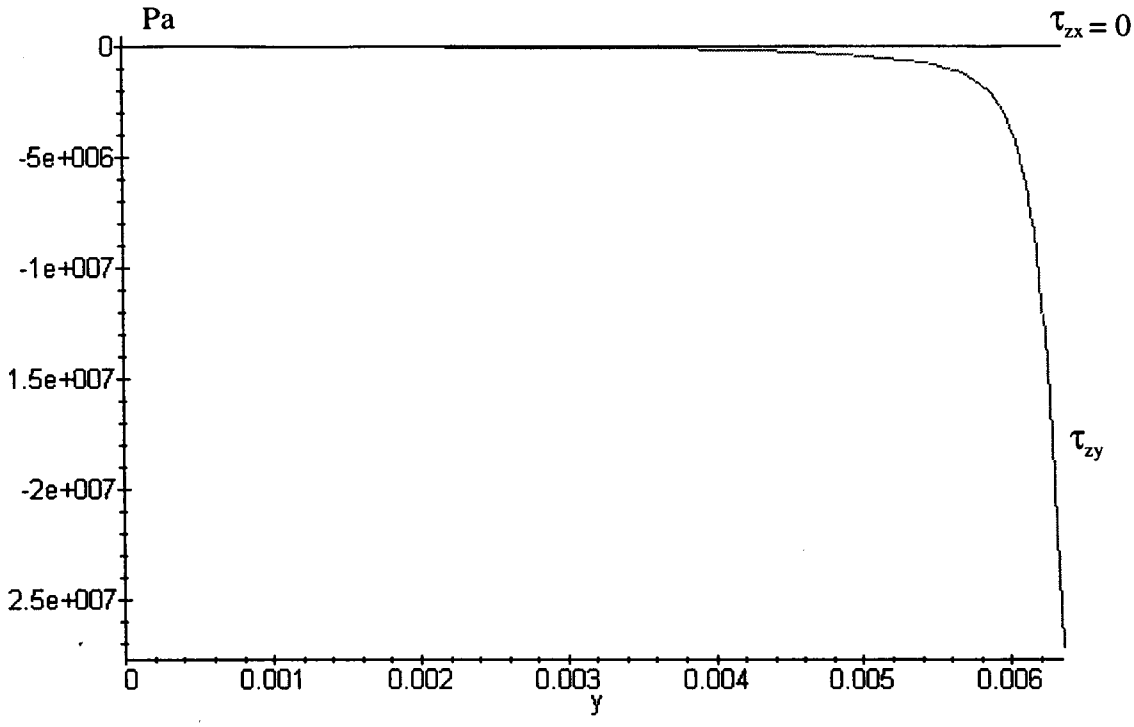

Figure C.19: Plots of τ_{zx} and τ_{zy} as a function of y $(0 < y < Wi/2)$ for u_a=-10^{-3} m. (Angle $\theta = 90^{o}$, Interface 2)

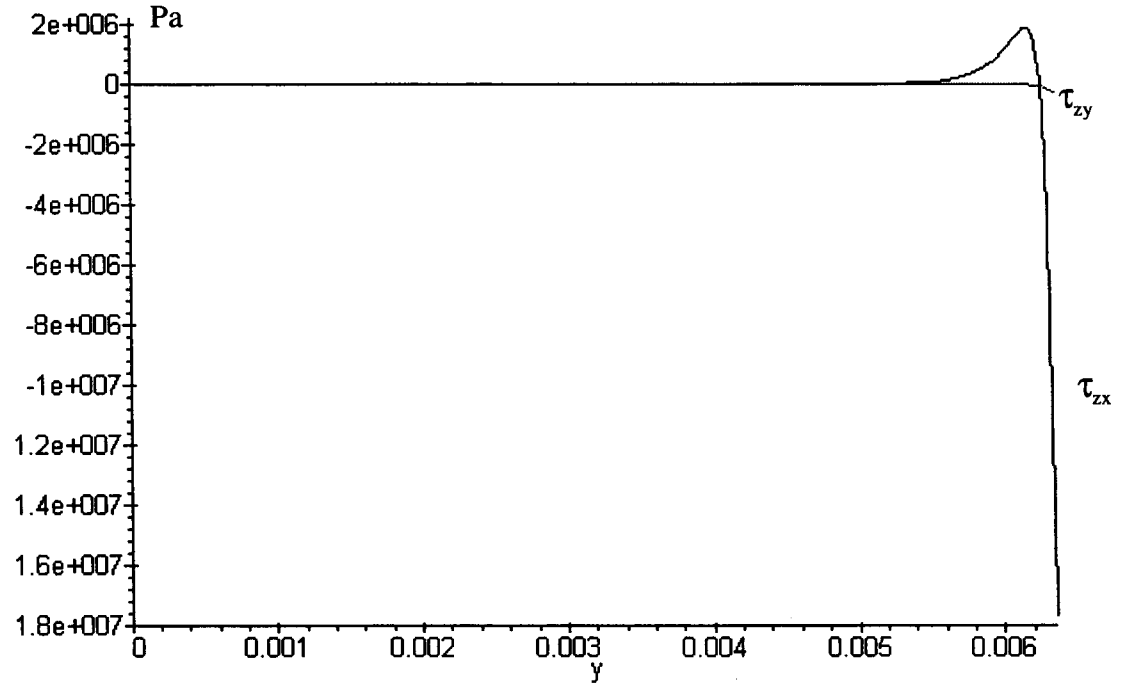

Figure C.20: Plots of τ_{zx} and τ_{zy} as a function of y $(0 < y < Wi/2)$ for u_a=-10^{-3} m. (Angle $\theta = 1^{o}$, Interface 3)

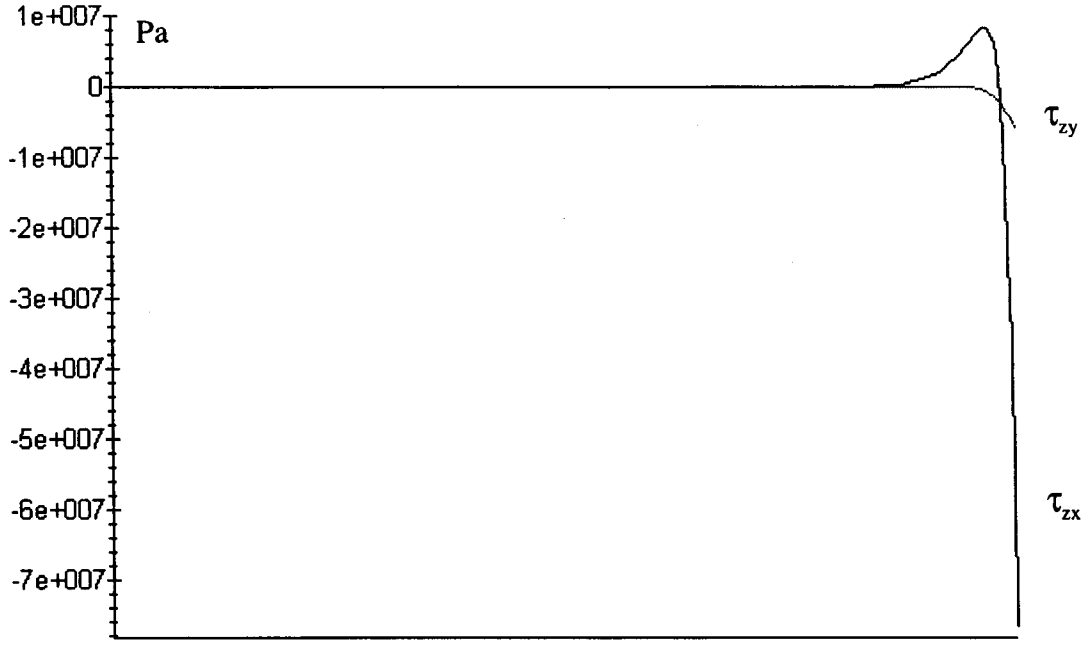

Figure C.21: Plots of τ_{zx} and τ_{zy} as a function of y $(0 < y < Wi/2)$ for u_a=-10^{-3} m. (Angle $\theta = 5^o$, Interface 3)

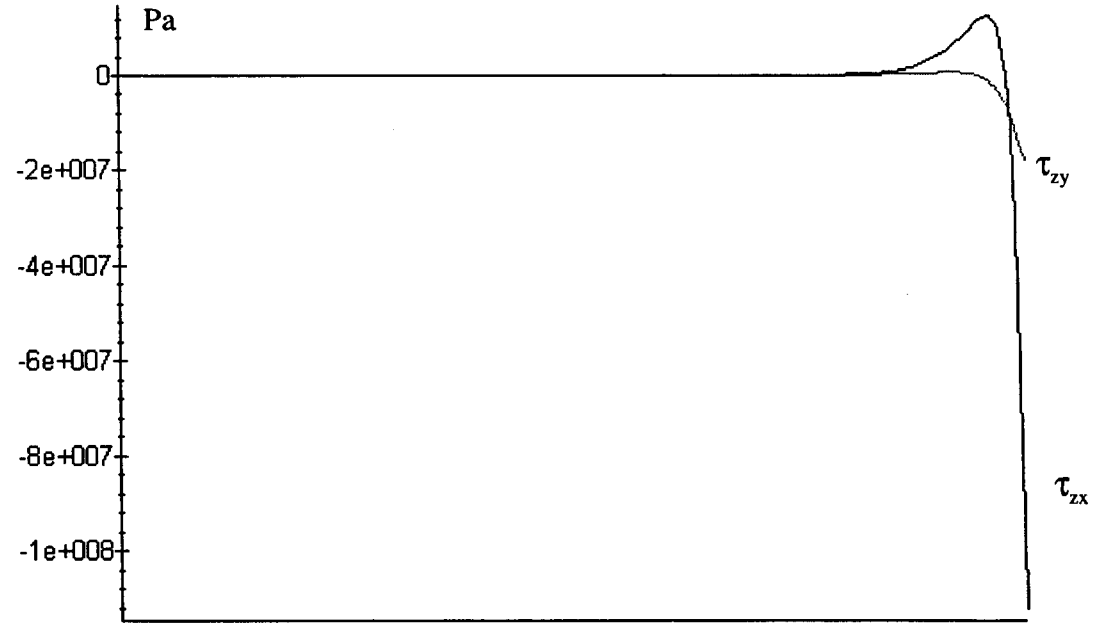

Figure C.22: Plots of τ_{zx} and τ_{zy} as a function of y $(0 < y < Wi/2)$ for u_a=-10^{-3} m. (Angle $\theta = 10^o$, Interface 3)

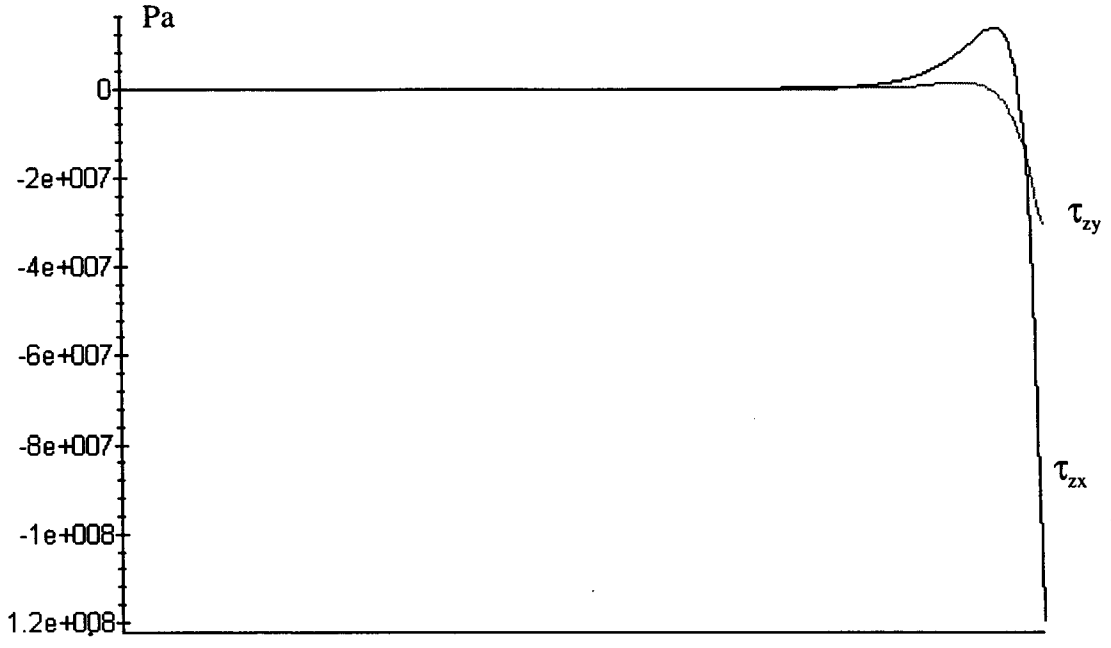

Figure C.23: Plots of τ_{zx} and τ_{zy} as a function of y $(0 < y < Wi/2)$ for u_a=-10^{-3} m. (Angle $\theta = 15^{o}$, Interface 3)

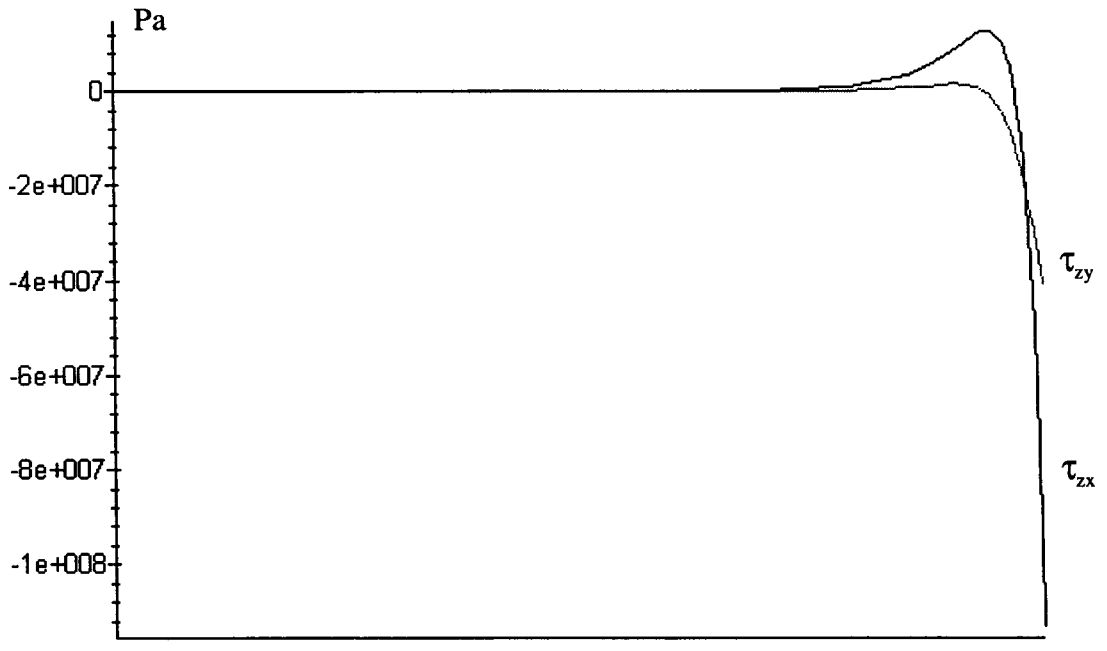

Figure C.24: Plots of τ_{zx} and τ_{zy} as a function of y $(0 < y < Wi/2)$ for u_a=-10^{-3} m. (Angle $\theta = 20^{o}$, Interface 3)

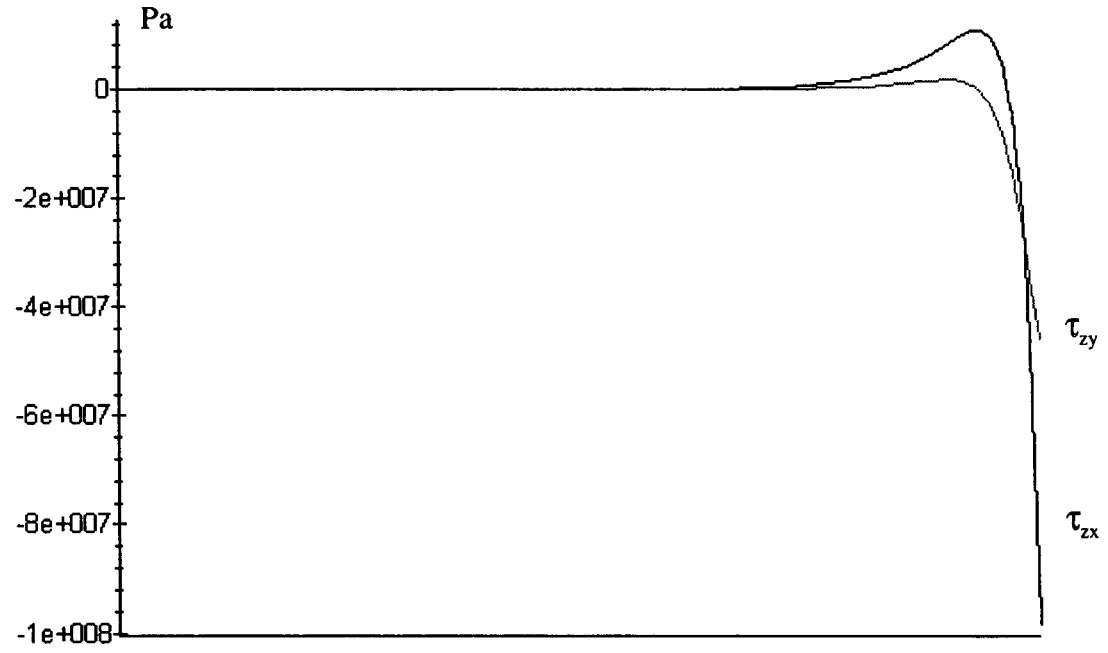

Figure C.25: Plots of τ_{zx} and τ_{zy} as a function of y $(0 < y < Wi/2)$ for u_a=-10^{-3} m. (Angle $\theta = 25^{o}$, Interface 3)

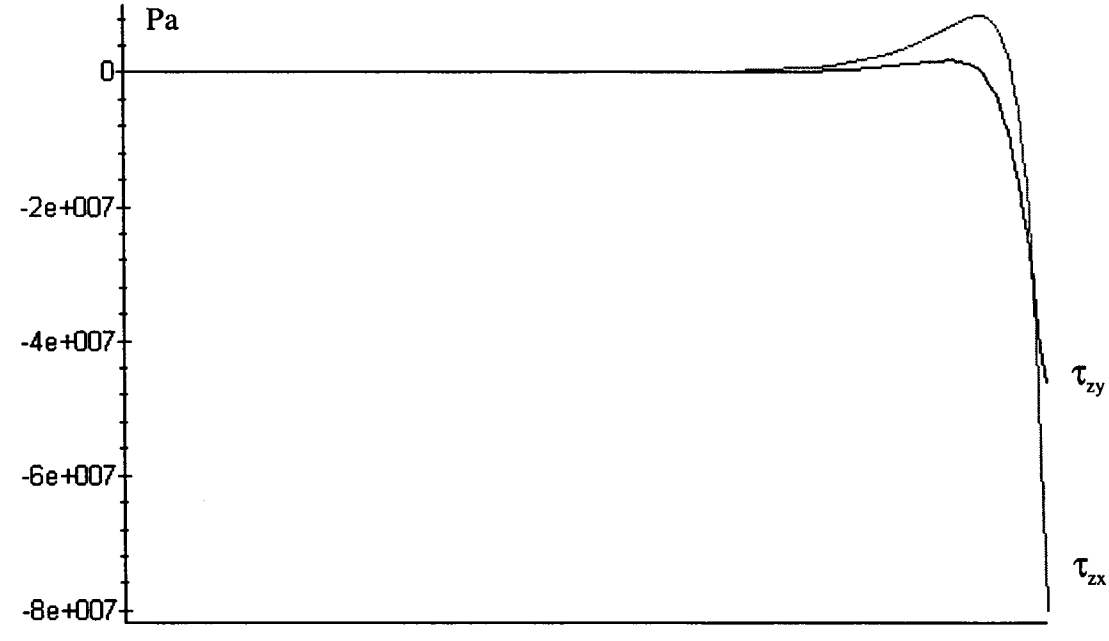

Figure C.26: Plots of τ_{zx} and τ_{zy} as a function of y $(0 < y < Wi/2)$ for u_a=-10^{-3} m. (Angle $\theta = 30^{o}$, Interface 3)

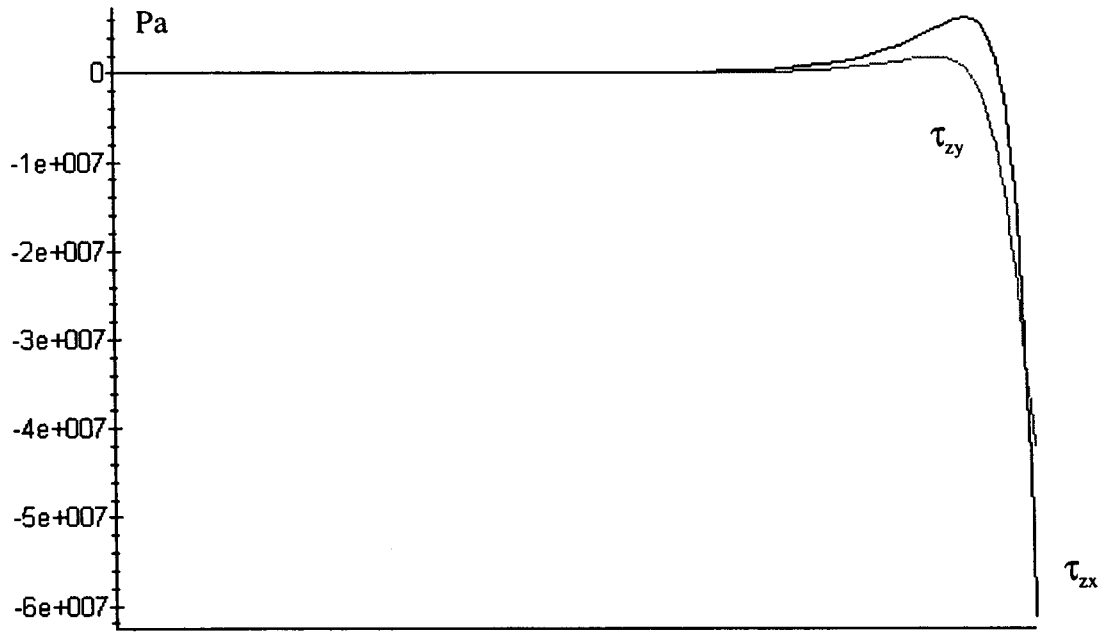

Figure C.27: Plots of τ_{zx} and τ_{zy} as a function of y $(0 < y < Wi/2)$ for u_a=-10^{-3} m. (Angle $\theta = 35^{o}$, Interface 3)

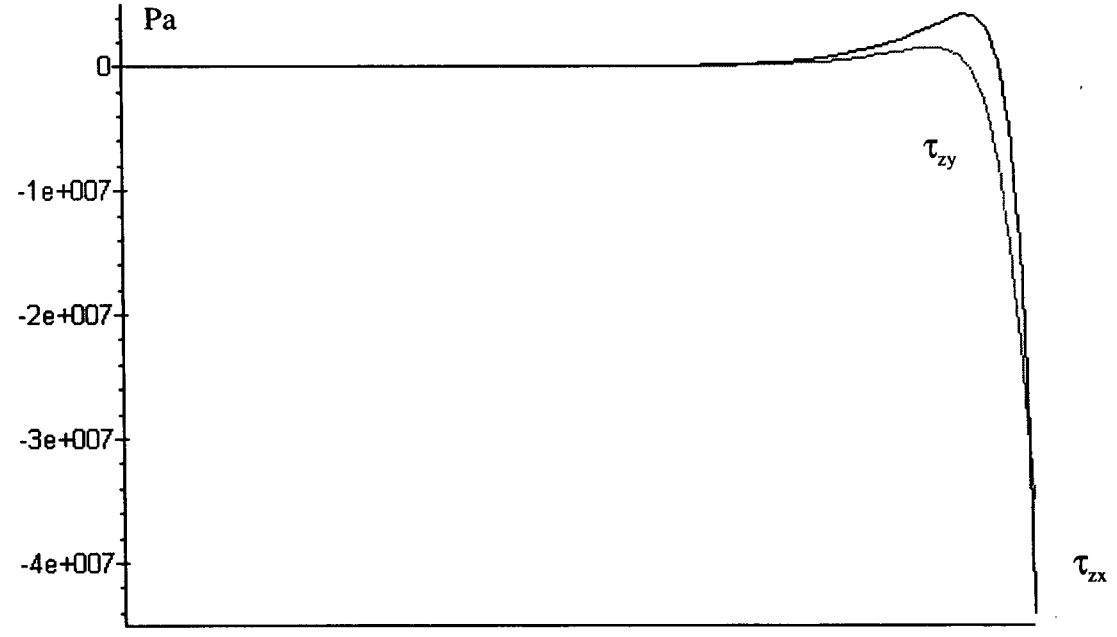

Figure C.28: Plots of τ_{zx} and τ_{zy} as a function of y $(0 < y < Wi/2)$ for u_a=-10^{-3} m. (Angle $\theta = 40^{o}$, Interface 3)

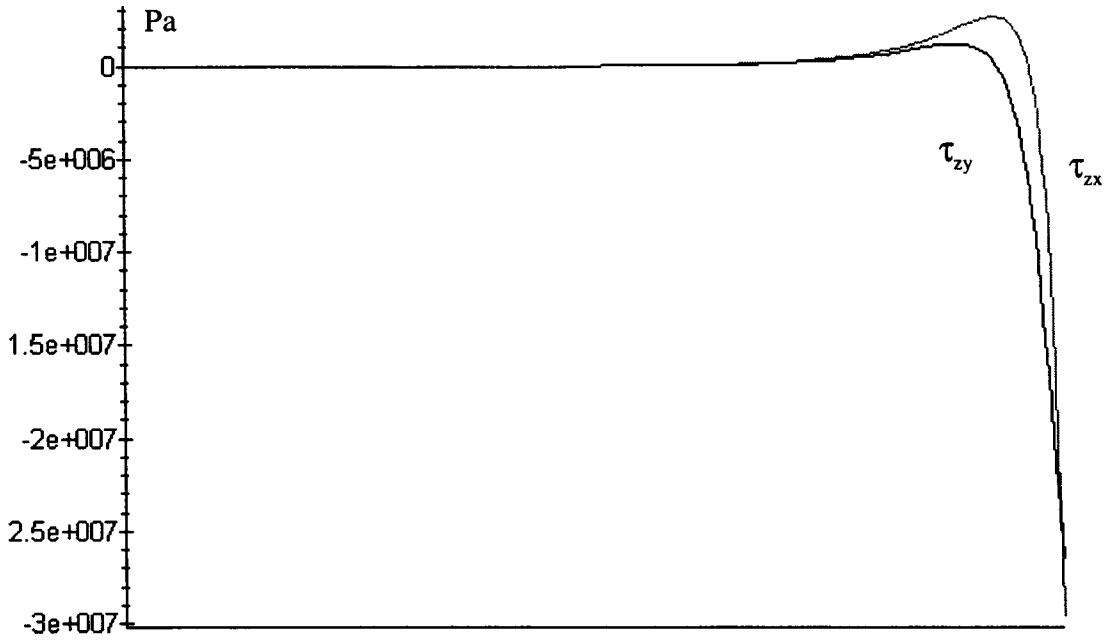

Figure C.29: Plots of τ_{zx} and τ_{zy} as a function of y $(0 < y < Wi/2)$ for u_a=-10^{-3} m. (Angle $\theta = 45^o$, Interface 3)

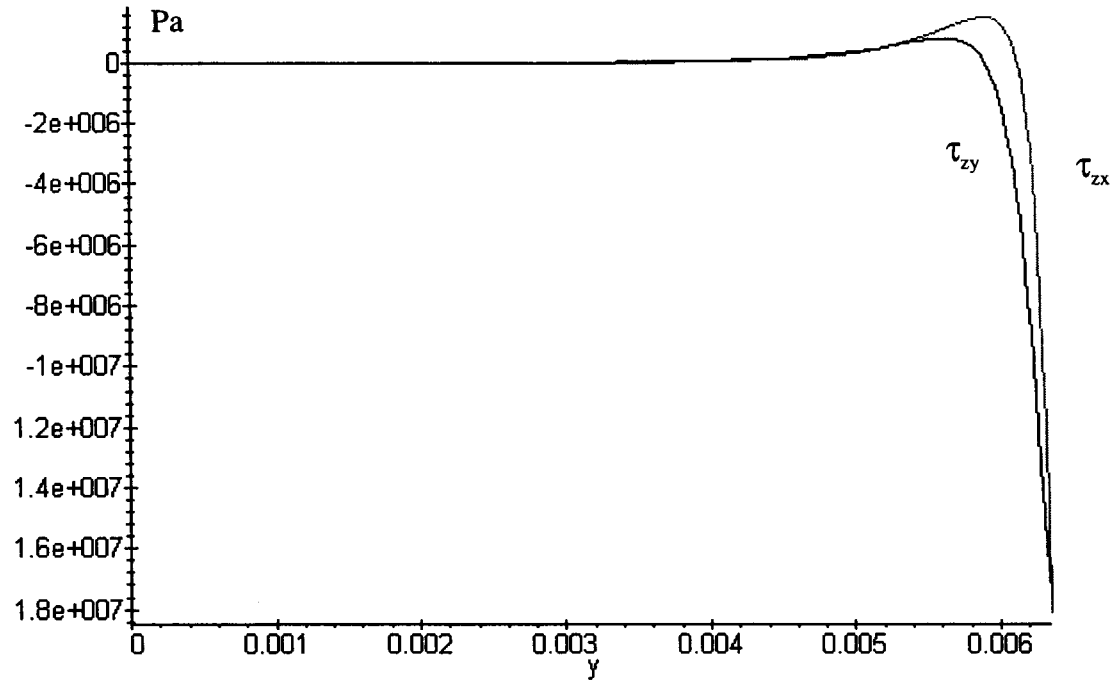

Figure C.30: Plots of τ_{zx} and τ_{zy} as a function of y $(0 < y < Wi/2)$ for u_a=-10^{-3} m. (Angle $\theta = 50^o$, Interface 3)

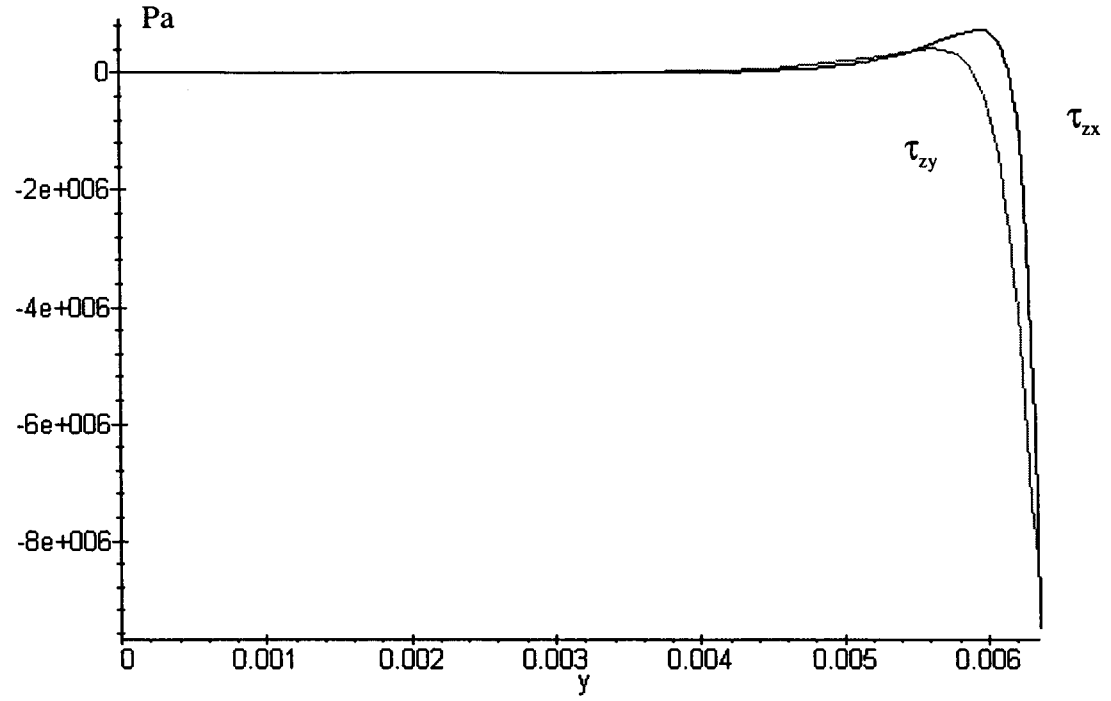

Figure C.31: Plots of τ_{zx} and τ_{zy} as a function of y $(0 < y < Wi/2)$ for u_a=-10^{-3} m. (Angle $\theta = 55^{o}$, Interface 3)

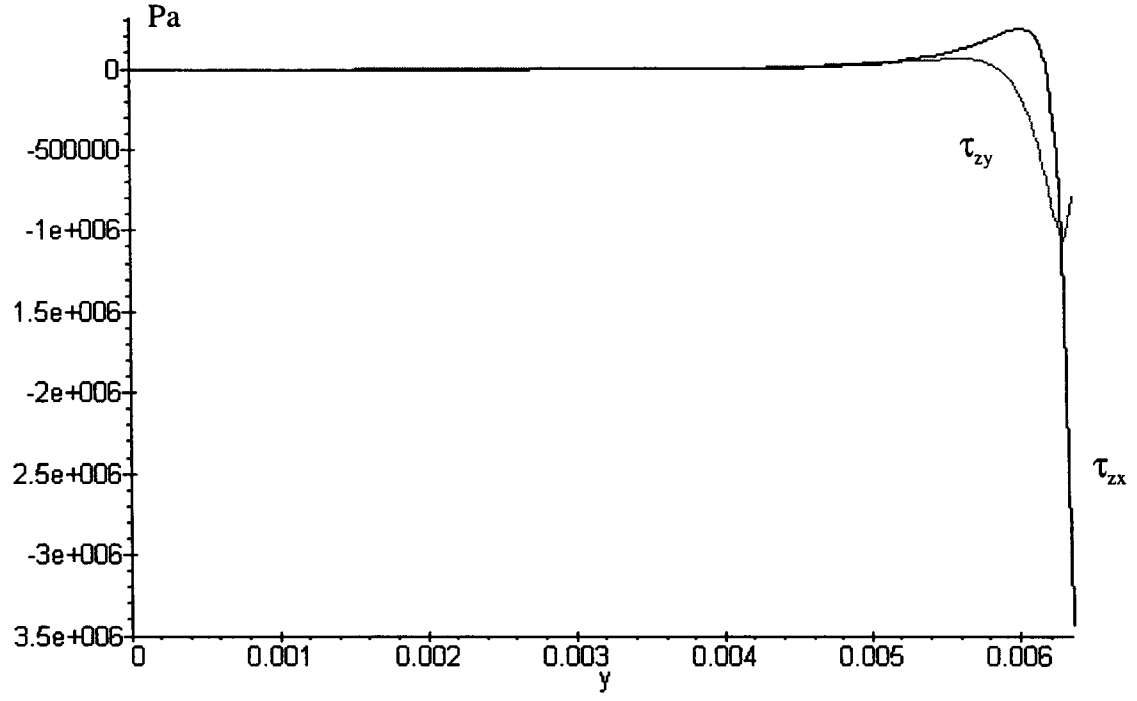

Figure C.32: Plots of τ_{zx} and τ_{zy} as a function of y $(0 < y < Wi/2)$ for u_a=-10^{-3} m. (Angle $\theta = 60^{o}$, Interface 3)

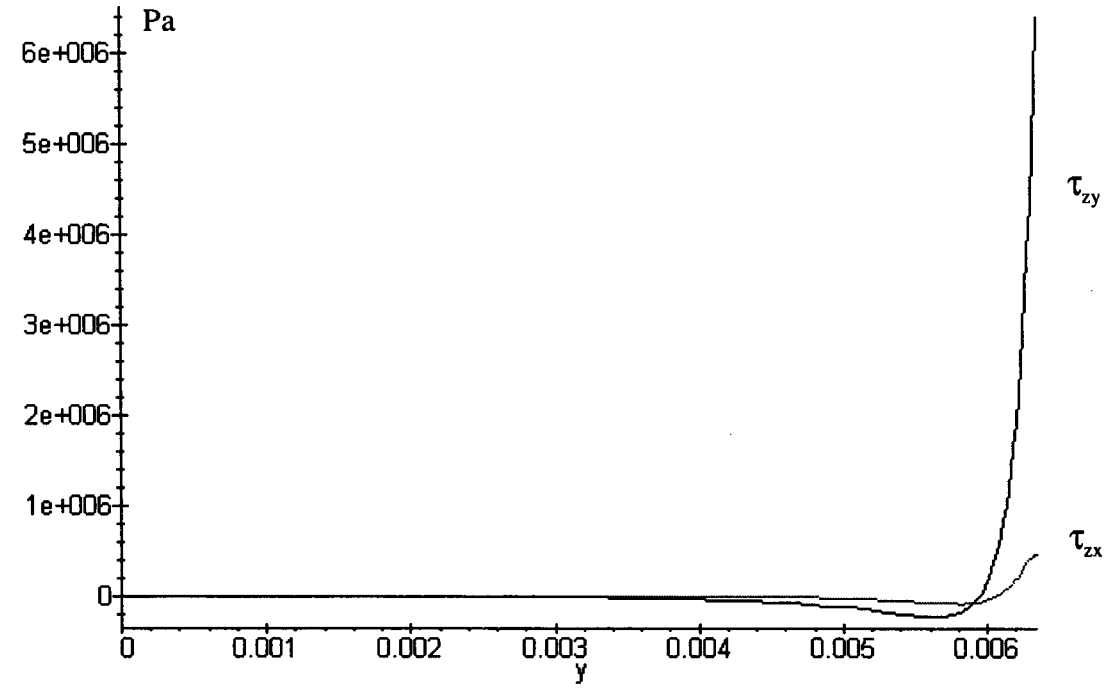

Figure C.33: Plots of τ_{zx} and τ_{zy} as a function of y $(0 < y < Wi/2)$ for u_a=-10^{-3} m. (Angle $\theta = 65^{o}$, Interface 3)

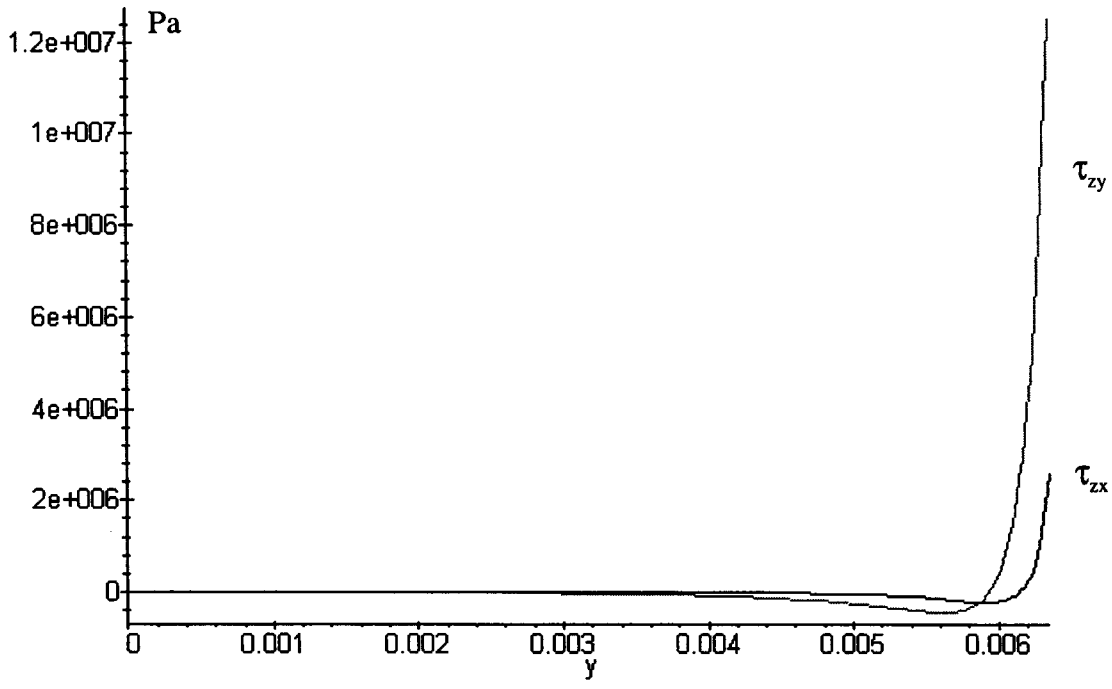

Figure C.34: Plots of τ_{zx} and τ_{zy} as a function of y $(0 < y < Wi/2)$ for u_a=-10^{-3} m. (Angle $\theta = 70^{o}$, Interface 3)

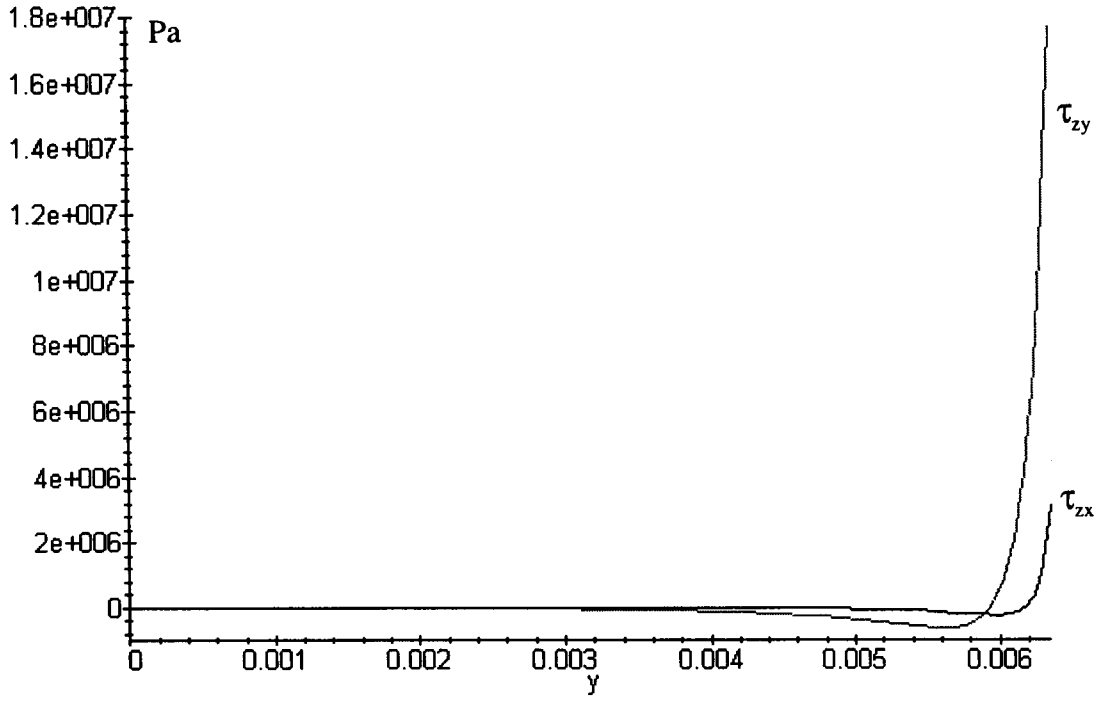

Figure C.35: Plots of τ_{zx} and τ_{zy} as a function of y $(0 < y < Wi/2)$ for u_a=-10^{-3} m. (Angle $\theta = 75^{o}$, Interface 3)

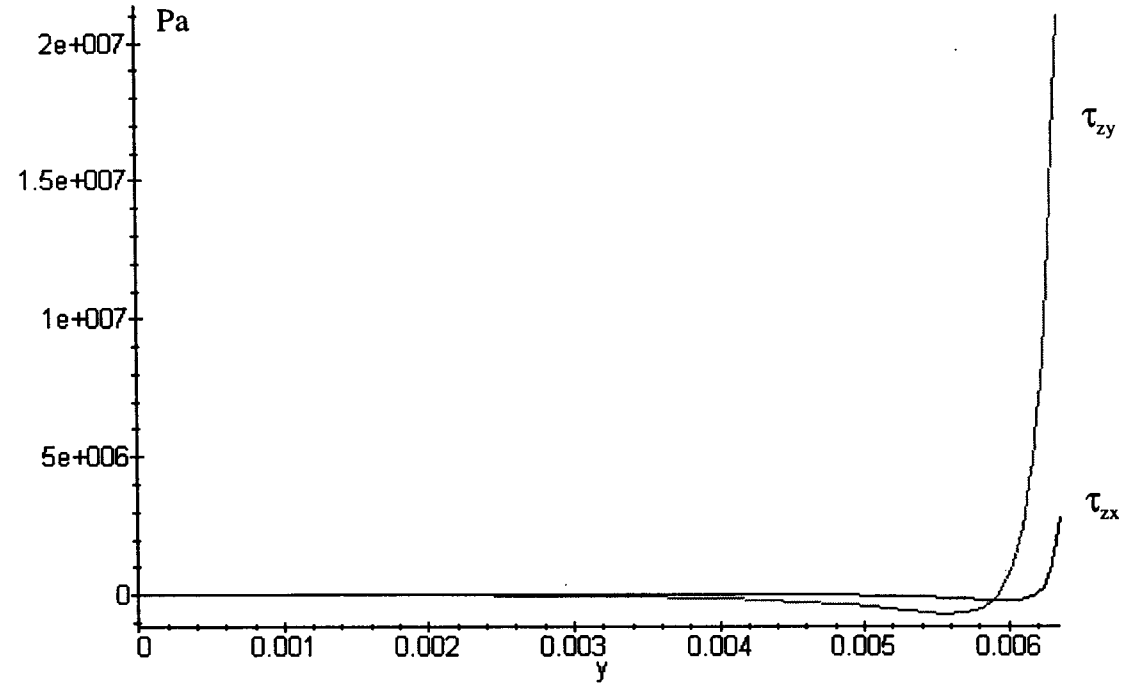

Figure C.36: Plots of τ_{zx} and τ_{zy} as a function of y $(0 < y < Wi/2)$ for u_a=-10^{-3} m. (Angle $\theta = 80^{o}$, Interface 3)

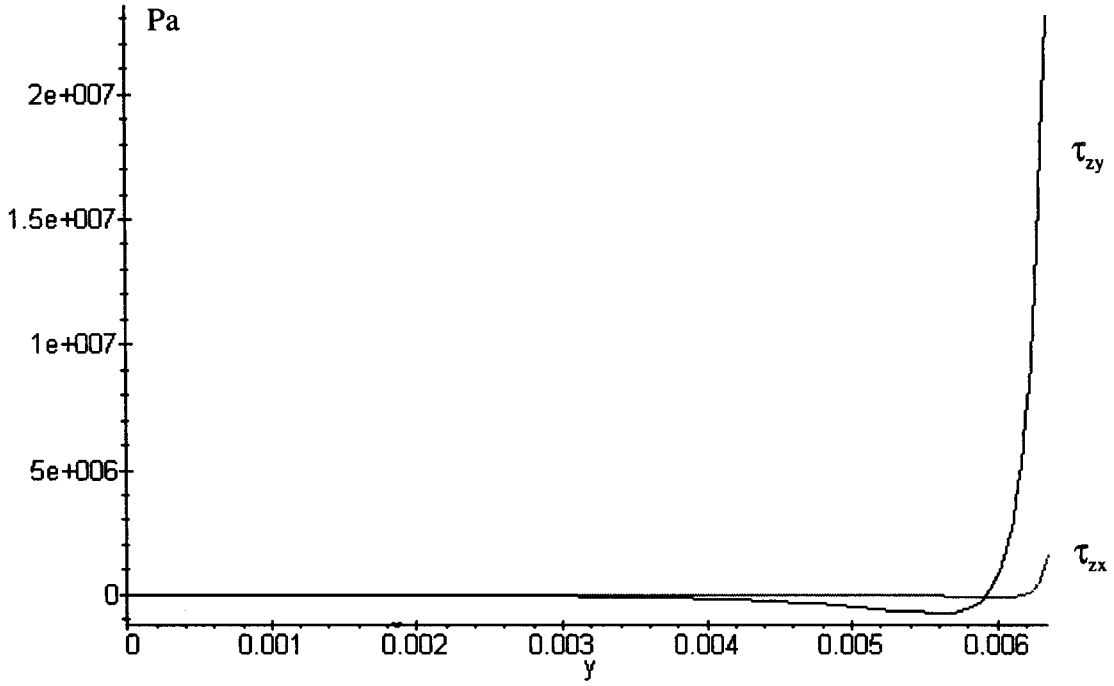

Figure C.37: Plots of τ_{zx} and τ_{zy} as a function of y $(0 < y < Wi/2)$ for u_a=-10^{-3} m. (Angle $\theta = 85°$, Interface 3)

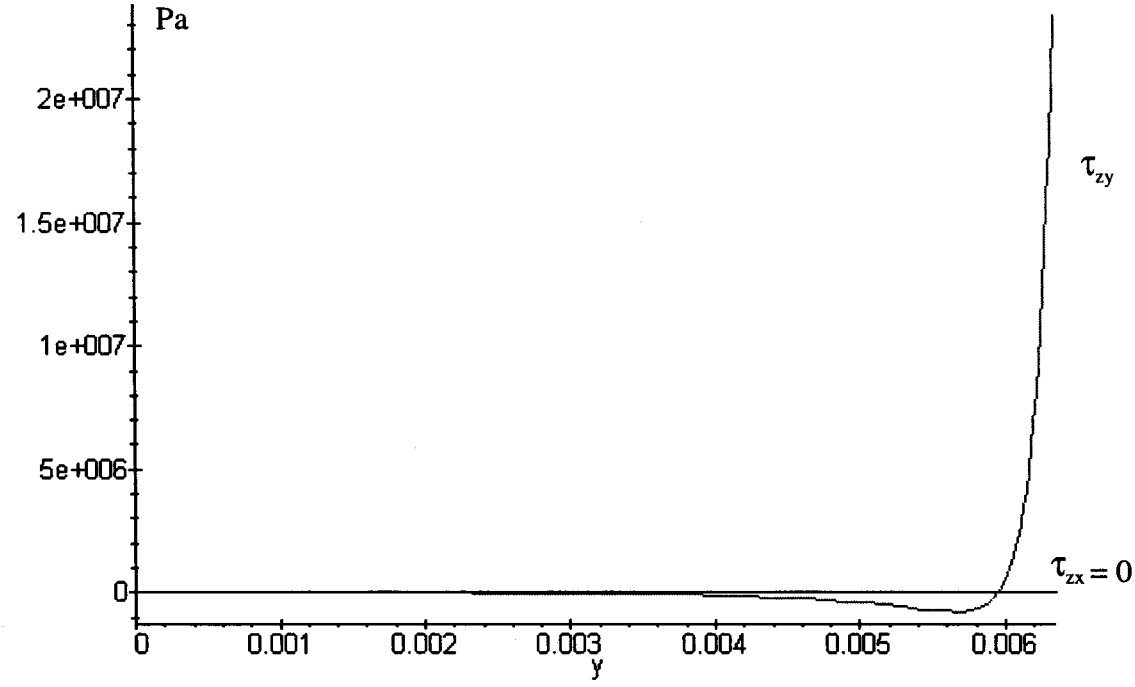

Figure C.38: Plots of τ_{zx} and τ_{zy} as a function of y $(0 < y < Wi/2)$ for u_a=-10^{-3} m. (Angle $\theta = 90°$, Interface 3)

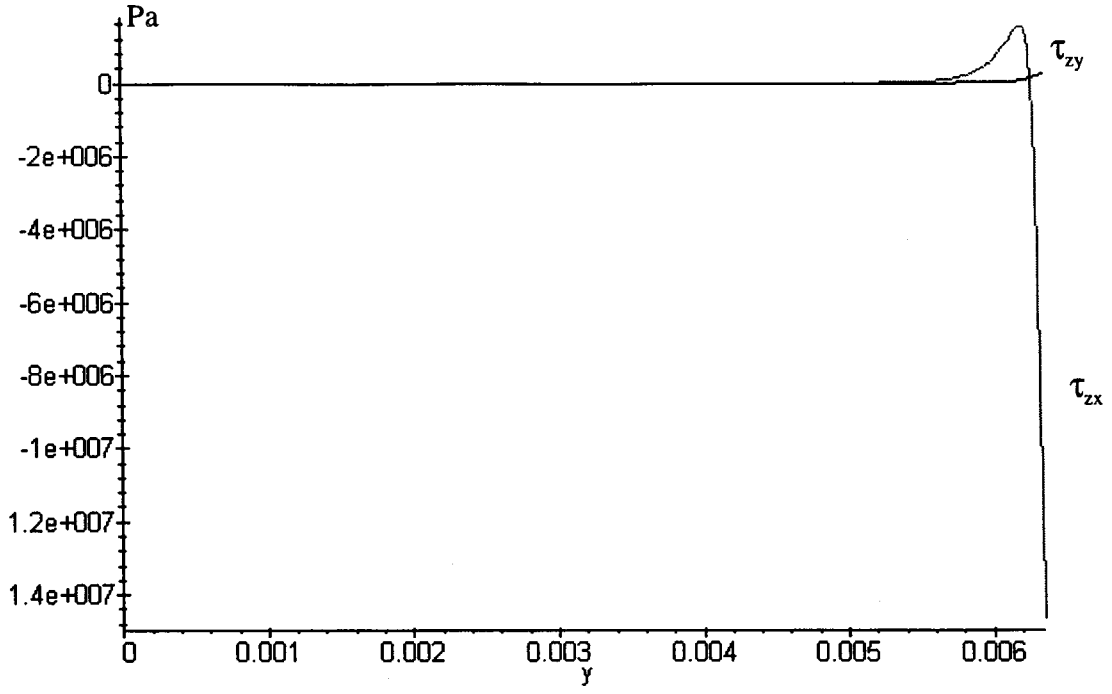

Figure C.39: Plots of τ_{zx} and τ_{zy} as a function of y $(0 < y < Wi/2)$ for u_a=-10^{-3} m. (Angle $\theta = 1^{o}$, Interface 5)

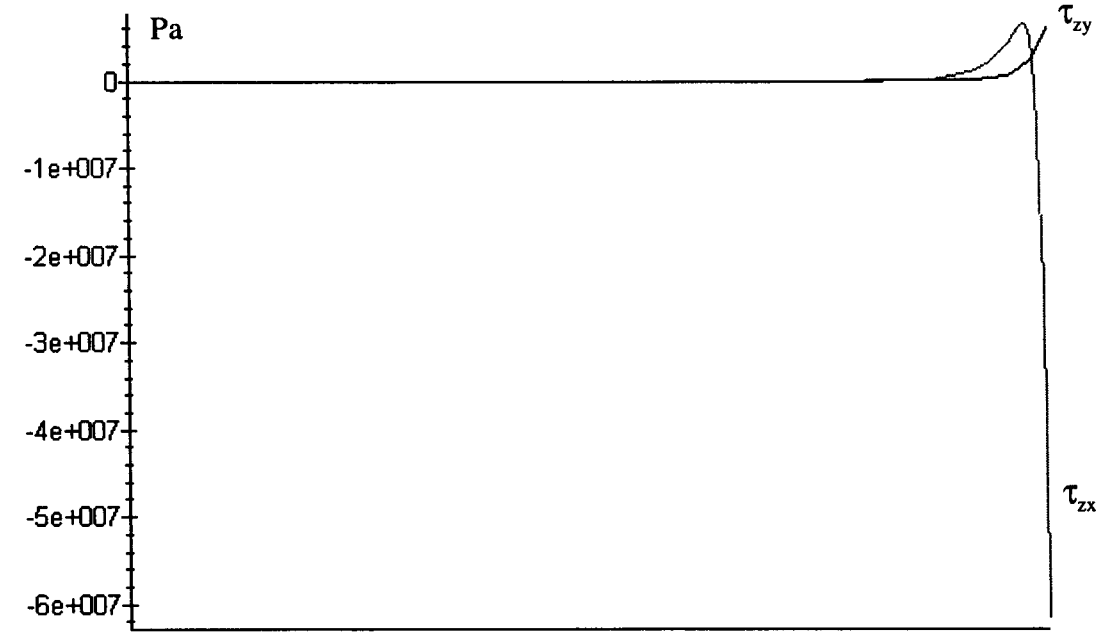

Figure C.40: Plots of τ_{zx} and τ_{zy} as a function of y $(0 < y < Wi/2)$ for u_a=-10^{-3} m. (Angle $\theta = 5^{o}$, Interface 5)

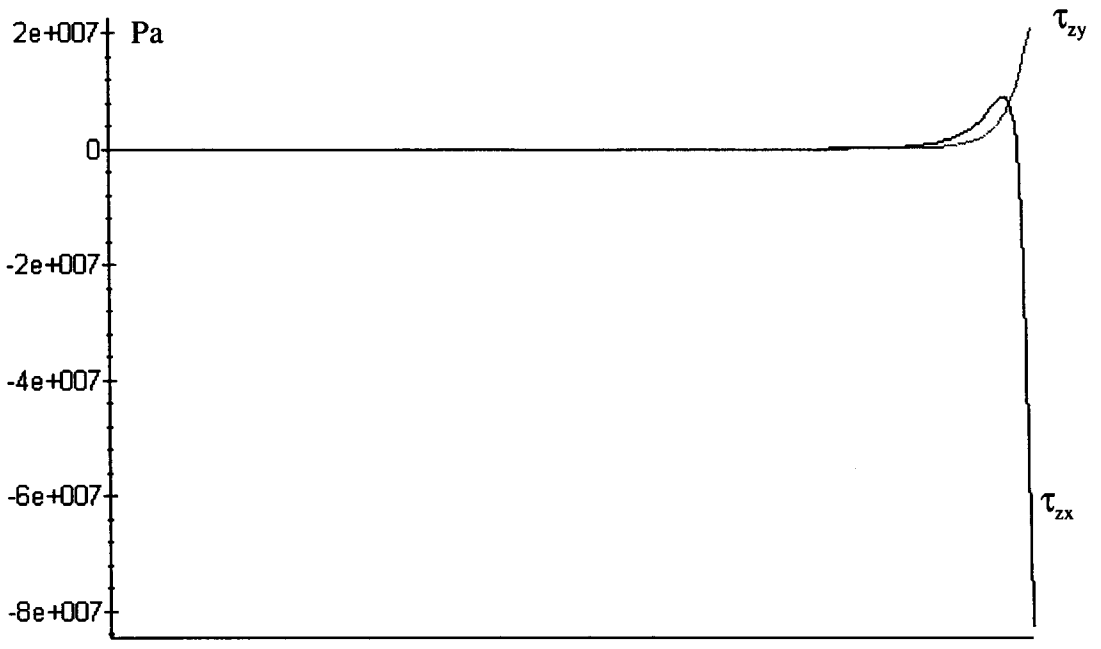

Figure C.41: Plots of τ_{zx} and τ_{zy} as a function of y $(0 < y < Wi/2)$ for u_a=-10^{-3} m. (Angle $\theta = 10^o$, Interface 5)

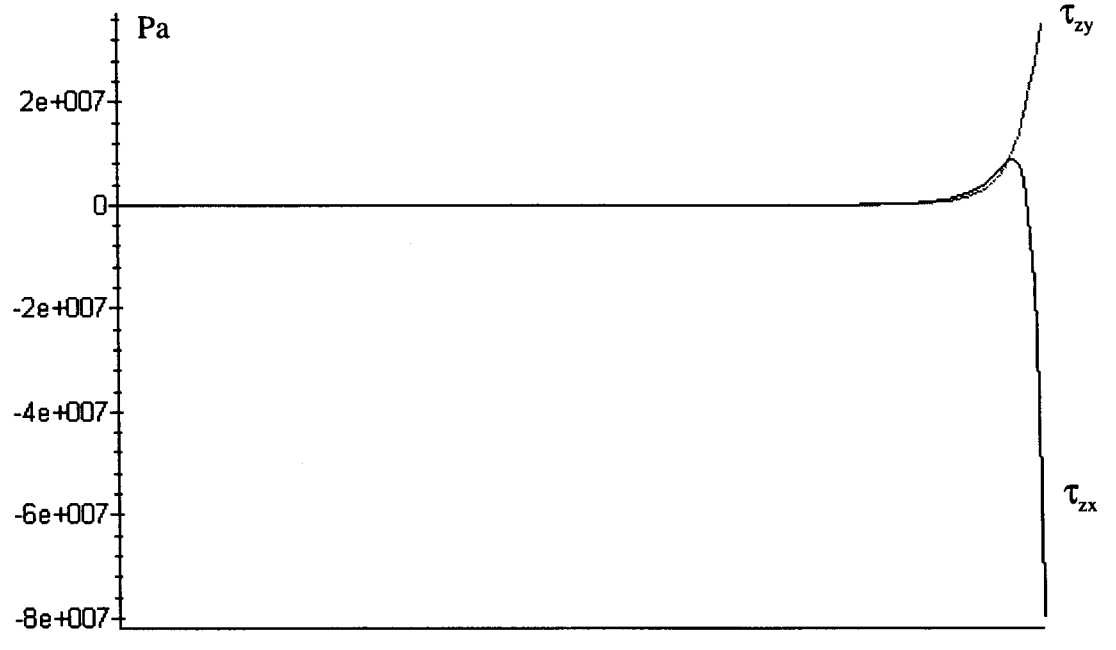

Figure C.42: Plots of τ_{zx} and τ_{zy} as a function of y $(0 < y < Wi/2)$ for u_a=-10^{-3} m. (Angle $\theta = 15^o$, Interface 5)

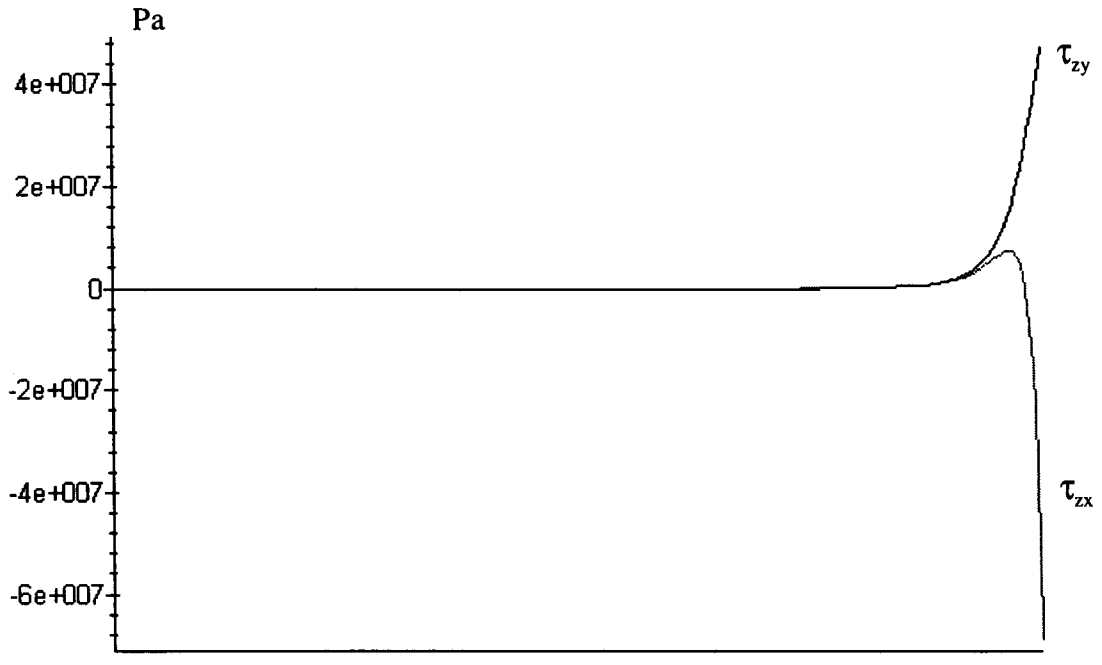

Figure C.43: Plots of τ_{zx} and τ_{zy} as a function of y $(0 < y < Wi/2)$ for u_a=-10^{-3} m. (Angle $\theta = 20^{o}$, Interface 5)

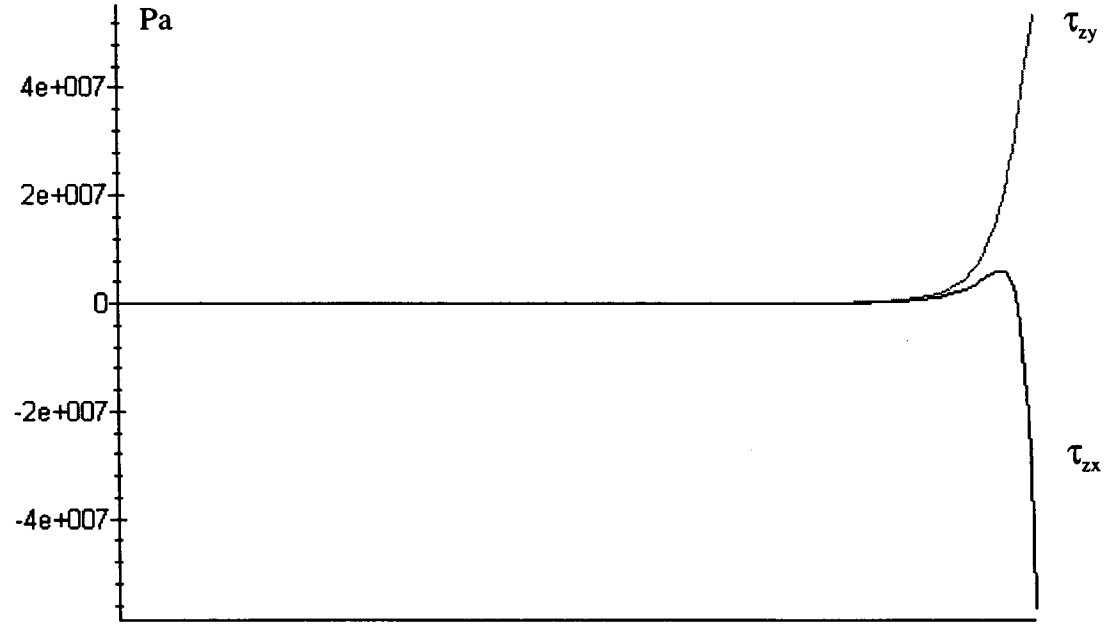

Figure C.44: Plots of τ_{zx} and τ_{zy} as a function of y $(0 < y < Wi/2)$ for u_a=-10^{-3} m. (Angle $\theta = 25^{o}$, Interface 5)

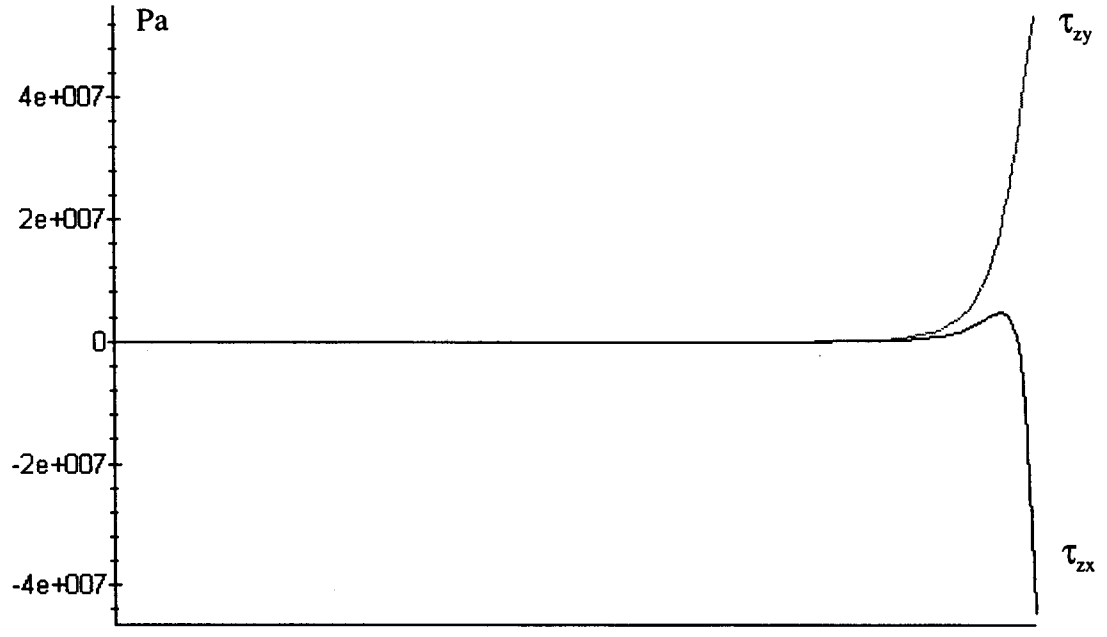

Figure C.45: Plots of τ_{zx} and τ_{zy} as a function of y $(0 < y < Wi/2)$ for u_a=-10^{-3} m. (Angle $\theta = 30^{o}$, Interface 5)

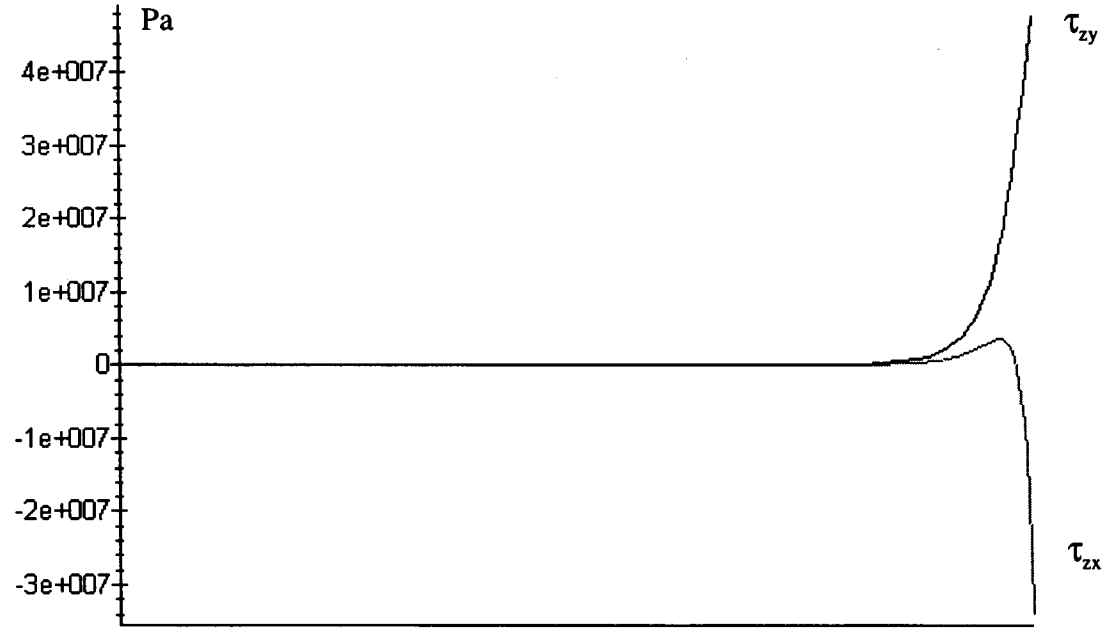

Figure C.46: Plots of τ_{zx} and τ_{zy} as a function of y $(0 < y < Wi/2)$ for u_a=-10^{-3} m. (Angle $\theta = 35^{o}$, Interface 5)

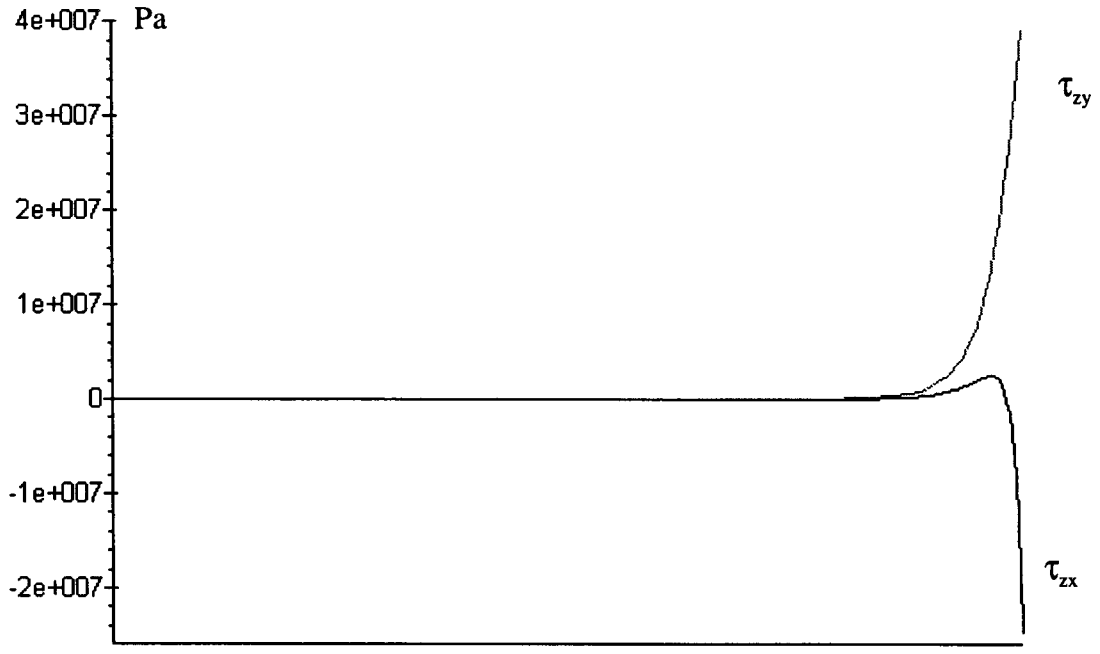

Figure C.47: Plots of τ_{zx} and τ_{zy} as a function of y $(0 < y < Wi/2)$ for u_a=-10^{-3} m. (Angle $\theta = 40^{o}$, Interface 5)

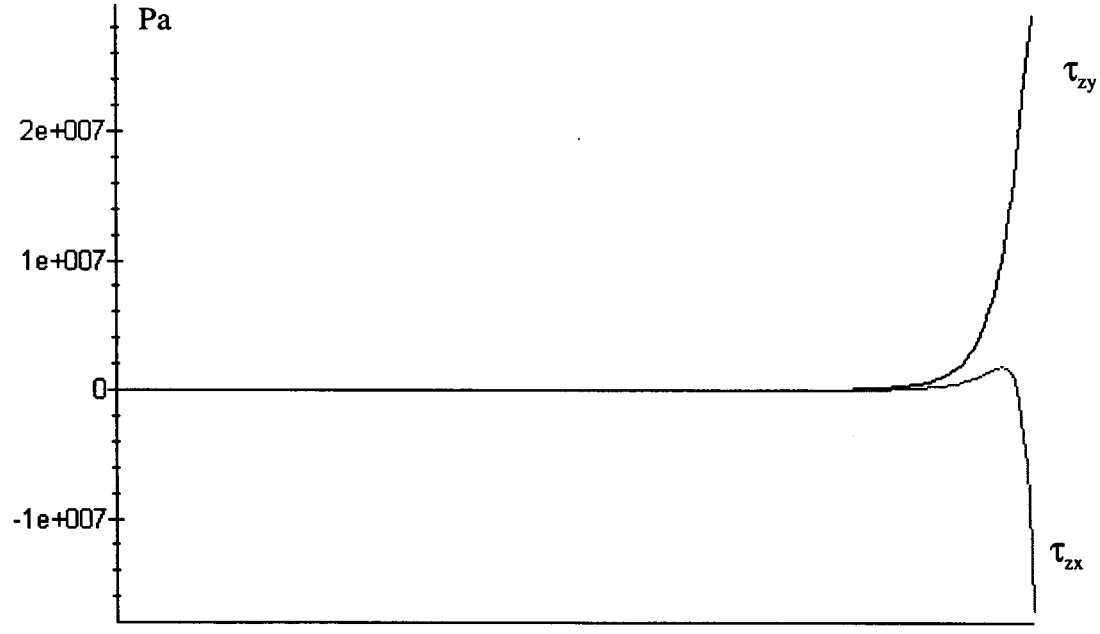

Figure C.48: Plots of τ_{zx} and τ_{zy} as a function of y $(0 < y < Wi/2)$ for u_a=-10^{-3} m. (Angle $\theta = 45^{o}$, Interface 5)

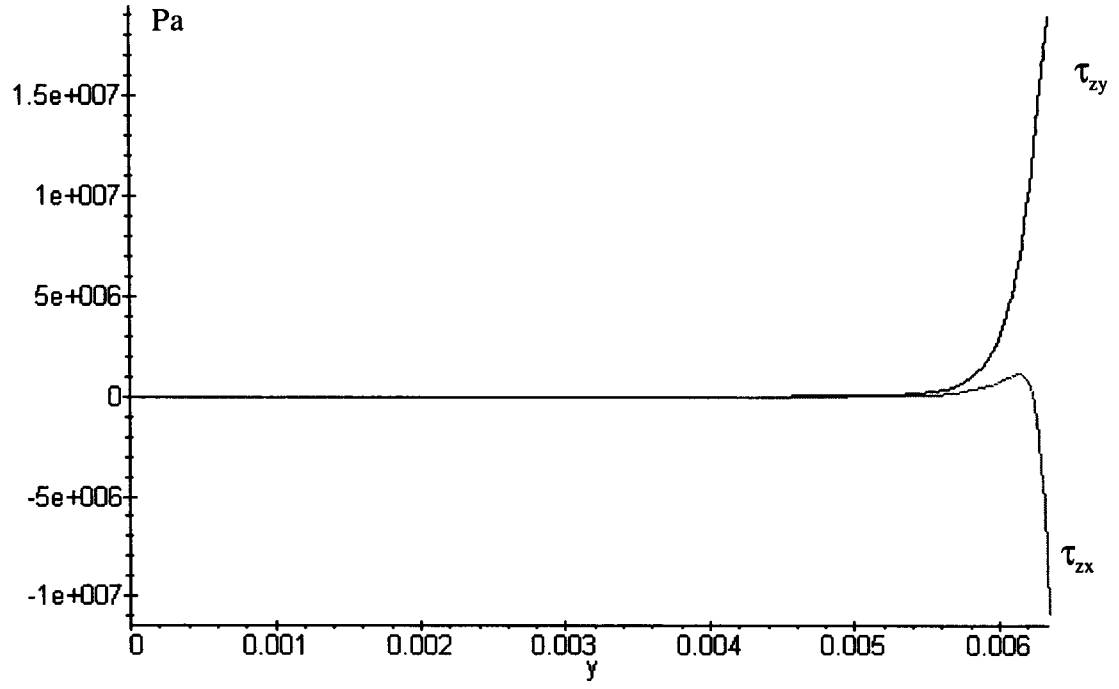

Figure C.49: Plots of τ_{zx} and τ_{zy} as a function of y $(0 < y < Wi/2)$ for u_a=-10^{-3} m. (Angle $\theta = 50^{o}$, Interface 5)

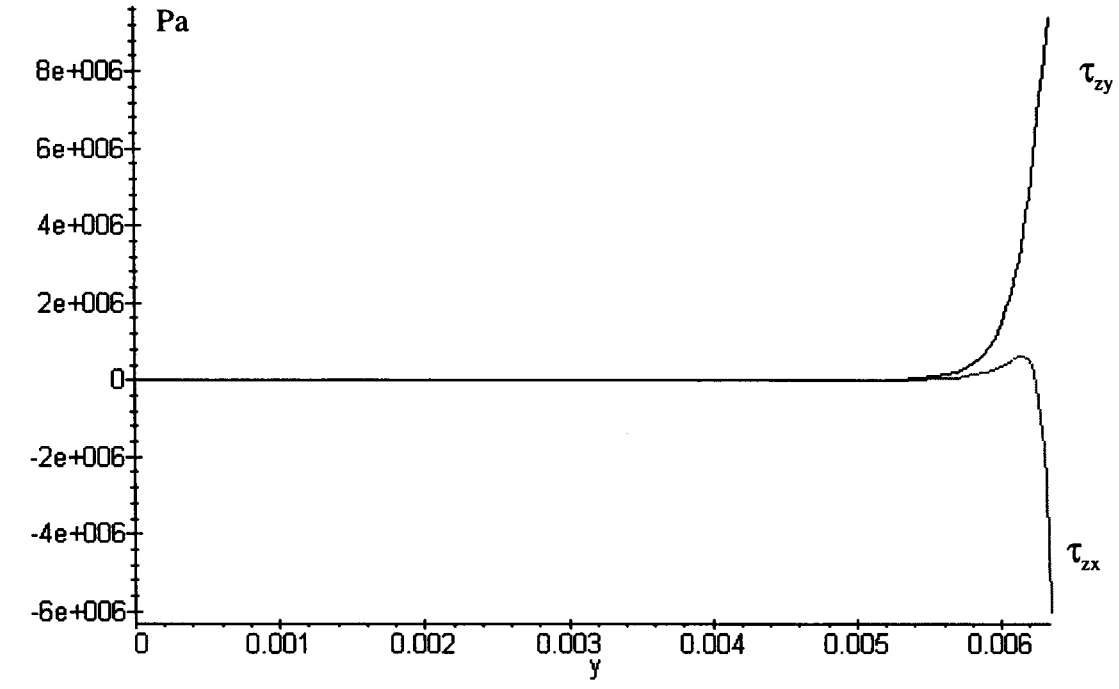

Figure C.50: Plots of τ_{zx} and τ_{zy} as a function of y $(0 < y < Wi/2)$ for u_a=-10^{-3} m. (Angle $\theta = 55^{o}$, Interface 5)

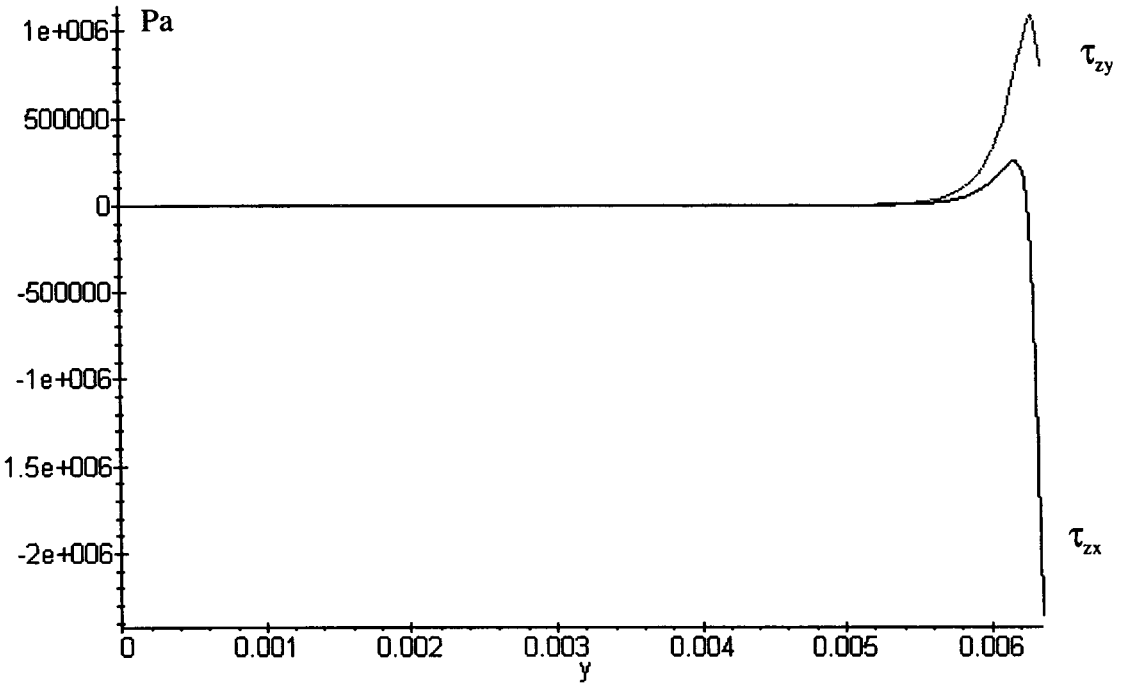

Figure C.51: Plots of τ_{zx} and τ_{zy} as a function of y $(0 < y < Wi/2)$ for u_a=-10^{-3} m. (Angle $\theta = 60^o$, Interface 5)

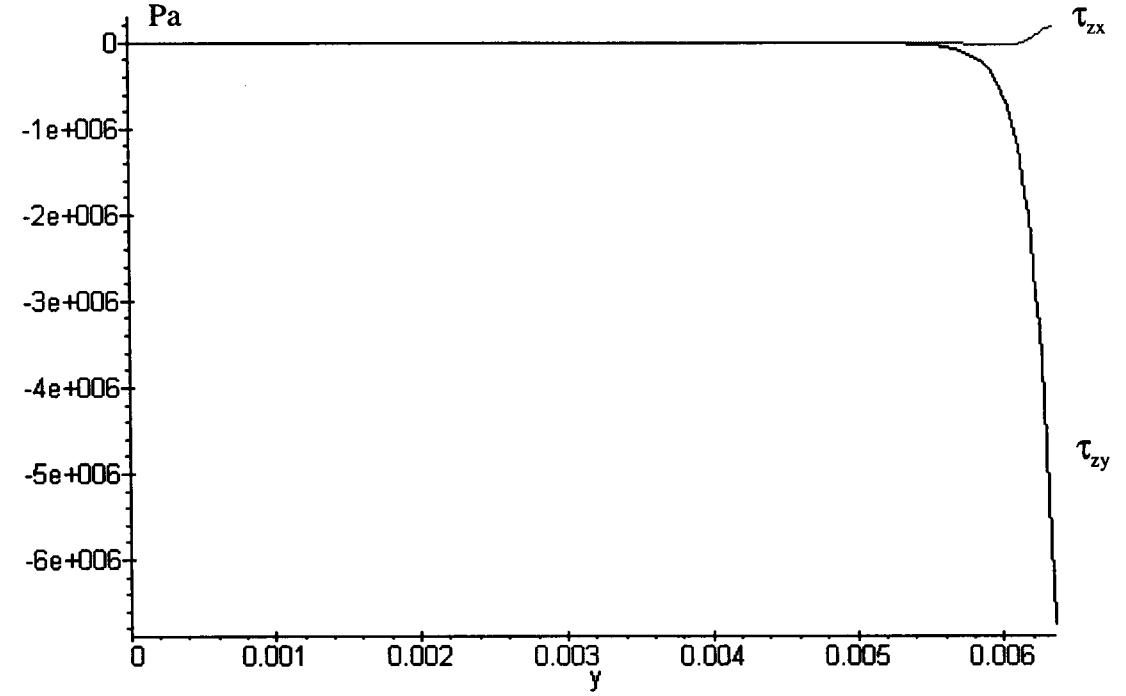

Figure C.52: Plots of τ_{zx} and τ_{zy} as a function of y $(0 < y < Wi/2)$ for u_a=-10^{-3} m. (Angle $\theta = 65^o$, Interface 5)

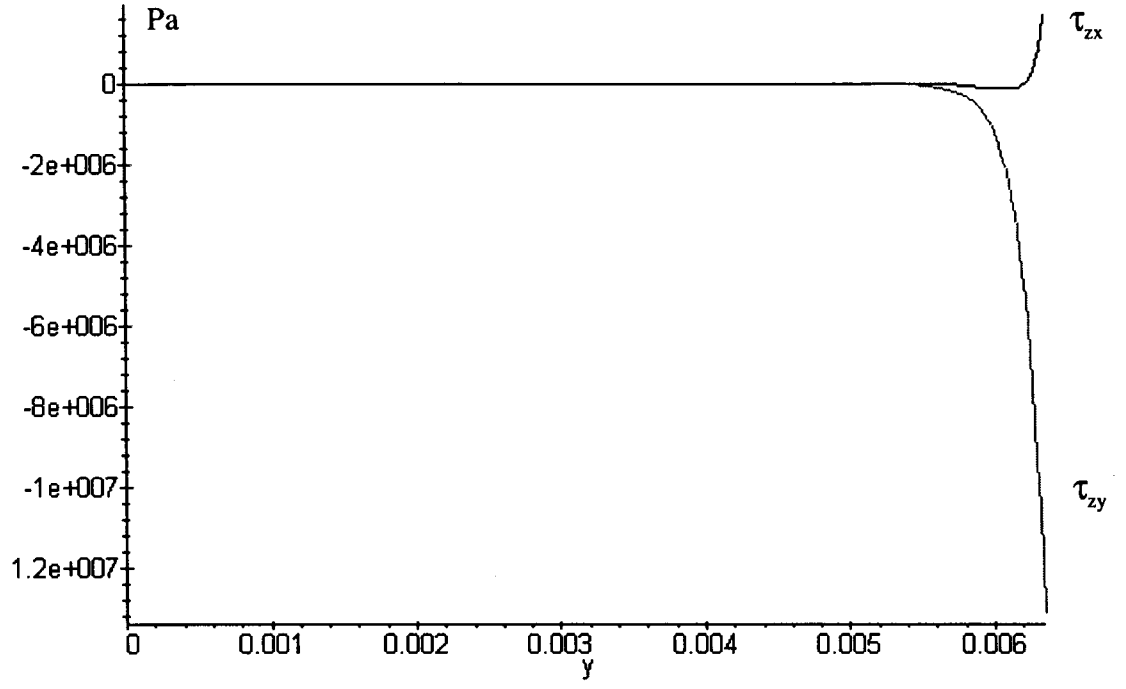

Figure C.53: Plots of τ_{zx} and τ_{zy} as a function of y $(0 < y < Wi/2)$ for u_a=-10^{-3} m. (Angle $\theta = 70^o$, Interface 5)

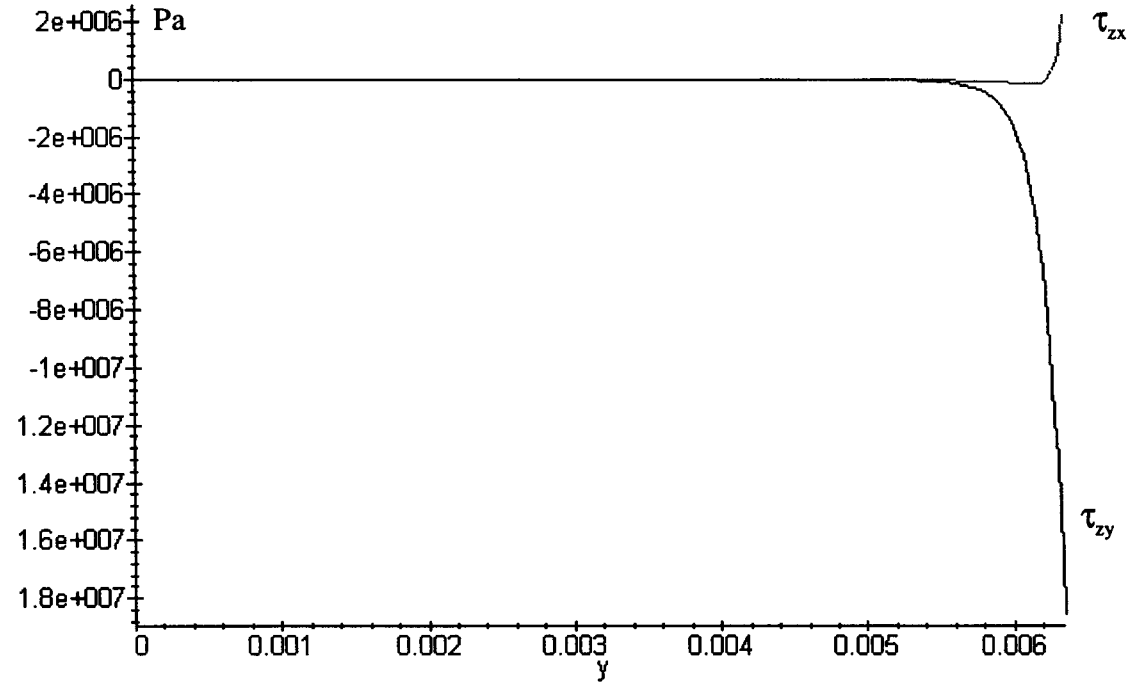

Figure C.54: Plots of τ_{zx} and τ_{zy} as a function of y $(0 < y < Wi/2)$ for u_a=-10^{-3} m. (Angle $\theta = 75^o$, Interface 5)

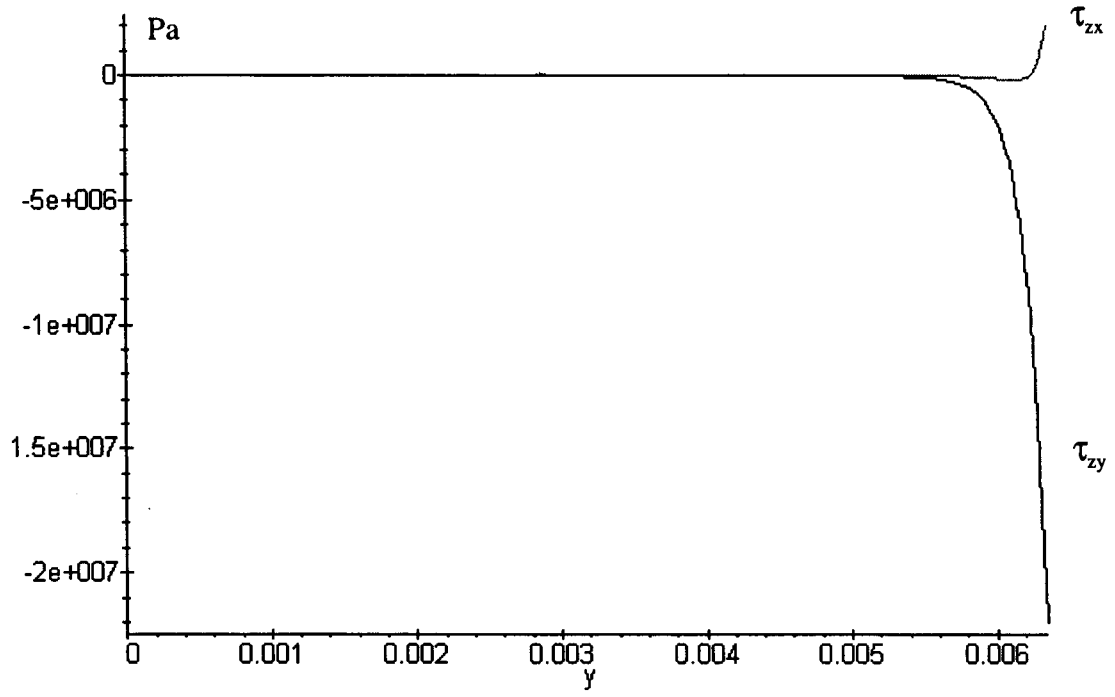

Figure C.55: Plots of τ_{zx} and τ_{zy} as a function of y $(0 < y < Wi/2)$ for u_a=-10^{-3} m. (Angle $\theta = 80^{o}$, Interface 5)

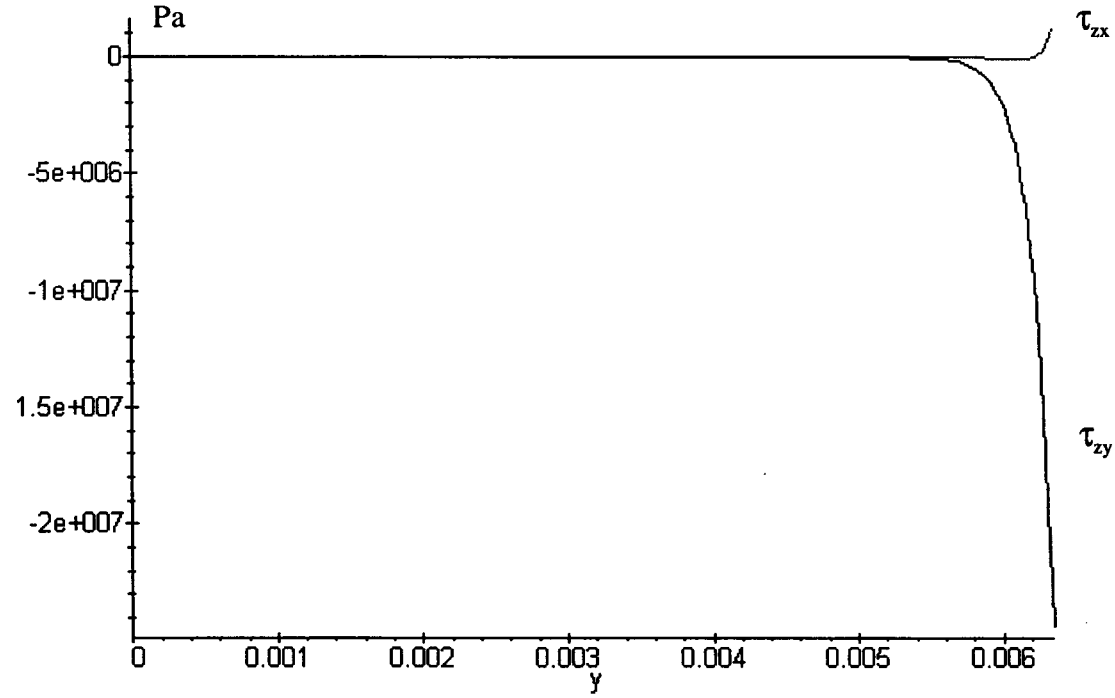

Figure C.56: Plots of τ_{zx} and τ_{zy} as a function of y $(0 < y < Wi/2)$ for u_a=-10^{-3} m. (Angle $\theta = 85^{o}$, Interface 5)

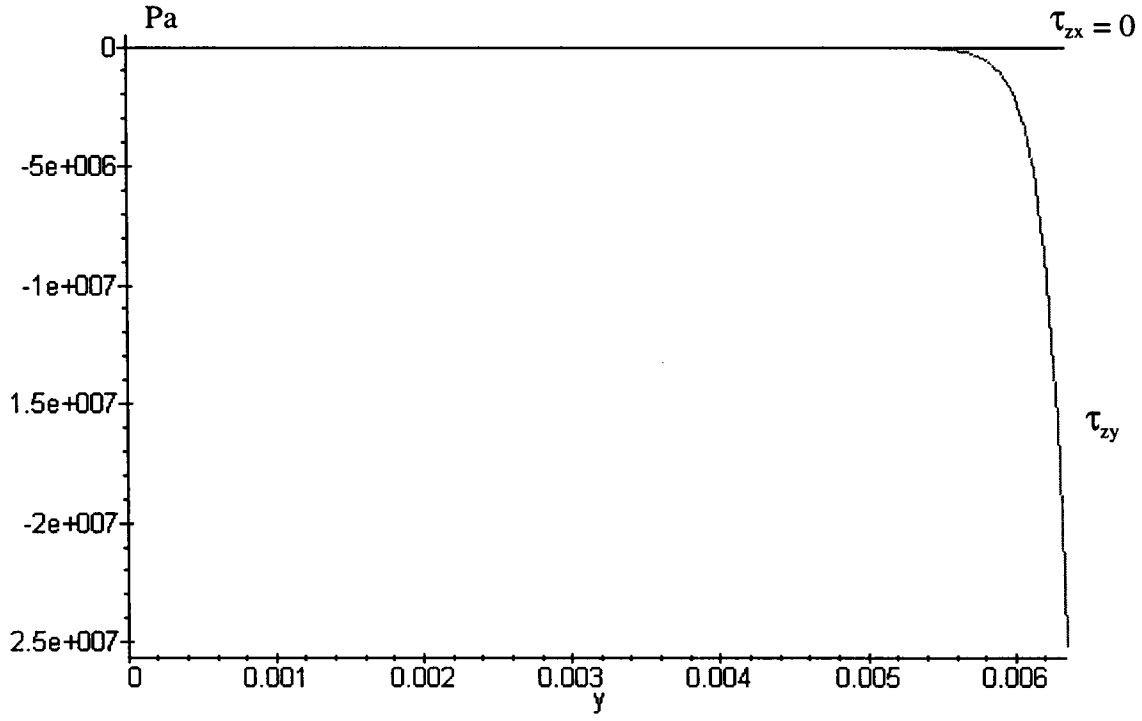

Figure C.57: Plots of τ_{zx} and τ_{zy} as a function of y $(0 < y < Wi/2)$ for u_a=-10^{-3} m. (Angle $\theta = 90^{o}$, Interface 5)

APPENDIX D

Program "Maple V" for the calculation
of interlaminar stresses τ_{zx} and τ_{zy}
and failure strain ε_f for the laminate $[\theta_1/\theta_2/\theta_3/\theta_4]_s$
with application to the laminate $[45/-45/0/90]_s$

EXAMPLE: CALCULATION OF INTERLAMINAR SHEAR STRESSES FOR: [theta1, theta2, theta3, theta4]s.

All quantities are in S.I. units, except stiffnesses which are in GPa. Final shear stresses are in Pa.

```
> Ef:=214:

> Em:=34*10^(-1):

> Gm:=13*10^(-1):

> nu12:=3*10^(-1):

> Vf:=6*10^(-1):

> E1:=Ef*Vf + Em*(1-Vf):

> E2:=Ef*Em/(Vf*Em + (1-Vf)*Ef):

> G:=Gm/(1-Vf):

> nu21:=nu12*E2/E1:

> e:=123*10^(-7):

> h:=123*10^(-6):

> L:=8*10^(-2):

> Wi:=127*10^(-4):
```

All calculations performed with an accuracy of "Digits" given below:

```
> Digits:=30:

> Q:=array([ [E1/(1-nu12*nu21), E2*nu12/(1-nu12*nu21),0], [E2*nu12/(1-nu12*n
> u21), E2/(1-nu12*nu21),0], [0,0,G] ]):


> Qb:=array(1..3,1..3):

> Qb[1,1]:=Q[1,1]*((cos(the/180*Pi))^4)+(2*Q[1,2]+4*Q[3,3])*((cos(the/180*Pi))^
> 2)*((sin(the/180*Pi))^2)+Q[2,2]*((sin(the/180*Pi))^4):
```

```
> Qb[1,2]:=(Q[1,1]+Q[2,2]- 4*Q[3,3])*((cos(the/180*Pi))^2)*((sin(the/180*Pi))^2)+
> Q[1,2]*(((sin(the/180*Pi))^4)+((cos(the/180*Pi))^4)):

> Qb[2,2]:=Q[1,1]*((sin(the/180*Pi))^4)+(2*Q[1,2]+4*Q[3,3])*((cos(the/180*Pi))^
> 2)*((sin(the/180*Pi))^2)+Q[2,2]*((cos(the/180*Pi))^4):

> Qb[1,3]:=(Q[1,1]- Q[1,2]- 2*Q[3,3])*(sin(the/180*Pi))*((cos(the/180*Pi))^3)+(Q[
> 1,2]- Q[2,2]+2*Q[3,3])*((sin(the/180*Pi))^3)*(cos(the/180*Pi)):

> Qb[2,3]:=(Q[1,1]- Q[1,2]- 2*Q[3,3])*((sin(the/180*Pi))^3)*(cos(the/180*Pi))+(Q[
> 1,2]- Q[2,2]+2*Q[3,3])*(sin(the/180*Pi))*((cos(the/180*Pi))^3):

> Qb[3,3]:=(Q[1,1]+Q[2,2]- 2*Q[1,2]- 2*Q[3,3])*((sin(the/180*Pi))^2)*((cos(the/18
> 0*Pi))^2)+Q[3,3]*(((sin(the/180*Pi))^4)+((cos(the/180*Pi))^4)):

> Qb[2,1]:=Qb[1,2]:  Qb[3,1]:=Qb[1,3]:  Qb[3,2]:=Qb[2,3]:

> Qb1:=array(1..3,1..3):   for m to 3 do for n to 3 do Qb1[m,n]:=evalf(subs(the=th
> eta1,Qb[m,n])) od od:

> Qb2:=array(1..3,1..3):   for m to 3 do for n to 3 do Qb2[m,n]:=evalf(subs(the=th
> eta2,Qb[m,n])) od od:

> Qb3:=array(1..3,1..3):   for m to 3 do for n to 3 do Qb3[m,n]:=evalf(subs(the=th
> eta3,Qb[m,n])) od od:

> Qb4:=array(1..3,1..3):   for m to 3 do for n to 3 do Qb4[m,n]:=evalf(subs(the=th
> eta4,Qb[m,n])) od od:


> H:=array([Gm/(2*e*h),Gm/(2*e*h),Gm/(2*e*h),Gm/(2*e*h)]):

> AA:=array([ [Qb1[3,3]*rho-H[1], Qb1[2,3]*rho, H[1], 0, 0, 0, 0, 0],  [Qb1[2,3]*rh
> o, Qb1[2,2]*rho-H[1], 0, H[1], 0, 0, 0, 0], [H[2], 0, Qb2[3,3]*rho-2*H[2], Qb2[2,3]
> *rho, H[2], 0, 0, 0], [0, H[2], Qb2[2,3]*rho, Qb2[2,2]*rho-2*H[2], 0, H[2], 0, 0],  [
> 0, 0, H[3], 0, Qb3[3,3]*rho-2*H[3], Qb3[2,3]*rho, H[3], 0], [0, 0, 0, H[3], Qb3[2,3
> ]*rho, Qb3[2,2]*rho-2*H[3], 0, H[3]], [0, 0, 0, 0, H[4], 0, Qb4[3,3]*rho-H[4], Qb4
> [2,3]*rho], [0, 0, 0, 0, 0, H[4], Qb4[2,3]*rho, Qb4[2,2]*rho-H[4]] ]):

> with(linalg):
  Warning: new definition for   norm
  Warning: new definition for   trace

> detAA:=det(AA):
```

Input of the 4 angles (theta1, theta2, theta3, theta4):

```
> theta1:=45:  theta2:=-45:  theta3:=0:  theta4:=90:

> rang := fsolve(detAA=0,rho,fulldigits):


> rhos:=vector( [ rang[3], rang[4], rang[5], rang[6], rang[7], rang[8] ] ):

> Identity:=array([ [1, 0, 0], [0, 1, 0], [0, 0, 1] ]):

> R1:=array(1..3,1..3): for m to 3 do for n to 3 do R1[m,n]:=evalf(Qb1[m,n]*rhos[i
> ] - H[1]*Identity[m,n]) od od:

> R2:=array(1..3,1..3): for m to 3 do for n to 3 do R2[m,n]:=evalf(Qb2[m,n]*rhos[i
> ] - 2*H[2]*Identity[m,n]) od od:

> R3:=array(1..3,1..3): for m to 3 do for n to 3 do R3[m,n]:=evalf(Qb3[m,n]*rhos[i
> ] - 2*H[3]*Identity[m,n]) od od:

> R4:=array(1..3,1..3): for m to 3 do for n to 3 do R4[m,n]:=evalf(Qb4[m,n]*rhos[i
> ] - H[4]*Identity[m,n]) od od:


> eq1:=R133*A1+H[1]*A2+R123*B1=0:

> eq2:=R123*A1+R122*B1+H[1]*B2=0:

> eq3:=R233*A2+H[2]*A3+H[2]*A1+R223*B2=0:

> eq4:=R223*A2+R222*B2+H[2]*B3+H[2]*B1=0:

> eq5:=R333*A3+H[3]*A4+H[3]*A2+R323*B3=0:

> eq6:=R323*A3+R322*B3+H[3]*B4+H[3]*B2=0:

> eq7:=R433*A4+H[4]*A3+R423*B4=0:

> A1:='A1': A2:='A2': A3:='A3': A4:='A4': B1:='B1': B2:='B2': B3:='B3': B4:
> ='B4':


> Z:=solve( {eq1,eq2,eq3,eq4,eq5,eq6,eq7}, {A2,A3,A4,B1,B2,B3,B4} ):
```

```
> assign (Z):

> FacA2:=subs(R122=R1[2,2], R222=R2[2,2], R322=R3[2,2],  R123=R1[2,3], R223
> =R2[2,3], R323=R3[2,3], R423=R4[2,3], R133=R1[3,3], R233=R2[3,3], R333=R3[
> 3,3],R433=R4[3,3], A1=1, A2):

> FacA3:=subs(R122=R1[2,2], R222=R2[2,2], R322=R3[2,2],  R123=R1[2,3], R223
> =R2[2,3], R323=R3[2,3], R423=R4[2,3],R133=R1[3,3], R233=R2[3,3], R333=R3[
> 3,3],R433=R4[3,3], A1=1, A3):

> FacA4:=subs(R122=R1[2,2], R222=R2[2,2], R322=R3[2,2],  R123=R1[2,3], R223
> =R2[2,3], R323=R3[2,3], R423=R4[2,3],R133=R1[3,3], R233=R2[3,3], R333=R3[
> 3,3],R433=R4[3,3], A1=1, A4):


> FacB1:=subs(R122=R1[2,2], R222=R2[2,2], R322=R3[2,2],  R123=R1[2,3], R223
> =R2[2,3], R323=R3[2,3], R423=R4[2,3],R133=R1[3,3], R233=R2[3,3], R333=R3[
> 3,3],R433=R4[3,3], A1=1, B1):

> FacB2:=subs(R122=R1[2,2], R222=R2[2,2], R322=R3[2,2],  R123=R1[2,3], R223
> =R2[2,3], R323=R3[2,3], R423=R4[2,3],R133=R1[3,3], R233=R2[3,3], R333=R3[
> 3,3],R433=R4[3,3], A1=1, B2):

> FacB3:=subs(R122=R1[2,2], R222=R2[2,2], R322=R3[2,2],  R123=R1[2,3], R223
> =R2[2,3], R323=R3[2,3], R423=R4[2,3],R133=R1[3,3], R233=R2[3,3], R333=R3[
> 3,3],R433=R4[3,3], A1=1, B3):

> FacB4:=subs(R122=R1[2,2], R222=R2[2,2], R322=R3[2,2],  R123=R1[2,3], R223
> =R2[2,3], R323=R3[2,3], R423=R4[2,3],R133=R1[3,3], R233=R2[3,3], R333=R3[
> 3,3],R433=R4[3,3], A1=1, B4):


> eq8:=R122*A1-R122=0:

> ZZ:=solve( {eq8}, {A1} ):

> assign (ZZ):

> FacA1:=subs(R122=R1[2,2], A1):


> MM21:=subs( i=1, ( Qb2[2,2]*(FacB2-FacB1)+Qb2[2,3]*(FacA2-FacA1) )*sqrt(
> rhos[i] )*cosh( sqrt( rhos[i] )*Wi/2 )):
```

```
> MM31:=subs( i=1, ( Qb3[2,2]*(FacB3-FacB1)+Qb3[2,3]*(FacA3-FacA1) )*sqrt(
> rhos[i] )*cosh( sqrt( rhos[i] )*Wi/2 )):

> MM41:=subs( i=1, ( Qb4[2,2]*(FacB4-FacB1)+Qb4[2,3]*(FacA4-FacA1) )*sqrt(
> rhos[i] )*cosh( sqrt( rhos[i] )*Wi/2 )):

> MM22:=subs( i=2, ( Qb2[2,2]*(FacB2-FacB1)+Qb2[2,3]*(FacA2-FacA1) )*sqrt(
> rhos[i] )*cosh( sqrt( rhos[i] )*Wi/2 )):

> MM32:=subs( i=2, ( Qb3[2,2]*(FacB3-FacB1)+Qb3[2,3]*(FacA3-FacA1) )*sqrt(
> rhos[i] )*cosh( sqrt( rhos[i] )*Wi/2 )):

> MM42:=subs( i=2, ( Qb4[2,2]*(FacB4-FacB1)+Qb4[2,3]*(FacA4-FacA1) )*sqrt(
> rhos[i] )*cosh( sqrt( rhos[i] )*Wi/2 )):

> MM23:=subs( i=3, ( Qb2[2,2]*(FacB2-FacB1)+Qb2[2,3]*(FacA2-FacA1) )*sqrt(
> rhos[i] )*cosh( sqrt( rhos[i] )*Wi/2 )):

> MM33:=subs( i=3, ( Qb3[2,2]*(FacB3-FacB1)+Qb3[2,3]*(FacA3-FacA1) )*sqrt(
> rhos[i] )*cosh( sqrt( rhos[i] )*Wi/2 )):

> MM43:=subs( i=3, ( Qb4[2,2]*(FacB4-FacB1)+Qb4[2,3]*(FacA4-FacA1) )*sqrt(
> rhos[i] )*cosh( sqrt( rhos[i] )*Wi/2 )):

> MM24:=subs( i=4, ( Qb2[2,2]*(FacB2-FacB1)+Qb2[2,3]*(FacA2-FacA1) )*sqrt(
> rhos[i] )*cosh( sqrt( rhos[i] )*Wi/2 )):

> MM34:=subs( i=4, ( Qb3[2,2]*(FacB3-FacB1)+Qb3[2,3]*(FacA3-FacA1) )*sqrt(
> rhos[i] )*cosh( sqrt( rhos[i] )*Wi/2 )):

> MM44:=subs( i=4, ( Qb4[2,2]*(FacB4-FacB1)+Qb4[2,3]*(FacA4-FacA1) )*sqrt(
> rhos[i] )*cosh( sqrt( rhos[i] )*Wi/2 )):

> MM25:=subs( i=5, ( Qb2[2,2]*(FacB2-FacB1)+Qb2[2,3]*(FacA2-FacA1) )*sqrt(
> rhos[i] )*cosh( sqrt( rhos[i] )*Wi/2 )):

> MM35:=subs( i=5, ( Qb3[2,2]*(FacB3-FacB1)+Qb3[2,3]*(FacA3-FacA1) )*sqrt(
> rhos[i] )*cosh( sqrt( rhos[i] )*Wi/2 )):

> MM45:=subs( i=5, ( Qb4[2,2]*(FacB4-FacB1)+Qb4[2,3]*(FacA4-FacA1) )*sqrt(
> rhos[i] )*cosh( sqrt( rhos[i] )*Wi/2 )):

> MM26:=subs( i=6, ( Qb2[2,2]*(FacB2-FacB1)+Qb2[2,3]*(FacA2-FacA1) )*sqrt(
```

```
> rhos[i] )*cosh( sqrt( rhos[i] )*Wi/2 )):

> MM36:=subs( i=6, ( Qb3[2,2]*(FacB3-FacB1)+Qb3[2,3]*(FacA3-FacA1) )*sqrt(
> rhos[i] )*cosh( sqrt( rhos[i] )*Wi/2 )):

> MM46:=subs( i=6, ( Qb4[2,2]*(FacB4-FacB1)+Qb4[2,3]*(FacA4-FacA1) )*sqrt(
> rhos[i] )*cosh( sqrt( rhos[i] )*Wi/2 )):


> NN21:=subs( i=1, ( Qb2[2,3]*(FacB2-FacB1)+Qb2[3,3]*(FacA2-FacA1) )*sqrt( r
> hos[i] )*cosh( sqrt( rhos[i] )*Wi/2 )):

> NN31:=subs( i=1, ( Qb3[2,3]*(FacB3-FacB1)+Qb3[3,3]*(FacA3-FacA1) )*sqrt( r
> hos[i] )*cosh( sqrt( rhos[i] )*Wi/2 )):

> NN41:=subs( i=1, ( Qb4[2,3]*(FacB4-FacB1)+Qb4[3,3]*(FacA4-FacA1) )*sqrt( r
> hos[i] )*cosh( sqrt( rhos[i] )*Wi/2 )):

> NN22:=subs( i=2, ( Qb2[2,3]*(FacB2-FacB1)+Qb2[3,3]*(FacA2-FacA1) )*sqrt( r
> hos[i] )*cosh( sqrt( rhos[i] )*Wi/2 )):

> NN32:=subs( i=2, ( Qb3[2,3]*(FacB3-FacB1)+Qb3[3,3]*(FacA3-FacA1) )*sqrt( r
> hos[i] )*cosh( sqrt( rhos[i] )*Wi/2 )):

> NN42:=subs( i=2, ( Qb4[2,3]*(FacB4-FacB1)+Qb4[3,3]*(FacA4-FacA1) )*sqrt( r
> hos[i] )*cosh( sqrt( rhos[i] )*Wi/2 )):

> NN23:=subs( i=3, ( Qb2[2,3]*(FacB2-FacB1)+Qb2[3,3]*(FacA2-FacA1) )*sqrt( r
> hos[i] )*cosh( sqrt( rhos[i] )*Wi/2 )):

> NN33:=subs( i=3, ( Qb3[2,3]*(FacB3-FacB1)+Qb3[3,3]*(FacA3-FacA1) )*sqrt( r
> hos[i] )*cosh( sqrt( rhos[i] )*Wi/2 )):

> NN43:=subs( i=3, ( Qb4[2,3]*(FacB4-FacB1)+Qb4[3,3]*(FacA4-FacA1) )*sqrt( r
> hos[i] )*cosh( sqrt( rhos[i] )*Wi/2 )):

> NN24:=subs( i=4, ( Qb2[2,3]*(FacB2-FacB1)+Qb2[3,3]*(FacA2-FacA1) )*sqrt( r
> hos[i] )*cosh( sqrt( rhos[i] )*Wi/2 )):

> NN34:=subs( i=4, ( Qb3[2,3]*(FacB3-FacB1)+Qb3[3,3]*(FacA3-FacA1) )*sqrt( r
> hos[i] )*cosh( sqrt( rhos[i] )*Wi/2 )):

> NN44:=subs( i=4, ( Qb4[2,3]*(FacB4-FacB1)+Qb4[3,3]*(FacA4-FacA1) )*sqrt( r
> hos[i] )*cosh( sqrt( rhos[i] )*Wi/2 )):
```

```
> NN25:=subs( i=5, ( Qb2[2,3]*(FacB2-FacB1)+Qb2[3,3]*(FacA2-FacA1) )*sqrt( r
> hos[i] )*cosh( sqrt( rhos[i] )*Wi/2 )):

> NN35:=subs( i=5, ( Qb3[2,3]*(FacB3-FacB1)+Qb3[3,3]*(FacA3-FacA1) )*sqrt( r
> hos[i] )*cosh( sqrt( rhos[i] )*Wi/2 )):

> NN45:=subs( i=5, ( Qb4[2,3]*(FacB4-FacB1)+Qb4[3,3]*(FacA4-FacA1) )*sqrt( r
> hos[i] )*cosh( sqrt( rhos[i] )*Wi/2 )):

> NN26:=subs( i=6, ( Qb2[2,3]*(FacB2-FacB1)+Qb2[3,3]*(FacA2-FacA1) )*sqrt( r
> hos[i] )*cosh( sqrt( rhos[i] )*Wi/2 )):

> NN36:=subs( i=6, ( Qb3[2,3]*(FacB3-FacB1)+Qb3[3,3]*(FacA3-FacA1) )*sqrt( r
> hos[i] )*cosh( sqrt( rhos[i] )*Wi/2 )):

> NN46:=subs( i=6, ( Qb4[2,3]*(FacB4-FacB1)+Qb4[3,3]*(FacA4-FacA1) )*sqrt( r
> hos[i] )*cosh( sqrt( rhos[i] )*Wi/2 )):


> RR2:=Qb1[1,2]*(Qb2[2,2]*Qb1[3,3] - Qb2[2,3]*Qb1[2,3])/(Qb1[2,2]*Qb1[3,3] -
> Qb1[2,3]*Qb1[2,3]) - Qb2[1,2] + Qb1[1,3]*(Qb2[2,3]*Qb1[2,2] - Qb2[2,2]*Qb1[2
> ,3])/(Qb1[2,2]*Qb1[3,3] - Qb1[2,3]*Qb1[2,3]):

> RR3:=Qb1[1,2]*(Qb3[2,2]*Qb1[3,3] - Qb3[2,3]*Qb1[2,3])/(Qb1[2,2]*Qb1[3,3] -
> Qb1[2,3]*Qb1[2,3]) - Qb3[1,2] + Qb1[1,3]*(Qb3[2,3]*Qb1[2,2] - Qb3[2,2]*Qb1[2
> ,3])/(Qb1[2,2]*Qb1[3,3] - Qb1[2,3]*Qb1[2,3]):

> RR4:=Qb1[1,2]*(Qb4[2,2]*Qb1[3,3] - Qb4[2,3]*Qb1[2,3])/(Qb1[2,2]*Qb1[3,3] -
> Qb1[2,3]*Qb1[2,3]) - Qb4[1,2] + Qb1[1,3]*(Qb4[2,3]*Qb1[2,2] - Qb4[2,2]*Qb1[2
> ,3])/(Qb1[2,2]*Qb1[3,3] - Qb1[2,3]*Qb1[2,3]):

> SS2:=Qb1[1,2]*(Qb2[2,3]*Qb1[3,3] - Qb2[3,3]*Qb1[2,3])/(Qb1[2,2]*Qb1[3,3] -
> Qb1[2,3]*Qb1[2,3]) - Qb2[1,3] + Qb1[1,3]*(Qb2[3,3]*Qb1[2,2] - Qb2[2,3]*Qb1[2
> ,3])/(Qb1[2,2]*Qb1[3,3] - Qb1[2,3]*Qb1[2,3]):

> SS3:=Qb1[1,2]*(Qb3[2,3]*Qb1[3,3] - Qb3[3,3]*Qb1[2,3])/(Qb1[2,2]*Qb1[3,3] -
> Qb1[2,3]*Qb1[2,3]) - Qb3[1,3] + Qb1[1,3]*(Qb3[3,3]*Qb1[2,2] - Qb3[2,3]*Qb1[2
> ,3])/(Qb1[2,2]*Qb1[3,3] - Qb1[2,3]*Qb1[2,3]):

> SS4:=Qb1[1,2]*(Qb4[2,3]*Qb1[3,3] - Qb4[3,3]*Qb1[2,3])/(Qb1[2,2]*Qb1[3,3] -
> Qb1[2,3]*Qb1[2,3]) - Qb4[1,3] + Qb1[1,3]*(Qb4[3,3]*Qb1[2,2] - Qb4[2,3]*Qb1[2
> ,3])/(Qb1[2,2]*Qb1[3,3] - Qb1[2,3]*Qb1[2,3]):
```

```
> eq21:=MM21*At1+MM22*At2+MM23*At3+MM24*At4+MM25*At5+MM26*
> At6=RR2:

> eq22:=MM31*At1+MM32*At2+MM33*At3+MM34*At4+MM35*At5+MM36*
> At6=RR3:

> eq23:=MM41*At1+MM42*At2+MM43*At3+MM44*At4+MM45*At5+MM46*
> At6=RR4:

> eq24:=NN21*At1+NN22*At2+NN23*At3+NN24*At4+NN25*At5+NN26*At6=S
> S2:

> eq25:=NN31*At1+NN32*At2+NN33*At3+NN34*At4+NN35*At5+NN36*At6=S
> S3:

> eq26:=NN41*At1+NN42*At2+NN43*At3+NN44*At4+NN45*At5+NN46*At6=S
> S4:


> At1:='At1': At2:='At2': At3:='At3': At4:='At4': At5:='At5': At6:='At6':

> At:=solve( {eq21,eq22,eq23,eq24,eq25,eq26},{At1,At2,At3,At4,At5,At6} ):

> assign (At):

> Atf:=vector( [At1,At2,At3,At4,At5,At6] ):

> FacA:=vector( [1, FacA2, FacA3, FacA4] ):

> FacB:=vector( [FacB1, FacB2, FacB3, FacB4] ):
```

Definition of shear stresses at the interface k (between ply 'k' and ply 'k+1'):

```
> k:=3:

> ua:=-1*10^(-3):

> Tauzx:=(ua/L)*(Gm/(2*e))*( Atf[1]*(subs(i=1, FacA[k]-FacA[k+1]))*sinh( sqrt(
> rhos[1] )*y ) +Atf[2]*(subs(i=2, FacA[k]-FacA[k+1]))*sinh( sqrt( rhos[2] )*y ) +
> Atf[3]*(subs(i=3, FacA[k]-FacA[k+1]))*sinh( sqrt( rhos[3] )*y ) +Atf[4]*(subs(i=
> 4, FacA[k]-FacA[k+1]))*sinh( sqrt( rhos[4] )*y ) +Atf[5]*(subs(i=5, FacA[k]-Fac
> A[k+1]))*sinh( sqrt( rhos[5] )*y ) +Atf[6]*(subs(i=6, FacA[k]-FacA[k+1]))*sinh(
> sqrt( rhos[6] )*y ) ):
```

```
> Tauzy:=(ua/L)*(Gm/(2*e))*( Atf[1]*(subs(i=1, FacB[k]-FacB[k+1]))*sinh( sqrt(
> rhos[1] )*y ) +Atf[2]*(subs(i=2, FacB[k]-FacB[k+1]))*sinh( sqrt( rhos[2] )*y ) +A
> tf[3]*(subs(i=3, FacB[k]-FacB[k+1]))*sinh( sqrt( rhos[3] )*y ) +Atf[4]*(subs(i=4,
> FacB[k]-FacB[k+1]))*sinh( sqrt( rhos[4] )*y ) +Atf[5]*(subs(i=5, FacB[k]-FacB[
> k+1]))*sinh( sqrt( rhos[5] )*y ) +Atf[6]*(subs(i=6, FacB[k]-FacB[k+1]))*sinh( sq
> rt( rhos[6] )*y ) ):

> Tauzxedge:=subs(y=Wi/2,Tauzx*10^9):

> Tauzyedge:=subs(y=Wi/2,Tauzy*10^9):

> Digits:=10:

> Tauzxedge; Tauzyedge;
```

$$-.475198438\ 10^{7}$$

$$.1112215302\ 10^{9}$$

```
> plot({Tauzx*10^9,Tauzy*10^9},y=0..Wi/2);
```

Calculation of the amplitude of microbuckling V and fiber maximum tensile strain epsfiber (at the interface of the 0* ply where Tauzy is maximum).

```
> Digits:=20:

> lambda0:=5*10^(-4):

> V0:=(lambda0/Pi)*tan(3*Pi/180):
```

(a positive u displacement indicates compression)

```
> slopeTauzy:=(-u/ua)*(subs(y=Wi/2,Tauzy*10^9)-subs(y=(Wi/2)-2*evalf(V0),Tau
> zy*10^9))/(2*evalf(V0)):

> sigma0:=Q[1,1]*(10^9)*abs(u)/L:

> rf:=35*10^(-7):  Af:=Pi*rf^2:  Ifib:=Pi*(rf^4)/4:

> V:=V0/(1-((sigma0*Af/Vf)+2*2*rf*slopeTauzy*(lambda0/Pi)^2)/(Ef*(10^9)*Ifib
> *((Pi/lambda0)^2)+(6*10^(-1))*Gm*(10^9)*Af/(1-Vf))):

> epsfiber:=-(sigma0)/(Vf*Ef*(10^9))+rf*((Pi/lambda0)^2)*V:
```

Calculation of the strain (epsfailure) which cause fiber failure (in microstrains).

```
> epstf:=14*10^(-3):

> dispfailure:=fsolve(epsfiber-epstf=0, u):  epsfailure:=dispfailure/L:

> Digits:=5:

> abs(epsfailure)*10^6;
```

5272.4

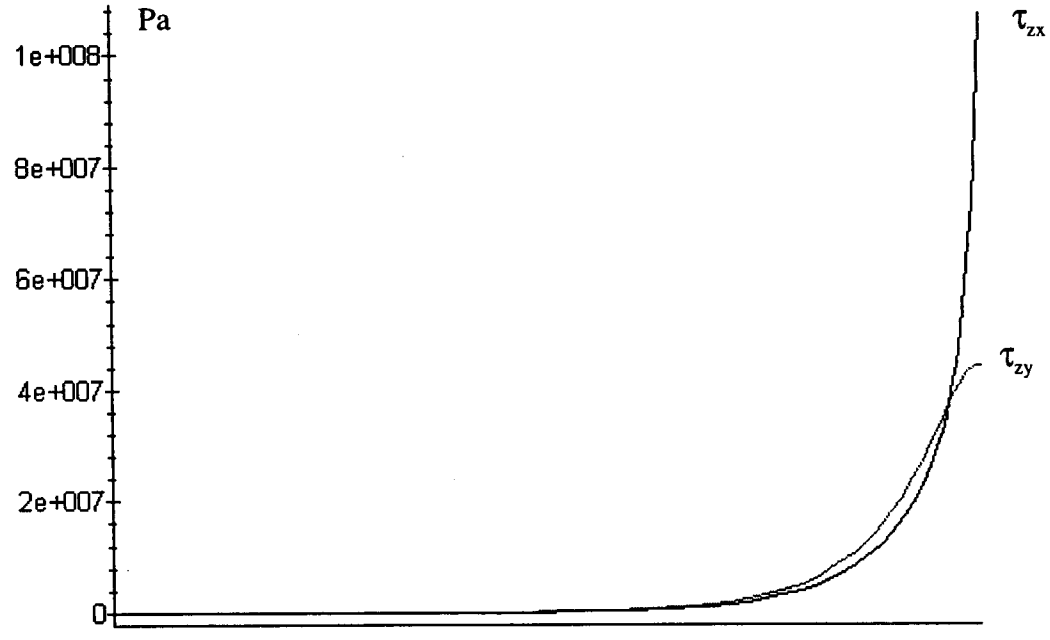

Figure D.1: Laminate $[45/-45/0/90]_s$: Laminate $[45/-45/0/90]_s$:
Plots of τ_{zx} and τ_{zy} as a function of y $(0 < y < Wi/2)$ for u_a=-10^{-3} m. (Interface 1)

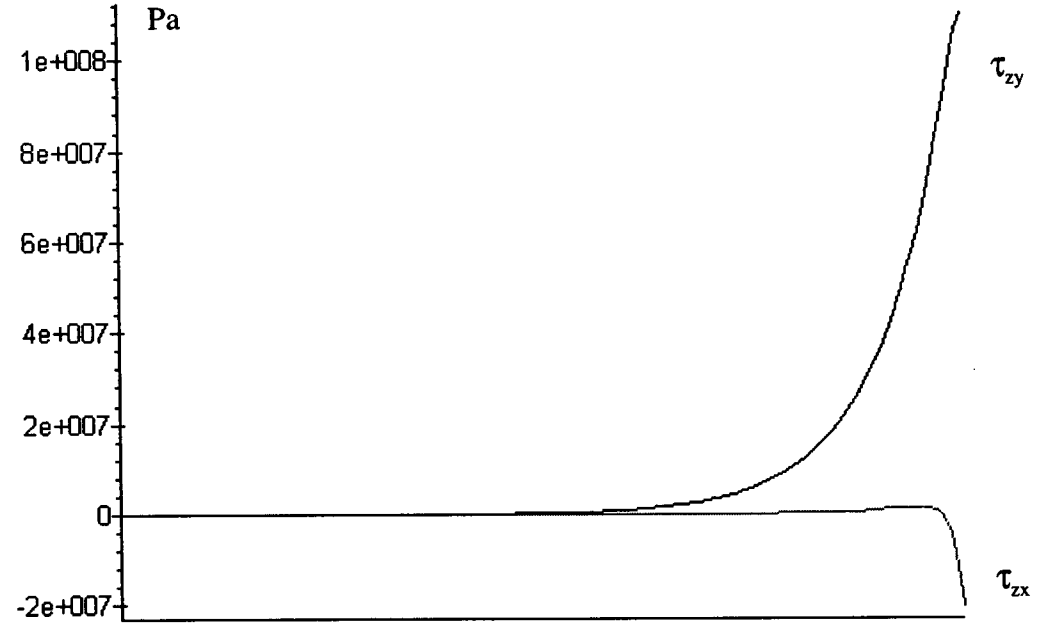

Figure D.2: Laminate $[45/-45/0/90]_s$:
Plots of τ_{zx} and τ_{zy} as a function of y $(0 < y < Wi/2)$ for u_a=-10^{-3} m. (Interface 2)

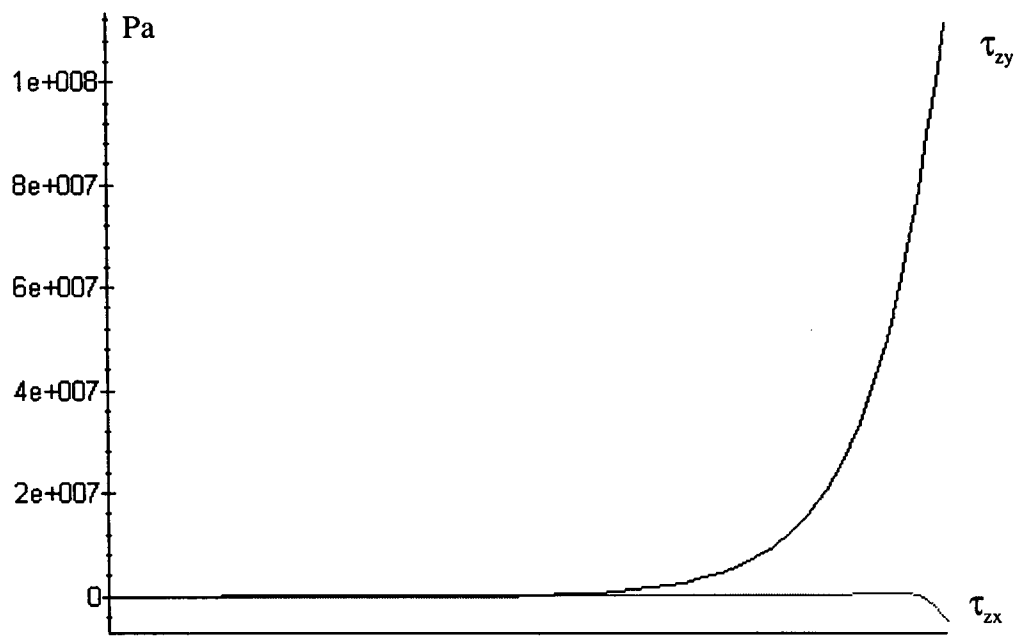

Figure D.3: Laminate $[45/-45/0/90]_s$:
Plots of τ_{zx} and τ_{zy} as a function of y $(0 < y < Wi/2)$ for $u_a=-10^{-3}$ m. (Interface 3)